Bioactive Materials 51 (2025) 650–719

Contents lists available at ScienceDirect

Bioactive Materials

journal homepage: www.keaipublishing.com/en/journals/bioactive-materials

Review article

Electrically conductive biopolymer-based hydrogels and fibrous materials fabricated using 3D printing and electrospinning for cardiac tissue engineering

Arnaud Kamdem Tamo [a,b,c,d,*], Ingo Doench [a,b], Kaveh Roshanbinfar [d], Alexandra Montembault [c], Anatoli Serghei [c], Felix B. Engel [d,**], Anayancy Osorio-Madrazo [a,b,***]

[a] Laboratory of Organ Printing, University of Bayreuth, 95447, Bayreuth, Germany
[b] Laboratory for Bioinspired Materials for Biomedical Engineering, Department of Microsystems Engineering IMTEK, University of Freiburg, 79110, Freiburg, Germany
[c] Ingénierie des Matériaux Polymères (IMP), UMR 5223, Université Claude Bernard Lyon 1, CNRS, INSA Lyon, Université Jean Monnet, 69622, Villeurbanne, France
[d] Department of Nephropathology, Experimental Renal and Cardiovascular Research, Institute of Pathology and Department of Cardiology, Friedrich-Alexander-Universität Erlangen-Nürnberg (FAU), 91054, Erlangen, Germany

ARTICLE INFO

Keywords:
Cardiac tissue engineering
3D (bio)printing
Electrospinning
Biopolymer-based hydrogels
Fiber-filled hydrogels
Electroconductive materials
Electroconductive hydrogels

ABSTRACT

Cardiovascular diseases pose a significant global health challenge, driving ongoing efforts to develop effective treatments. Various biofabrication technologies utilizing numerous materials have been employed to design functional cardiac tissues. Choosing the right material is crucial to support cardiac cell growth, proliferation, tissue maturation and functionality. 3D printing enables the fabrication of structures that mimic the hierarchical organization of native cardiac tissue, further enhancing its function. Electrospinning produces nanofibrous scaffolds with a high surface area and porosity, mimicking the extracellular matrix and promoting the cell behaviors required for tissue formation. Although typically employed independently, combining these technologies can enable the fabrication of patches with properties closely resembling those of native cardiac tissues. Recent research focuses on the use of electroconductive materials, which enhance cell-to-cell communication and promote the maturation of cardiomyocytes, thereby preventing arrhythmic contractions and improving the functionality of engineered cardiac tissues. In this review, recent studies showcasing the applications of electroconductive biopolymer-based fibrous materials and hydrogels designed using 3D printing and/or electrospinning for cardiac tissue engineering are discussed. Furthermore, the review evaluates the synergistic effects of biopolymer-based materials and electrical components in 3D printed electroconductive hydrogels. It also discusses the challenges faced in fabricating these hydrogels and explores their future prospects for biomedical applications.

1. Introduction

Heart disease remains the leading cause of death worldwide [1,2]. Heart transplantation is currently the only effective treatment for patients with end-stage heart failure, but the severe shortage of donor hearts poses a major challenge. While progress has recently been made in xenotransplantation [3], its application in humans has so far failed, and we are still far from achieving successful clinical implementation [4]. Similarly, stem cell therapies have not been successful [5]. The approach of inducing cardiomyocyte proliferation presents limitations, with its efficacy in adult hearts still being unclear [6]. In recent years, engineered cardiac tissues have emerged as valuable tools for modeling

Peer review under the responsibility of editorial board of Bioactive Materials.
* Corresponding author. Laboratory of Organ Printing, University of Bayreuth, 95447, Bayreuth, Germany.
** Corresponding author. Department of Nephropathology, Experimental Renal and Cardiovascular Research, Friedrich-Alexander-Universität Erlangen-Nürnberg (FAU), 91054, Erlangen, Germany.
*** Corresponding author. Laboratory of Organ Printing, University of Bayreuth, 95447, Bayreuth, Germany.
E-mail addresses: arnaud.kamdem-tamo@uni-bayreuth.de, arnaudkamdem38@yahoo.com (A.K. Tamo), felix.engel@uk-erlangen.de (F.B. Engel), anayancy.osorio-madrazo@uni-bayreuth.de (A. Osorio-Madrazo).

https://doi.org/10.1016/j.bioactmat.2025.05.014
Received 7 February 2025; Received in revised form 21 April 2025; Accepted 14 May 2025
Available online 9 June 2025
2452-199X/© 2025 The Authors. Publishing services by Elsevier B.V. on behalf of KeAi Communications Co. Ltd. This is an open access article under the CC BY-NC-ND license (http://creativecommons.org/licenses/by-nc-nd/4.0/).

disease and studying drug responses. Preclinical animal studies suggested that engineered cardiac tissues can improve heart function [1,7–10], and their suitability for patients is currently being evaluated in a clinical trial (ClinicalTrials.gov Identifier: NCT04396899). The clinical trial aims to test the hypothesis that cardiomyocyte implantation using an engineered heart muscle (EHM), the proposed investigational medicinal product (IMP) known as "Biological ventricular assist tissue" or BioVAT, can lead to sustainable remuscularization and improve myocardial function in patients with heart failure. The engineered heart muscle are created from a precise mixture of induced pluripotent stem cell (iPSC)-derived cardiomyocytes and stromal cells, encapsulated in a bovine collagen type I hydrogel. Extensive preclinical testing has supported the clinical viability of this myocardial remuscularization approach via the EHM implantation. The trial targets patients with advanced heart failure and reduced ejection fraction (HFrEF; EF $\leq$ 35 %), who have no viable options for heart transplantation (ClinicalTrials.gov Identifier: NCT04396899). Moreover, Jebran et al. [11] investigated the use of epicardial EHM allografts made from induced pluripotent stem cell-derived cardiomyocytes and stromal cells to treat heart failure in rhesus macaques. The goal was to achieve structural and functional remuscularization of the failing heart without severe side effects like arrhythmia and tumor growth. The researchers confirmed that the new rhesus macaque EHM model was comparable to an established human EHM formulation [11]. Long-term retention of EHM grafts (up to 6 months) and dose-dependent enhancement of the heart wall were demonstrated, including improvements in heart contractility and ejection fraction. The EHM allografts were shown to be safe, as no arrhythmias or tumors were observed. Histopathological and magnetic resonance imaging analyses confirmed cell retention and vascularization. These findings led to the approval of a first-in-human clinical trial, where EHM implantation successfully remuscularized the heart in a patient with advanced heart failure [11]. Cardiac tissue engineering (cardiac TE) stands at the forefront of biomedical research, driven by the imperative to address challenges posed by traditional methodologies [12,13].

The cardiovascular system, with its complex network of blood vessels including arteries, veins and capillaries, along with the heart muscle and valves, is susceptible to various pathologies and injuries that need advanced strategies for effective tissue repair [14–16]. Traditional approaches to cardiovascular TE, such as the use of synthetic grafts and the injection or transplantation of cells directly into the damaged heart tissue, face significant challenges [17]. Synthetic grafts, while widely used, often lack the intricate cellular and extracellular matrix (ECM) architecture necessary for optimal functionality and integration within the host tissue [18]. Furthermore, cardiac cell injection and cell transplantation for regenerating cardiac tissue functions and properties face several limitations that hinder their efficacy and practical clinical application [19,20]. One significant challenge is the low survival rate of transplanted cells, often due to the hostile environment of the infarcted heart, characterized by inflammation, hypoxia, and oxidative stress. This environment can cause rapid cell death, reducing the overall therapeutic potential [21]. Immunogenicity is another concern, as the immune system may reject the transplanted cells, especially if they are allogeneic rather than autologous [22]. Furthermore, the lack of appropriate vascularization at the damaged heart site where cells are introduced, can impede nutrient and oxygen supply, compromising cell survival and function [23,24]. The newly introduced cells often struggle to establish strong connections with existing myocardial cells, leading to poor mechanical and electrical coupling. This lack of integration disrupts the synchronized contraction of the heart muscle, crucial for effective blood pumping [25]. This increases the risk of arrhythmias, which are life-threatening abnormal heart rhythms. The difference in electrical properties between the transplanted cells and native myocardium worsens this issue, as the transplanted cells may fail to propagate electrical signals efficiently or synchronously [25,26].

Due to tissue complex microstructure and limited regenerative capacity, the human heart struggles to repair itself after injury [5,27]. Myocardial infarction often leads to non-functional scar tissue formation, distorting tissue structure, increasing stiffness, and reducing contractility, which impaires cardiac function [28]. The normal pumping action of the heart causes deformation, leading to remodeling and reduced cardiac output over time. Despite lots of efforts, complete elimination of scar tissue and restoration of cardiac output to pre-myocardial infarction levels remain elusive [29]. Additionally, coordinated interactions among cardiomyocytes, endothelial cells and other cell types are crucial for proper cardiac function. Traditional methods often falter in recreating this intricate cellular environment, which hinders the seamless integration of engineered tissues with the native cardiac milieu [30,31]. Traditional methods often struggle to induce proper vascularization within engineered tissues [18,32,33]. Similarly, integrating the necessary neural innervation for proper cardiac function presents an additional challenge. The intricate interplay between the autonomic nervous system and the myocardium is crucial for physiological control [34,35]. Moreover, traditional regenerative strategies encounter difficulties in mimicking the biomechanical properties of native myocardium. Achieving optimal scaffold design and material selection to withstand the cyclic mechanical stresses remains a persistent challenge, affecting the functionality and long-term stability of engineered tissues [36,37].

The multidisciplinary field of cardiac TE integrates principles from biology, medicine, chemistry, biophysics, materials science and engineering, to develop advanced strategies for repairing or replacing damaged cardiovascular tissues [37–39]. Mechanically, TE scaffolds should possess strength and elasticity mimicking the heart muscles, providing structural support while accommodating dynamic contractions and expansions [40,41]. Additionally, biocompatibility is paramount to ensure that the scaffold does not elicit an adverse immune response, thereby promoting cellular adhesion, proper cell functions such as contractions and maturation [18,41]. Tuned biodegradability is another crucial feature; some scaffolds are designed to degrade at a rate that matches tissue regeneration, ensuring they provide temporary support without causing long-term complications or requiring removal [42]. Moreover, anisotropy, reflecting the directional dependency of mechanical properties, is essential to guide the alignment of cardiomyocytes, promoting the formation of functional and contractile tissue [43,44]. To design scaffolds approaching cardiac tissue functionalities, advanced biofabrication techniques such as 3D (bio)printing and electrospinning can be combined. The tissue engineering of cardiac tissue, with heart intricate architecture and network of vessels, along with its diverse cell types and dynamic mechanical forces, requires a level of precision typically provided by 3D (bio)printing technologies when designing 3D cardiac bioconstructs [45–47]. 3D printing enables the precise layer-by-layer deposition of materials as inks, allowing for the fabrication of intricately designed structures that mimic the complex architecture of native tissues [48,49]. In the field of cardiovascular TE, 3D printing offers remarkable control over scaffold geometry and porosity, essential factors influencing cell adhesion, proliferation, and overall tissue integration [48–50]. The ability to customize cell/biomaterial scaffolds based on patient-specific anatomical data holds great promise, paving the way for personalized regenerative therapies to more effectively enhance patient care and improve quality of life [51,52]. Moreover, 3D (bio)printing can play a crucial role in the integration of electrically conductive biomaterials into the tissue. This technological process enables the precise layering of materials, allowing for the strategic placement of electrically conductive elements and cells within the polymer-based structured scaffold. Electrically conductive materials, such as metal nanoparticles and carbon-based nanomaterials, impart a set of properties to the electroactive engineered tissues [53–55]. They enable the transmission of electrical signals, fostering synchronized cell communication and enhancing the functionality of the regenerated cardiovascular tissues [53,56]. In addition to 3D printing, electrospinning plays a pivotal role in fabricating functional fiber/hydrogels for

cardiac TE, offering a versatile and effective approach to fabricate biomimetic scaffolds with tailored properties [57–60]. Electrospinning enables the production of nanofibrous structures which can mimic the ECM fiber reinforcement [61]. Furthermore, this innovative technique allows for precise control over fiber diameter, alignment, and overall fibrous scaffold architecture, thereby facilitating the development of functional patches or implants for applications in regenerative medicine [61,62]. In tandem with these biofabrication technologies, bioactive hydrogels have emerged as a cornerstone in cardiovascular TE [63]. Hydrogels, owing to their high-water content and biocompatibility, provide an ideal environment for cell encapsulation and proliferation. The integration of bioactive components, such as growth factors, peptides, ECM-mimicking molecules, or even bioactive polymers, further enhances the regenerative potential of these hydrogels [64,65]. The bioactive functionalities contributes to create a microenvironment conducive to cellular cues, orchestrating signaling pathways that guide tissue development and maturation [66,67]. The potential synergy between advancing fabrication technology and hydrogels is highly promising [68,69].

The originality of this review lies in the thorough examination of 3D printing and electrospinning technologies for designing electroconductive biopolymer-based hydrogels for cardiac TE applications. While both fabrication techniques are mainly independently studied in this work, it also emphasizes the combined potential of these techniques to fabricate scaffolds that replicate the microstructural, functionality, including mechanical and electrical properties of native cardiac tissues. Additionally, the review highlights how incorporating electroconductive materials into biopolymer-based hydrogels enhances cell-to-cell communication and electrical coupling as well assupport cardiomyocyte maturation. The review discusses recent studies on the use of 3D printing and/or electrospinning to engineer the electroconductive hydrogels for cardiac TE. The interplay between electrical conductivity and other bioactive functionalities in electroconductive composite hydrogels is explored. The role of 3D (bio)printing and electrospinning, their advantages, limitations, and applications in designing electrically conductive biopolymer composite hydrogels is discussed, while providing insights into these biofabrication technologies. The review also highlights the electrically conductive materials and biopolymers commonly used in the design of electroactive hydrogels, focusing on their properties, characteristics, and significance.

2. Cardiac tissue architecture and electroconductive properties

The architecture of cardiac tissue is defined by a meticulously organized and interconnected network of cells that serves as the cornerstone of the heart remarkable rhythmic contractility and its crucial function in pumping blood throughout the body [70]. In terms of volume, mainly consisting of cardiomyocytes, the cardiac tissue is organized to ensure the seamless integration of electrical conduction and mechanical contraction [70,71]. The alignment of cardiomyocytes into myocardial fibers, layered in a precise pattern, facilitates synchronized contraction, optimizing the heart ability to generate the force needed for effective blood circulation [72,73].

The myocardium serves as the essential structural muscle layer of the heart, playing a crucial role in coordinating cardiac function (Fig. 1A). This cardiac muscle layer constitutes the thickest portion of the heart wall, encompassing the muscular substance responsible for the forceful contractions that propel blood throughout the circulatory system [74]. These elongated cells exhibit a remarkable degree of organization and coordination to ensure the synchronous contraction essential for efficient cardiac performance [75]. The cellular arrangement in the myocardium allows for optimal force generation while maintaining the structural integrity required to withstand the continuous mechanical demands of the cardiac cycle. Within the cardiac muscle fiber, the

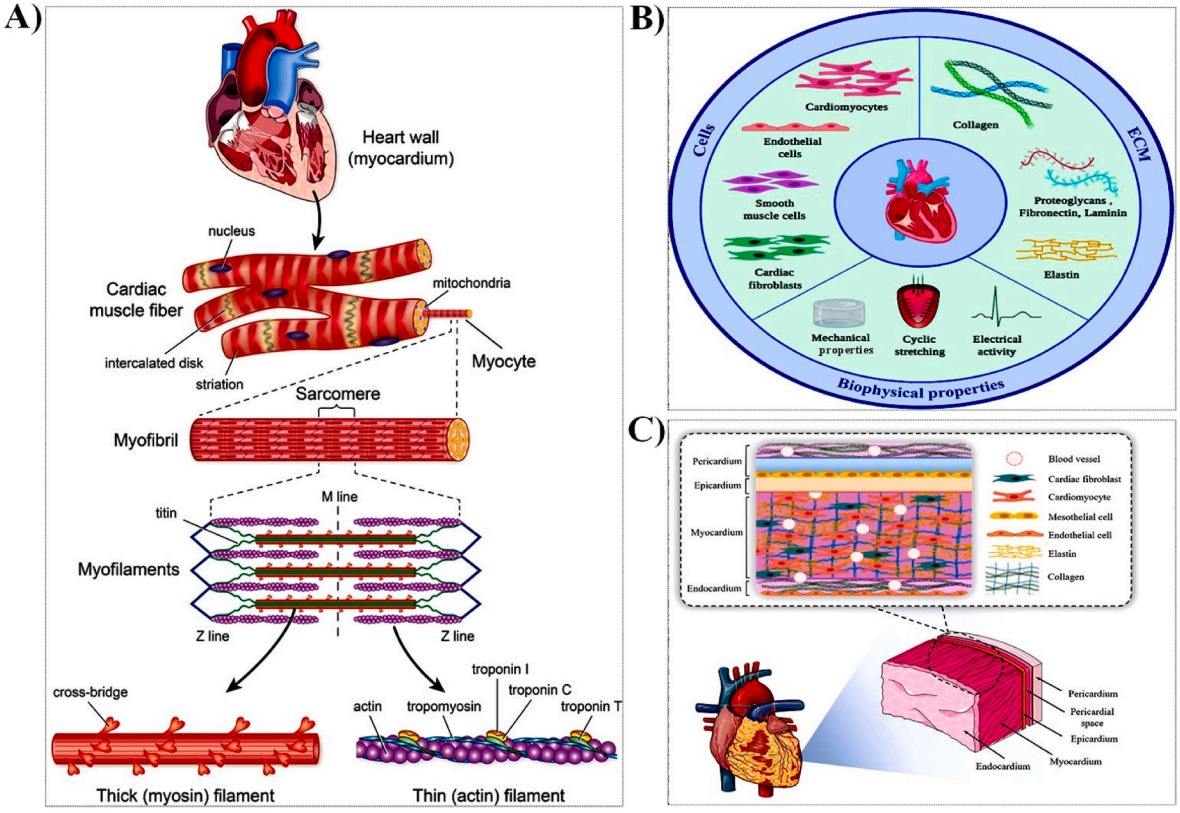

Fig. 1. (A) Structure of cardiac muscle fiber and sarcomeres—the functional units of muscle contraction. Reproduced with permission from Ref. [81] Copyright © 2014 Springer Nature. (B) Key components of the heart tissue, highlighting cardiac cells of myocardium, ECM, and biophysical properties. (C) Overview of cardiac multi-layered structure. Reproduced with permission from Ref. [76] Copyright © 2020 Frontiers.

myofibril emerges as the fundamental structural unit responsible for contractility. These thread-like structures extend longitudinally throughout the entire length of the cardiac muscle cell, housing the contractile machinery necessary for myocardial function [76,77]. The myofibril is characterized by a striated appearance, a result of the orderly arrangement of contractile proteins within its structure. Comprising the myofibril are sarcomeres, the smallest functional units of the cardiac muscle (Fig. 1A). These repeating units encapsulate the actin and myosin filaments responsible for the intricate process of muscle contraction [78]. The harmonious interplay of these contractile filaments is regulated by the controlled release of calcium ions, a process fundamental to the myocardium ability to contract rhythmically and efficiently [79]. The composition of the cardiac muscle fiber extends beyond its contractile apparatus to encompass specialized intercellular structures known as intercalated discs. These discs facilitate mechanical and electrical coupling between adjacent cardiac muscle fibers, ensuring the coordinated contraction essential for the heart pump function [75,76]. Comprising desmosomes and gap junctions, intercalated discs contribute to the myocardium unique ability to contract as a synchronized unit [80]. The intrinsic characteristics that collectively enable the heart to efficiently pump blood are contractility, elasticity, and conductivity [81]. Contractility relies on the myofibrillar machinery, while elasticity ensures the myocardium prompt recoil after contraction, allowing for optimal blood filling during the diastolic phase [82]. In addition, the conductivity of cardiac muscle fibers ensures the propagation of electrical signals, maintaining the rhythmicity and synchronization necessary for a coordinated heartbeat [26].

The various cell types of cardiac tissue contribute uniquely to the structural integrity and functional harmony of the heart (Fig. 1B) [76]. Cardiomyocytes are responsible cells for the forceful contractions that propel blood throughout the circulatory system [83]. Interspersed among them are fibroblasts, which play a crucial role in maintaining the structural framework of the heart by synthesizing and organizing the ECM [84]. The endothelial cells, which form the inner lining of blood vessels, provide a seamless microenvironment for nutrient and oxygen exchange [31]. Furthermore, smooth muscle cells, found in the walls of blood vessels, regulate vascular tone and blood flow. Moreover, the conduction system cells, including pacemaker cells, orchestrate the electrical impulses that synchronize and regulate the rhythmic contractions of the heart [85]. In addition, single-cell RNA-seq experiments revealed that around 5 % of the cells in the heart are macrophages. Furthermore, it has been shown that macrophages contribute to the electrical coupling of cardiomyocytes [86].

Beyond the singular alignment of cardiomyocytes, the parallely arranged myocardial fibers are artfully organized in distinct layers, each strategically oriented at different angles. This multi-layered architectural design serves as evidence of heart adaptability, optimizing its mechanical performance to meet the dynamic demands inherent in the rhythmic pumping of blood during each cardiac cycle [87,88]. The innermost layer, the endocardium, comprises endothelial cells lining the heart chambers, ensuring smooth blood flow (Fig. 1C). In the myocardium, the middle layer of the heart, cardiomyocytes rhythmically contract to pump blood throughout the circulatory system [76]. The epicardium, which is the outermost layer of the heart, is primarily composed of epicardial cells. These cells form a thin, protective layer that covers the surface of the heart (Fig. 1C). The ECM, rich in collagen and elastin, provides structural support and regulates heart elasticity. Additionally, blood vessels and nerves contribute to the overall complexity of cardiac tissue, forming a cohesive and dynamic structure essential for cardiac function (Fig. 1C) [76].

The ECM of cardiac tissue, which forms the structural framework of the heart (Fig. 1B), is constituted of an intricate interplay of proteins, glycoproteins, and polysaccharides. The ECM is not merely a passive scaffold but a dynamic entity that profoundly influences cellular behavior, tissue architecture, and overall cardiac function (Fig. 1B) [89]. Collagen is a key component of the cardiac ECM, forming a dense, organized matrix that provides tensile strength to the myocardium. Its fibers align in parallel with the orientation of cardiac muscle fibers, contributing to the mechanical integrity of the heart. Specifically, this collagen network not only provides tensile strength but also facilitates the transmission of mechanical signals to the cells, which is essential for proper cardiac function [54,90,91]. Elastin is another crucial protein within the cardiac ECM, imparting elasticity to cardiac tissues. This elasticity is essential for accommodating the dynamic movements of the heart, allowing it to stretch and recoil with each heartbeat. Elastin contributes to the resilience of blood vessels, heart valves, and the myocardium itself, influencing overall cardiac performance [92]. Proteoglycans, composed of a core protein and glycosaminoglycan chains, constitute a significant portion of the cardiac ECM. These molecules confer water-retaining properties to the matrix, contributing to its hydration and lubrication. This hydrated ECM facilitates nutrient exchange and serves as a reservoir for various signaling molecules, influencing cellular activities and maintaining tissue homeostasis [15,93]. Glycoproteins such as fibronectin and laminin play pivotal roles as adhesion molecules within the cardiac ECM. They establish connections between cells and the surrounding matrix, influencing crucial cellular processes such as adhesion, migration, and signaling [94]. The cardiac ECM undergoes constant remodeling, a process where cells deposit and degrade matrix components. This remodeling is essential for adapting to mechanical forces, responding to injury, and facilitating tissue regeneration. However, dysregulated ECM remodeling is implicated in various cardiovascular pathologies, including myocardial infarction and heart failure [95].

The intricacies of cardiac tissue architecture are fundamentally intertwined with its electroconductive properties, a dynamic interplay that orchestrates the synchronized contraction essential for effective cardiac function [96]. At the core of this complex system are cardiomyocytes, the specialized muscle cells of the heart, whose coordinated activity is meticulously regulated by precisely timed electrical signals. Cardiac cells communicate with remarkable precision through a complex network of intercellular connections known as gap junctions [25]. These microscopic channels facilitate direct communication between adjacent cardiomyocytes, enabling the seamless transmission of electrical signals. This interconnected web of gap junctions serves as the communication highway for rapid signal propagation, ensuring that the entire myocardium contracts and relaxes in unison [97,98]. The electroconductive nature of cardiac tissue is intricately linked to the movement of ions across cell membranes, a process governed by specialized proteins known as ion channels [99]. These channels are embedded within the cell membrane and act as gatekeepers, regulating the influx and efflux of ions such as sodium, potassium, and calcium [100,101]. The orchestrated opening and closing of these ion channels generate electrical impulses known as action potentials. As the action potential initiates in one cardiomyocyte, it rapidly propagates through the gap junctions, transmitting the electrical signal to neighboring cells [102]. This phenomenon leads to the coordinated depolarization and subsequent repolarization of each cell, creating a cascade of events that results in the rhythmic electrical activity fundamental to proper heart function. The synchronized contraction and relaxation of cardiomyocytes, driven by these precisely orchestrated electrical signals, culminate in the pumping action of the heart [102,103]. The concept of electroconductivity within cardiac tissue goes beyond being a passive attribute; instead, it represents an active and dynamic process essential for orchestrating the intricate coordination of electrical impulses, ensuring the heart's efficient and synchronized pumping. This complex interplay involving cellular communication, ion movement, and harmonized electrical activity is fundamental to cardiac physiology. It serves as the foundation for comprehending and developing interventions in the fields of cardiovascular health and regenerative medicine [104–106].

The heart as a muscular organ, relies on a precisely regulated electrical signal to coordinate the contraction and relaxation of its chambers

[25,107]. The initiation of the cardiac electrical signal occurs in the sinoatrial node, often referred to as the heart natural pacemaker. Specialized pacemaker cells generate rhythmic electrical impulses, establishing the heart baseline rate [108,109]. These impulses propagate through the atria, causing them to contract and pump blood into the ventricles. The electrical signal then encounters the atrioventricular node, where there is a momentary delay, allowing the ventricles to fill completely [110]. Subsequently, the signal travels through the His bundle and its branches, reaching the Purkinje fibers, consisting of specialized cardiomyocytes with fewer myofibrils and many mitochondria, that spread throughout the ventricles, initiating their contraction [111]. The electroconductive properties of cardiac tissue are vital for the seamless transmission of these electrical signals. This conductivity allows for the rapid and coordinated depolarization of cardiomyocyte cells [112,113]. Disruptions in the electroconductive properties can lead to a range of cardiac disorders, particularly arrhythmias. In the field of cardiovascular TE, replicating the native architecture and electroconductive features of cardiac tissue is an important goal. There is a need to fabricate engineered structures that not only mimic the structural complexity of the heart, but also possess functional electroconductive properties to facilitate proper electrical signaling [55,60,90,114,115]. To achieve this goal, scientists are actively exploring innovative approaches, including the utilization 3D (bio)printing and electrospinning techniques for fabricating functional biomimetic hydrogel scaffolds for cardiac repair [116,117]. These scaffolds often incorporate a combination of natural and synthetic materials, offering structural support and cues for cellular alignment and proliferation [49,90,118].

3. 3D printing and electrospinning technologies for fabricating functional hydrogels for cardiac tissue engineering

3.1. 3D printing

3D printing technologies such as inkjet-based printing, extrusion-based printing, stereolithography, selective laser sintering, fused deposition modeling, and laser-assisted printing, along with electrospinning technology, are commonly employed in the fabrication of hydrogels for cardiac TE [41,119]. These technologies allow the fabrication of 3D structures with precise control over spatial organization and geometric intricacies, offering the opportunity to customize hydrogel properties for biomedical applications [41,120]. Fig. 2 illustrates advanced 3D printing technologies, including laser-based stereolithography, digital light projection (DLP) systems, selective laser sintering (SLS), fused deposition modeling (FDM), inkjet-based printing, extrusion-based printing, and laser-assisted printing (LAB) for fabricating complex 3D functional structures. In the field of 3D printing, the used material used must satisfy specific criteria as apropriate viscosity, flow behavior, high resolution, precision, biocompatibility and stability of 3D printed object. The required properties of the ink differ from one technology to another, as each printing method demands distinct material behavior during deposition, gelation/solidification, or curing processes [41,48,64]. In biofabrication, in addition to the 3D printing technologies, the appropriate setup for electrospinning of nanofibers should be accordingly designed.

Stereolithography (SLA), a precise and advanced 3D printing technique, has found profound applications in the fabrication of hydrogels

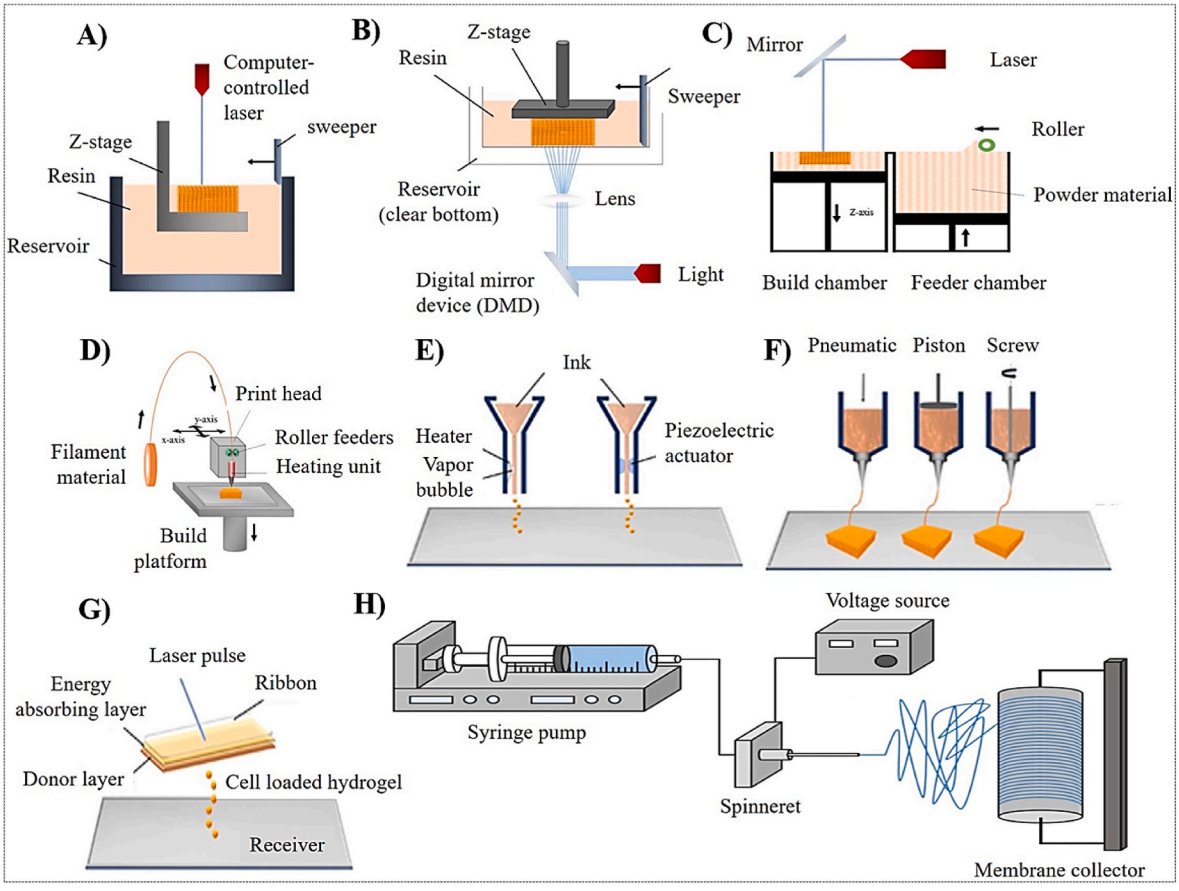

Fig. 2. 3D printing and electrospinning technologies: (A) laser-based stereolithography, (B) digital light projection (DLP), (C) selective laser sintering (SLS), (D) fused deposition modeling (FDM), (E) inkjet-based printing, (F) extrusion-based printing (EBB), (G) laser-assisted printing (LAB). Reproduced with permission from Ref. [121] Copyright © 2019 Frontiers, and (H) electrospinning setup for nanofiber fabrication. Reproduced with permission from Ref. [122] Copyright © 2018 MDPI.

for cardiovascular TE. In the SLA process, a liquid photopolymer resin is selectively exposed to a laser or ultraviolet (UV) light in a controlled pattern using a laser (Fig. 2A) or a digital light source (Fig. 2B). The photopolymerization process in SLA can potentially compromise the viability of encapsulated cells. The resin should have a carefully controlled viscosity, typically ranging from 100 to 1000 mPa s, to ensure smooth flow and consistent recoating, while preventing excessive spreading [123]. The high resolution inherent in SLA is advantageous for the replication of the complex cardiac microarchitecture. The smooth surface finish of SLA-generated constructs seems to reduce the risk of thrombosis, making them suitable for cardiovascular tissue regeneration [124,125]. Furthermore, SLA allows for the creation of bioartifitial blood vessels that closely mimic the intricate network found in the heart, fostering improved nutrient delivery and waste removal within engineered cardiac tissues [123,126,127]. The choice of suitable biocompatible materials for SLA can be limited. Cardiac TE often requires materials with specific mechanical and biological properties, and not all resins used in SLA may meet these criteria [123,128].

Selective laser sintering (SLS) is also a 3D printing technology that provides a versatile and precise approach for fabricating cardiovascular TE hydrogels [129]. In SLS, a high-powered laser selectively fuses powdered materials, typically polymers or metals, layer upon layer, based on a 3D digital model (Fig. 2C). The polymers typically used are polyamide or thermoplastic elastomers. A key requirement is the uniformity and control of the particle size distribution, ensuring that the powder maintains a consistent size within this range. This balance is essential for optimizing flowability, packing density, and sintering behavior, while also enabling high resolution in the printed layers [130,131]. Sufficient flowability is essential for consistent powder spreading and preventing recoater clogging, influenced by particle shape, size distribution, and surface treatment. efficient post-processing is reqired to remove loose powder and achieve the desired surface finish and dimensional accuracy for the final part [132–134]. A noteworthy advantage of SLS lies in its capacity to craft 3D scaffolds tailored for cardiac regeneration, featuring a precisely controlled and interconnected porous structure [135,135,136]. SLS supports a wide range of materials suitable for cardiac engineering applications [132,137]. Furthermore, SLS-produced cardiac constructs often exhibit good mechanical strength. This property is vital for maintaining structural integrity during implantation and ensuring that the construct can withstand physiological forces within the cardiovascular environment [138,139]. Yeong et al. [129] used SLS technology to fabricate a porous polycaprolactone (PCL) scaffold. The sintered PCL strut exhibited a tensile stiffness of 0.43 ± 0.15 MPa. The scaffold had a porosity of 85 %, with pores of 40–100 μm [129]. C2C12 myoblast cells were cultured on the scaffold at a high cell density of 1.2×10^6 cells/mL. Cell fusion and differentiation were confirmed by myosin heavy chain immunostaining. This study demonstrated the successful application of SLS technology for tailoring high-performance scaffolds for cardiac TE applications [129]. Moreover, SLS is amenable to scaling up production without compromising precision. This scalability is crucial for potential clinical applications, allowing the fabrication of larger constructs suitable for transplantation or other therapeutic interventions [131,140]. While SLS offers impressive resolution, it may not achieve the level of precision provided by some other 3D printing techniques. This limitation may impact the fabrication of very fine features within the cardiac constructs [141]. Proper removal of residual powder after the sintering process is important for not affecting biocompatibility, which may require additional post-processing steps to ensure the construct suitability for biological applications as well as to enhance the mechanical properties of the construct [141].

Fused deposition modeling (FDM) has emerged as a versatile 3D printing technology that involves layer-by-layer extrusion of thermoplastic filaments (Fig. 2D), with notable applications in the fabrication of TE cardiovascular constructs. In FDM, the material, typically a thermoplastic filament, must possess specific characteristics to ensure successful 3D printing and optimal performance of finished parts. A key requirement is a well-defined melting point, allowing for smooth extrusion through the heated nozzle while ensuring the filament solidifies quickly upon cooling to maintain the integrity of the printed structure [142,143]. Moreover, the extruded filament must exhibit adequate mechanical properties, such as tensile strength, impact resistance, and stiffness, to meet the functional demands of the final part. Additionally, it should have low hygroscopicity to avoid moisture absorption, which can cause problems like bubbling or weak interlayer bonding, compromising the print quality. Domínguez-Robles et al. [144] explored the use of FDM 3D printing to fabricate thermoplastic polyurethane (TPU)-based tubular cardiovascular grafts with antiplatelet properties. Dipyridamole (DIP) was incorporated into TPU filaments via hot-melt extrusion. The 3D-printed grafts exhibited sustained DIP release for 30 days [144]. The inclusion of 5 % DIP significantly reduced platelet adhesion compared to pristine TPU, while higher DIP concentrations increased surface roughness and platelet adhesion. Biocompatibility tests showed that 5 % DIP-loaded TPU promoted higher HUVEC proliferation than pristine TPU. Additionally, double-layered grafts combining DIP-loaded TPU with rifampicin-loaded TPU displayed antimicrobial activity against *Staphylococcus aureus* and *Escherichia coli* [144]. FDM accommodates a wide range of thermoplastic materials, offering researchers the flexibility to tailor constructs with diverse mechanical properties suited for cardiac applications [145]. However, achieving high resolutions with FDM can be challenging, potentially impacting the precision of intricate features within 3D fabricated constructs [146]. While the thermoplastic materials may provide suitable mechanical properties, they might lack the necessary biological properties required for cardiac tissue regeneration. Finding materials that meet both mechanical and biological criteria is crucial for successful cardiac TE [147]. Besides, the printing process, which involves high temperatures, may pose challenges for maintaining cell viability of cells embedded in the printing material [147,148].

Inkjet-based printing has emerged as a promising and high resolution 3D (bio)printing technique for fabricating hydrogels [149,150]. This technology relies on the controlled deposition of bioink droplets often containing living cells onto a substrate, offering unparalleled control over the spatial arrangement of cellular components (Fig. 2E) [41,151]. In inkjet-based printing, the properties of the ink are primarily governed by the need for high fluidity and precise droplet deposition. The ink must possess a low viscosity to facilitate smooth flow through the narrow nozzles of the printhead, preventing clogging and ensuring consistent material delivery. The viscosity of ink used in inkjet-based printing typically ranges from 3.5 to 12 mPa s [41,151]. The ink must possess a low surface tension, as this facilitates the formation of uniform and well-defined droplets upon ejection from the printhead. Cui and Boland [152] used human microvascular endothelial cells (HMVEC) and fibrin as bioinks to construct microvasculature using a drop-on-demand (inkjet printing) polymerization technique. They successfully fabricated micron-sized fibrin channels, which induced minimal cell damage [152]. When HMVECs were printed alongside fibrin, the cells aligned within the channels and proliferated to form confluent linings. The 3D tubular structures were observed in the printed patterns. The results demonstrated that the combined simultaneous printing of cells and scaffolds promoted HMVEC proliferation and microvasculature formation, highlighting a promising approach for engineering vascular tissues [152]. The precision extends to the deposition of multiple biological components, allowing for the creation of heterogeneous structures within the hydrogel constructs [151,153,154]. Inkjet-printed tissues may need time to develop the appropriate mechanical and biological characteristics, which can limit the speed at which functional tissues can be generated [151,155,156].

Extrusion-based printing involves the extrusion (pneumatic, piston, or screw-driven) of viscous inks through a nozzle and their controlled deposition, allowing for the precise layering of materials to form 3D constructs (Fig. 2F) [41,157–160]. The ability to work with different

inks of extended viscosity values, often containing living cells, enables the fabrication of constructs with cellular complexity resembling native cardiac tissues [158,161–163]. However, achieving high resolution may be constrained by the nozzle diameter, affecting the precision of 3D printed hydrogel constructs. [164,165]. Moreover, the rheological behavior of ink in extrusion-based 3D printing should be well-controlled for ensuring consistent material deposition and structural integrity. This behavior ensures that the material flows easily when subjected to the mechanical stress of extrusion, but maintains higher viscosity once deposited, preventing unwanted spreading or sagging [41,159,160,166]. The ink must possess a viscosity within a specific range, typically between 30 mPa/s and above 6×10^7 mPa s, which varies depending on the material and the intended resolution of the print [41,165]. Additionally, the shear forces experienced by cells during the extrusion process may impact cell viability, requiring careful consideration of bioink rheology and formulation [166,167]. Depending on the biomaterial used, post-printing steps such as crosslinking, may be necessary. These steps can influence the mechanical and biological properties of

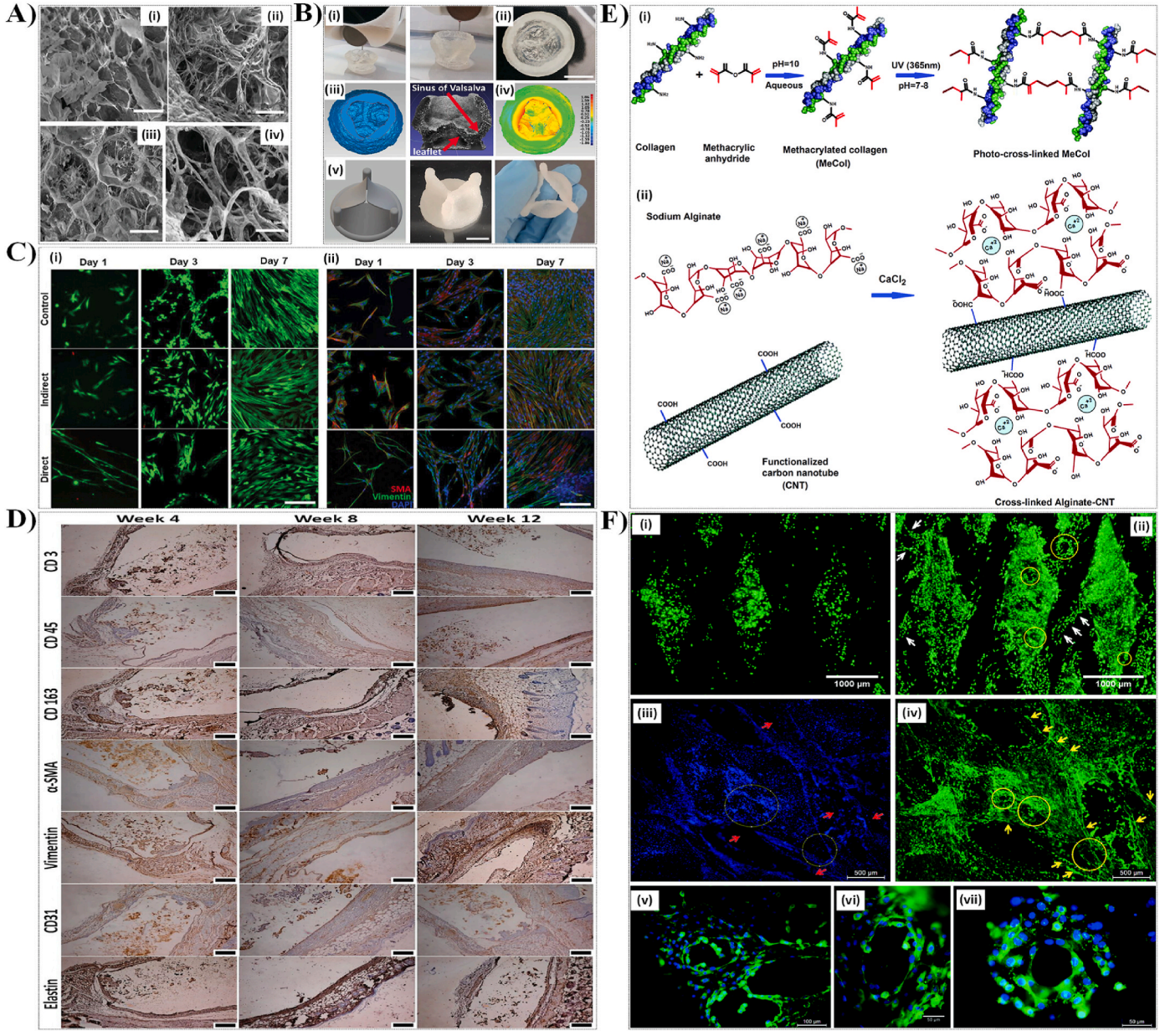

Fig. 3. (A) SEM micrographs of freeze-dried hydrogels obtained by 3D printing of tissue-engineered heart valve models by using P/G/C ink formulations containing poly(vinyl alcohol) (P), gelatin (G), and carrageenan (C): (i) P5/G2.5/C2, (ii) P5/G2.5/C2.5, (iii) P10/G2.5/C2, (iv) P10/G2.5/C2.5 (scale bar = 50 μm). (B) Development of a tri-leaflet heart valve model by 3D printing processing, showing successful printing with leaflets and sinus of Valsalva (scale bars: 1 cm). (C) In vitro assessment with: (i) Fluorescent images of porcine cardiac valve interstitial cells (PVICs) cultured on hydrogels, showing live (green) and dead (red) cells (scale bar: 200 μm). (ii) Immunofluorescent staining for Vimentin (green), α-SMA (red), and nuclei (blue) of PVICs. (D) Immunohistochemistry analysis of hydrogels implanted subcutaneously in mice, investigating immune response (CD3, CD45, CD163), cell phenotype (α-SMA, Vimentin), endothelization (CD31), and elastin deposition for P10/G2.5/C2.5 hydrogels. Reproduced with permission from Ref. [170], Copyright © 2023 WILEY-VCH Verlag GmbH & Co. KGaA, Weinheim. (E) (i) Synthetic pathway for modification of collagen into light-sensitive methacrylated collagen (MeCol), and (ii) calcium ion-induced cross-linking between alginate and carboxylated carbon ananotubes (CNTs). (F) Fluorescence images of live HCAECs stained with Calcein-AM and/or Hoechst after (i) 3 days, (ii) 7 days, and (iii, iv) 10 days of culture. Immunohistochemistry images (v–vii) show HCAEC morphology via phalloidin F-actin and DAPI staining, highlighting lumen formation in CNT-incorporated MeCol of the hybrid implant. Reproduce with permission from Ref. [161], Copyright © 2018 Mary Ann Liebert, Inc.

the printed cardiac tissue [168,169]. Microextrusion also facilitates the incorporation of bioactive agents, such as growth factors, enhancing the regenerative potential of printed biomaterials [164,165]. Extrusion-based printing remains a powerful technology for cardiac TE [170,171]. For instance, Jafari et al. [170] developed a series of inks combining poly(vinyl alcohol), gelatin, and carrageenan (P/G/C) for 3D printing tissue-engineered heart valves. These inks/hydrogels were analyzed for their physico-chemical, morphological, mechanical, and rheological properties (Fig. 3A). The microstructure and porosity of the fabricated scaffolds were crucial for performance post-implantation [170]. Specifically, an ink was successfully printed as tri-leaflet heart valves demonstrating the ability to fabricate large constructs without support materials. The printed valves maintained structural features essential for functionality, as confirmed by micro-CT (μCT) scans (Fig. 3B) [170]. Additionally, biocompatibility tests showed minimal cytotoxicity and a suitable immune response. Porcine cardiac valve interstitial cells (PVICs) cultured on hydrogels maintained high viability and proliferated, expressing relevant markers like Vimentin and alpha-smooth muscle actin (α-SMA) (Fig. 3C). In vivo implantation in subcutaneous tissue revealed favorable remodeling and integration without chronic inflammation or foreign body reactions (Fig. 3D) [170].

Biofabricating cell-supportive cardiac patches for direct implantation into myocardial infarctions offers a promising approach for repairing heart damage [161,162,172]. These patches should ideally replicate the ECM of the myocardium to ensure rapid integration with the host tissue, highlighting the need for cardiac constructs with complex characteristics. Specifically, cardiac patches must be electrically conductive, mechanically robust and elastic, biologically active, and prevascularized to effectively support tissue regeneration [161,162,172]. For instance, Esser et al. [162] developed a method to directly 3D-bioprint human induced pluripotent stem cell (hiPSC)-derived cardiomyocytes embedded in a collagen–hyaluronic acid ink, producing centimeter-sized functional cardiac tissues with ring- and ventricle-like shapes in a precise and reproducible manner [162]. The printed tissues, containing well-organized sarcomeres, displayed spontaneous and regular contractions that lasted for several months, with the ability to contract against passive resistance. Notably, the beating frequency of these tissues could be modulated through pharmacological stimulation. This technique offers new potential for creating complex, functional cardiac tissues for use in advanced drug screening and as grafts for organ repair or replacement [162]. Izadifar et al. [161] biofabricated a nanoreinforced hybrid cardiac patch loaded with human coronary artery endothelial cells (HCAECs) to improve electrical, mechanical, and biological properties for myocardial infarction repair. Methacrylated collagen (MeCol) was photo-crosslinked using safe ultraviolet (UV) exposure to create micropatterns (Fig. 3E(i)) [161]. Carboxyl-functionalized carbon nanotubes (CNTs) were incorporated into MeCol and alginate matrices, forming a nanofibrous network that significantly enhanced viscoelastic properties, electrical conductivity, and HCAEC attachment and elongation compared to pristine alginate (Fig. 3E(ii)). Using a UV-integrated 3D bioprinting, they created hybrid hydrogel constructs incorporating a CNT-infused alginate framework and cell-laden MeCol [161]. Over 10 days, HCAECs showed significant proliferation, migration, and differentiation, including lumen-like formation within the constructs. The CNT-functionalized constructs improved mechanical and electrical properties, with CNT-reinforced alginate exhibiting a nanofilamentous network that supported better cell attachment and elongation compared to pristine alginate. Fluorescence microscopy images (Fig. 3F) demonstrated that after 7 days, HCAECs proliferated and migrated from MeCol regions, forming lumen-like structures. After 10 days, elongation and interconnection of actin filaments were observed in the hybrid patch, showing effective HCAEC differentiation (Fig. 3F) [161].

Laser-assisted printing (LAP) technology, which operates on the principle of using laser energy to precisely deposit inks, onto a substrate to fabricate complex 3D structures (Fig. 2G), offers control over cell placement and the ability to fabricate constructs with biomimetic architectures [173–175]. The materials used in LAP should exhibit a high degree of optical absorbance at the laser wavelength to efficiently convert laser energy into thermal energy. This property is crucial for precise material deposition and controlled melting or sintering during the printing process [175]. Additionally, materials need to possess excellent thermal conductivity to dissipate heat uniformly and prevent thermal stresses that could lead to deformation [174–176]. The material should exhibit low thermal expansion to minimize dimensional distortions, ensuring high shape fidelity and precision in the printed object. Moreover, chemical stability and resistance to oxidation are important for maintaining the material integrity and performance over time, especially under the intense heat encountered during LAP process [174,176]. Laser-based printing technology has been successfully applied to fabricate scaffolds for cardiac TE. Gaebel et al. [173] used laser-induced-forward-transfer (LIFT) cell printing to fabricate a cardiac patch seeded with human umbilical vein endothelial cells (HUVEC) and human mesenchymal stem cells (hMSC) in a specific pattern for cardiac regeneration (Fig. 4A). cells were seeded in defined patterns on polyester urethane urea cardiac patches (Fig. 4B) [173]. Patches were cultured in vitro or transplanted into the infarcted zone of rat hearts post LAD-ligation. LIFT-derived cell seeding significantly enhanced vessel formation and improved cardiac function in infarcted hearts, demonstrating increased capillary density and integration of human cells into the murine vascular system (Fig. 4C) [173]. LAP offers distinct advantages in hydrogel production for TE. LAP excels in achieving high resolution, enabling the fabrication of complex structures that closely mimic the native architecture of cardiac tissues [173,177]. Nevertheless, the use of lasers, especially in direct laser writing process, can expose cells to potentially harmful levels of heat or radiation, impacting cell viability [41,176]. Additionally, LAP may face limitations in scalability and speed, influencing its applicability for large-scale cardiac tissue constructs [175,176].

3.2. Electrospinning

Electrospinning has emerged as a pivotal technology providing a distinctive method for crafting hydrogels tailored for cardiac TE applications [60,178]. Electrospinning is used in the fabrication of nanofibrous structures. Its principle involves the application of an electric field to a polymer solution or melt. which induces a repulsive force overcoming the surface tension of the polymer, causing a fine jet to form (Fig. 2H) [179]. The application of electrospinning for fabricating fibrous hydrogels holds several advantages [178,180]. The high surface area-to-volume ratio of electrospun nanofibers and of fibrous hydrogel hybrid materials enhances cellular interactions and nutrient exchange, promoting tissue regeneration [181,182]. Achieving 3D fibrous structures by electrospinning can be challenging, as electrospun materials typically form two-dimensional membranes. This limitation restricts the biomimicry of complex cardiac tissues with intricate 3D architectures [183]. In electrospinning, the fibrous architecture and properties can be altered by a variety of parameters in the polymer solution (e.g., molecular weight, concentration, mixture of polymers); in the operation of the apparatus (voltage, distance from needle tip to collector plane, injection flow rate, and duration); and in the setup of the collector or other processing conditions (e.g., humidity) [184].

Traditionally, post-seeding of cardiac cells onto these electrospun scaffolds after fabrication is a common approach to promote tissue formation [185,186]. However, innovative studies have introduced cell electrospinning, a technique where cells are directly incorporated into the fibers during the electrospinning process itself [187]. This approach enables the immobilization of multiple cell types within the fibers, creating complex, three-dimensional architectures that better replicate the natural ECM environment. By embedding cells directly into the fibers, this method can enhance cell survival, promote better organization, and improve overall cellular function, making it an attractive and

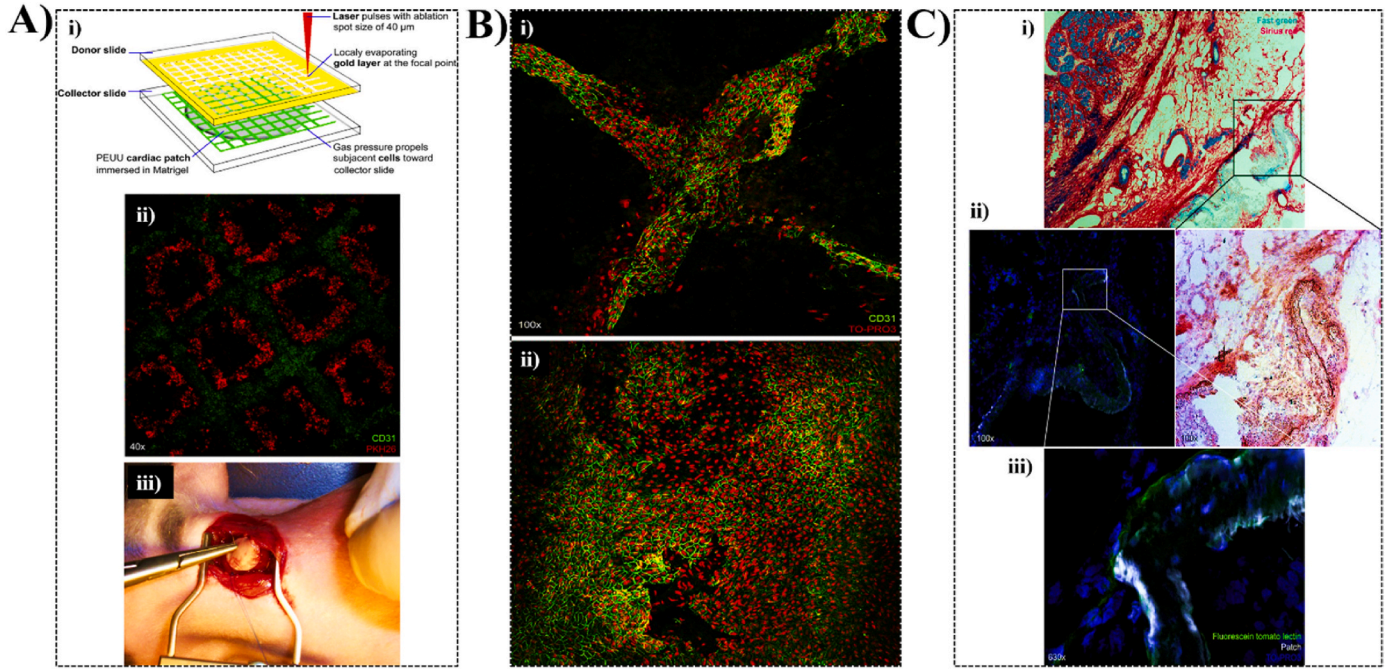

Fig. 4. (A) (i-ii) Design of a LIFT bioprinting process for cell arrangement in grid-patterned for the development of tissue engineering patches. (iii) Patch implantation in vivo onto the blanched myocardium area in rat animal models. (B) (i) Immunofluorescent micrographs of Pecam1-stained patches treated with HUVEC/hMSC co-culture, showing vessel formation in the printed pattern 8 days post-seeding. (ii) Minimal vessel formation observed on randomly seeded control matrix. (C) (i-iii) Cell infiltration in the cardiac patch, with immunofluorescence (left) and HE staining (right) after 8 weeks post-MI. Functional fluorescein tomato lectin-stained vessels are visible in the scaffold (iii, white). Reproduced with permission from Ref. [173], Copyright © 2011 Elsevier.

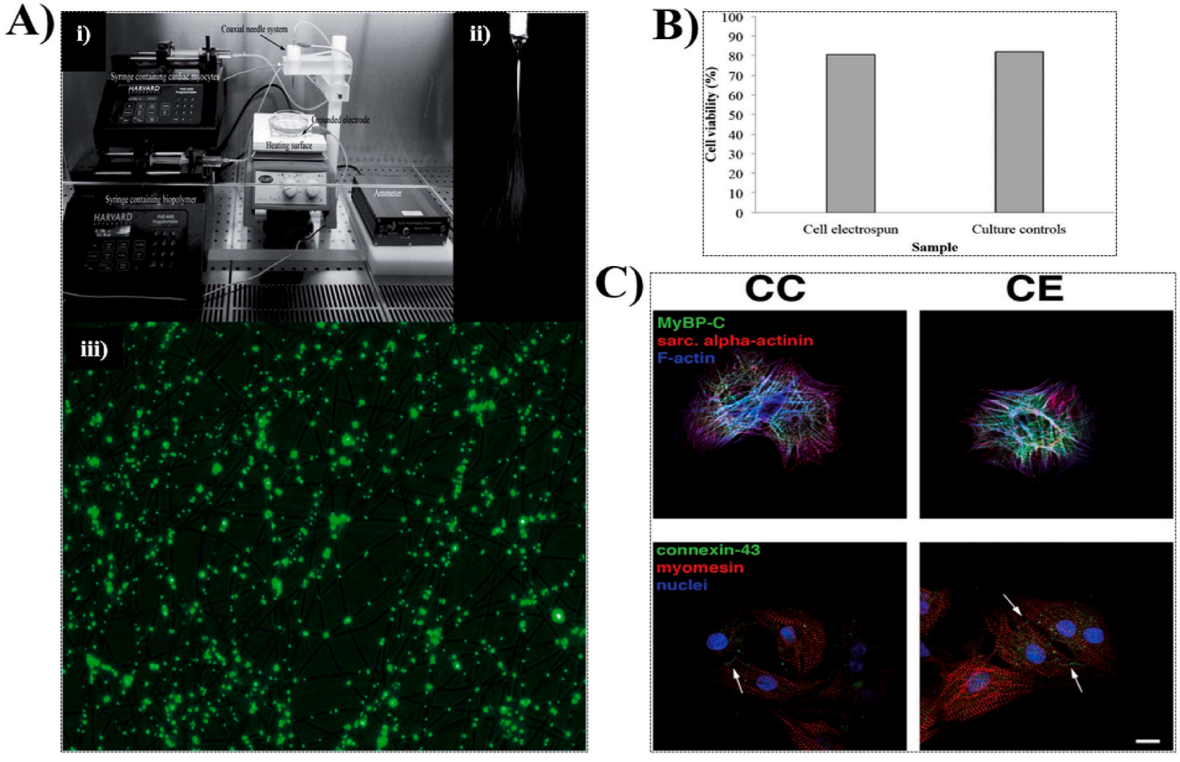

Fig. 5. (A) (i-ii) Cell electrospinning setup, with (iii) showing a fluorescent image of cardiac cell-bearing fibers/scaffolds. (B) Cellular viability in cell electrospun samples, and culture controls. (C) Confocal micrographs of neonatal rat cardiomyocytes plated with (cell electrospun cells (CE)) or without (culture controls (CC)). Staining reveals well-structured myofibrils with A-band protein MyBP-C (green, top row), Z-disc protein sarcomeric alpha-actinin (red, top row), and M-band protein myomesin (red, bottom row). Gap junctions between neighboring cardiomyocytes, indicated by Cx43 staining (green, bottom row; arrows), were evident in both groups. Scale bar: 10 μm. Reproduced with permission from Ref. [187], Copyright © 2014 Royal Society of Chemistry.

promising technique for developing functional tissues [187,188]. The integration of cells during the electrospinning process not only streamlines scaffold preparation but also potentially improves the physiological relevance and effectiveness of the engineered cardiac tissues, offering significant advancements in the field of TE and regenerative medicine [187,188]. Ehler et al. [187] demonstrated, for the first time, the ability to directly cell-electrospin primary cardiomyocytes into living fibers and scaffolds, presenting a breakthrough for developing 3D cardiac patches for tissue repair and rejuvenation. Using a coaxial needle system (Fig. 5A(i)), they successfully produced cardiomyocyte-laden fibers while maintaining cell viability (Fig. 5A (ii) and Fig. 5A(iii)). They also investigated the effects of cell electrospinning on primary cardiomyocytes to form living cardiac fibers and scaffolds [187]. They found that the electrospinning procedure did not affect cell viability or the integrity of cardiomyocytes (Fig. 5B). Staining for contractile proteins, such as sarcomeric alpha-actinin, MyBP-C, and myomesin, showed no differences between electrospun and control cells (cultured cells), indicating intact myofibrils. Additionally, gap junctions, visualized by connexin-43 (Cx43) staining, were present in both groups, suggesting electrical coupling (Fig. 5C). The study demonstrated that cell electrospinning preserved the structural and functional integrity of cardiomyocytes, opening new possibilities for creating functional 3D cardiac tissues [187].

3.3. Combining 3D printing and electrospinning technologies for cardiac tissue engineering

Nanofibrous hydrogels can be generated via various methods, such as layering, mixing of short fibers, and concurrent electrospinning and electrospraying [62,189], although this system is not widely used and has low mechanical stability compared to scaffold-based techniques. However, the methodology to make nanofibrous hydrogels is easily miniaturized and automated to produce composite structures [62]. Combining 3D printing technologies with electrospinning holds immense promise in the biofabrication of nanofibrous hydrogels for cardiac TE, offering a synergistic approach that capitalizes on the unique advantages of each technology [190]. 3D printing excels in creating complex 3D structures with high precision, enabling the recreation of intricate cardiac architectures [191,192]. Electrospinning contributes by generating nanofibrous scaffolds, introducing a level of micro and nanoscale detail that is challenging to achieve with 3D printing alone. The electrospun nanofibers provide a fibrous biomimetic environment, resembling the fiber-filled native ECM, promoting cell adhesion, proliferation, and tissue integration [192,193]. Nevertheless, when considered separately, each technique exhibits specific drawbacks. For instance, 3D printing is hindered by its low resolution, while the shape of electrospun products can remain uncontrollable, thereby restricting their application performances. Consequently, innovative approaches are emerging that integrate both 3D printing and electrospinning methods. This integration aims to harness their respective strengths and alleviate their weaknesses, resulting in an efficient and robust platform. This combined approach proves instrumental in manufacturing novel structural materials and well-organized fibrous 3D scaffolds endowed with enhanced mechano-biological properties [190,194]. Moreover, the use of both electrospinning and 3D printing technologies has led to the fabrication of anisotropic functional structures characterized by precise fiber orientation, facilitating cellular alignment in engineered scaffolds [190,195]. The heart experiences mechanical forces and electrical signaling that are directionally dependent, making fiber orientation a key factor that should be carefully controlled to restore cardiac tissue functionality. By designing anisotropic scaffolds with aligned fibers, these materials support the directional alignment of cardiomyocytes, promoting their synchronization and coordinated contraction, which is essential for efficient cardiac muscle function. In the heart, fibers are aligned in specific orientations to withstand the mechanical forces generated during each heartbeat [196,197]. Engineering anisotropic scaffolds with fibers aligned in a similar direction, provide mechanical strength and flexibility along specific axes, which is essential for replicating the heart natural behavior. This directional strength allows the scaffold to endure the tensile and compressive forces that occur during heart contraction and expansion. Additionally, the aligned fibers help distribute the mechanical load evenly, preventing deformation and enhancing the scaffold stability under the cyclic stress of heartbeats [120,198,199].

Elastomeric biodegradable poly(glycerol sebacate) (PGS):gelatin nanofibrous anisotropic scaffolds were fabricated by electrospinning [62,200]. The anisotropy capable of mimicking the left ventricular myocardial architecture which improved its functionality was demonstrated using neonatal rat cardiac fibroblast cells in PGS:gelatin scaffolds, evaluated for cell attachment, proliferation, differentiation, and contractile function of the cardiomyocytes. A study regarding nanofibers and hydrogels used the combination of both material forms in a supporting system for cardiomyocytes for cardiac TE [201]. In this study, one of six different collagen-like synthetic self-assembling nanofiber hydrogels supported the culture of both neonatal rat cardiomyocytes and human embryonic stem-cell-derived cardiomyocytes, as observed via cell attachment, growth and function [201]. Jayakumar et al. [202] generated a unique fibrous scaffold consisting of multilayers for vascular TE. The inner layer was made up of poly (lactic acid) (PLA) nanofibers, and the outer layer was composed of PCL/PLA. The multi-layers had large pores for smooth muscle cells (SMCs) penetration. The PLA fiber showed enhanced cellular functionality, and the PCL/PLA outer fiber supported SMC adhesion and proliferation [202]. Studies have demonstrated that designed tubular scaffolds can mimic the morphology of native vessels [202,203]. Several works have demonstrated several applications using fibers and stem cells, fabricated methods, and differentiation routes for heart tissue regeneration, vascular tissue regeneration [204,205]. Cardiomyogenic differentiation of human MSC seeded on scaffolds has been assessed in fibers composed of poly(L-lactic acid)-co-PCL, gelatin and VEGF. Cardiomyogenic differentiation of MSCs on the scaffolds was observed [206]. Moreover, a porous scaffold composed of multilayers with MSCs was used as a bioengineered cardiac patch in a syngeneic rat model [207].

Aligned nanofibers prepared by electrospinning technique have been increasingly investigated in cardiac TE [61,208], because the aligned structures can mimic the anisotropic structural organization of native cardiac tissue and their nano or micro-environment and excellent mechanical properties, provided the guidance cues to enhance cardiomyocyte maturation [186,209]. However, insufficient cell migration into the dense nanofibrous structures and the limited thickness of scaffolds are significant challenges in developing a well-defined scaffold that can control cardiomyocyte orientation within a 3D environment and further mimic the highly organized anisotropic structure of myocardium. This is where the combination of electrospun fibers with a highly hydrated porous support provided by hydrogels plays a crucial role in a hybrid fiber-filled biomaterial [190,197,199,210]. A 3D hybrid scaffold, composed of an aligned conductive nanofiber yarn network made of polycaprolactone, silk fibroin, and carbon nanotubes, encapsulated within a hydrogel shell, was developed to replicate the native structure of cardiac tissues. This design highlights the significant potential of electrospinning and 3D printing techniques in engineering cardiac tissue anisotropy [43]. The aligned conductive nanofiber yarn network effectively enabled control cellular orientation and promoted cardiomyocyte maturation. These 3D hybrid scaffolds, formed by embedding the aligned conductive yarn layers within the hydrogel shell, facilitated the alignment and elongation of cardiomyocytes, enhancing their maturation. Furthermore, the scaffolds supported the co-culture of cardiomyocytes and endothelial cells, providing a more complex, tissue-like environment [43]. Besides, Qiu et al. [210] investigated the construction of 3D aligned nanofiber scaffolds for cardiac TE. They introduced a trench-guided electrospinning strategy that combined electrospinning and direct ink writing to fabricate aligned nanofiber

scaffolds. Their investigation revealed that the trench width/height ratio significantly influenced nanofiber alignment, with a ratio of 1.5 achieving over 60 % alignment [210]. They successfully fabricated scaffolds with controllable porosity (60–80 %) and alignment (30–60 %). When hiPSC-derived cardiomyocytes were cultured on these scaffolds, a uniform 3D distribution of aligned cells was achieved, with a thickness of approximately 1000 μm. This study demonstrated the potential of this combined approach for efficiently constructing engineered tissues with improved structure and functionality [210].

Furthermore, the high porosity and fiber orientation in the scaffolds enable the customization of mechanical properties, promoting both cell growth and the diffusion of vital nutrients and oxygen essential for optimal tissue functionality [197,211]. The combination of 3D printing and electrospinning offers a highly precise approach for creating patient-specific cardiac patches. By integrating these advanced technologies with computational modeling and patient-specific medical imaging, it becomes possible to design and fabricate scaffolds that are precisely tailored to the anatomical and physiological needs of each patient [212,213]. Mayoral et al. [212] designed an in-vitro, patient--specific cardiac patch combining 3D printing and vascular smooth muscle cell (VSMC) differentiation. Using medical images of a 2-month--old girl with aortic arch hypoplasia, they employed computational modeling to identify the most hemodynamically efficient aortic patch for surgical repair. Hybrid FDM printing and electrospinning techniques were used to fabricate the scaffold, which was then seeded with multipotent mesenchymal stem cells (MSC) for maturation into derived VSMC (dVSMC) [212]. The graft demonstrated resistance to physiological aortic pressure (burst pressure 101 ± 15 mmHg) and featured a porosity gradient from 80 to 10 μm, facilitating cell infiltration. The bio-scaffolds exhibited good cell viability at days 4 and 12 and a functional vasoactive response to endothelin-1. The study showed that the method generated a patient-specific patch with favorable hemodynamic, mechanical, and functional properties, indicating its potential in regenerative medicine and heart disease prevention [212]. Lee et al. [213] combined 3D printing and electrospinning to fabricate artificial blood vessels from a blend of chitosan and polycaprolactone polymers. The water absorption and hydrophilicity of the composites increased as the proportion of chitosan increased [213]. The fabricated tubular scaffolds exhibited favorable surface morphology and mechanical properties, which were significantly enhanced by the addition of polycaprolactone strands printed onto the electrospun nanofiber substrate. The resulting tubular vessels demonstrated excellent mechanical properties and highlighted that this process might be useful for vascular reconstruction [213].

Recent research has explored the utilization of uniaxially aligned

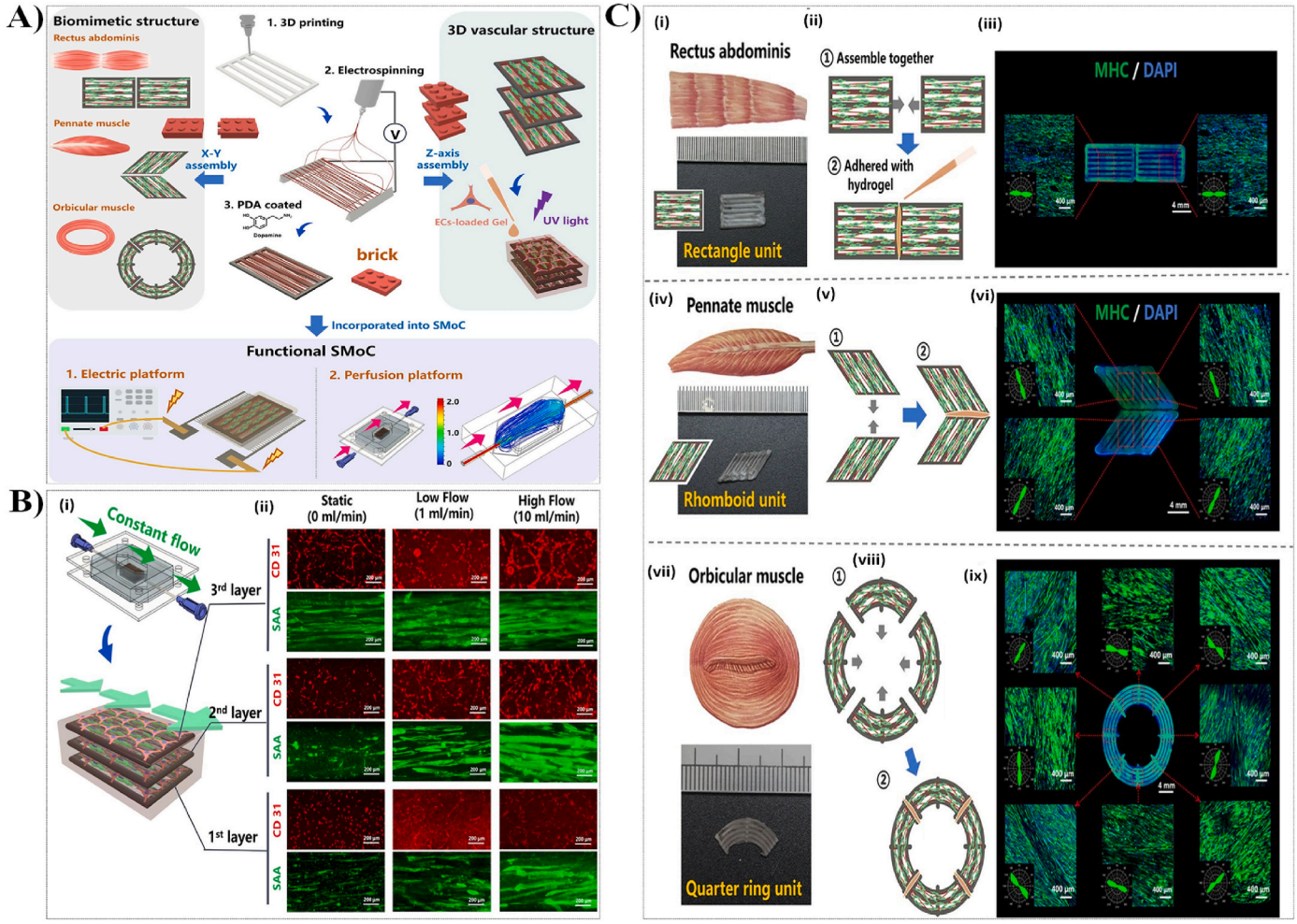

Fig. 6. (A) LEGO-like assembly of modular nanofibrous scaffold bricks developed using a 3D printing-electrospinning hybrid method, for a functional skeletal muscle-on-a-chip (SMoC) platform, with electrical and perfusion stimulation. Left: Scaffold bricks assembled in a configuration to mimic various native skeletal muscle structures: rectus abdominis, pennate, and orbicular muscle. Right: Scaffold bricks were assembled to create 3D muscle tissue with vascularization. (B) (i) Impact of fluid on 3D engineered muscle and the layered arrangement on biological properties, (ii) Fluorescence images (red = vessel, green = myotube, blue = cell nucleus) of different layers within the 3D vascular muscle under different flow rates. (C) LEGO-like assembly of modular scaffold bricks mimicking directional cell growth orientation by using the nanofibrous template: (i–iii) rectus abdominis, (iv–vi) pennate muscle, (vii–ix) orbicular muscle. Reproduced with permission from Ref. [211], Copyright © 2024 Springer.

electrospun fibers to functionalize the surfaces of 3D printed spacers, with the aim of inducing directional cell arrangements and enhancing viability in 3D cell cultures [196,214–216]. For instance, Xu et al. [217] implemented a hybrid approach involving electrospinning and inkjet bioprinting of cells. [217]. This process resulted in electrospun layers and thick layers of printed bioink. The hybrid constructs exhibited superior mechanical properties compared to printed hydrogels alone, with viable cells [217]. Wang et al. [211] developed a LEGO-like assembly strategy for fabricating complex muscle structures using combination of 3D printing and electrospinning technologies. They designed modular nanofibrous scaffold bricks with precise micro- and nanoscale structures. These bricks were assembled along the x–y axis to emulate various skeletal muscles, and along the z-axis for complex 3D structures. The bricks were joined using a photopolymerizable fibrinogen-gelatin methacryloyl hydrogel, promoting cell proliferation and migration [211]. Scaffolds mimicking rectus abdominis, bipennate, and orbicular muscles were fabricated by assembling rectangular, parallelogram, and quarter-ring bricks, respectively (Fig. 6A). Fluorescence images showed, alignment of the seeded muscle cells mimicking natural muscle structures (Fig. 6B). This method allowed for the replication of diverse muscle morphologies and facilitated vascularization within a microfluidic system (Fig. 6C). The LEGO-like approach provided a versatile strategy for constructing functional muscle tissue and organ-on-a-chip platforms for biomedical research [211].

Wu et al. [196] developed a novel method termed 3D nanofiber-assisted embedded bioprinting (3D-NFEP) that combines 3D printing and electrospinning technologies to create cardiac tissue constructs with oriented morphology. As shown in Fig. 7A, this approach used aligned nanofiber scaffolds fabricated via divergence electrospinning to provide structural support for low-viscosity bioinks, mimicking ECM environment. The aligned fibers induced cell orientation, as confirmed through immunofluorescence staining and microscopy (Fig. 7B), revealing enhanced alignment of hiPSC-derived cardiomyocytes along nanofiber directions compared to isotropic distribution on Petri dishes. Quantitative analysis further demonstrated superior alignment within a $0^\circ \pm 20^\circ$ range (Fig. 7B). Over 7 days, cells cultured in nanofiber scaffolds exhibited morphological maturation, as evidenced by organized sarcomeres and intercellular gap junctions (Fig. 7C), with improved anisotropic sarcomere length and nuclear eccentricity (Fig. 7C). These results highlighted 3D-NFEP as a promising platform for engineering structured cardiac tissues with high precision and enhanced cellular alignment. Lou et al. [216] designed multiscale hybrid patches for cardiac TE using 3D printing and electrospinning as biofabrication technologies. They compared three patch types: pure silicone and silicone-poly(lactic-co-glycolic acid) (PLGA) with random (S-PLGA-R) and aligned (S-PLGA-A) fibers. The S-PLGA-A patches were fabricated by applying a secondary electrical field to achieve fiber orientations of 95–115°, providing structural and biomechanical properties mimicking native myocardium (Fig. 7D) [216]. These patches improved cellular interaction and supported hiPSC derived cardiomyocyte growth. Cells on pure silicone patches formed irregular spheroids, while fibers on S-PLGA-R and S-PLGA-A patches promoted organized myofibrils and cell maturation (Fig. 7E). Contractility tests demonstrated that fiber alignment enhanced functional properties, with S-PLGA-A patches showing superior contractility, directional strain, and synchronization compared to S-PLGA-R (Fig. 7F) [216]. Additionally, the aligned fibers facilitated better communication between hiPSC-derived cardiomyocytes, enhancing mechanical and electrical properties of patches, and promoting maturation toward an adult-like phenotype. This was confirmed by enhanced contractility observed with digital image correlation and strain analysis, showing that aligned fibers improved maturation and synchronization of the tissue (Fig. 7F). These findings suggest that fiber alignment plays a crucial role in optimizing the mechanical and electrophysiological properties of engineered cardiac tissues, providing a promising approach for regenerative therapies in ischemic heart disease [216].

Significant advancements have been made in cardiac safety assessments for drug discovery, targeting drug-induced cardiotoxicity (DIC), a primary cause of drug attrition. Despite the increasing popularity of heart-on-a-chip (HoC) technology, challenges persist in its development due to the anisotropic structure of the native myocardium. A recent study introduced an anisotropic multiscale cardiac scaffold, fabricated through a hybrid biofabrication method that combined 3D printing with electrospinning technology (Fig. 8A) [197]. The 3D printed scaffolds were generated by varying the printing speed rates and adjusting the printing pressures. The diameters (D) of the printed parallel filaments were specified as 200, 400, and 600 μm, while the gap spaces (S) between two parallel filaments were set at 200 and 400 μm [197]. The 3D-printed micrometer-scale scaffold frames mimicked the interwoven anatomical structure of the myocardium, while a network of branched-aligned polycaprolactone/carbon nanotubes (PCL/CNT) electrospun nanofibers guided cellular arrangements. To augment the capability of these multiscale scaffolds for promoting cell adhesion and proliferation, polydopamine (PDA) was introduced as a modification on the nanofiber networks. In vitro 3D bioengineered cardiac tissues were fabricated by encapsulating three-layer multiscale scaffolds within a photocurable methacrylated gelatin (GelMA) hydrogel shell [197]. The resulting anisotropic multiscale structure enhanced cardiomyocyte maturation and synchronous beating behavior (Fig. 8B). Integrating these 3D bioengineered cardiac tissues with a self-designed microfluidic perfusion system established a 3D anisotropic HoC platform for evaluating DIC and cardioprotective efficacy, showcasing its potential as a valuable preclinical tool for testing drug efficacy and cardiotoxicity [197].

4. Biopolymer-based hydrogel materials fabrication for cardiac tissue engineering

In the aim of optimizing hydrogel performance for cardiac TE, researchers have increasingly explored the use of biopolymer-based materials to fabricate robust hydrogels. These biopolymer-based materials, sourced from natural origins, like the polysaccharides and protein-based materials, commonly inherently possess biocompatibility and bioactivity [1,218,219]. Integrating these biopolymer-based materials in hydrogel formulations enhances overall biocompatibility and functionality, bringing the hydrogel scaffolds more in line with the biological environment of the heart [49,63]. However, to emulate the electrophysiological features of cardiac tissues, these biopolymer-based materials are frequently combined with electroconductive polymers to create composite hydrogels tailored for cardiac TE [96,114,162]. Table 1 highlights various approaches and advancements in utilizing electroconductive biopolymer-based materials to that end. Those studies explore a range of electrically conductive biopolymer-based material compositions and fabrication technologies (electrospinning and 3D printing) to fabricate scaffolds that mimic properties and features of native cardiac tissues and enhance cellular interactions.

For instance, scaffolds incorporating polyaniline with poly(lactic acid) (PLA) or poly(ethylene glycol) (PEG) demonstrated electroactivity and biocompatibility, crucial for supporting cardiomyocytes and other cell types [185]. Similarly, hydrogels combining GelMA, DF-PEG, and carbon nanotubes (CNTs) showed enhanced conductivity and mechanical stability, suitable for applications in cardiac and nerve tissue regeneration [220]. Conductive polypyrrole-encapsulated silk fibroin fiber hydrogels supported cardiomyocyte functionality with optimized ratios providing sufficient conductivity for cardiac cell contraction [221]. Additionally, conductive hydrogel patches incorporating graphene oxide and mesenchymal stem cells effectively repaired myocardial infarction damage, underscoring their therapeutic potential for cardiac repair [222]. Furthermore, the fabrication of multifunctional scaffolds combining synthetic and natural polymers, including poly (glycerol sebacate)-polyurethane and gelatin with or without simvastatin, showcased improved bioactivity and mechanical properties while

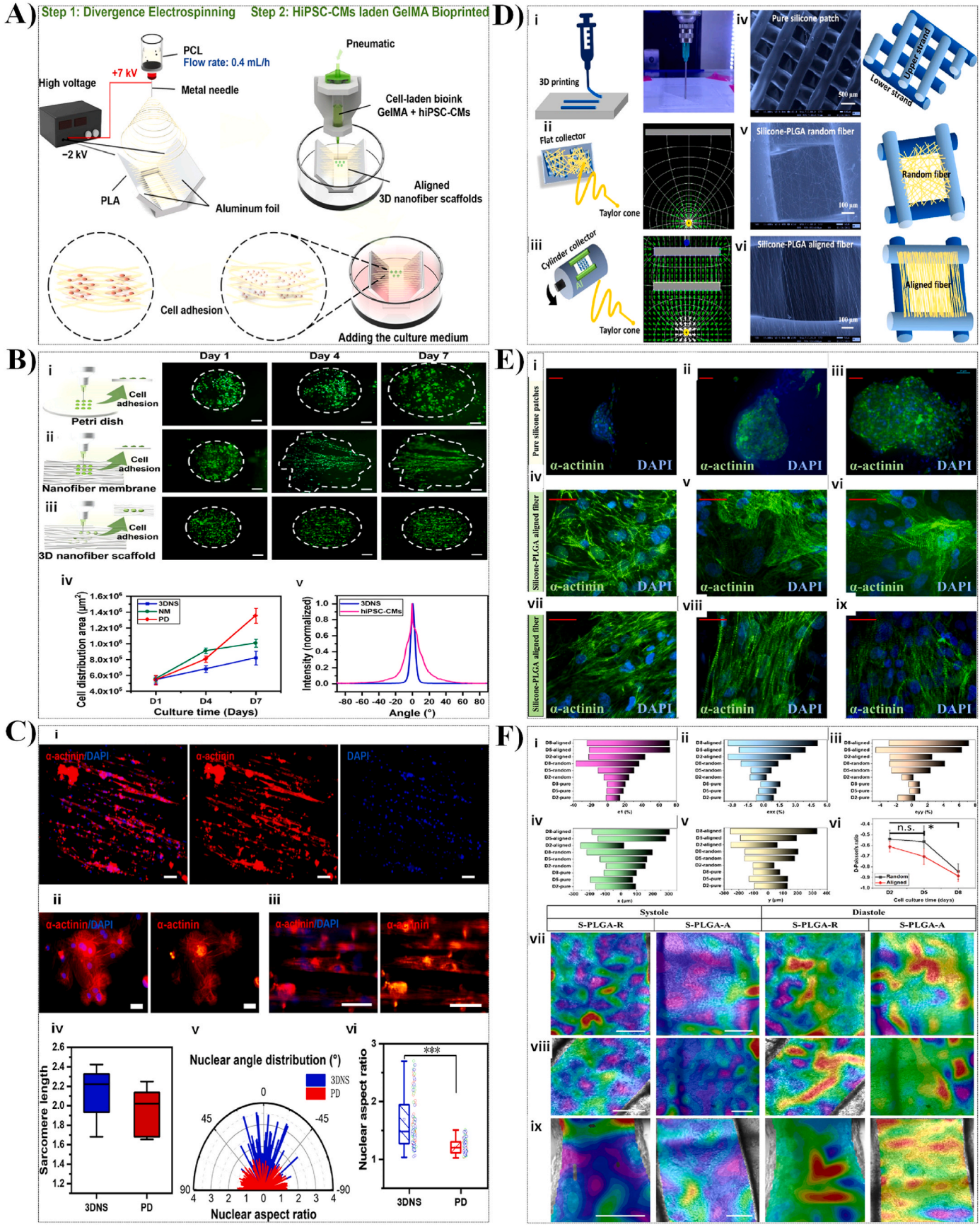

(caption on next page)

Fig. 7. (A) 3D-NFEP process for the fabrication of oriented engineered cardiac tissue. Step 1: Aligned 3D nanofiber scaffolds created through divergence electrospinning. Step 2: Controlled deposition of hiPSC-derived cardiomyocytes into the 3D nanofiber scaffolds forms an oriented cardiac tissue layer. (B) hiPSC-derived cardiomyocyte growth in 3D-NFEP. Cardiomyocyte growth at days 1, 4, and 7: (i) on Petri dishes (PD), (ii) printed on nanofiber membranes (NM), (iii) printed inside 3D nanofiber scaffolds (3DNS) (scale bar = 200 μm), (iv) Distribution area of the three cell groups measured during incubation, (v) Comparison of 3DNS and cardiomyocyte alignment. (C) (i-iii), Immunofluorescence staining and cell morphology analysis of hiPSC-derived cardiomyocytes printed in 3D nanofiber scaffolds (i, scale bar = 100 μm; iii, scale bar = 50 μm), in comparison to 2D culture directly on Petri dish (ii, scale bar = 100 μm). (iv) Comparison of cardiomyocyte sarcomere lengths on 3D nanofiber scaffolds and Petri dishes at day 7 (n = 3, **P < 0.005). (v) Distribution of nuclear shape and orientation. vi) Nuclear aspect ratio (n = 3, ***P < 0.001). Reproduced with permission from Ref. [196] Copyright © 2024, American Chemical Society. (D) (i,ii) Fibrous-layered patches obtained by 3D printing of silicone-poly(lactic-co-glycolic acid) (PLGA) (S-PLGA) with random (R) or aligned (A) fibers, with simulated electrical charge distribution. (iii) Schematic of aligned fiber layer formation on a 3D printed silicone patch (S-PLGA-A) using a cylinder drum and static electric field aluminum enhancers with simulated electrical charge distribution. (iv) 3D printed pure silicone patch. (v) Silicone–PLGA random fiber patch. (vi) Silicone–PLGA aligned fiber patch. (E) Confocal images and sarcomere structure of the cellular 3D-printed patches. Cellular pure silicone patches (i-iii), silicone–PLGA random fiber (S-PLGA-R) patches (iv-vi), silicone–PLGA aligned fiber (S-PLGA-A) patches (vii-ix), at days 2, 5, and 8, respectively. Scale bar = 25 μm. Immunofluorescence confocal images of α-actinin (green) and hiPSC-CM nuclei (blue). (F) Spontaneously beating dynamics of cellular patches. Average minimum (systole) to maximum (diastole) mechanical range of (i) major principal strain, (ii) strain in the x direction, (iii) strain in the y direction, (iv) x-direction displacement, (v) y-direction displacement, (vi) D-Poisson's ratio. (vii-ix) Time-dependent full-field major principal strain, color maps for systole and diastole phases of silicone–PLGA random (S-PLGA-R) and aligned (S-PLGA-A) fiber patches at days 2, 5 and 8. Scale bar = 150 μm. Reproduced with permission from Ref. [216] Copyright © 2024, American Chemical Society.

highlighting their utility as drug release carriers in cardiac TE [223]. Moreover, innovative approaches highlighted the fabrication of layered cardiac patches using brown adipose-derived stem cells and electrospun nanofibers containing multi-walled carbon nanotubes. These patches accelerated angiogenesis and reduced inflammation in myocardial infarction models, emphasizing their pivotal role in cardiac remodeling [224]. Electrospun polycaprolactone/gold nanoparticles composite scaffolds coated with gelatin/spironolactone exhibited interconnected porous structures and controlled drug release profiles, promoting cell attachment and viability, thus positioning them as viable candidates for myocardial TE applications [225]. In examining Table 1, several important aspects emerge from the diverse studies on electroconductive biopolymer-based materials for cardiac TE. First, the choice of cells used varied widely, from cardiomyocytes derived from both postnatal rats [60] and hiPSCs [60] to MSCs [226], fibroblasts [185,227], cardiomyoblasts [223], endothelial cells [228] and specific cell lines like H9c2 myoblasts [225]. Each cell type influenced scaffold function differently, impacting their suitability for cardiac tissue regeneration. Cardiomyocytes are fundamental as they are the contractile cells responsible for generating the force needed for cardiac contraction. Their integration into engineered tissues is essential for mimicking the beating function of the heart [60]. MSCs contribute significantly to cardiac repair and regeneration by secreting paracrine factors that promote tissue healing and modulate inflammation. They can differentiate into various cell types further supporting tissue remodeling and vascularization [226]. Fibroblasts play an important role in the structural integrity of cardiac tissues by producing ECM proteins such as collagen and elastin. Their presence helps maintain tissue architecture and mechanical strength [185,227]. Cardiomyoblasts are precursor muscle cells capable of differentiating into cardiomyocytes, the contractile cells of the heart. They are widely used in research to explore heart development, disease mechanisms, and regenerative strategies. A notable example is the H9c2 cell line, derived from rat heart tissue, which serves as a valuable model in cardiac studies [223,229,230]. H9c2 myoblasts served as a model for studying cardiac cell behavior, testing drug responses, and optimizing TE protocols [225]. However, it is important to note that H9c2 cells are not contractile, but they are proliferative and can exhibit characteristics of skeletal muscle under specific conditions, such as differentiation into multinucleated myotubes [229,231]. Endothelial cells are essential for forming new blood vessels in the engineered tissue. They ensure proper vascularization, which is crucial for providing oxygen and nutrients to the regenerating cardiac tissue and removing metabolic waste, thereby supporting cell survival and function [173,228]. In addition, biofabrication technologies like electrospinning have facilitated the design of fibrous scaffolds with tailored fiber diameters and enhanced mechanical properties [60,221,226], while 3D bioprinting has enabled the precise placement of cells in hydrogels, crucial for mimicking native tissue architecture [222,228]. Moreover, hydrogel compositions can significantly vary, allowing the integration of various biopolymer-based materials, electroconductive components and cells. Their formulation has been tailored to improve scaffold biocompatibility, mechanical strength and electrical conductivity, crucial for supporting cardiac tissue function [220,225–227].

The subsequent sections delve into various biopolymers and biopolymer-based materials commonly used in fabricating hydrogels for cardiac TE. Table 2 provides details on several biopolymers, their sources, chemical compositions, and properties, highlighting their scientific and practical significance. Chitosan, mainly derived from crustacean shells and fungal cell walls, is flexible, hydrogel-forming, antimicrobial and bioactive, suitable for wound healing due to its self-healing properties [160,232]. Alginate, obtained from brown seaweeds, forms hydrogels with divalent cations and is widely used in TE due to its water solubility and biocompatibility [233,234]. Hyaluronic acid, naturally present in connective tissues, retains water and lubricates joints, making it ideal for preparation of hydrogels which have found applications for example in cosmetics and biomedicine [235,236]. Cellulose present in plant cell walls, is the most abundant biopolymer in Earth, which exhibits high tensile strength and has been increasingly used in medical applications despite its water insolubility [40]. Carrageenan and pectin, derived from red seaweeds and plant cell walls respectively, form gels and are used in food, biomedicine and pharmaceutical industry due to their biocompatibility and biodegradability [237–239]. Besides, proteins such as collagen, gelatin, fibrin, elastin, silk fibroin form TE biomaterials with appropriate tunable mechanical properties and biocompatibility. Collagen, with high tensile strength and flexibility, constitute the ECM in tissues together with other biomolecules [240]; while gelatin, derived from collagen, is used in biomedicine and pharmaceuticals due to its gel-like consistency [220,241]. Fibrin forms stable clots and is crucial in wound healing [242], elastin provides tissue elasticity [243,244], and silk fibroin offers biocompatibility as well as high flexibility and toughness [245].

4.1. Polysaccharide-based materials for cardiac tissue engineering

The use of polysaccharides in hydrogel preparation has become a central focus in cardiac TE [271]. This trend is propelled by their outstanding attributes, including inherent biocompatibility, biodegradability, and adept mimicry of the native ECM [160,272]. Polysaccharides closely emulate the ECM composition and architecture enhancing cellular adhesion, proliferation, and differentiation. Polysaccharides such as chitosan, cellulose, pectin and dextran are biomaterials that not only offer structural support but also establish a bioactive microenvironment for cellular interactions [41,273]. Their biocompatibility ensures minimal adverse reactions in physiological contexts, while biodegradability permits controlled degradation over

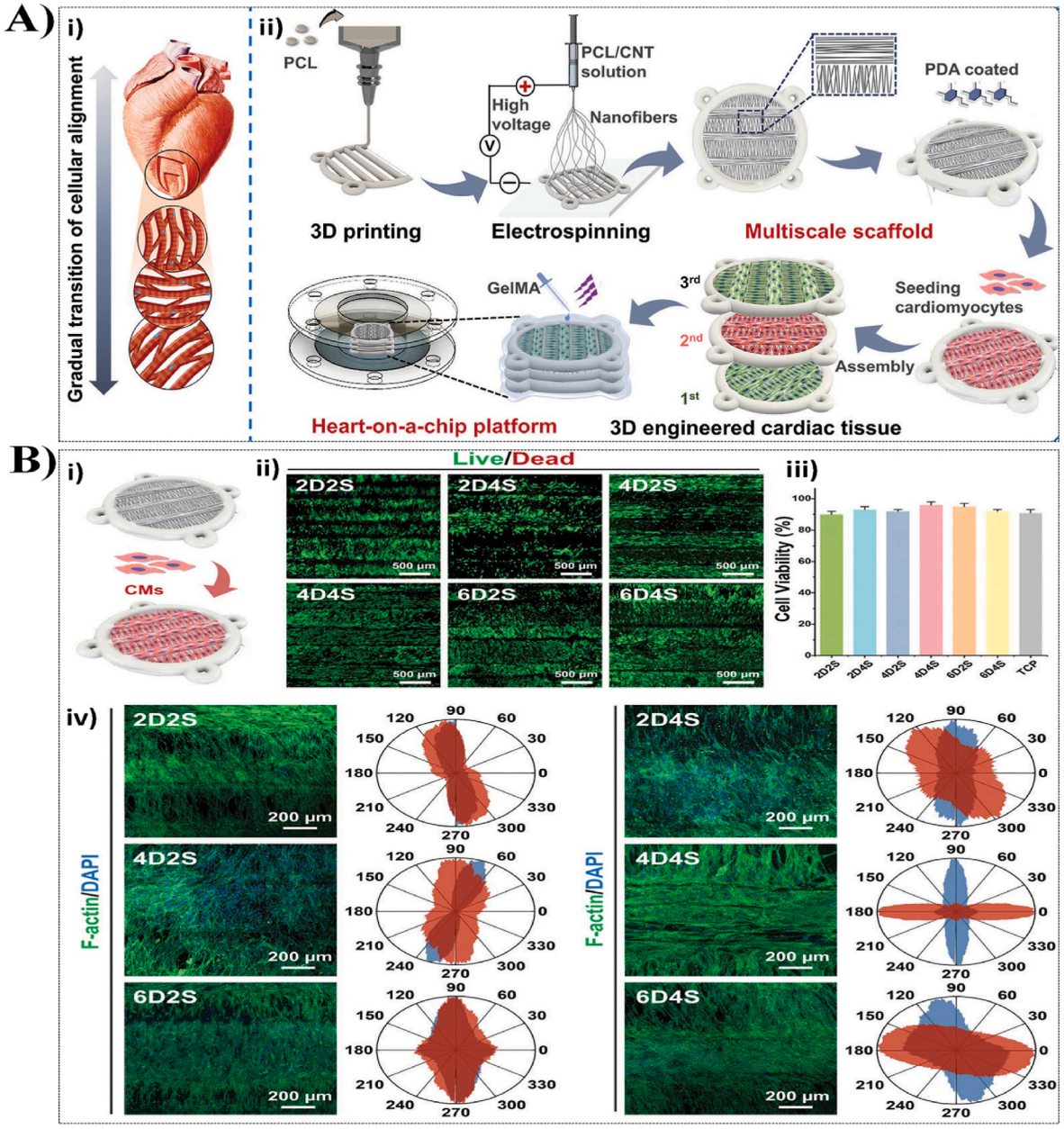

Fig. 8. (A) Scaffold design and fabrication to replicate the native cardiac tissue structure. (i) Schematic illustrating a gradual transition of aligned cell layers with an interwoven structure from the endocardium to the epicardium. (ii) Fabrication of multiscale anisotropic scaffolds using integrated 3D printing and electrospinning techniques, further combining the engineered cardiac tissue with a microfluidic chip to create a heart-on-a-chip platform for drug research. (B) Culture of cardiomyocyteson multiscale scaffolds with varying diameters and spaces. (i) Schematic depiction of cardiomyocytes seeded on multiscale scaffolds. (ii) Live/Dead images demonstrating normal cardiomyocyte growth on multiscale scaffolds. (iii) Evaluation of cardiomyocyte viability percentages on multiscale scaffolds. (iv) Confocal images of cardiomyocytes on multiscale scaffolds, stained with F-actin (green) and DAPI (blue) after 5 days of cultivation. Quantitative analysis of cellular orientation distribution indicates alignment with the direction of branched-aligned nanofibers. Reproduced with permission from Ref. [197], Copyright © 2023 WILEY-VCH Verlag GmbH & Co. KGaA, Weinheim.

time, aligning with the dynamic nature of tissue regeneration processes [159,254]. As a result, they are components of great interest in tailoring functional hydrogels for cardiac TE [248,273].

Polysaccharides are essential in the development of hydrogels for TE due to their biocompatibility, biodegradability, and water retention capabilities, which help create a hydrated environment that supports cell survival and tissue growth [40,41,159,160,248]. These polysaccharides form networks that trap significant amounts of water, maintaining the moisture necessary for cellular functions and offering a customizable matrix for various biomedical applications, such as drug delivery and wound healing [40,41]. However, several polysaccharides like alginate lack natural cell recognition sites, such as the RGD (arginyl-glycyl-aspartic acid) motif, which are crucial for cell adhesion. As a result, cells often do not attach strongly to these materials, leading to improper cellular interactions [274,275]. Besides the RGD sequence, other recognition sites commonly grafted to alginate for cell adhesion include peptides containing the IKVAV (isoleucine-lysine-valine-alanine-valine) sequence and peptides containing the YIGSR (tyrosine-isoleucine-glycine-serine-arginine) sequence [276,277]. These sequences are recognized by specific cell surface receptors, promoting cell attachment and spreading [276,277]. To address this limitation, researchers commonly modify these hydrogels by

Table 1
Overview of several research studies on 3D printed and electrospun electroactive biopolymer-based materials for cardiac TE.

Hydrogel compositions	Cell used	Biofabrication technology	Main features	Ref.
Collagen/hyaluronic acid/polyaniline	Postnatal rat cardiomyocytes; Human-induced pluripotent stem cell–derived cardiomyocytes	Electrospinning	• Electrospun fiber mats with polyaniline, collagen, and hyaluronic acid were assessed for cardiomyocyte compatibility. • Collagen fiber mats exhibited a wide range of fiber diameters after crosslinking, from ≈300 nm to ≈5 μm. • All other fiber mats had fiber diameters ranging from ≈120 to ≈300 nm. • Fiber mats demonstrated comparable electrical conductivity and superior mechanical properties to native myocardium. • Fiber mats containing collagen, hyaluronic acid, and polyaniline showed optimal properties for cardiac TE.	[60]
Polyaniline (PANi) doped with dodecylbenzenesulfonic acid (DBSA) combined with poly(lactic acid) (PLA) and PLA/poly(ethylene glycol) (PEG) mixtures	Fibroblasts; Epithelial cells; Cardiomyocytes	Electrospinning	• Electroactive and biocompatible fibrous scaffolds were prepared using PANi/DBSA combined with PLA and PLA/PEG. • Simple and core-shell fibers were obtained via uniaxial and coaxial electrospinning, confirmed by spectroscopic analyses. • PEG enhanced PLA and PANi chain packing, influencing fiber thickness regulation and electrical properties. • Cell studies showed reduced cytotoxicity with PANi/PLA fibers due to favorable PANi···PLA interactions, suitable for cardiac TE.	[185]
Chitosan (CS)/polyvinyl alcohol (PVA)/poly(3,4-ethylenedioxythiophene) polystyrene sulfonate (PEDOT:PSS)	Mesenchymal stem cells	Electrospinning	• CS/PVA scaffolds containing poly(3,4-ethylenedioxythiophene):polystyrene sulfonate (PEDOT:PSS) were fabricated for cardiac TE. • The addition of PEDOT:PSS significantly enhanced scaffold mechanical properties and electrical conductivity. • Cell viability and biocompatibility were improved with PEDOT:PSS incorporation. • Results suggested potential use of these scaffolds in cardiac TE applications.	[226]
Hydrogels composed of methacrylated gelatin (GelMA)/dibenzaldehyde-terminated telechelic polyethylene glycol (DF-PEG)/carbon nanotubes (CNTs)	Mouse embryo osteoblast precursor cells	3D printing	• Gelatin was used in 3D printing due to its bioactivity and RGD sequences promoting cell growth. • A 3D printed hydrogel was prepared via a two-step cross-linking of GelMA and DF-PEG. • GelMA was UV-cured during 3D printing, enhancing the structure mechanical strength and stability. • CNTs in GelMA/DF-PEG hydrogel increased conductivity, with optimal composition being 30 % GelMA and 25 % DF-PEG. • G30D25-CNTs hydrogel with 4 % CNTs showed suitable conductivity and properties for cardiac and nerve TE.	[220]
Conductive polypyrrole-encapsulated silk fibroin fiber hydrogels	Neonatal rat cardiomyocytes; Human-induced pluripotent stem cell-derived cardiomyocytes	Electrospinning	• Polypyrrole (PPy) improved engineered cardiac tissue functionality when blended with silk fibroin (SF). • PPy-encapsulated SF nanofibers were electrospun with various SF concentrations and PPy-to-SF ratios. • PPy reduced fiber diameter, mimicking myocardium fibrils, with 7 % SF matching myocardium mechanical properties. • A PPy-to-SF ratio of 15:85 provided sufficient conductivity for cardiomyocytes (CMs). • PPy-encapsulated SF mats supported CM contraction, with 30:70 ratio showing strongest contractions in human-derived CMs.	[221]
Conductive hydrogel patch made of fibrinogen scaffolds and mesenchymal stem cells (MSCs) combined with graphene oxide (GO) flakes (MSC@GO)	Cardiomyocytes, Human umbilical cord mesenchymal stem cells	3D bioprinting	• Conductive hydrogel patches, incorporating MSCs and graphene oxide (GO), repaired myocardial infarction (MI) damage effectively. • The MSC@GO hydrogel patch adhered to the epicardium, integrating electrically and mechanically with infarcted hearts. • GO flakes in the hydrogel protected MSCs from apoptosis, crucial for enhancing MI repair.	[222]

(*continued on next page*)

Table 1 (*continued*)

Hydrogel compositions	Cell used	Biofabrication technology	Main features	Ref.
			• In a mouse MI model, MSC@GO patches reduced cardiomyocyte apoptosis and increased Cx43 expression. • The study highlighted the hydrogel potential as a robust therapy for cardiac repair post-MI.	
Four different types of multifunctional scaffolds, including synthetic-based poly (glycerol sebacate)-polyurethane (PGU), PGU-Soy scaffold, and a series of trilayer scaffolds containing two outer layers of PGU-Soy and a middle (inner) layer of gelatin (G) as a natural and biodegradable macromolecule without simvastatin (S) and with simvastatin (GS), an anti-inflammatory agent, were fabricated	Cardiomyoblasts	Electrospinning	• Multifunctional scaffolds were electrospun using synthetic (PGU) and natural (gelatin, Soy) polymers. • Incorporation of simvastatin enhanced bioactivity and promoted cardiomyoblast attachment and growth. • Nanofibrous scaffolds showed uniform morphology with fiber diameters ranging from 361 nm to 417 nm. • Soybean oil improved electrical conductivity; scaffolds exhibited delayed blood clotting indicating anticoagulant properties. • PGU-Soy/GS scaffold demonstrated superior cytocompatibility and potential as a drug release carrier in cardiac TE.	[223]
Nanofibrillated cellulose/single-walled carbon nanotube ink 3-dimensionally printed in conductive patterns onto bacterial nanocellulose were developed.	–	3D printing	• Carbon nanotube patches printed on bacterial nanocellulose were electrically conductive, flexible, and stretchable. • The patches were applied to canine epicardium post-surgery, showing improved cardiac conduction during pacing. • Surgical disruption initially caused conduction impairment, which was restored with the patch application. • This study highlights the potential of 3D-printed nanotube patches for enhancing cardiac conduction post-surgery.	[246]
Carbon nanotubes (CNTs)/polycaprolactone (PCL)/gelatin scaffolds	NIH 3T3 murine fibroblasts	Electrospinning	• CNTs were incorporated into PCL and gelatin scaffolds using novel electrospinning methods: "sandwich" (sCNT) and dual deposition (DD CNT). • DD CNT scaffolds contained higher CNT quantities compared to sCNT scaffolds. • Electrical conductance increased with CNT inclusion: 0.54 ± 0.10 kS (sCNT) and 5.22 ± 0.49 kS (DD CNT) parallel to CNT arrays. • Orthogonal to CNT arrays, conductance was 0.25 ± 0.003 kS (sCNT) and 2.85 ± 1.12 kS (DD CNT). • CNT incorporation increased fiber diameter, pore size, and promoted cellular migration into scaffolds. • CNTs decreased scaffold degradation rate, increased hydrophobicity, Young's modulus, and failure load. • Murine fibroblasts showed high cytocompatibility on CNT-incorporated scaffolds for 30 days, suggesting suitability for cardiac and neural TE.	[227]
Alginate/graphene oxide (GO)/poly(ε-caprolactone) (PCL) conductive scaffolds	Cardiac progenitor cells	Electrospinning	• Tri-layered alginate-GO/PCL conductive scaffolds were fabricated using a sequential electrospinning method. • The middle PCL layer provided mechanical support for the scaffold. • Top and bottom alginate-GO layers ensured cell viability, attachment, and electroconductivity. • Scaffold electroconductivity reached 7.29 ± 0.91 μS with 1 wt% GO in alginate layers. • Tensile strength and Young's modulus of alginate-0.5 wt% GO/PCL scaffold were 22.46 ± 0.07 MPa and 4.35 ± 0.56 MPa. • GO in alginate nanofibers improved cell viability, adhesion, and proliferation for cardiac tissue regeneration.	[247]
Hydrogels were composed of GelMA (gelatin methacryloyl) and fibrin	• Human pluripotent stem cells induced cardiomyocytes (iPSC-CM) • Human umbilical vein endothelial cells (HUVEC)	3D bioprinting	• Bioinks included GelMA/fibrin hydrogel, iPSC-CM, and HUVEC for bioprinting engineered cardiac tissues (ECTs). • Electrical stimulation (ES) promoted elongation, migration, and interconnection of HUVECs in ECTs.	[228]

(*continued on next page*)

Table 1 (*continued*)

Hydrogel compositions	Cell used	Biofabrication technology	Main features	Ref.
Polycaprolactone/gold nanoparticles (PCL/GNPs) 3D composite coated with gelatin/spironolactone (GEL/SPL)	Myoblasts (H9c2) cell line	3D printing using the fused deposition modeling (FDM)	• ES increased the expression of genes related to HUVECs in engineered cardiac tissues. • ES enhanced secretion of signaling factors between cardiomyocytes and HUVECs. • ES improved vascularization and contractility in ECTs, aiding clinical transplantation applications. • PCL/GNPs 3D scaffolds were 3D printed using FDM and coated with GEL/SPL. • The microstructural observation of the scaffolds revealed interconnected pores with 150–300 μm in diameter. • 3D scaffolds degraded significantly in stimulated body fluid (SBF) after 28 days, with maximum rate for GEL-coated scaffolds. • SPL release from GEL coating balanced after 14 days, demonstrating controlled drug delivery systems. • GNPs addition enhanced H9c2 cell proliferation; GEL/SPL coating improved cell attachment and viability. • Findings suggested 3D PCL/GNPs scaffolds coated with GEL/SPL were suitable for myocardial TE.	[225]

incorporating bioactive molecules or peptides or by combining polysaccharides with other natural and synthetic polymers to fabricate robust and functional hydrogels that promote cell adhesion [276–279]. Functionalizing polysaccharides with these recognition sites enables the hydrogels to better mimic the natural ECM, thereby creating a more conducive environment for tissue regeneration and repair [276,277].

4.1.1. Chitosan

Chitosan (CHI), a natural polysaccharide, stands out as a versatile and extensively used polymer in hydrogel formulations. It possesses a myriad of properties that make it exceptionally well-suited for creating hydrogels tailored to meet the intricate demands of cardiac tissue [160,256,280]. Chitosan is a polysaccharide derived from chitin, a major component mainly found in the exoskeletons of crustaceans such as shrimps, crabs, and lobsters. It is a linear polysaccharide composed of β-(1 → 4)-linked D-glucosamine and N-acetyl-D-glucosamine units [249,281,282]. In weakly acidic aqueous media, CHI undergoes protonation of amino groups (-NH_2) to form positively charged ammonium groups (-NH_3^+) [160]. Chitosan-based hydrogels have shown potential in cardiac TE [182,250,251,283], but they face several challenges, particularly regarding their mechanical properties. These hydrogels often have lower mechanical strength compared to other materials, limiting their ability to provide adequate support and durability in the heart dynamic environment. Additionally, their elasticity is often insufficient to mimic the natural flexibility of cardiac tissue, which is essential for proper heart function [284,285].

Several noteworthy research studies highlighted the application of biofabrication technologies such as electrospinning and 3D printing in the fabrication of chitosan-based hydrogels for cardiac tissue regeneration [182,283,286]. For example, varying weight percentages of conductive electrospun polypyrrole (PPy) nanofibers (5–25 %) in combination with chitosan, collagen, and polyethylene oxide were developed to expedite tissue healing [287]. Increasing PPy content in developed composites reduced fiber diameter, and at 10 %, it achieved optimal conductivity (164.274 × 10^{-3} S/m), falling within the semi-conductive to conductive polymer range. MTT assay (3-(4, 5-dimethylthiazol-2-yl)-2,5-diphenyl tetrazolium bromide (MTT) assay) and SEM analyses revealed superior cell adhesion and proliferation at that 10 % PPy content, making these nanofiber scaffolds particularly suitable for regenerating electrically active tissues like cardiovascular, heart muscles, or nerve tissues [287]. In another work, patterned membranes composed of chitosan-gelatin-guar gum were fabricated using 3D printing, resulting in significantly enhanced elasticity and tensile resistance [288]. A numerical model was developed to predict the elasticity of membranes with specific internal patterns, allowing for the modeling of complex membranes with tunable elastic properties matching myocardium anisotropy [288]. The study also involved evaluating the developed membrane ability to withstand cyclic fatigue tests, requiring potential adjustments to the model for viscoelasticity, considering heartbeat rates [288]. In the pursuit of addressing global heart failure stemming from myocardial infarction, a range of electrospun polyurethane/chitosan/carbon nanotubes composite nanofibrous scaffolds, exhibiting both random and aligned orientations, were crafted to emulate the ECM structure [182]. Comprehensive characterizations highlighted their electroconductivity and biocompatibility with H9c2 cells. The aligned nanofibers demonstrated particular promise as nanoscale scaffolds for regenerating infarcted myocardium [182].

To optimize the performance of cardiac cells, various methodologies are employed, with electrical stimulation being a prominent technique aimed at bolstering their functionality and fostering tissue maturation [25]. This approach involves applying controlled electrical impulses to the cells, which is designed to mimic natural physiological conditions and encourage the cells to develop and function more effectively [25,228]. By simulating the electrical signals that cells would typically experience in the heart, researchers aim to enhance the maturity and functionality of cardiac tissues, potentially advancing therapeutic strategies for heart disease and other cardiac-related conditions [289–291]. Abedi et al. [289] combined chitosan (CHI)-based electrically conductive scaffolds, small molecules (SMs), electrical stimulation (ES), and stem cells in cardiac TE applications (Fig. 9A). Electrospun composite scaffolds made of CHI and polyvinyl alcohol (PVA) with multiwall carbon nanotubes (MWCNTs) were fabricated. Fig. 9B highlights the SEM images of the electrospun composites obtained. The optimal MWCNT concentration was determined to be 2 % w/w, which reduced the average fiber diameter from 225 nm to 110 nm, increased electrical conductivity from 8 × 10^{-5} S/m to 9 × 10^{-3} S/m, and tripled tensile strength [289]. Using a 10-day differentiation protocol with SMs and ES, unrestricted somatic stem cells (USSCs) were differentiated into cardiomyocytes. Scaffold + SM + ES showed significant overexpression of cardiac-associated genes troponin I, CX43, and β-MHC, increasing by

Table 2
Overview of features and properties of polysaccharides and proteins highlighted in this review.

Polymers	Sources	Chemical Composition	Physical Properties	Solubility	Biocompatibility	Mechanical Properties	Biodegradability	Ref.
Polysaccharides								
Chitosan	Mainly derived from crustaceans (e.g., shrimp shells) and squids.	Composed of glucosamine and N-acetylglucosamine units.	Film-forming, and antimicrobial property. Forms hydrogels for wound healing; Self-healing property	Soluble in acidic solutions (pH < 6.5). Insoluble at neutral pH.	Generally well-tolerated in vivo, it is used in wound healing and TE.	Varies depending on degree of deacetylation and cross-linking density. Can form hydrogels.	Biodegrades due to enzymatic action.	[159,160, 248–253]
Alginate	Derived from brown seaweeds (e.g., kelp).	Composed of linear chains of guluronic acid (G) and mannuronic acid (M) units.	Forms hydrogels in the presence of divalent cations (e.g., Ca^{2+}, Mg^{2+}, Sr^{2+}, Ba^{2+})	Soluble in water. Its solubility is influenced by factors such as pH, temperature, and ionic strength.	Generally biocompatible. Used in wound dressings and TE.	Varies depending on alginate source and composition. Can be stiff or flexible.	Biodegrades in natural environments through microbial action.	[32,214, 254]
Hyaluronic Acid	Naturally present in connective tissues, synovial fluid, and skin.	Consists of repeating disaccharide units (glucuronic acid and N-acetylglucosamine).	High-water retention capacity. Lubricates joints and maintains skin hydration.	Soluble in water. Forms viscous solutions.	Highly biocompatible. Used in cosmetics, joint injections, and wound healing.	Provides elasticity and cushioning. Found in skin and cartilage.	Biodegrades slowly due to its large molecular size.	[235,236, 241,255]
Cellulose	Abundant in plant cell walls (e.g., wood, cotton).	Composed of linear chains of glucose units linked by β-1,4 glycosidic bonds.	High tensile strength. Insoluble in water.	Insoluble in water. Swells in some solvents.	Generally biocompatible. Used in wound dressings, drug delivery, and scaffolds.	Strong and stiff. Used in paper, textiles, and medical applications.	Biodegrades slowly in natural environments due to crystalline structure.	[40, 256–260]
Carrageenan	Extracted from red seaweeds (e.g., Irish moss).	Composed of repeating galactose units (κ-carrageenan, ι-carrageenan, λ-carrageenan).	Forms gels in the presence of potassium ions.	Soluble in water. Forms viscous solutions.	Generally safe for consumption. Used as a food thickener and in pharmaceuticals.	Varies based on carrageenan type. Can be flexible or rigid.	Biodegrades in natural environments through microbial action.	[170,261, 262]
Pectin	Found in plant cell walls (e.g., citrus fruits, apples).	Composed of galacturonic acid units. Forms a branched structure.	Forms gels in the presence of calcium ions.	Soluble in water. Forms viscous solutions.	Generally safe for consumption. Used in food industry (jams, jellies) and drug delivery.	Varies based on degree of methylation and amidation. Can form gels.	Biodegrades in natural environments through microbial action.	[237,239, 263]
Proteins								
Collagen	Found in skin, tendons, bones, and connective tissues of animals (especially mammals).	Triple helix of polypeptide chains, composed of repeating amino acid sequences (Gly-Pro-X); Rich in glycine, proline, and hydroxyproline; Forms fibrils	High tensile strength, flexibility, and resilience; Forms the ECM in tissues	Insoluble in water and organic solvents	Biocompatible, widely used in medical applications (e.g., sutures, wound dressings)	Provides structural support and elasticity; Resists deformation under stress	Slowly biodegradable, broken down by enzymes (collagenases) in the body	[240,264, 265]
Gelatin	Derived from denaturation of collagen through hydrolysis.	Composed of amino acids (Gly, Pro, X); Forms gel-like structures when hydrated. Chemical structure similar to collagen but less ordered	Gel-like consistency, used in food (jellies, gummies) and pharmaceuticals (capsules)	Soluble in hot water, forms gels upon cooling	Biocompatible, used in drug delivery and TE	Varies based on gelatin type (e.g., bloom strength); Forms soft, elastic gels	Biodegradable, enzymatically broken down by proteases in the body	[220,266, 267]
Fibrin	Forms during blood clotting (from fibrinogen)	Fibrinogen molecules polymerize into fibrin fibers. Composed of fibrinogen subunits (α, β, γ chains); Forms a mesh-like network in blood clots	Forms stable clots to stop bleeding; Used in wound healing and TE	Insoluble in water, forms fibrin strands during clotting	Biocompatible, promotes wound healing and tissue regeneration	Provides mechanical stability to clots; Resists shear forces and maintains integrity	Biodegradable, broken down by plasmin into soluble fragments	[242, 268]
Elastin	Found in elastic tissues (e.g., skin, blood vessels, lungs).	Composed of hydrophobic amino acids (glycine, proline, valine); Rich in desmosine and isodesmosine	High elasticity and resilience; Allows tissues to stretch and recoil	Insoluble in water and organic solvents	Biocompatible, provides elasticity to tissues (e.g., skin, lungs)	Highly elastic, can be stretched up to 150 % of its original length; Recovers its shape after deformation	Slowly biodegradable, broken down by elastases and other enzymes in the body	[92,243, 244,269]

(*continued on next page*)

Table 2 (*continued*)

Polymers	Sources	Chemical Composition	Physical Properties	Solubility	Biocompatibility	Mechanical Properties	Biodegradability	Ref.
Silk fibroin	Derived from silkworm cocoons	Composed of amino acids (glycine, alanine, serine); Forms silk fibers with high tensile strength; Antiparallel β-sheet structure	Strong, lightweight, and biocompatible; Used in sutures, textiles, and TE	fibrin is hydrophobic and quite insoluble, not only through specific cross-binding, but through physical acid-base and Lifshitz-van der Waals attraction	Biocompatible, supports cell adhesion and growth in TE	High tensile strength, similar to steel; Flexible and resilient	Biodegradable, enzymatically broken down by proteases and other enzymes (sericinase) in the body	[221,245, 270]

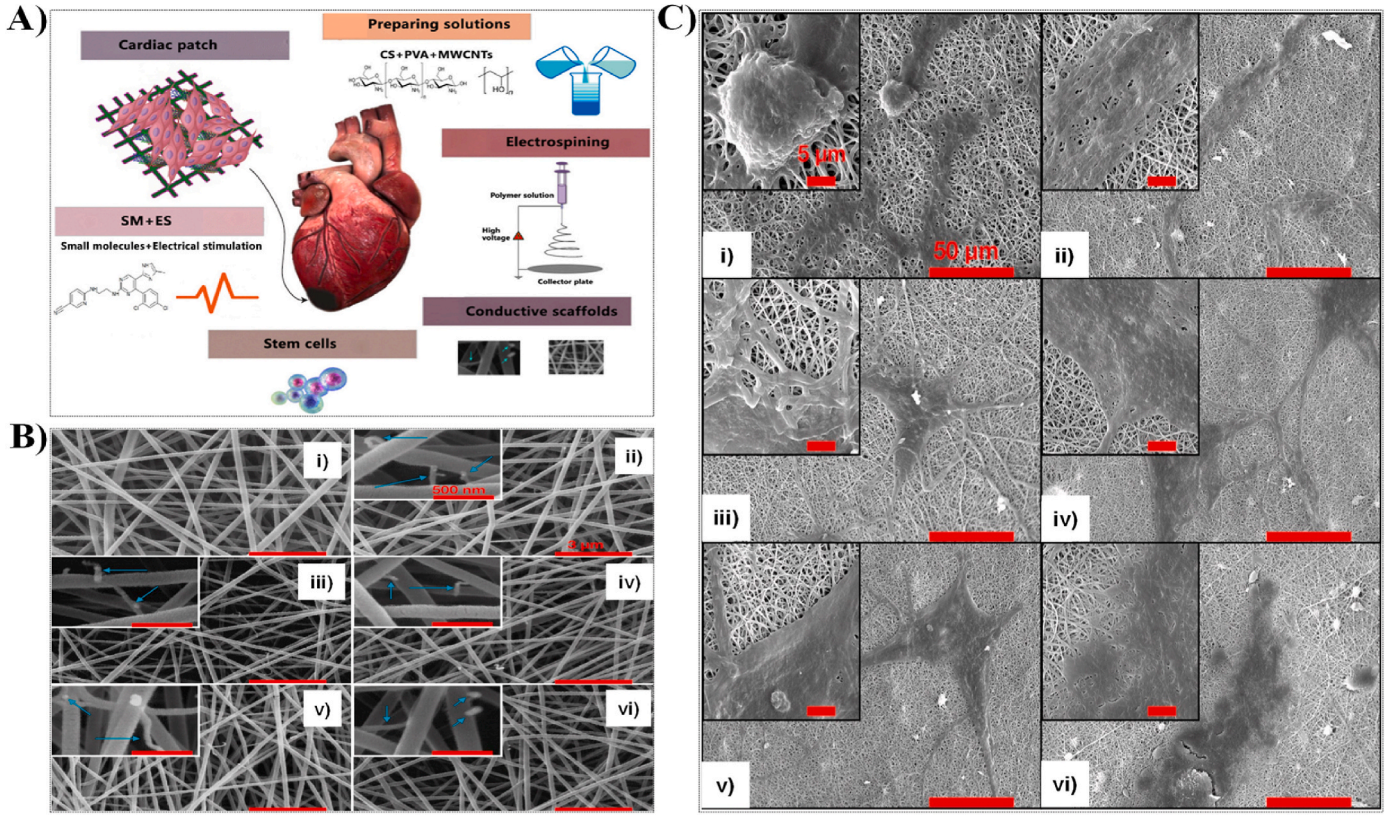

Fig. 9. (A) Schematic representation of the synergistic application of conductive polymeric CHI/PVA/MWCNTs nanofibers, intracellular signaling modulators, and electrical stimulation for enhanced cardiac TE. (B) SEM images showing fabricated scaffolds: (i) CHI/PVA, (ii) CHI/PVA/MWCNT (0.5), (iii) CHI/PVA/MWCNT (1), (iv) CHI/PVA/MWCNT (1.5), (v) CHI/PVA/MWCNT (2), and (vi) CHI/PVA/MWCNT (2.5). Scale bars for large and small images are 3 µm and 500 nm, respectively. MWCNTs are indicated with arrows in the small images (insets). Increasing MWCNT concentration resulted in decreased fiber diameter, as previously noted. (C) SEM images depicting cell attachment after 24 h of seeding on fabricated scaffolds: (i) CHI/PVA, (ii) CHI/PVA/MWCNT (0.5), (iii) CHI/PVA/MWCNT (1), (iv) CHI/PVA/MWCNT (1.5), (v) CHI/PVA/MWCNT (2), and (vi) CHI/PVA/MWCNT (2.5). Scale bars for large and small images are 50 µm and 5 µm, respectively. Reproduced with permission from Ref. [289] Copyright © 2021 Elsevier.

172, 5.3, and 64 times, respectively. Cells were cultured on fabricated scaffolds to assess the impact of the physical and chemical properties of these latter on cell viability and proliferation [289]. By the first day of culture, CHI/PVA samples showed more cells than MWCNT-containing samples. MWCNT scaffolds, with smaller fiber diameters, higher surface area, and electrical conductivity, facilitated cell signaling and promoted cellular extensions. SEM imaging of cell attachment on fabricated scaffolds showed cells on CHI/PVA/MWCNT forming polygonal shapes with extensions, while CHI/PVA samples showed limited cell extension growth (Fig. 9C). These findings highlighted the importance of integrating multiple additives and stimuli to achieve cardiac tissue functionality in TE biomaterials [289].

Chitosan also exhibits inherent antimicrobial properties. This attribute can arise from its cationic charge, which can disrupt microbial cell membranes, leading to the inhibition of bacterial and fungal growth [292]. Furthermore, chitosan-based hydrogels can interfere with microbial metabolism by binding to DNA, inhibiting replication and transcription [293]. The hydrogels can also create a barrier effect, physically trapping bacteria and limiting their proliferation within the hydrogel matrix [292,293]. In the context of cardiac TE, where preventing infections is of paramount importance, CHI antimicrobial characteristics contribute to the overall safety and efficacy of hydrogel-based therapeutic interventions. Chitosan has improved the engraftment and survival of cells, thereby contributing to the process of

myocardial repair [286,294]. Additionally, CHI mechanical properties can be tailored to suit the specific requirements of cardiac tissue. Through adjustments in processing methods, crosslinking, and blending with other polymers, the mechanical strength of CHI-based hydrogels can be finely tuned. This is crucial for mimicking the mechanical properties of biomaterials, ensuring optimal support for cell growth and tissue regeneration [295,296]. Almasi-Jaf et al. [297] developed mechanically reinforced CHI-based grafts that successfully supported growth and proliferation of cardiac cells. A heparinized bilayer graft was developed, comprising an inner layer of heparinized polycaprolactone, polyurethane and gelatin co-electrospun, and an outer layer of chitosan, gelatin, and silk fibroin freeze-dried hydrogel [297]. The graft exhibited high ultimate stress (4.16 ± 0.25 MPa), Young's modulus (8.24 ± 2.59 MPa), and suture retention (4.83 ± 0.31 N). Heparin release from developed grafts was sustained at approximately 70 % over 4 weeks. The heparinized samples showed suitable anti-thrombogenic properties in platelet adhesion assays. The outer hydrogel layer, crosslinked with non-toxic materials, achieved high porosity (64.63 %), suitable for smooth muscle cell activity. Both layers supported high cell viability, with endothelial cells at 78.96 % and smooth muscle cells at 57.77 % [297].

4.1.2. Alginate

Alginate (Alg), a polysaccharide derived from brown seaweed, plays a pivotal role in hydrogel formulations tailored for cardiac TE. This natural polymer, characterized by its biocompatibility and hydrophilic nature, is frequently used to construct hydrogel matrices for cardiac TE, either in combination with other polymeric materials or by functionalizing it with bioactive molecules [278,279,298]. Alginate is composed of linear chains of (1–4)-linked β-D-mannuronic acid (M) and α-L-guluronic acid (G) residues [254,299]. The ratio of M to G units, as well as the distribution along the alginate chains, influences its physical and chemical properties [299]. One of Alg distinctive features is its ionogelation, a property that significantly influences its use in hydrogel fabrication. Alginate undergoes gelation when exposed to divalent cations, with Ca^{2+} ions being the most commonly employed [299,300]. While Alg possesses several advantageous properties for certain applications in cardiac TE such as biocompatibility and ease of gelation, its mechanical properties may need enhancement for cardiac TE applications. Alg hydrogels are known for their relatively low stiffness and lack of contractility, which are important considerations when aiming to replicate the dynamic and contractile nature of heart tissues [298,301,302]. To address these limitations, researchers often modify Alg or combine it with other materials to improve its mechanical properties. Common strategies include reinforcing Alg with nanomaterials, other polymers, including natural ones like proteins. These modifications aim to increase the overall stiffness, strength and elasticity of the Alg-based hydrogels [303,304].

3D printing and electrospinning technologies have become potent technology for producing Alg-based hydrogels [247,279]. Each year, numerous aortic valve replacements are required for valve diseases, prompting the pursuit of TE heart valves with remodeling capabilities [234]. Despite challenges in replicating the intricate 3D anatomy, Rioux et al. [234] introduced a novel technique for swift fabrication of tricuspid aortic valve scaffolds using Alg-based hydrogels. This method involved injecting a Alg hydrogel into a mold crafted by a custom-made sugar glass 3D printer, followed by dissolution of the mold using a custom-made dissolving module [234]. Tested in a cardiac bioreactor mimicking physiological conditions, the scaffolds demonstrated functional repeatability, establishing the potential for swift fabrication of cell-seeded Alg scaffolds for heart valve TE [234]. In another study, cardiac constructs with a unique angular structure mimicking cardiac architecture were developed using 3D printing with alginate (Alg) and gelatin (Gel) composites. Various composite ratios were examined for cytotoxicity and printability, with the optimal combinations (Alg2Gel1 and Alg3Gel1) chosen [279]. The 3D-printed structures were characterized, revealing that Alg3Gel1 exhibited higher elastic modulus, lower swelling, and less mass loss compared to Alg2Gel1. Cell viability studies demonstrated that the 3D constructs with the angular design maintained significantly more viable cells, exceeding 99 % viability for both H9c2 and HUVECs cells. This approach showcased the potential of 3D-printed Alg-Gel composites for cardiac TE [279]. Electrospinning technology was also employed to design Alg based hybrid hydrogels. In a sequential electrospinning method, tri-layered electrospun Alg–-graphene oxide (GO)/poly(ε-caprolactone) (PCL) conductive scaffolds were developed, simulating the cardiac ECM. The middle PCL layer provided mechanical support, while the top and bottom Alg–GO layers offered cell viability, attachment, and electroconductivity [247]. The scaffolds exhibited GO presence and Alg nanofiber crosslinking. Incorporating 1 wt% GO, the electroconductivity reached 7.29 ± 0.91 μS. Mechanical properties of the scaffold, with Alg–0.5 wt% GO/PCL, demonstrated ultimate tensile strength and Young's modulus of 22.46 ± 0.07 and 4.35 ± 0.56 MPa, respectively [247]. Despite accelerated degradation in PBS solution, the scaffolds enhanced cardiac progenitor cell viability, adhesion, and proliferation. These tri-layered electroconductive Alg–PCL nanofibrous scaffolds have shown promise for cardiac TE [247]. However, H9c2-based studies are limited in their significance for cardiac TE. H9c2 cells lack the spontaneous contractile properties typical of primary cardiomyocytes. While they exhibit some cardiac-like features and are commonly used as a model for cardiac research, they do not possess the ion channel activity or sarcomeric organization required for spontaneous contraction. As a result, they are less suitable for investigating contractile functions in cardiac TE [229–231].

4.1.3. Hyaluronic acid

Hyaluronic acid (HA), a glycosaminoglycan (GAG) inherent in the ECM, emerges as an interesting material in the design of hydrogels for cardiac TE [305]. Composed of repeating disaccharide units of glucuronic acid and N-acetylglucosamine, HA forms a linear and non-sulfated GAG polymer. Its high biocompatibility and water-binding capacity contribute to its prominence in hydrogel formulations [306]. Its high water retention capacity enables it to maintain tissue hydration and elasticity. HA plays a vital role in wound healing, cell adhesion and proliferation due to its interactions with cell surface receptors like CD44 [307]. It exhibits low immunogenicity and can be chemically modified for enhanced stability or functionality in applications such as drug delivery, TE and cosmetic formulations. This biopolymer brings a unique set of attributes, orchestrating essential cell signaling events [235,305]. It can be sourced from various biological origins or produced through microbial fermentation [236]. HA-based hydrogels exhibit an exceptional water-retaining capacity, creating an environment akin to the physiological conditions within the cardiac tissue [308]. The interactions between HA and cell surface receptors, such as CD44, initiate signaling cascades that influence cell behavior [309,310].

HA is usually blended with other components to fabricate composite hydrogels using 3D printing technologies [241,311]. HA alone lacks the mechanical strength and bioactivity to mimic the cardiac ECM. When combined with other biomaterials or synthetic polymers, HA-based hydrogels can better support cell growth, provide structural integrity, and promote tissue regeneration, offering tunable properties like elasticity, mechanical strength, and biocompatibility essential for cardiac repair [241,305,311]. For example, a 3D-printed patch, consisting of cardiac progenitor cells embedded in a hyaluronic acid/gelatin (HA/gel) matrix was evaluated for therapeutic potential, which demonstrated enhanced cardiac cell therapy. The 3D printed HA/Gel biocomplex loaded with hCMPCs maintained the cell viability, proliferation and differentiation capabilities [311]. Transplanting the 3D printed biocomplex into a mouse model of myocardial infarction resulted in a significant reduction in adverse remodeling, preservation of cardiac function, and sustained in vivo survival and engraftment of hCMPCs. This study underscored the effectiveness of this translational approach

in improving the delivery and impact of hCMPCs in cardiac tissues [311]. Bioinks were developed utilizing decellularized human heart ECM (dhECM) incorporating gelatin methacryloyl (GelMA) or GelMA-methacrylated hyaluronic acid (MeHA) hydrogels, dual cross-linked with UV light and microbial transglutaminase (mTGase). The resulting composite GelMA–MeHA–dhECM hydrogels exhibited significantly enhanced mechanical properties compared to GelMA–dhECM hydrogels [312]. These hydrogels exhibited biocompatibility with human induced pluripotent stem cell-derived cardiomyocytes and human cardiac fibroblasts. They facilitated the creation of tissue-like constructs with precise control over mechanical properties, cellular content, and macromolecular composition, demonstrating their potential for modeling myocardial infarct boundaries in vitro [312].

4.1.4. Dextran

Dextran, a polysaccharide derived from glucose linked by α-1,6 glycosidic bonds, has also gained prominence in TE hydrogel formulations [272]. The innate biocompatibility of dextran ensures minimal adverse reactions when introduced into biological systems [313]. Banerjee et al. [314] developed dextran-derived hydrogels as a chemically-defined matrix for in vitro cardiac TE. Hydrogels were fabricated in situ using hydrazone crosslinking, with material properties adjusted by varying dextran derivatization and molecular weight [314]. To enhance bioactivity of hydrogels, cyclic pentapeptide RGD was added to dextran. Blends of modified dextran and human collagen combined with iPSC-derived cardiomyocytes and fibroblasts, supported tissue formation and functional maturation, demonstrating the potential of hydrogels for cardiac grafts [314]. Moreover, dextran-based hydrogels exhibit controlled degradation profiles, which can be beneficial in cardiac TE, where a balanced degradation profile is essential to provide sustained support during tissue regeneration [315]. In addition, the versatility of dextran extends to applications requiring the controlled release of bioactive molecules in the cardiac microenvironment [316]. This is particularly valuable in cardiac TE, where precise delivery of growth factors, cytokines, or other signaling molecules is essential for orchestrating the regenerative processes within the damaged tissue [316–318]. A study has tackled the issue of inadequate vascularization, which restricts the ability to effectively support prolonged cell survival, by developing hydrogels with tubular geometries, replicating the structures of human small arteries/veins and arterioles/venules [319]. Surface coating with ECM proteins has promoted endothelial cell monolayer adhesion. Notably, small-diameter channels composed of neutral pullulan and dextran within hydrogels initially unsupportive of endothelial cell adhesion, have transformed them into active materials guiding cell behavior solely through internal microarchitecture modifications, eliminating the need for added proteins [319]. The materials have induced endothelial cell adhesion, migration, proliferation, and polarization, emphasizing the influence of internal channel curvature. This work has showcased a geometrically guided, pro-vascularizing material, marking a significant stride in TE biomaterials [319]. Electrospun dextran-based hydrogels were fabricated for cardiovascular regeneration. Emulsion electrospinning was used to fabricate core-shell nanofibers, offering advantages such as reduced initial burst release and preserved bioactivity of drugs or proteins. Vascular endothelial growth factor (VEGF) was encapsulated with protective agents or bovine serum albumin (BSA) in the core of poly(l-lactic acid-co-ε-caprolactone) (PLCL) nanofibers for sustained release scaffolds in cardiovascular tissue regeneration [320]. Uniform nanofibers were obtained with diameters of 572 ± 92 nm for PLCL, 460 ± 63 nm for PLCL-VEGF-BSA, and 412 ± 61 nm for PLCL-VEGF-dextran. Release studies demonstrated controlled VEGF release over 28 days. Human bone marrow-derived mesenchymal stem cells confirmed scaffold functionality. This study highlighted emulsion electrospun core-shell PLCL/dextran nanofibers as potential substrates for controlled-release applications in cardiac TE [320].

4.1.5. Cellulose

Cellulose is a linear polysaccharide composed of glucose repeating units connected by β-1,4-glycosidic linkages [40,254,256,321]. Multiple cellulose chains align through hydrogen bonding, forming microfibrils that contribute to the strength and rigidity of plant cell walls. The arrangement of cellulose molecules in a crystalline structure provides remarkable mechanical strength and stability to biomaterials as well as finely modulate porosity [160,256,322,323]. Cellulose and its derivatives have emerged as components in hydrogel fabrication for cardiac TE [40,324,325]. Cellulose, renowned for its robust mechanical properties, serves as a cornerstone in the fabrication of mechanically reinforced hydrogels for TE [160,326]. In addition, the fibrous nature of cellulose contributes to the formation of a reinforcing network in hydrogels, elevating their mechanical strength [160,248,326]. Beyond its mechanical prowess, cellulose stands out for its inherent biocompatible nature, making it an invaluable component in the field of TE [160,327,328].

Numerous research studies have emphasized the effectiveness and versatility of cellulose-based hydrogels in tackling significant challenges in cardiac tissue regeneration [324,329]. Cellulosic scaffolds with an inherent 3D origami crease pattern were designed for cardiac TE. The study explored various cellulosic materials, such as cotton linters, fibers from eucalyptus, pine, spruce, and lyocell [329]. Cotton linters sheets were chosen for further investigation due to their optimal biocompatibility and mechanical properties for cardiomyocytes in both wet and dry conditions: Young's modulus of 0.8 GPa, tensile strength of 4.7 MPa, and tensile strength in a wet environment of 2.28 MPa were determined. To achieve cell alignment, different methods, including a dynamic sheet former and Rapid Köthen sheet former, were explored. Despite minimal orientation, cells cultured on the cellulose fibers grew and aligned along them [329]. In another study, a biomaterial system comprising 2,2,6,6-tetramethylpiperidine-1-oxyl radical-oxidized nanocellulose (TOCNF), poly(glycerol sebacate (PGS), and polypyrrole (PPy) was fabricated for myocardial TE. Direct ink writing (DIW) was employed to fabricate multifunctional lattice structures suitable for myocardial infarction treatment (Fig. 10A). These structures, exhibiting elasticity and electrical conductivity, supported extensive cell growth, making them ideal cardiac patches [330]. The nanocellulose-based scaffolds showed high porosity (94 ± 1 %) beneficial for cell growth and interaction. Scaffolds with single-component TEMPO-oxidized cellulose nanofibers (TOCNF) were significantly more porous compared to those with PGS-PPy or multicomponent counterparts (Fig. 10B). The biocompatibility of 3D-printed composites undergoing degradation was assessed using the MTT assay and compared with a positive control. As shown in Fig. 10C(i), degradation did not affect H9c2 cardiomyoblast viability, with no cytotoxicity detected over 28 days [330]. The histogramm shown in Fig. 10C(ii) demonstrates that all 3D-printed biocomposites supported cardiomyoblast proliferation, with no significant differences between PPy loadings. The proliferation rate of H9c2 cells on the biocomposites was comparable to that of the TOCNF porous structure, doubling every two weeks. SEM analysis demonstrated strong cell attachment, with bodies assembling on pore surfaces and elongating along pore walls. Fig. 10C(iii) and Fig. 10C(iv) illustrate the control and cell-seeded biocomposite, confirming positive cell-scaffold interactions. The hydrophilicity, high porosity, and surface area of TOCNF and PGS facilitated adhesion while maintaining cell viability [330]. An electrospun scaffold crafted from polyurethane (PU) and ethyl cellulose (EC), featuring uniform fibrous nanostructures and a 3D porous network was also achieved. The research established the correlation between processing conditions and fibrous nanostructures, enabling rational processing with tunable fiber diameters [324]. The resulting scaffold demonstrated high biocompatibility, supporting the proliferation of H9c2 cells. Boasting remarkable mechanical strength, the PU/EC scaffolds allowed the fabrication of ultrathin patches compatible with contractile tissues, demonstrating promising potential in the field of cardiac TE [324].

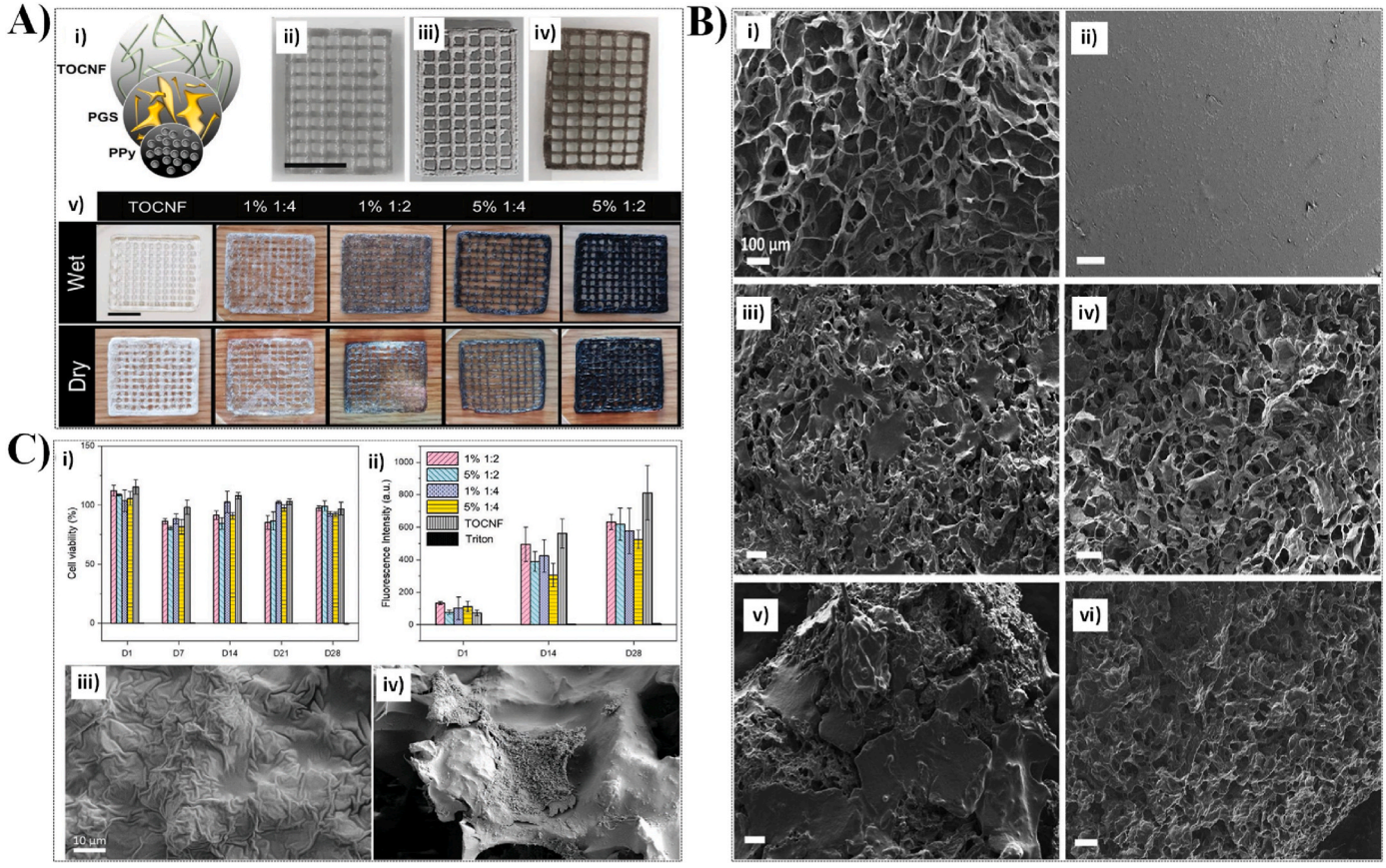

Fig. 10. (A) (i) Schematic illustration depicting TOCNF, pre-PGS, and PPy used in DIW ink formulation and 3D-printed scaffold fabrication. (ii) Scaffold appearance before and (iii) after freeze-drying. (iv) Scaffold after curing pre-PGS for 48 h at 120 °C. (v) 3D-printed samples with specified component ratios, shown in wet and cured states. Scale bar in (ii-iv) is 1 cm. (B) Scanning electron microscope (SEM) images: (i) Neat TOCNF, (ii) PGS-PPy 5 % cast and cured, (iii) 5 % 1:4 and (iv) 5 % 1:2 before PGS synthesis, indicating TOCNF and pre-PGS phase separation. (v) 5 % 1:4 and (vi) 5 % 1:2 after pre-PGS curing, showing formation of PGS-PPy-TOCNF biocomposite. Scale bars correspond to 100 µm. (C) (i) Cytotoxicity and (ii) H9c2 cardiomyoblast proliferation over 28 days assessed by MTT and alamarBlue assays, respectively. Blank incubated medium served as positive control for cytotoxicity tests (n = 4). (iii) Cell attachment on control sample 5 % 1:2 and (iv) 5 % 1:2 sample containing H9c2 cells. Reproduced with permission from Ref. [330] Copyright © 2020 WILEY-VCH Verlag GmbH & Co. KGaA, Weinheim.

4.1.6. Carrageenan

Carrageenan, derived from red seaweeds, has a molecular structure consisting of galactose repeating units and 3,6-anhydrogalactose, forming linear chains with various sulfation patterns [331]. It exhibits biocompatibility, biodegradability, and gelation properties, making it suitable for hydrogel fabrication, as well as for cell encapsulation and proliferation [262]. Carrageenan ability to form thermally reversible gels allows for easy processing and incorporation of bioactive agents [238].

Research studies have emphasized the utilization of 3D printing in the fabrication of carrageenan-based hydrogels for applications in cardiac TE [170,331]. κ-carrageenan-based hydrogels fabricated through 3D printing revealed controllable structures and improved cell viability [331]. Varying the shear stress produced small-diameter (<6 mm) gel filaments simulating blood vessel structures. HUVECs cultured on κ-carrageenan and composite gels (carrageenan/carbon nanotube and carrageenan/alginate) showed enhanced cell attachment and proliferation on composite gels compared to pure κ-carrageenan [331]. In addition, carrageenan-based composite bioinks exhibited superior printability, mechanical stiffness, interconnectivity and biocompatibility. Optimizing printing parameters allowed precise adjustment of hydrogel structure, facilitating the preparation of 3D TE scaffolds with optimal pore size, porosity, and distribution [331]. Another research work highlighted the formulation and evaluation of carrageenan composite inks for 3D printing of functional of TE heart valves (TEHVs) [170]. In vitro and in vivo assessments of 3D hydrogels encompassed biocompatibility, immune response, hemolysis, thrombogenicity, and hydrodynamics under physiological conditions. The results demonstrated that these 3D-printed TEHVs exhibited mechanical characteristics comparable to native leaflets, minimal hemolysis, low thrombogenicity, and the ability to withstand aortic conditions, presenting a promising solution for valve replacement challenges [170].

4.1.7. Pectin

Pectin, a complex polysaccharide found in the cell walls of plants, has garnered significant attention in the field of cardiac TE [278,332]. Comprising a linear chain of α-1,4-linked D-galacturonic acid units, pectin exhibits a high degree of structural variability depending on its source and extraction method [239]. In cardiac TE, pectin based hydrogels have demonstrated potential in emulating the ECM, and promoting cell adhesion and proliferation [278]. Pectin is a versatile biomaterial for developing cardiovascular constructs with enhanced structural support and the potential for vascular applications in TE [263,332]. Li et al. [263] prepared hydrogel nanofiber scaffolds with varying oxidation degrees (25 % and 50 %) using periodate oxidation, electrospinning, and adipic acid dihydrazide crosslinking. Nano-sized fibrous structures with fiber diameters ranging from 300 to 400 nm were achieved. Mesenchymal stem cells cultured on these scaffolds for 14 days showed high viability [263]. Scaffolds of different stiffness were evaluated for their potential in MSC differentiation into vascular cells using gene expression analysis. Stiffer scaffolds promoted MSC differentiation into vascular smooth muscle cells, while softer mats favored

differentiation into endothelial cells. These findings highlight the capability of pectin hydrogel nanofibers to provide mechanical cues that facilitate MSC differentiation into vascular cells, showcasing their potential in stem cell-based TE [263].

To enhance its bioactivity, particularly in promoting cell attachment and interaction, pectin has been subjected to biochemical modification. One prevalent method involved the use of RGD (Arginine-Glycine-Aspartic Acid) sequences to modify pectin and augment its biological properties. The RGD sequence is recognized for its ability to facilitate cell adhesion by interacting with specific cell receptors, including integrins present on the cell surface. This modification is frequently applied in the field of TE and regenerative medicine to enhance the functionality of biomaterials like hydrogels, aiming to provide better support for cell growth and tissue regeneration [237,332,333]. By employing a coaxial flow wet-spinning system, Campiglio et al. [332] ingeniously produced 3D fibrous patches laden with cells, incorporating RGD-modified pectin to exploit the advantageous properties of hydrogel and fibrous architecture. The rapid fabrication of self-standing patches, ranging from 100 to 200 μm in diameter, was achieved through precise adjustments of pectin and calcium ions concentrations [332]. These patches exhibited high cell density and uniform dispersion, with cells remaining highly viable for up to 2 weeks, showcasing the potential of modified-pectin in scaffolds to support muscle tissue regeneration. The inherent porosity, favorable cell–material interaction, and the ability to guide cell alignment make these microfibers conducive to fostering functional tissue formation [332].

4.2. Protein-based materials for cardiac tissue engineering

Proteins, being integral components of the native ECM, play a fundamental role in the formulation of hydrogels for cardiac TE [42,90,221,334]. Proteins can either serve as a key component in the development of hydrogel matrices or be incorporated into matrices composed of polysaccharides and other materials to more closely mimic cardiac tissues. By integrating proteins into biopolymer-based matrices, these hybrid matrices can better replicate the bioactive environment of the heart, enhancing cell adhesion and proliferation. This approach helps in fabricating more functional and physiologically relevant models for cardiac TE [60,221,279]. In hydrogel formulations for cardiac TE, various proteins are commonly used to mimic the natural ECM. Among the most frequently employed proteins are collagen, gelatin, fibrin, elastin and silk fibroin [335,336].

4.2.1. Collagen

Collagen is a fibrous helical protein primarily extracted from animal connective tissues. It is composed of three polypeptide chains, which helical structure. This triple helix confers stability and strength to collagen [264]. The primary structure of collagen includes glycine, proline and hydroxyproline, where glycine due to its small size allows for tight packing of the helical structure. Hydroxyproline provides additional stability through hydrogen bonding between the polypeptide chains [265]. Collagen is highly resistant to tension, making it an essential component in tissues requiring strength, such as tendons and ligaments [337,338]. Its ability to self-assemble into fibrillar networks contributes to its role in the ECM, providing mechanical support to tissues [339]. Collagen is biodegradable, allowing controlled degradation over time as tissues remodel [340]. Additionally, it can interact with cell surface receptors promoting cell adhesion, migration and signaling. These features make collagen a versatile and valuable biomaterial in TE and regenerative medicine [341].

Through 3D printing, collagen-based inks can be precisely deposited in controlled architectures, mimicking the complex structures of native cardiac tissue. Lee et al. [172] innovatively 3D-printed collagen hydrogels using the freeform reversible embedding of suspended hydrogels (FRESH) method for human heart components, achieving versatile scales from capillaries to complete organs. resulted in a filament resolution of 20 μm, porous microstructure enabling rapid cellular infiltration, and mechanical strength for fabricating multiscale vasculature and tri-leaf valves [172]. FRESH 3D-printed hearts accurately mirrored patient-specific anatomies, validated by micro–computed tomography. Cardiac ventricles with human cardiomyocytes exhibited synchronized contractions, directional action potential propagation, and up to 14 % wall thickening during peak systole [172]. Recently, an adaptation of the FRESH method has been used for directly 3D bioprinting hiPSC-derived cardiomyocytes into ring and ventricle-shaped constructs which exhibited spontaneous construction for several month [162]. Electrospinning has been also used to fabricate collagen-based fibrous hydrogels for cardiac TE [342,343]. Karapehlivan et al. [342] developed electrospun nanofibers composed of polycaprolactone (PCL), graphene oxide, and collagen as a potential treatment for cardiac injuries as illustrated in Fig. 11A. Graphene oxide was incorporated in nanofiber fabrication to enhance electrical stimulation and support cardiomyocyte contraction and elongation, while collagen was added due to its role in the myocardial extracellular matrix. The SEM images of cardiomyocyte cells on the nanofibers highlighted their excellent biocompatibility, showing cell growth and proliferation on the nanofibers (Fig. 11B) [342]. Cell fluorescence imaging further confirmed the results of the MTT assay, showing that cells proliferated on the nanofibers (Fig. 11C). The response of nanofibers to alternating current (AC) signals was assessed over frequencies ranging from 40 Hz to 10^5 Hz (Fig. 11D). Direct current (DC) conductivity values of fabricated nanofibers ranged from 1.10^{-10} to 6.10^{-10} S m^{-1} at 25 °C (Fig. 11D), while AC conductivity displayed frequency-dependent behavior (Fig. 11E) [342]. Among the tested formulations, 17 % PCL/1.5 % graphene oxide/5 % collagen nanofibers exhibited the highest DC and AC conductivity compared to 17 % PCL/1.5 % graphene oxide nanofibers. The findings highlights the potential of these collagen-based electroconductive nanofibers for cardiac TE [342]. Collagen was also blended with synthetic materials such as polylactic acid (PLA) and polyethylene glycol (PEG) to fabricate composites. Electrospinning successfully produced random polylactic acid (PLA), polylactic acid/polyethylene glycol (PLA/PEG), random or aligned polylactic acid/polyethylene glycol/collagen (PLA/PEG/COL) nanofiber patches [343]. The resulting patches exhibited beadles and smooth structures, with a collagen fiber diameter of 755 nm [343]. Mechanical characterization revealed that aligned patches had the highest tensile strength (5.90 MPa), and in vitro degradation tests showed the highest degradation percentage for the aligned patch. These patches exhibited promising potential as tissue-like cardiac patches for the regenerative properties expected after myocardial infarction [343].

4.2.2. Gelatin

Gelatin is derived from denaturation of collagen through its controlled hydrolysis [344]. Thus, the chemical structure of gelatin is constituted by the amino acids been glycine, proline, and hydroxyproline, forming its polypeptide chains [345]. Gelatin is soluble in warm water and forms thermo-reversible hydrogels upon cooling. This property is pivotal in its applications for drug delivery systems and TE. Gelatin is also responsive to pH changes. Its biodegradability and biocompatibility further enhance its utility in various biomedical applications [346,347]. Its gel-forming, emulsifying, and foaming capabilities, extend its applications in the food and pharmaceutical industries. The properties and features of Gel, combined with its natural origin, position it as a valuable biomaterial with diverse functionalities in biomedical sciences [346,348].

The thermo-reversible nature of gelatin facilitates the fabrication of 3D structures, crucial for mimicking the complex architecture of cardiac tissues [291]. Gelatin-based hydrogels produced using 3D printing provide a supportive environment for cell encapsulation and growth [349]. Gelatin-based hydrogels cross-linked with the biocompatible agent genipin, were developed as scaffolds for cardiac cell culture studies [349]. Using a microcontact printing technique, microstructured

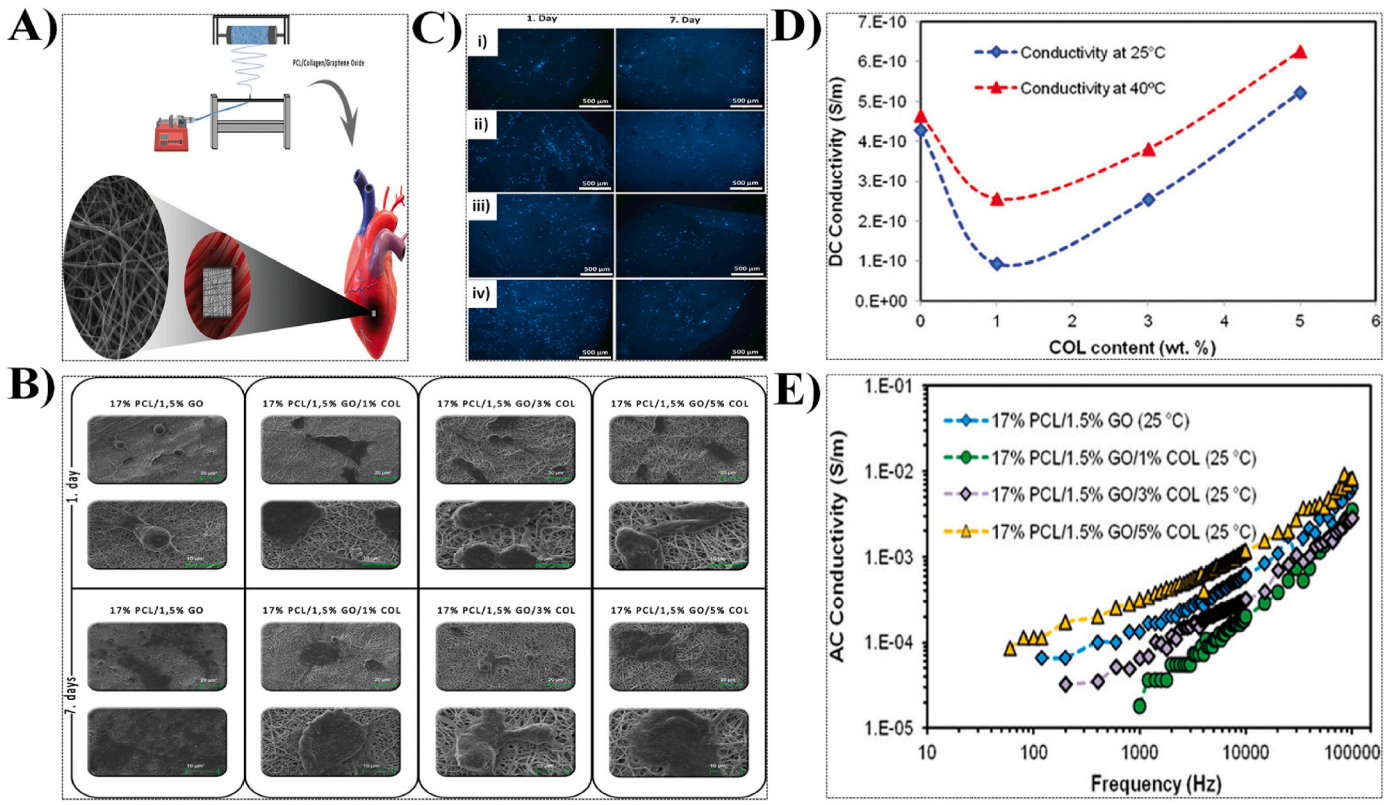

Fig. 11. (A) Schematic illustration of the experimental setup. (B) SEM images of cardiomyocyte cells cultured on nanofibers after 1 and 7 days of incubation. (C) Fluorescent images of cardiomyocytes on (i) 17 % PCL/1.5 % GO, (ii) 17 % PCL/1.5 % GO/1 % COL, (iii) 17 % PCL/1.5 % GO/3 % COL, and (iv) 17 % PCL/1.5 % GO/5 % COL nanofibers. (D) Variation in DC conductivity of the films as a function of COL content (wt%) in a vacuum environment (10^{-3} mbar) at 25 and 40 °C. (E) Frequency-dependent AC conductivity of nanofiber films with different COL contents in vacuum (10^{-3} mbar) at 25 °C. In this study, polycaprolactone is referred to as PCL, graphene oxide as GO, and collagen as COL. Reproduced with permission from Ref. [342] Copyright © 2024 WILEY-VCH Verlag GmbH & Co. KGaA, Weinheim.

gelatin-based hydrogels were fabricated to promote the alignment and maturation of neonatal rat ventricular cardiomyocytes. Additionally, graphene oxide (GO) was incorporated into the gelatin matrix to enhance cardiomyocyte functionality [349]. The results demonstrated that micropatterned genipin-cross-linked gelatin hydrogels contributed to the alignment and maturation of cardiomyocytes, while the presence of GO further improved functional performance, leading to synchronized contractions lasting up to 3 months [349]. Moreover, Tijore et al. [350] developed a 3D bioprinted microchannel gelatin hydrogel that enhanced human mesenchymal stem cell commitment to myocardial lineage and supported native cardiomyocytes functionality (Fig. 12A). The study investigated the effects of microchannel hydrogel on hMSC alignment, elongation, and differentiation, revealing well-defined F-actin anisotropy and elongated cell morphology [350]. Aligned stem cells showed increased myocardial lineage commitment, confirmed by mature cardiac markers and fluorescence-activated cell sorting analysis (Fig. 12B). Zhang et al. [291] also developed gelatin-based hydrogels crosslinked with genipin as scaffolds for cell culture. Neonatal rat cardiomyocytes demonstrated synchronous beating within 2 days on these hydrogels. Additionally, electrical stimulation was employed to enhance cardiomyocyte maturation (Fig. 12C), resulting in improved sarcomere organization, gap junction establishment, calcium-handling capacity, and pacing signal propagation (Fig. 12D) [291]. This system holds promise for promoting physiological maturation in engineered cardiac tissues, contributing to advancements in cardiac TE [291].

Electrospinning technology was also used to fabricate biocompatible gelatin-based fibrous scaffolds mimicking cardiac tissues. In a study, three types of electrospun scaffolds including furfuryl-gelatin (f-gelatin) alone, f-gelatin mixed with polycaprolactone (PCL), and coaxial scaffolds with PCL (core) and f-gelatin (sheath) were developed. Scaffolds were fabricated through single-nozzle or coaxial electrospinning to achieve uniform fibrous structures with varied average fiber diameters (760 ± 80 nm for f-gelatin, 420 ± 110 nm for f-gelatin/PCL, and 810 ± 60 nm for coaxial f-gelatin > PCL) [351]. Despite the absence of polymer interactions in blended scaffolds, differences in elastic moduli were significant, with coaxial f-gelatin > PCL having the highest one (164 ± 3.85 kPa) [351]. The coaxial scaffold demonstrated superior biocompatibility with hiPSC-derived cardiomyocytes, highlighting its potential for cardiac tissue-on-a-chip models. The study showcased a simple method to produce nanofibrous scaffolds that are biodegradable and crosslinkable under visible light [351].

4.2.3. Fibrin

Fibrin is an important protein in the clotting cascade, playing a fundamental role in wound healing and tissue repair. It is formed through the proteolytic cleavage of fibrinogen by thrombin, resulting in the polymerization of fibrin monomers into a mesh-like network [268]. This 3D fibrin matrix can provide a supportive environment for cell migration, adhesion, and proliferation. Additionally, fibrin mechanical properties, such as flexibility and visco-elasticity, can be leveraged to develop hydrogels that closely mimic the mechanical properties of natural tissues [352]. Fibrin exhibits remarkable biocompatibility and biodegradability, contributing to its widespread use in TE. Its ability to be easily manipulated and functionalized further enhances its utility in creating scaffolds for various regenerative medicine applications, particularly in cardiac TE, where fibrin-based hydrogels have shown promise in supporting cell survival and tissue regeneration [242]. Fibrin is commonly used in cardiac TE hydrogels due to its ability to support cell attachment and proliferation [242,353]. However, a major challenge is its rapid degradation by various cell types, which can undermine

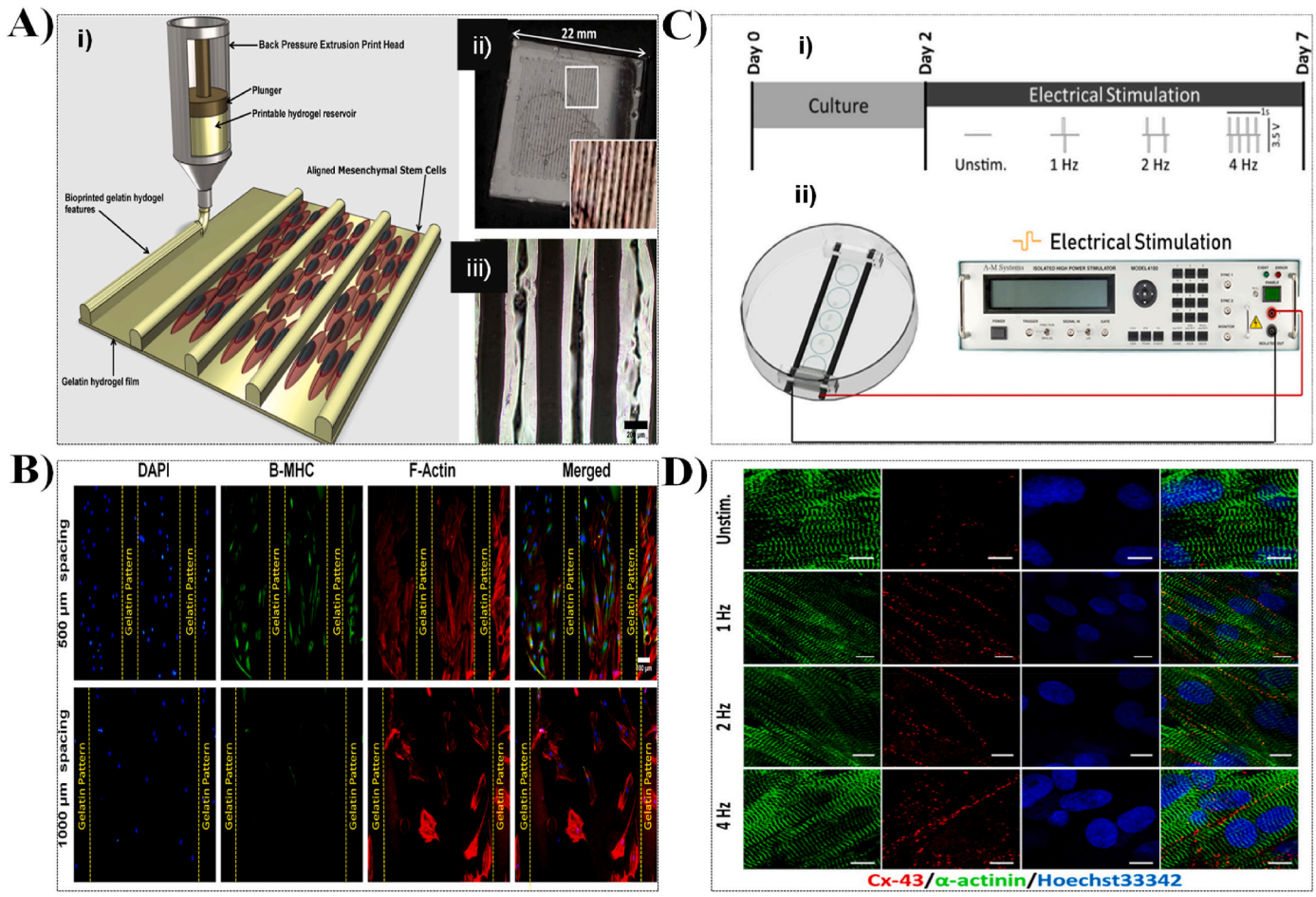

Fig. 12. (A) 3D bioprinting and characterization of gelatin hydrogel features. (i) Schematic representation of the process. (ii) Image of the 3D patterned gelatin hydrogel captured with an 8-megapixel digital camera. The outlined area of the printed pattern is shown magnified in the inset. (iii) Bright field microscope image of bioprinted gelatin pattern on a gelatin film-coated coverslip. Scale bar = 200 μm. (B) Effect of microchannel width on cell alignment and cardiomyogenic lineage commitment: Fluorescent images after 5 days of culturing hMSCs on microchannel hydrogels with 500 or 1000 μm spacing, showing morphology, cytoskeletal orientation, and lineage commitment. Cells on microchannel surfaces with 500 μm spacing exhibited greater alignment and upregulation of β-MHC expression compared to cells on microchannels with 1000 μm spacing. Scale bar = 100 μm. Reproduced with permission from Ref. [350] Copyright © 2018 IOP Publishing Ltd. (C) Experimental setup for applying electrical field stimulation to cardiomyocytes: (i) CMs cultured on hydrogels 2 days after seeding, followed by 5 days of electrical stimulation or cultured without electrical stimulation (unstimulated controls). (ii) Scheme of the electrical stimulation device, with hydrogels placed in the circular glass groove between the two electrodes. (D) Electrical stimulation enhances expression of cardiac-specific proteins: Immunofluorescent staining of cardiac-specific proteins (Cx43 in red, α-actinin in green, nucleus in blue) with and without electrical stimulation. Scale bars: 10 μm. Reproduced with permission from Ref. [291] Copyright © 2020 Springer.

the structural integrity and longevity of the hydrogel scaffold. This fast degradation may result in inadequate support for regenerating cardiac tissue, potentially hindering the success of the TE process [354]. To overcome this, researchers are investigating cross-linking techniques and modifications aimed at slowing the degradation rate while preserving the beneficial properties of fibrin [353–355].

Fibrin-based hydrogels can be designed using methods like 3D printing and electrospinning to create structures that mimic the native cardiac tissue environment [353,356,357]. Kumar et al. [357] developed a fibrin-enhanced gelatin-based bioink to fabricate cardiac cell-laden constructs using hiPSC-derived cardiomyocytes and cardiac fibroblasts. The bioink incorporated platelet-rich fibrin and improved bioactivity, with a two-step cross-linking process involving visible light cross-linking of furfuryl-gelatin and fibrinogen cross-linking via thrombin and calcium chloride [357]. The resulting constructs exhibited a porous, stable network and supported long-term in vitro culture. Printed cardiomyocytes demonstrated high viability, proliferation, and troponin I marker expression. Additionally, the constructs enabled cardiomyocytes and cardiac fibroblasts coculture, crucial for cardiac wall physiology, with applications in drug screening and heart disease modeling [357]. Sreerekha et al. [356] developed a multiscale electrospun composite scaffold based on fibrin and poly(lactic-co-glycolic acid) (PLGA) for myocardial regeneration (Fig. 13A). Leveraging the biological potential of fibrin, the scaffold provided an ideal environment for cell attachment and proliferation [356]. SEM micrographs revealed greater cell attachment on PLGA–fibrin fibers than on pure PLGA fibers, with MSCs spreading more on the composite fibers after 24 h compared to pure PLGA (Fig. 13B). Cell viability assays showed that MSCs maintained normal morphology on both scaffolds after 24 h, but those on PLGA–fibrin exhibited better survival and proliferation, with fewer dead cells observed at both 24 and 72 h (Fig. 13C) [356]. Cardiomyocyte differentiation was evaluated using immunofluorescence and flow cytometry, which revealed that cells cultured on PLGA–fibrin scaffolds expressed higher levels of cardiac markers, including α-sarcomeric actinin, cardiac troponin, and tropomyosin, compared to those grown on pure PLGA scaffolds. After 14 days in differentiation medium, MSCs on PLGA–fibrin scaffolds showed differentiation into myogenic cells, as evidenced by confocal microscopy images (Fig. 13D) [356].

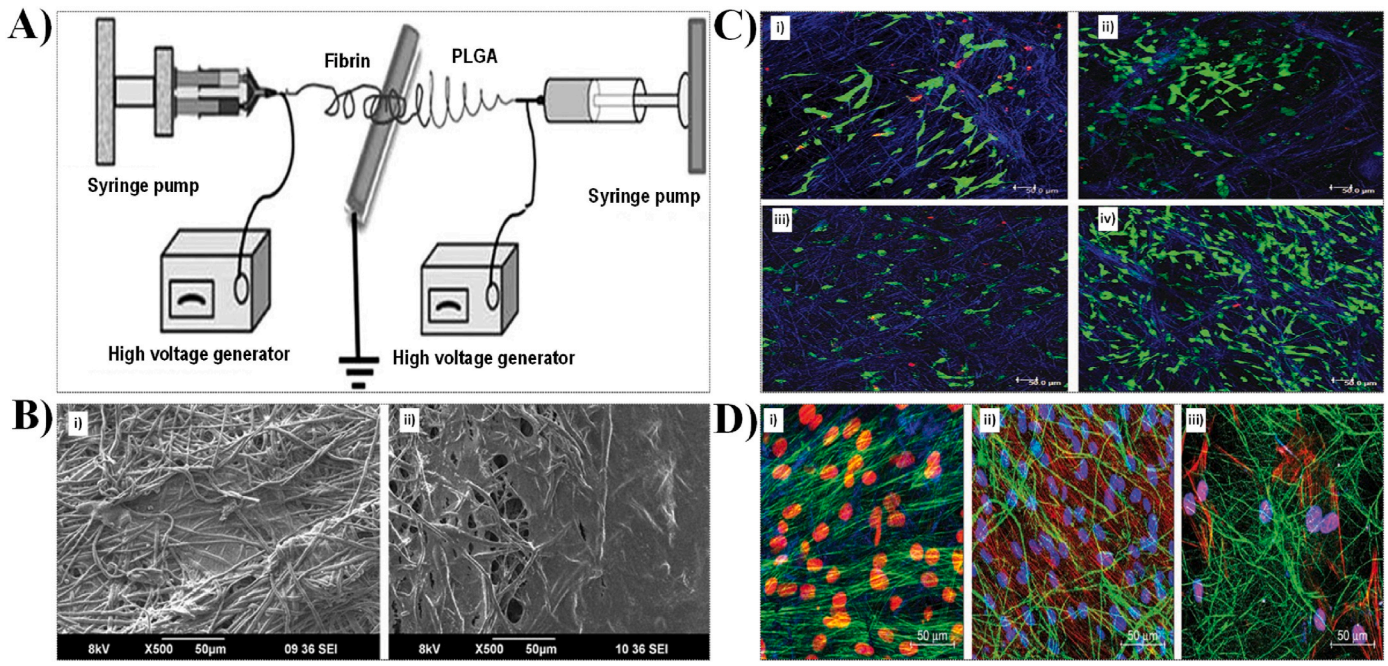

Fig. 13. (A) Schematic representation of simultaneous electrospinning of fibrin and poly(lactide-co-glycolide) (PLGA) onto a rotating mandrel. (B) SEM images of hMSCs cultured on (i) PLGA scaffold and (ii) PLGA–fibrin composite scaffold after 24 h. (C) Cell survival and morphology of hMSCs on electrospun fibers, assessed by live/dead assay. Confocal microscopy images of cells on PLGA (i, iii) and PLGA-fibrin composite fibers (ii, iv) after 24 and 72 h, respectively. Live cells appear green, dead cells appear red, and fibers are shown in blue. (D) Confocal microscopy images of MSCs cultured on PLGA–fibrin composite fibers for 14 days during cardiac differentiation. (i) Expression of cardiac troponin (green), with nuclei stained by Sytox Orange (orange), and fibers shown in blue. (ii) Expression of α-sarcomeric actinin (red), with nuclei stained by DAPI (blue), and fibers in green. (iii) Expression of tropomyosin (red), with nuclei stained by DAPI (blue), and fibers in green. Reproduced with permission from Ref. [356] Copyright © 2013 Mary Ann Liebert, Inc.

4.2.4. *Elastin*

Elastin is a key structural protein that contributes to the elasticity and resilience of various tissues in the human body [358]. It is rich in lysine-derived cross-links, which contribute to its elastic properties [243,358]. The remarkable elasticity of elastin arises from its ability to recoil after being stretched, attributed to the inherent properties of its molecular structure [359]. Elastin functionality extends beyond its mechanical properties. It interacts with other ECM components, such as fibrillin and collagen, influencing tissue organization and strength. Moreover, elastin is involved in cell signaling, impacting cellular behavior and tissue homeostasis [92,360].

Incorporating elastin into hydrogel formulations enhances their mechanical properties, mirroring the elasticity of native cardiac tissues [243]. Through 3D printing technologies, elastin-rich hydrogels can be precisely engineered to mimic the complex architecture of the heart. This aids in the fabrication of scaffolds with tailored elasticity, promoting cell adhesion, proliferation, and overall functionality [269]. Furthermore, elastin not only influences cell behavior through interactions with other ECM components but also contributes to tissue organization and cell signaling. Its multifaceted involvement enhances the microenvironment for cardiac cells, promoting survival and supporting tissue regeneration [269,361]. A research work demonstrated the use of recombinant human tropoelastin as a highly biocompatible and elastic bioink for 3D printing [244]. Vascularized elastin-based cardiac constructs have been bioprinted, exhibiting endothelium barrier function and spontaneous beating of cardiomyocytes in vitro and in vivo. The bioink specifically consisted of two ECM-derived biopolymers: gelatin methacryloyl (GelMA) and methacryloyl-substituted recombinant human tropoelastin (MeTro) [244]. Cardiomyocytes, cardiac fibroblasts, and HUVECs were encapsulated within the MeTro/GelMA bioink for 3D bioprinting of constructs containing multiple cell types (Fig. 14A). The constructs showed minimal inflammatory responses and efficient in vivo biodegradation when subcutaneously implanted in rats. This highlighted the potential of the elastic bioink for 3D printing functional cardiac tissues (Fig. 14A) [244]. Wang et al. [362] designed a 3D collagen-elastin scaffold emulating heart valve ECM encapsulated valve interstitial cells (VICs) and cultured valve endothelial cells (VECs) to create an in vitro 3D VEC-VIC co-culture. Cells aligned more prominently as cultures became highly confluent, orienting parallel to each other along their long axis, possibly influenced by collagen fiber orientation (Fig. 14B). This alignment, observed from day 3 onwards, reflected sustained cell elongation and enhanced with culture confluence. Over 7 days, VICs exhibited stable integrin β1 expression and proliferation with altered morphology. VECs maintained endothelial phenotype up to day 5, transforming to mesenchymal phenotype by day 7 (Fig. 14C). The fabricated 3D collagen-elastin scaffolds proved being a valuable biomaterial for studying cell interactions, advancing valvular endothelial cell research [362].

4.2.5. *Silk fibroin*

Silk fibroin, a natural protein derived from silkworms, exhibits a unique crystalline structure, imparting exceptional strength, toughness and stability suitable for various biomedical applications [221,245,363,364]. Silk fibroin-based hydrogels are gaining significant interest in cardiac TE due to their interesting biocompatibility, biodegradability and mechanical properties. These hydrogels provide a supportive scaffold that can mimic the natural ECM, promoting cell adhesion, proliferation, and differentiation [363,365]. Additionally, silk fibroin low immunogenicity and tunability make it an ideal candidate for creating customized tissue constructs. Recent studies have demonstrated the potential of silk fibroin hydrogels in enhancing cardiac tissue repair and regeneration, offering a promising approach for treating heart diseases [42,363,365].

Silk fibroin-based materials can be processed into different forms including fibers, films, hydrogels [366,367]. A research study presented a fully aqueous process for fabricating conductive carbon nanotube/silk fibroin (CNT/silk) electrospun scaffolds. Scanning electron microscopy images showed that the nanofibers in all the study groups exhibited a

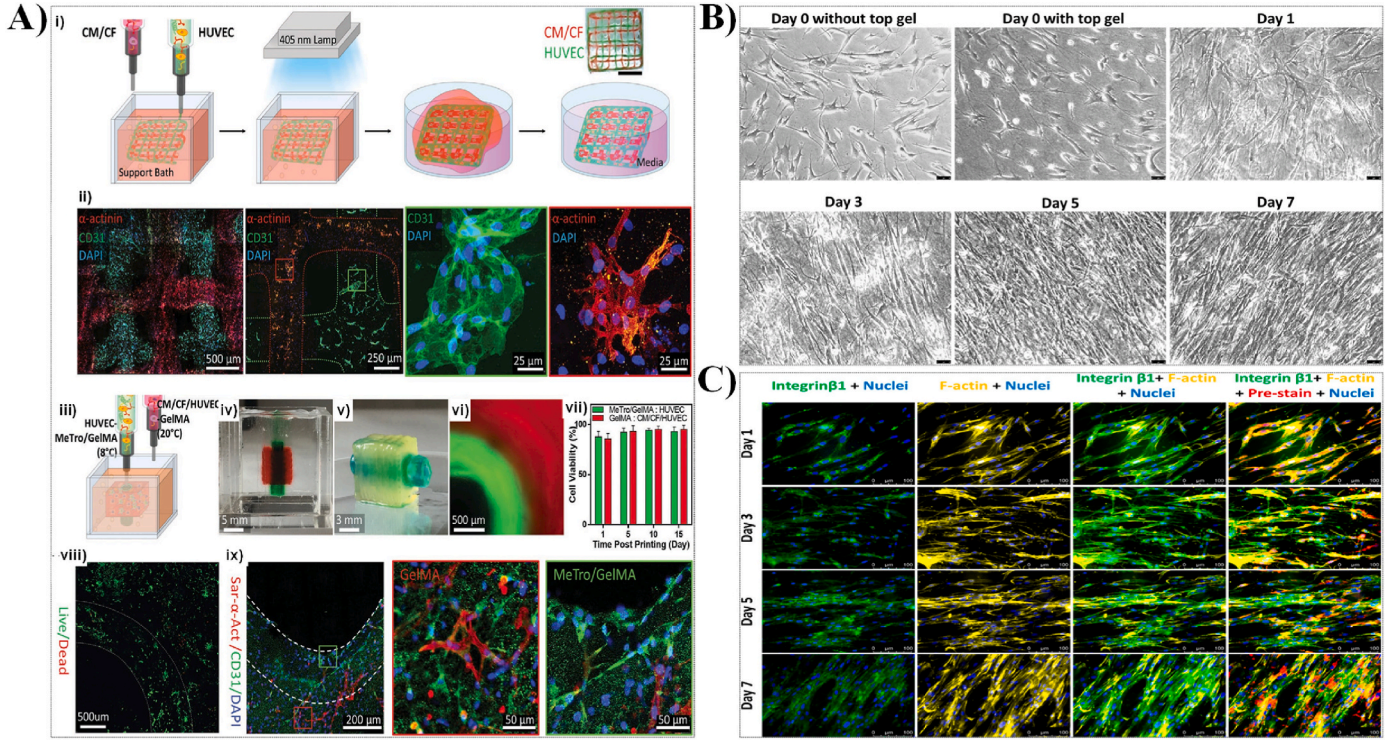

Fig. 14. (A) 3D bioprinting of cell-laden constructs using MeTro/GelMA bioink. (i) Schematic representation of lattice scaffold bioprinting with HUVECs- and cardiomyocytes/cardiac fibroblasts -laden MeTro/GelMA bioinks, distinguished by green and red food colors for imaging. (ii) Immunostaining against sarcomeric α-actinin (red), CD31 (green), and DAPI (blue) at day 7 post bioprinting. (iii) Schematic depicting vascularized cardiac construct bioprinting using HUVECs-laden MeTro/GelMA and cardiomyocytes/cardiac fibroblasts/HUVECs-laden GelMA bioinks. (iv) Vascularized cardiac construct immediately post-printing, and (v) after photo-cross-linking and washing. Green and red food colors distinguish MeTro/GelMA and GelMA bioinks for imaging. (vi) Cross-sectional fluorescence image of the vascularized cardiac construct. (vii) Viability assessment of HUVECs (MeTro/GelMA bioink) and cardiomyocytes/cardiac fibroblasts/HUVECs (GelMA bioink) within constructs. (viii) Live/dead staining at day 10 post bioprinting. (ix) Immunostaining against sarcomeric α-actinin (red), CD31 (green), and DAPI (blue) at day 10 post bioprinting, with HUVECs (green) and cardiomyocytes/cardiac fibroblasts/HUVECs (red) highlighted. Reproduced with permission from Ref. [244] Copyright © 2020 WILEY-VCH Verlag GmbH & Co. KGaA, Weinheim. (B) Phase-contrast images showing VICs elongation and alignment over time. Scale bar: 50 μm. (C) Fluorescent images of VICs in the middle layer: Integrin β1 (green), F-actin (yellow), Nuclei (blue), Cell membrane (red). Scale bar: 100 μm. Reproduced with permission from Ref. [362] Copyright © 2018 MDPI.

smooth and bead-free morphology (Fig. 15A), indicating the interesting electrospinnability of the solutions. The well-dispersed CNT enhanced scaffold conductivity without compromising biocompatibility [368]. Culturing neonatal rat cardiomyocytes on these scaffolds resulted in improved cell spreading and increased expression of cardiac-specific proteins. Aligned CNT/silk fibroin composite scaffolds guided the oriented organization of cardiac tissues, mimicking natural sarcomeres and gap junctions (Fig. 15B). This aqueous processing method showed great potential for supporting the formation of enhanced functional cardiac tissues [368]. In another study, a biodegradable polyvinyl alcohol/silk fibroin (PVA/SF) nanofibrous heart patch with unique tensile properties was crafted using an electrospinning technique in a water-solvent system [42]. Patches with pronounced and interconnected composite fibrous structures were achieved, with enhanced mechanical properties and tunable degradation rates. Culturing human cardiac fibroblast cells on these patches demonstrated favorable cell proliferation and attachment on the bio-interface [42]. Moreover, Mehrotra et al. [369] developed a novel, mechanically robust nonmulberry silk fibroin bioink [369]. The developed nonmulberry silk fibroin (n-SF) based ink consisted of n-SF, polyethylene glycol dimethacrylate (PEGDMA) and GelMA as its major components. The silk fibroin-based bioink exhibited suitable mechanical properties, including suitable elasticity and stiffness (≈40 kPa), essential for constructing clinically relevant cardiac tissue constructs. Through a dual crosslinking method, this ink was used for the fabrication of anisotropic scaffolds that supported the formation of aligned sarcomeres and maintained synchronized beating of cardiomyocytes (Fig. 15C). Macrophages released pro-inflammatory biomarkers (IL-1β, NO) when exposed to the constructs, showing low immunogenicity comparable to GelMA and tissue culture plates (TCP). In vivo implantation in rats demonstrated minimal macrophage infiltration, with fibroblasts predominant in the zone of interaction with the host tissue interaction (Fig. 15D) [369]. In the field of vascularized myocardial tissue-on-a-chip fabrication, the silk-based ink has served as a supporting hydrogel for encapsulating human-induced pluripotent stem cell-derived cardiac spheroids (hiPSC-CSs) and fabricating perfusable vascularized channels through embedded bioprinting. The silk-based hydrogel demonstrated its capability to support the maturation and viability of hiPSC-CSs and endothelial cells, offering a versatile platform for drug toxicity evaluation in cardiac TE [369]. 3D scaffolds were fabricated through electrospinning and microfluidics, incorporating silk fibroin nanofibers and uniform microspheres. The resulting bridge-shaped structures featured nanofibers (250–350 nm in diameter) doped with microspheres (2–10 μm) [370]. Endothelial cells (ECs) were seeded on these 3D microsphere-nanofiber silk fibroin scaffolds with a mean fiber diameter of 300 nm. Notably, a 10 % higher cell proliferation ratio was observed compared to microporous and sponge-like SF scaffolds made through freeze-drying [370]. Moreover, gene transcript levels, such as CD146, VE-C, and PECAM-1, showed superior preservation on the 3D microsphere-nanofiber silk fibroin scaffolds, which hierarchical structure is promising for cardiovascular TE [370]. Patra et al. [363] investigated the potential of non-mulberry silk fibroin from *Antheraea mylitta* as a scaffold for cardiac TE. Testing 3-day postnatal rat cardiomyocytes, they assessed cell adhesion, metabolic activity, extracellular response, cell communication, and contractility [363]. The

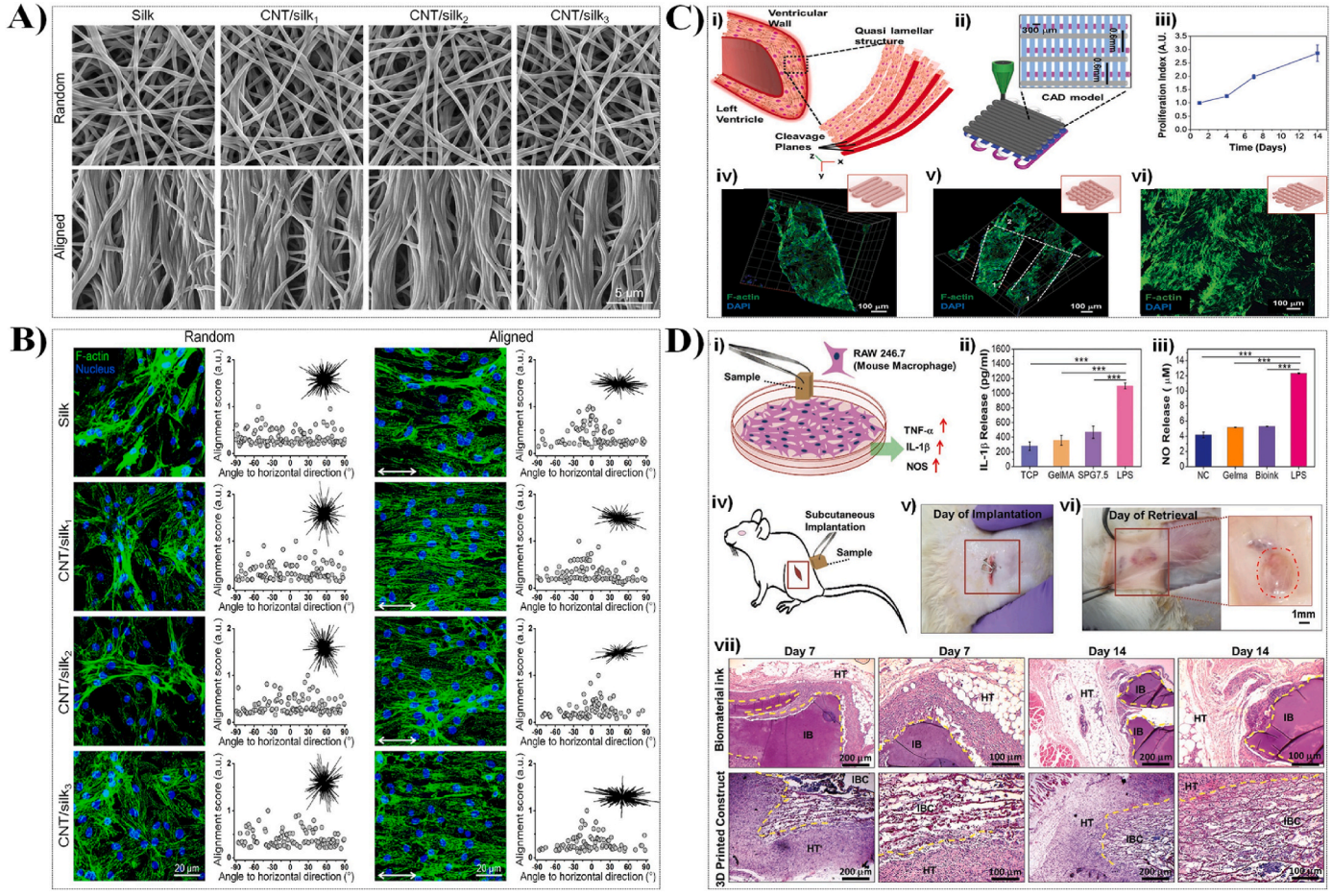

Fig. 15. (A) SEM images showing surface morphology of silk and CNT/silk scaffolds. (B) F-actin staining and nucleus alignment of cardiomyocytes on day 7. Reproduced with permission from Ref. [368] Copyright © 2020 American Chemical Society. (C) Design and characterization of an anisotropic 3D printed cardiac-like construct: (i) Schematic representation of native heart tissue with quasi-lamellar structure; (ii) Design schematic of 3D printed microfibrous scaffold to mimic quasi-lamellar 3D cardiac tissue; (iii) Assessment of proliferation index of seeded NRCMs on printed 3D microfibrous scaffold; (iv-vi) Confocal fluorescence images showing F-actin and DAPI staining of cellular attachment and alignment along iv) a single printed microfiber, (v) 2 layers of the 3D printed construct (represented as 1 and 2), and (vi) 4 layers of the 3D printed construct. (D) Immunocompatibility assessment of biomaterial ink and 3D printed constructs: i) Schematic illustrating release of pro-inflammatory molecules by mouse macrophage when exposed to 3D printed samples; Quantification of (ii) IL-1β and iii) NO release by macrophages as indicators of in vitro immunocompatibility of 3D printed SPG scaffolds compared to control samples; (iv) Schematic showing implantation of samples in left subcutaneous pocket of Sprague-Dawley rats; Images depicting (v) 3D printed scaffolds after implantation and (vi) on day 14 post-retrieval. In vivo immunocompatibility assessment via (vii) H&E staining of implanted biomaterial ink and 3D printed scaffolds post-retrieval at both low and high magnifications. Host cell infiltration observed for IBC on subcutaneous implantation at day 7 and day 14. Reproduced with permission from Ref. [369] Copyright © 2020 WILEY-VCH Verlag GmbH & Co. KGaA, Weinheim.

results showed that *A. mylitta* silk fibroin exhibited properties comparable to fibronectin, a key matrix component for cardiomyocytes, and outperformed mulberry *Bombyx mori* silk fibroin due to its RGD domains. Additionally, cardiomyocytes loaded onto *A. mylitta* 3D scaffolds formed contractile patches. These findings demonstrated that silk fibroin is a promising material for engineering functional cardiac patches [363]. In another study, Liu et al. [371] designed a biomimetic nanofiber electrospun membrane with a sandwich structure. The composite patch consisted of a stretchable polyurethane (PU) base, a middle layer of biocompatible silk fibroin methacryloyl (Silk-MA) via electrospinning, and a surface layer of Bio-ILs (biocompatible ionic liquids) for electrical conductivity [371]. The incorporation of Bio-ILs significantly enhanced electrical conductivity to 2877 mS/m and provided mild adhesive properties, minimizing tissue damage. The PU layer increased film stretchability to 250 %, while Silk-MA made the film hydrophilic, promoting a biocompatible microenvironment. In vitro cell experiments using H9c2 cells seeded on the developed membranes demonstrated low cytotoxicity and excellent biocompatibility, making the membrane a promising solution for cardiac TE [371].

Silk-based biomaterials can be genetically engineered to enhance their properties. Recombinant silk, produced through genetic engineering in organisms like bacteria or yeast, includes proteins such as fibroin [363,368] or eADF4(C16) [365,372,373]. These engineered silk proteins are used to create materials with tailored properties for diverse applications, including cardiac TE. In this field, recombinant silk proteins serve as scaffolds to support the growth and organization of cardiomyocytes [363,365,368,372]. These scaffolds mimic the heart natural environment, promoting cell attachment and growth. Being biocompatible, they avoid adverse bodily reactions and possess mechanical properties suitable for the contractile activity of heart cells [363,372]. A notable example is the eADF4(C16)-RGD protein, which supports cardiomyocyte attachment and beating, highlighting its potential for developing artificial cardiac tissues. Such materials could aid in repairing heart damage after events like heart attacks, offering a pathway to restore cardiac function [365,372].

In summary, the integration of polysaccharides, proteins and other biopolymers in the development of fiber/hydrogels for cardiac TE offers considerable potential, but each material comes with its own set of

advantages and limitations. Polysaccharides are highly biocompatible and biodegradable, making them ideal for supporting tissue regeneration as they can mimic the natural ECM [41]. Their inherent biological properties promote cell growth and tissue formation, which is important for cardiac repair. However, their generally non-conductive nature presents a significant challenge for cardiac TE, as heart tissue relies on electrical conductivity for coordinated contractions [40,41,271]. This limitation can be addressed by combining these polysaccharides with electroconductive additives allowing them to support electrical signals and enhance cardiac tissue functionality [53,96,280]. In addition, proteins are also widely used due to their strong bioactivity, promoting cell adhesion, proliferation and signaling essential for tissue regeneration [232,353,363,374]. Proteins play a suitable role in ECM of cardiac tissue, providing both structural support and biochemical signals that regulate cellular behavior essential for tissue function and repair. Their mechanical properties, such as stiffness and elasticity as well as their degradation rates can be finely tuned to match the dynamic mechanical environment of the heart, making them highly adaptable for cardiac applications [336,353,374]. When combined with polysaccharides, protein materials can get improved mechanical strength and bioactivity in hydrogels, resulting in a more balanced and functional matrix for cardiac TE [60,279,355]. The synthetic polymers even if they offer highly tunable mechanical properties, they may pose biocompatibility challenges, as they could provoke inflammatory responses or fail to integrate seamlessly with surrounding tissues [129,182,216,324,325,375]. Additionally, many synthetic polymers lack biodegradability, meaning they may need to be removed after tissue integration, potentially complicating their use in long-term applications [41,376]. Incorporating electrically conductive components into biopolymer-based hydrogels presents an exciting opportunity to address the electrical conductivity issue and further enhance their biological functionality. These conductive elements can facilitate electrical stimulation, which is important for promoting the growth and proliferation of cardiac cells in electrically conductive biopolymer-based hydrogels as well as tissue maturation, ultimately improving the performance of engineered cardiac patches [90,368,374,377,378]. The incorporation of electrically conductive materials into biopolymer-based hydrogels for cardiac TE must be precisely regulated to improve the electrical conductivity of the composite, while preserving cardiac cell functionality during cell culture and tissue formation [96,379]. Excessive incorporation of these electroconductive materials may induce cytotoxic effects, adversely affecting cell viability and physiological function. Conversely, insufficient content of conductive materials in biopolymer-based hydrogels can result in inadequate electrical conductivity of resulting composites, impeding effective signal transmission and synchronization of cardiac cells, which is essential for replicating the natural electrophysiological properties of heart tissues [60,96,114,368,374,377]. Therefore, fine tuning both the content and spatial distribution of conductive components within the hydrogels is essential to achieve an optimal balance between enhanced electrical conductivity and the maintenance of a biocompatible microenvironment conducive to cardiac cell survival and function [368,374,377].

5. Electroconductive material-filled hydrogels for cardiac tissue engineering

In cardiac TE, it has been extensively explored the integration of electrically conductive materials into biopolymer-based composite hydrogels [54,55,114,257,368]. This section highlights the role of electroconductive materials including conductive polymers, carbon-based materials and metal nanoparticles in enhancing electrical signaling for TE cardiac biomaterials as well as their promising applications in this field. Cellular interactions in electroconductive hydrogels are crucial in TE, where the combination of electroconductive materials and functional biomaterials creates a dynamic environment that significantly impacts cell behavior. These hydrogels offer a unique platform for orchestrating cellular responses [96,378,380]. Central to this interaction is the cell ability to sense and respond to electrical, biochemical, and mechanical cues, mimicking physiological conditions. The electrical conductivity of these hydrogels not only facilitates efficient signal transduction but also plays a pivotal role in influencing cell adhesion, proliferation and differentiation [381,382]. In addition, the electrical conductivity of the hydrogel enhances integrin-mediated adhesion, influencing the strength and stability of cell-substrate interactions [383]. Importantly, the conductivity of the hydrogel also plays a role in promoting cell adhesion by providing electrical cues that can influence cell behavior and signal transduction pathways involved in adhesion, migration, and differentiation [384,385]. As cells adhere and spread on the conductive hydrogel, they establish an interconnected network, forming a three-dimensional framework akin to the native tissue microenvironment. This spatial organization plays a leading role in facilitating cell signaling, nutrient exchange, and the development of cell-cell interactions [386].

5.1. Conductive polymers for tissue engineering cardiac biomaterials

Conductive polymers such as polyaniline (PANi) [60,180], poly(3,4-ethylenedioxythiophene) (PEDOT) [90,378], and PPy [375,387], have garnered significant interest in the field of cardiac TE. They exhibit suitable electrical conductivity, mechanical flexibility, and biocompatibility, making them promising candidates for the development of biomaterials for cardiac TE applications.

5.1.1. Polyaniline

PANi is a synthetic polymer with notable electrical conductivity, making it well-suited for applications in cardiovascular TE [388]. Additionally, its inherent biocompatibility and favorable processability make PANi highly noteworthy [389]. This is particularly evident in applications like cardiac patch development, where PANi can contribute significantly to both the structural integrity and bioactive functionality of hydrogels [180,185]. Integrating PANi into biopolymer-based composite inks for hydrogel manufacturing allows precise control over the hydrogel electrical properties, promoting essential interactions vital for cardiac tissue development [388]. The microstructure of electrospun fiber mats containing PANi revealed homogeneous morphologies (Fig. 16A). PANi-based materials were obtained by incorporating PANi in collagen/hyaluronic acid (HA)/PANi composites [60]. Specific structures formed by phase separation and hydrogen bonding were observed in all mats, enhancing electrical conductivity, porosity, mechanical properties, and cell attachment. Quantifications revealed 60–64 % porosity, with PANi4 mats exhibiting aligned fibers (Fig. 16A) [60]. Cellular viability analysis after 48 h, revealed that PANi percentages exceeding 0.08 % in the composites decreased viability compared to collagen–HA (Fig. 16B(i,ii)) [60]. Beating behavior analysis at day 5 using muscle motion, showed a correlation between contraction duration and PANi concentration (Fig. 16C(i)). Compared to mats without PANi, PANi-based mats exhibited longer contraction times, greater amplitudes, and lower beating rates, making them more favorable for cardiac TE (Fig. 16C(ii–iv)). Graphs exhibiting speed of contraction of cells cultured in different materials demonstrated appropriate characteristics (Fig. 16C(v–x)) [60]. Electroactive and biocompatible fibrous scaffolds, composed of polyaniline (PANi) doped with dodecylbenzenesulfonic acid (DBSA) along with poly(lactic acid) (PLA) and PLA/poly (ethylene glycol) (PEG) mixtures were also developed. The structure of both simple and core–shell fibers, obtained through uniaxial and coaxial electrospinning respectively, was confirmed by Fourier-transform infrared and micro-Raman spectroscopies [185]. Morphological studies revealed that the addition of PEG improved the interactions between PLA and PANi polymeric chains, allowing for better control of fiber thickness. Both PANi and PEG affected the thermal and electrical properties of the composites, lowering the glass transition temperature and increasing electrical conductivity. Despite high cytotoxicity

observed for PANi/DBSA composites, studies on PLA/PANi fibers demonstrated a reduction in harmful effects as the conducting polymer is mainly retained inside the fibers through favorable PANi/PLA interactions [185]. Morphological and functional studies with cardiac cells suggested that the fabricated fibrous scaffolds were suitable for cardiac TE [185].

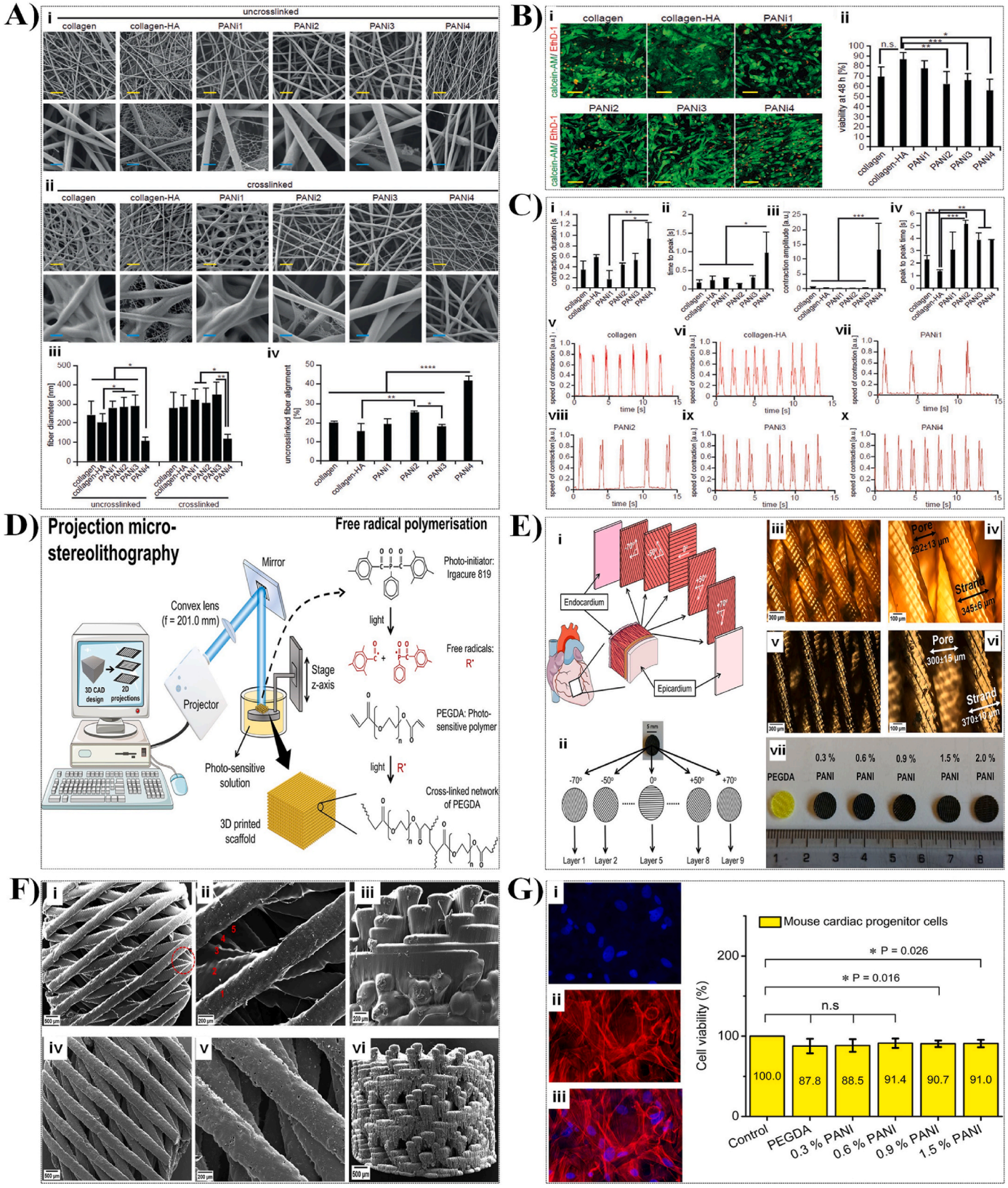

(caption on next page)

Fig. 16. (A) Morphological characterization of electrospun collagen, collagen/HA, and collagen/HA/PANi blends. (i) SEM images depicting the morphology of uncrosslinked electrospun fiber mats. (ii) SEM images illustrating the morphology of electrospun fiber mats after crosslinking with glutaraldehyde vapor. (iii) Quantitative assessment of fiber diameter. (iv) Quantitative evaluation of fiber alignment. Data presented as mean ± standard deviation (SD), Scale bars: yellow, 2 μm; blue, 0.2 μm. (B) Viability of cardiomyocytes on electrospun fiber mats. i) Representative images showing the viability of neonatal rat cardiac cells cultured on electrospun fiber mats at 48 h, based on live and dead staining by calcein (green, living) and ethidium homodimer-1 (EthD-1, red, dead). (ii) Quantitative analysis of live and dead staining in panel (i). Data presented as mean ± SD, Scale bars: 25 μm. (C) Muscle motion analysis of cardiomyocyte beating behavior on different fiber mats. Quantitative analysis of (i) contraction duration, (ii) time-to-peak, (iii) contraction amplitude, and (iv) peak-to-peak time at day 5. Examples of the speed of contraction on day 5 for (v) collagen, vi) collagen–HA, (vii) PANi1, (viii) PANi2, (ix) PANi3, and (x) PANi4. Data presented as mean ± SD. Reproduced with permission from Ref. [60], Copyright © 2020 WILEY-VCH Verlag GmbH & Co. KGaA, Weinheim. (D) Schematic of the custom-built 3D printing micro-stereolithography setup. (E) Structure and morphology of the printed scaffolds: (i) Myofibers in the myocardium are oriented at various angles in a hierarchical manner, (ii) scaffolds were fabricated by stacking layers aligned along these angles, (iii, iv) non-conductive PEGDA scaffold at 5X and 10X magnification, (v, vi) conductive scaffold (0.3 % PANI) at 5X and 10X magnification, (vii) scaffolds with varying PANi concentrations. Reproduced with permission from Ref. [390] Copyright © 2023 Springer Nature. (F) Hierarchical morphology: (i) PEGDA scaffold at 44X, (ii) PEGDA scaffold at 133X with layers rotating at certain angles, (iii) cross-section at 107X, (iv, v) PEGDA scaffold with 2.0 % PANI at 44X and 133X, (f) cross-section at 67X showing layered deposition. (G) Viability of mouse cardiac progenitor cells (mCPCs) on printed scaffolds: Micrographs showing mCPCs stained with (i) DAPI (blue nuclei), (ii) F-actin (red), and (iii) merged image. Right image: cell viability assessed via Trypan Blue assay after 5 days of culture. Bars represent cell viability relative to the control. Data shown as Mean ± S.D of triplicate experiments. Reproduced with permission from Ref. [390] Copyright © 2023 Springer Nature.

The integration of PANi into composite hydrogels using 3D printing has demonstrated remarkable success in achieving suitable electrical conductivity. Through precise 3D printing methods, PANi can be distributed within hydrogel scaffolds to create a conductive network. Studies have revealed that such composite hydrogel scaffolds exhibited conductivity levels suitable for supporting the alignment and functionality of cardiomyocytes [185,391]. This is of utmost importance in cardiac TE, where the orchestrated contraction of cardiomyocytes relies on complex electrical signals. For instance, Ul Haq et al. [390] fabricated electrically conductive scaffolds mimicking the directional alignment of muscle fibers in the myocardium using 3D printing micro-stereolithography (Fig. 16D). A composite ink was formulated using polyethylene glycol diacrylate (PEGDA), Irgacure 819 (photo--initiator), curcumin (dye), and PANi to enable free radical photo-polymerization [390]. The scaffold design replicated the varying angles of myofibers in the myocardium (Fig. 16E(i)), with each layer oriented accordingly (Fig. 16E(ii)). Optical images (Fig. 16E(iii–vi)) displayed the 3D-printed scaffolds, showing conductive scaffolds containing PANi with an average strand diameter of 370 ± 10 μm [390]. PANi imparted semi-conductive properties ((Fig. 16E(vii)). The scaffolds exhibited a conductivity of approximately 10^{-6} S/m. Structural analysis via SEM confirmed the hierarchical morphology of the scaffolds (Fig. 16F). The conductive nature of the scaffolds potentially improved the viability of mouse cardiac progenitor cells (mCPCs) compared to non-conductive scaffolds (Fig. 16G) [390].

5.1.2. Poly(3,4-ethylenedioxythiophene)

PEDOT is a conductive polymer which consists of a thiophene backbone with ethylenedioxy linkages, conferring outstanding electrical conductivity and electroactivity [392]. As a component in electrically conductive hydrogels, PEDOT can efficiently facilitate electron transport in the matrix, allowing for precise electrical signaling, vital in cardiac TE [393]. Roshanbinfar et al. [114] used PEDOT:poly(styrenesulfonate) (PEDOT:PSS) in a biohybrid hydrogel composed of collagen and alginate to engineer cardiac tissues by casting. They observed that these electroconductive biohybrid hydrogels enabled enhanced maturation and beating properties. Abedi et al. [226] developed chitosan scaffolds incorporating poly(3, 4-ethylenedioxythiophene):poly(styrenesulfonate) (PEDOT:PSS) using electrospinning technology for cardiac TE. The addition of PEDOT:PSS to the chitosan matrix not only enhanced mechanical and electrical aspects but also improved cell viability in composites. A substantial reduction in fiber diameter and a remarkable increase in electrical conductivity was achieved with a 1 wt% PEDOT:PSS content in the electrospun composites [226]. Luque et al. [394] developed a printable cardiac hydrogel to address the limited repair ability of damaged myocardium, a major contributor to myocardial cardiopathy. The hydrogel matrix was composed of poly(vinyl alcohol) cross-linked with gallic acid and PEDOT, yielding patches with suitable electrical conductivity, elasticity and mechanical strength, essential for enhancing cardiac contraction and impulse propagation [394]. The hydrogel was compatible with direct ink writing and demonstrated efficiency in propagating electrical signals in adult mouse cardiomyocytes by stimulating intracellular Ca^{2+} transients. Implanted in healthy mouse hearts, the patches showed biocompatibility and maintained essential cardiac function after two weeks, highlighting their therapeutic potential [394]. Roshanbinfar et al. [90] developed a collagen-PEDOT:PSS hydrogel for myocardial infarction treatment, aiming to address ventricular tachycardia (VT) and promote cardiac remuscularization. They demonstrated the use of PEDOT:PSS in hydrogels, improving collagen gel formation, micromorphology, and conductivity [90]. The combination of this bio-ink with hiPSC-derived cardiomyocytes enhanced contractility, calcium handling, and conduction velocity, with RNA-sequencing showing improved cell maturation and matrix interactions. The hydrogel, when injected into infarcted mouse hearts, reduced VT to levels similar to healthy hearts, offering a promising platform for cardiac injury treatment [90].

5.1.3. Polypyrrole

PPy is a leading electroconductive polymer possessing a chemical structure characterized by a conjugated backbone formed by a pyrrole monomer [221,387]. When integrated into hydrogels, PPy enhances both the mechanical and electrical properties of the composite material. Additionally, its influence extends to facilitating cell alignment, a key factor in fabricating functional and organized cardiac constructs [375]. Liang et al. [221] employed electrospinning to fabricate conductive nanofibers encapsulating PPy. The electrospun composites were prepared at different ratios PPy-to-silk fibroin. The resulting PPy-embedded mats exhibited reduced fiber diameters (0.431 ± 0.060 μm), closely resembling myocardium fibrils. Mats containing 7 % silk fibroin demonstrated interesting mechanical properties (1.437 ± 0.044 MPa) close to native myocardium and a PPy-to-silk fibroin ratio of 15:85 provided optimal electrical conductivity [221]. In this study, HL-1 cells were employed to assess biocompatibility. Neonatal rat cardiomyocytes (NRCMs) and hiPSC-derived cardiomyocytes were chosen for evaluating cardiac muscle contraction, due to their better contractility. Cell viability and metabolic activity of mats containing PPy, compared to those without PPy, showed interesting cytocompatibility (Fig. 17A and B). The metabolic rate of HL-1 cells increased across all groups from day 4 to day 8 (Fig. 17C). Cells cultured on PPy-containing mats showed higher absorbance compared to those on pure SF mats. NRCMs seeded PPy-silk fibroin electrospun scaffolds were examined for cell spreading [221]. The NRCMs successfully attached to and spread across the mats, interacting with PPy-silk fibroin fibers in various ways. Initially, NRCMs adhered to and grew along the fibers (Fig. 17D). They extended cellular processes to grip distant fibers, increasing their size (Fig. 17D). NRCMs

not only spread on the mat surface but also extended pseudopodia beneath fibers, establishing direct cell-cell contacts (Fig. 17E) [221]. Moreover, aligned fibers were observed in limited regions of the PPy-based mats, influencing NRCM morphology and orientation (Fig. 17F). The contraction of NRCM-seeded mats was monitored. By Day 7, 7 %PPy15 mats showed stable, regular contractions (average beat per minute: 39 ± 8, displacement: 5.68 ± 0.57 μm, Fig. 17G). Mats with higher PPy content exhibited vibrations; notably, 7 %PPy40 vibrated more intensely than 7 %PPy30 (Fig. 17H and I) [221]. Another research work focused on synthesized polypyrrole nanoparticles (PPy-NP) through the mini-emulsion method, followed by their integration in a gelatin (Gel)/hyaluronic acid (HA) hydrogel to fabricate electroconductive Gel:HA:PPy-NP composite scaffolds for electroactive TE [241]. These scaffolds exhibited commendable mechanical properties (1.08 ± 0.26 MPa), closely matching the spinal cord performance. Designed with controlled porosity and reaching electrical conductivities of $4.3 \times 10^{-6} \pm 1.1 \times 10^{-6}$ S cm^{-1}, Gel:HA:PPy-NP scaffolds underwent 3D printing into predefined lattice geometries with suitable post-printing shape fidelity (Fig. 17J) [241]. The in vitro biological assessments of the fabricated composites demonstrated their cytocompatibility, with high viability of mesenchymal stem cells (MSCs) and neuronal stem cells (NSCs) recorded as shown in Fig. 17K. MSC attachment was prominent, with cells growing in clusters in the scaffold grooves and pores [241]. The attached cells exhibited spindle-like projections, aligning with normal MSC morphology. Neuronal stem cells (NSCs) seeded and cultured on Gel:HA:PPy-NP scaffolds displayed successful attachment with visible cellular projections (Fig. 17L). Similar to MSCs, NSCs formed clusters on the scaffold surface, determined by the scaffold topography [241].

5.2. Carbon-based materials

Carbon-based materials, specifically carbon nanotubes and graphene are remarkable components for fabricating electroconductive hydrogels [53,55,374,377,395].

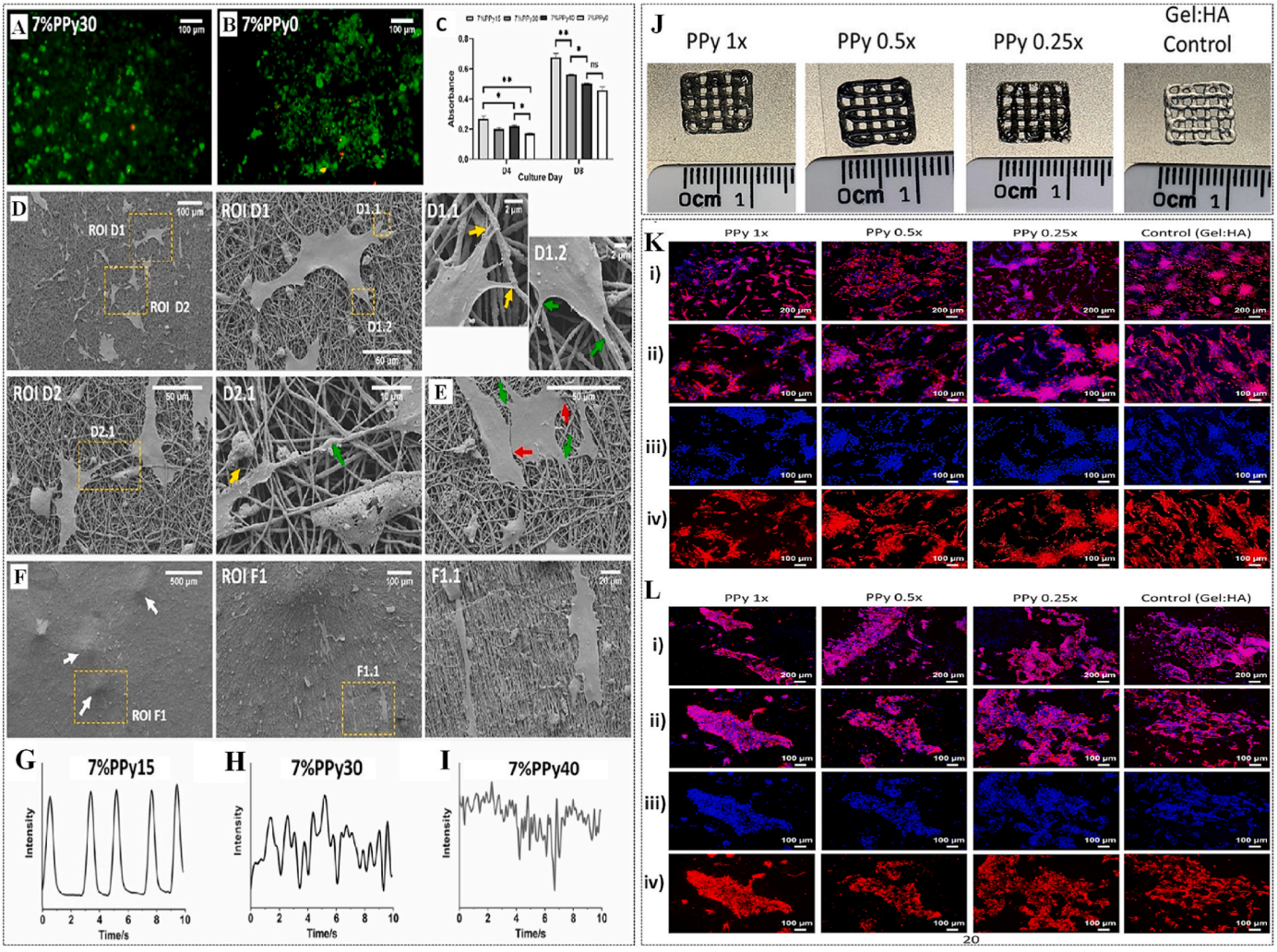

Fig. 17. (A–I) Cardiomyocytes (CMs) on electrospun (PPy, SF) mats. (A,B) Live/Dead staining of HL-1 cells cultured on 7 % PPy30 and 7 % PPy0. (C) Metabolic activities of HL-1 cells on electrospun (PPy, SF) mats from Day 4 to Day 8 (n = 3). (D–E) SEM images of Neonatal Rat Cardiomyocytes (NRCMs) on electrospun (PPy, SF) mats. (F) SEM images of NRCMs in regions with aligned PPy-SF fibers. Yellow dash boxes indicate Regions of Interest (ROIs). Yellow and white arrows denote cell adhesion sites on fibers and PPy-induced humps, respectively. Green and red arrows indicate CMs spreading on top of and beneath fibers. (G–I) Contraction cycles of NRCM-seeded mats. Reproduced with permission from Ref. [221] Copyright © 2021 Elsevier. (J) 3D printed lattices of Gel:HA:PPy-NP hydrogels before the introduction of a crosslinking regime. (K,L) Mesenchymal Stem Cells (MSCs) and Neuronal Stem Cells (NSCs) cultured on Gel:HA:PPy-NP scaffolds exhibit good cellular morphology and attachment in vitro. K) MSCs previously stained with DiI (red) seeded on Gel:HA:PPy-NP scaffolds with different PPy NP concentrations for 96 h, fixed with PFA, and stained with DAPI (blue). (i) DiI/DAPI, (ii) DiI/DAPI, (iii) DAPI, (iv) DiI [241]. L) NSCs previously stained with TdTomato (red) seeded on Gel:HA:PPy-NP scaffolds with different PPy NP concentrations for 96 h, fixed with PFA, and stained with DAPI (blue). (i) TdTomato/DAPI, (ii) TdTomato/DAPI, (iii) DAPI, and (iv) TdTomato. Reproduced with permission from Ref. [241] Copyright © 2023 Springer Nature.

5.2.1. Carbon nanotubes

Carbon nanotubes are cylindrical structures composed of carbon atoms arranged in hexagonal patterns, forming single or multiple layers. The two main types of CNTs are single-walled carbon nanotubes (SWCNTs) and multi-walled carbon nanotubes (MWCNTs) (Fig. 18A). SWCNTs consist of a single layer of carbon atoms composed of sp^2 hybridized carbon, resembling a rolled-up graphene sheet, while MWCNTs comprise multiple concentric layers [396]. The specific arrangement of carbon atoms imparts remarkable mechanical, electrical, and thermal properties to CNTs. The ballistic transport of electrons along the length of the nanotubes contributes to their superior conductive properties [397]. In addition, the tensile strength of CNTs render them invaluable for reinforcing the mechanical properties of hydrogels. Aside from their notable electrical conductivity, CNTs possess unique electronic and optical properties that render them instrumental in the development of electronic devices [396,398]. The high aspect ratio of CNTs facilitates the formation of a network-like structure in composites, even at low concentrations. This structural arrangement further enhances their utility in various potential applications, underlining the versatility of CNTs in electronic and structural domains [399]. However, the use of carbon nanotubes (CNTs) in hydrogels for cardiac TE can present several challenges and risks, particularly regarding their potential cytotoxicity. CNTs can enter cells through endocytosis or mechanically pierce the cell membrane like needles, leading to potential cellular damage and disruption of normal cellular functions, which can result in cell death [400,401]. These nanomaterials have sharp, rigid, and elongated structures that may mechanically puncture the lipid bilayer of cell membranes, potentially resulting in cell damage or death. Additionally, their small size enables easy penetration into tissues, which could trigger localized inflammation or oxidative stress through the production of reactive oxygen species (ROS), DNA damage, lysosomal disruption, mitochondrial dysfunction, and eventual cell death through apoptosis or necrosis [402,403]. While CNTs can improve the electrical conductivity and mechanical properties of hydrogels, their long-term biocompatibility is still uncertain. There is a significant concern about chronic inflammation and immune responses, which could impair the healing process and interfere with the integration of engineered tissue with the host myocardium. The risk of chronic toxicity and adverse immune reactions remains a major obstacle in ensuring the safe and effective use of CNT-based hydrogels for cardiac tissue regeneration [400,404]. Despite these disadvantages, upon integration into hydrogel matrices, CNTs significantly enhance electrical conductivity, playing an important role in the development of electrically conductive hydrogels tailored for TE [55,96,405]. The synergistic incorporation of CNTs into hydrogels imparts a dual advantage, reinforcing the mechanical integrity of the scaffold and endowing it with electrical conductivity. The resulting composite material could mimic the native myocardium more closely, facilitating optimal cell alignment and contractility [374]. The enhanced electrical properties enable efficient signal propagation, fostering synchronized cellular responses within the engineered cardiac tissue [55,374,406].

Mombini et al. [407] fabricated electrospun nanofiber scaffolds, comprising polyvinyl alcohol (PVA), chitosan, and varied CNT concentrations offering a biomimetic environment resembling the native cardiac tissue matrix [407]. An optimized PVA-CHI-CNT scaffold, incorporating 1 % CNT, demonstrated exceptional properties: an elastic modulus of 130 ± 3.605 MPa, electrical conductivity of 3.4×10^{-6} S/cm, high-water uptake, high cell adhesion, and over 80 % cell viability. Subsequent differentiation of rat mesenchymal stem cells (MSCs) into cardiomyocytes on the optimal scaffold, aided by electrical stimulation, significantly increased cardiac marker expression [407]. Gerasimenko et al. [408] developed a laser-based printing technology to fabricate structures from composite layers of lyophilized bovine serum albumin (BSA), bovine collagen (BC), and chitosan succinate (CS) with single-walled carbon nanotubes (SWCNT) for cardiovascular devices and TE implants [408]. SEM images revealed smooth surfaces for biopolymer composites, with increased roughness and porosity upon laser exposure at various energy thresholds (Eth) (Fig. 18B). Notably, bimodal pore distribution with large pores (100–200 μm) and small pores (1–5 μm) was achieved for BSA/BC/CS with SWCNT at specific Eth values, crucial for cell adhesion, proliferation, vascularization, and innervation processes (Fig. 18B) [408]. Laser-fabricated composite layers demonstrated higher conductivity, maximum hardness, and improved endothelial cell viability compared to thermostat layers. Fluorescence microscopy confirmed cell compatibility, highlighting the potential of these composite layers for tissue regeneration from implantation (Fig. 18C) [408]. Gelatin (Gel) and single-walled carbon nanotubes (SWCNTs) were used to physico-chemically and biologically modify polyurethane nanofibers followed by the application of electrospinning, a versatile technique for producing functional nanoscale fibers [409]. Mean diameters of nanofibrous Gel/SWCNTs scaffolds from 210 to 140 nm were obtained, impacting initial cell behavior [409]. Scaffold degradation was tailored by incorporating gelatin, contributing to biomimetic mechanical properties resembling normal blood vessels. SWNTs enhanced the Young's modulus and ultimate strength, reaching 16.47 ± 0.5 and 23.73 ± 0.5 MPa, respectively, while gelatin increased elongation at break. SWCNTs significantly improved electrical conductivity. Biological evaluation confirmed dense cell coverage after 7 days, indicating the potential effectiveness of these scaffolds for cardiovascular TE [409]. Furthermore, Kharaziha et al. [410] developed enhanced electrical properties in tough and flexible hybrid scaffolds by embedding CNTs within aligned poly(glycerol sebacate) (PG):gelatin electrospun nanofibers to mimic the native myocardium ECM (Fig. 18D). Gelatin cross-linking using 1-ethyl-3-(3--dimethylaminopropyl)carbodiimide/N-hydroxysuccinimide [410]. Varying CNT concentrations in PG-based nanofibrous scaffolds (CNT/PG scaffolds) significantly improved fiber alignment, electrical conductivity, and toughness while supporting cardiomyocyte (CM) viability, alignment, and contractile activities. CNT-PG scaffolds exhibited stronger beating behavior, lower excitation thresholds, and higher capture rates than PG scaffolds (Fig. 18D) [410]. Immunofluorescence staining demonstrated well-developed sarcomeric structures and enhanced Cx43 expression on CNT/PG scaffolds, indicating improved cell coupling and contractile properties (Fig. 18D). The aligned CNT/PG scaffold showcased superior mechanical properties compared to those of PG scaffolds, emphasizing its potential for generating well-organized and mature cardiac tissues [410].

5.2.2. Graphene

Graphene is a carbon-based material consisting of a single layer of carbon atoms arranged in a hexagonal lattice, forming a two-dimensional honeycomb pattern. It exhibits exceptional electrical conductivity and has a large surface area [411,412]. In addition, graphene possesses outstanding mechanical properties. Ideally, its Young's modulus can reach 1 TPa, and its tensile strength can reach 130 GPa [413,414]. Moreover, graphene is known for its outstanding flexibility, allowing it to bend and stretch without losing structural integrity. When graphene is incorporated into hydrogels, it enhances the overall performance of the composite material with its advantageous properties [415]. The integration of graphene in biomaterials enhances electrical coupling, a crucial factor in the development of functional cardiac tissue constructs.

Chemical modifications particularly oxidation and reduction, play a crucial role in tailoring graphene for the development of hydrogels with enhanced functional properties in cardiac TE [115]. These functional groups can enhance interactions with biomolecules and other components, facilitating the integration of graphene into complex hydrogel networks. In addition, these modifications also improve the dispersibility of graphene in aqueous solutions, preventing aggregation and enhancing its integration into the hydrogel matrix [115]. Graphene oxide (GO) is initially produced through oxidation, introducing oxygen-containing functional groups such as hydroxyl, epoxy, and

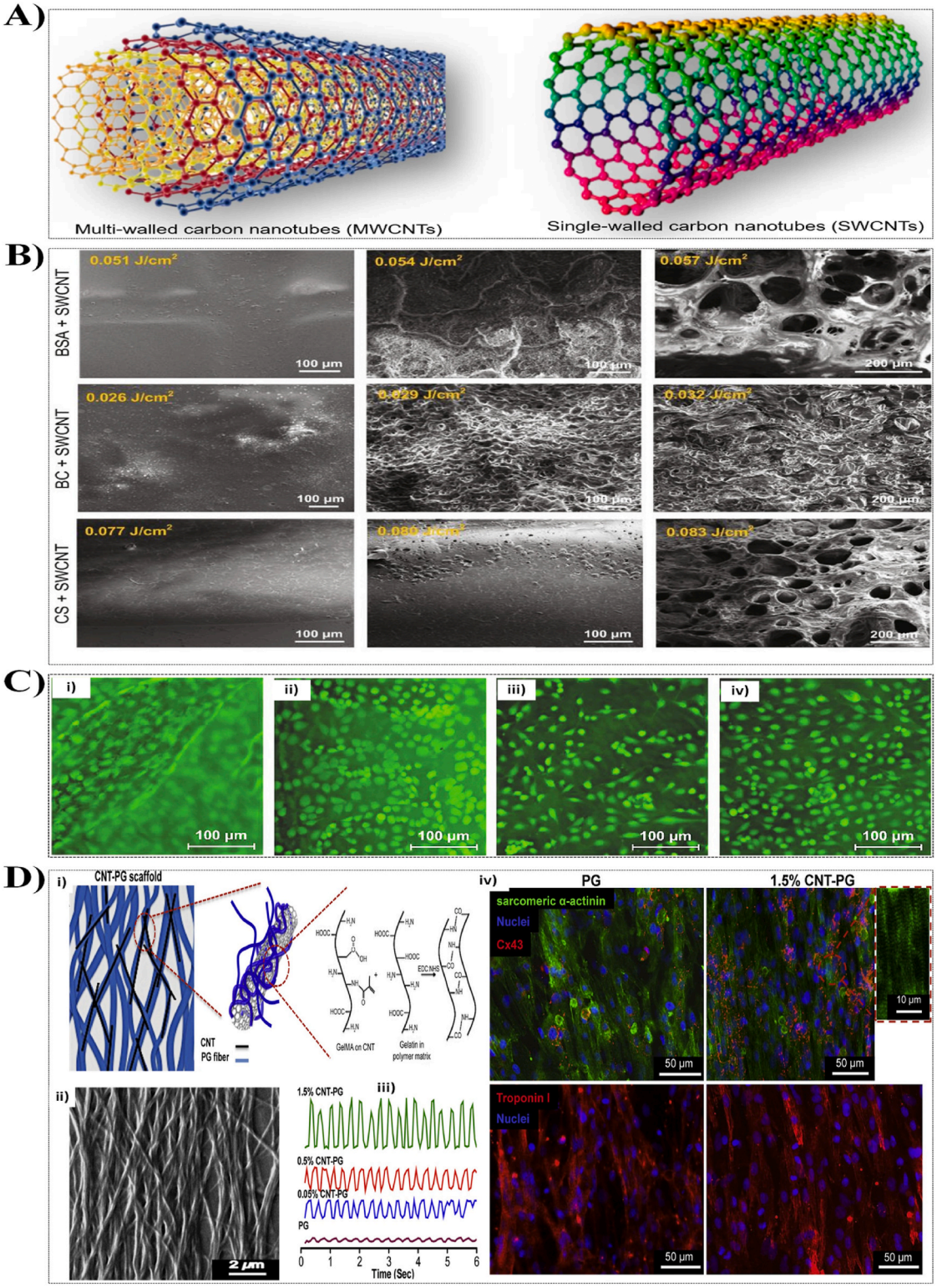

Fig. 18. (A) Nanostructures of multi-wall carbon nanotubes (MWCNTs) (left) and single-wall carbon nanotubes (SWCNTs). Reproduced with permission from Ref. [396] Copyright © 2020 Royal Society of Chemistry. (B) SEM images of developed composites. (C) Fluorescence microscopy images capture endothelial cells within the structure of composite layers from BSA (i), BC (ii), CS (iii) with SWCNT (0.01 wt%), and a control sample (iv). Reproduced with permission from Ref. [408] Copyright © 2021 Elsevier. (D) (i) Schematic representation illustrates CNT interactions with PG scaffold upon cross-linking with EDC/NHS, (ii) SEM images display cross-linked 1.5 % CNT-PG scaffold, (iii) Contraction patterns of electrically stimulated CMs on PG scaffold versus CNT-PG scaffold after 7 days of culture, (iv) Immunofluorescence staining for sarcomeric a-actinin (green), Cx43 (red), and DAPI (blue), as well as Troponin I (red) and DAPI (blue) after 7 days of culture, revealing organized sarcomeres with higher Cx43 expression on 1.5 % CNT-PG than PG scaffold. A high-magnification image (inset in Fig. 18D(iv) shows interconnected sarcomeric structures perpendicular to the direction of the nanofibers. Reproduced with permission from Ref. [410] Copyright © 2014 Elsevier.

carboxyl moieties onto graphene sheets. The resulting GO exhibits improved hydrophilicity, facilitating its integration into hydrogel matrices [416]. While GO exhibits improved hydrophilicity and dispersibility in aqueous solutions, it inherently compromises electrical conductivity due to disruptions in the sp^2 hybridization [417]. To enhance the mechanical and electrical properties of hydrogels, GO is subsequently reduced to form reduced graphene oxide (rGO). This reduction process removes some oxygen functionalities, partially restoring the sp^2 carbon network and increasing electrical conductivity [418]. Fig. 19A displays the structure of graphene, GO and rGO. The controlled balance achieved through oxidation and reduction allows for the optimization of graphene-based hydrogels, ensuring improved mechanical strength, electrical conductivity, and biocompatibility. These tailored hydrogels, laden with rGO, provide a supportive environment for cardiac tissue regeneration, promoting cell adhesion, alignment, and maturation [419,420].

Zhao et al. [421] conducted a research study aiming to develop silk nanofibrous biomaterials modified with reduced graphene oxide (rGO) to guide the formation of electrically interconnected networks in excitable tissues. Silk fibroin solutions were electrospun with a poly(ethylene oxide) (PEO) solution, and rGO solutions at various concentrations were applied onto the electrospun silk mat to achieve controlled rGO coating densities [421]. Various rGO/silk scaffolds were synthesized in this study. Scanning electron microscopy (SEM) images revealed a gradual blurring of the nanofibrous morphology in the rGO/silk materials as the rGO coating thickness increased (Fig. 19B). The composite nanofibrous scaffolds, applied for cardiac TE, demonstrated the ability to promote cardiomyocyte growth and proliferation, tissue formation, expression of cardiac-specific proteins, and the formation of sarcomeric structures and gap junctions (Fig. 19C–D) [421]. External electrical stimulation further enhanced the maturation of cardiomyocytes cultured on these scaffolds (Fig. 19D). The results highlighted the potential of rGO-functionalized silk biomaterials to mimic electrical microenvironments for regenerating functional excitable tissues [421]. Arici et al. [422] developed carboxymethyl cellulose (CMC)/gelatin (Gel)/graphene oxide (GO)-based scaffolds using extrusion-based 3D printing for cardiac tissue regeneration. SEM images of 3D printed scaffolds achieved are shown in Fig. 19E and images after 28 days of incubation in PBS buffer are shown in Fig. 19F. Rheological studies indicated that CMC enhanced the viscosity and printability of the inks. The printed cardiac patches were cross-linked using different concentrations of 1-Ethyl-3-(3-dimethylaminopropyl)carbodiimide (EDC)/N-hydroxysuccinimide (NHS), and their mechanical properties, electrical conductivity, contact angle, and degradation rates were analyzed [422]. Cell culture studies with H9c2 cardiomyoblasts showed good cell viability, with the optimal EDC/NHS concentration producing stable, flexible, and stiff scaffolds. The patches exhibited increased flexibility and mechanical strength compared to those that did not incorporate graphene, with CMC/Gel/GO patches showing improved electrical conductivity (7.0×10^{-3} S cm^{-1}), making them suitable for mimicking native myocardium. The addition of GO and higher CMC concentrations significantly improved cell viability (Fig. 19G) [422].

5.3. Metal nanoparticles for electroconductive TE cardiac biomaterials

Metal nanoparticles, including the silver and gold ones, play a vital role in augmenting the properties of electrically conductive hydrogels for cardiac TE [54,377,424–426].

5.3.1. Silver nanoparticles

Silver nanoparticles (AgNPs) exhibit a range of physicochemical attributes that make them particularly appealing for biomedical applications [427]. With diameters typically ranging from 1 to 100 nm, AgNPs offer a high surface area-to-volume ratio, optical tunability and potent antimicrobial properties [428,429]. The combination of their electrical conductivity and intrinsic antimicrobial properties positions them as valuable assets in addressing infection-related concerns in cardiac applications [427]. Research studies illustrated the efficacy of AgNPs in preventing bacterial contamination in hydrogels. AgNPs actively inhibited bacterial growth [430,431]. The synergistic combination of hydrogel flexibility and the enhanced strength imparted by AgNPs results in a scaffold capable of withstanding the dynamic mechanical forces inherent in the cardiac environment, providing a supportive matrix for cell growth and tissue organization [377]. Studies have also suggested that AgNPs can contribute to angiogenesis. The pro-angiogenic effects of AgNPs-based hydrogels enhance their utility in promoting a vascularized cardiac microenvironment [432].

AgNPs have recently emerged as interesting candidates for improving the electrical and mechanical characteristics of non-conductive scaffolds in cardiac TE through the fabrication of electroconductive nanocomposites [377]. Allison et al. [433] designed electrospun collagen-fibrous materials containing spherical AgNPs. The resulting composite displayed comparable morphology to the control (without AgNPs) but exhibited improved electrical conductivity (Fig. 20A). The incorporation of AgNPs resulted in an eightfold increase in the electrical conductivity of the fibers (Fig. 20A) [433]. Under electrical stimulation using chronic paced electrical cell stimulation system (CPACE® system), cells cultured on AgNPs-containing fibrous materials increased Cx43 expression and neonatal cardiomyocyte proliferation. Collagen fibers, with and without AgNPs, exhibited α-sarcomeric actinin (α-SA) expression, maintaining cardiomyocyte phenotype effectively (Fig. 20B(i)) [433]. Cx43 expression was notably doubled in cells seeded on fibers containing AgNPs that were electrically stimulated, while significantly lower Cx43 levels were observed in non-paced samples (Fig. 20B(ii)). These composites also prevented biofilm formation and did not activate macrophages [433]. Nazari et al. [377] synthesized reduced graphene oxide-silver (rGO-Ag) nanocomposites (1 and 2 wt%) and incorporated them into polyurethane (PU) nanofibers using the electrospinning technique. Human cardiac progenitor cells (hCPCs) were then seeded on these scaffolds for in vitro studies [377]. In vitro studies using PU and PU/nanocomposites scaffolds revealed good cytocompatibility of hCPCs, confirmed by MTT assay and scanning electron microscopy studies showing cell attachment (Fig. 20C) [377]. Real-time polymerase chain reaction (PCR) and immunostaining demonstrated upregulated cardiac-specific genes in the PU/rGO-Ag scaffolds, including GATA-4, T-box 18 (TBX 18), cardiac troponin T (cTnT), and alpha-myosin heavy chain (α-MHC), compared to neat PU (Fig. 20D), indicating the potential of these nanofibrous rGO-Ag–reinforced PU scaffolds for cardiac tissue repair [377].

5.3.2. Gold nanoparticles

Gold nanoparticles (AuNPs) are recognized for their significant potential in enhancing the fabrication of electrically conductive hydrogels [425]. AuNPs are composed of gold atoms arranged in a nanoscale configuration, with size typically ranging from 1 to 100 nm. Their properties include a high surface area-to-volume ratio and surface plasmon resonance, making them conducive for interaction with electromagnetic fields [434]. The surface of AuNPs can be functionalized with various molecules, enabling tailored interactions with surrounding environments [435]. AuNPs exhibit tunable electrical conductivity, providing researchers with a powerful tool to finely adjust the electrical properties of hydrogel matrices [325,436]. Research studies have demonstrated the ability to modulate the electrical conductivity of AuNPs by adjusting their size, shape or surface chemistry. This tunability ensures that the hydrogel precisely meets the specific electrical requirements for fostering cellular communication and tissue regeneration [54,437]. Recently, a biohybrid hydrogel was developed to enhance the beating properties of engineered cardiac tissues and enable drug release [54]. AuNPs of various sizes (18–241 nm) and surface charges (33.9–55.4 mV), synthesized using branched polyethyleneimine (bPEI) increased gel stiffness from 91 to 146 kPa and enhanced electrical conductivity from 40 to 49–68 mS cm^{-1} (Fig. 21A) [54]. These

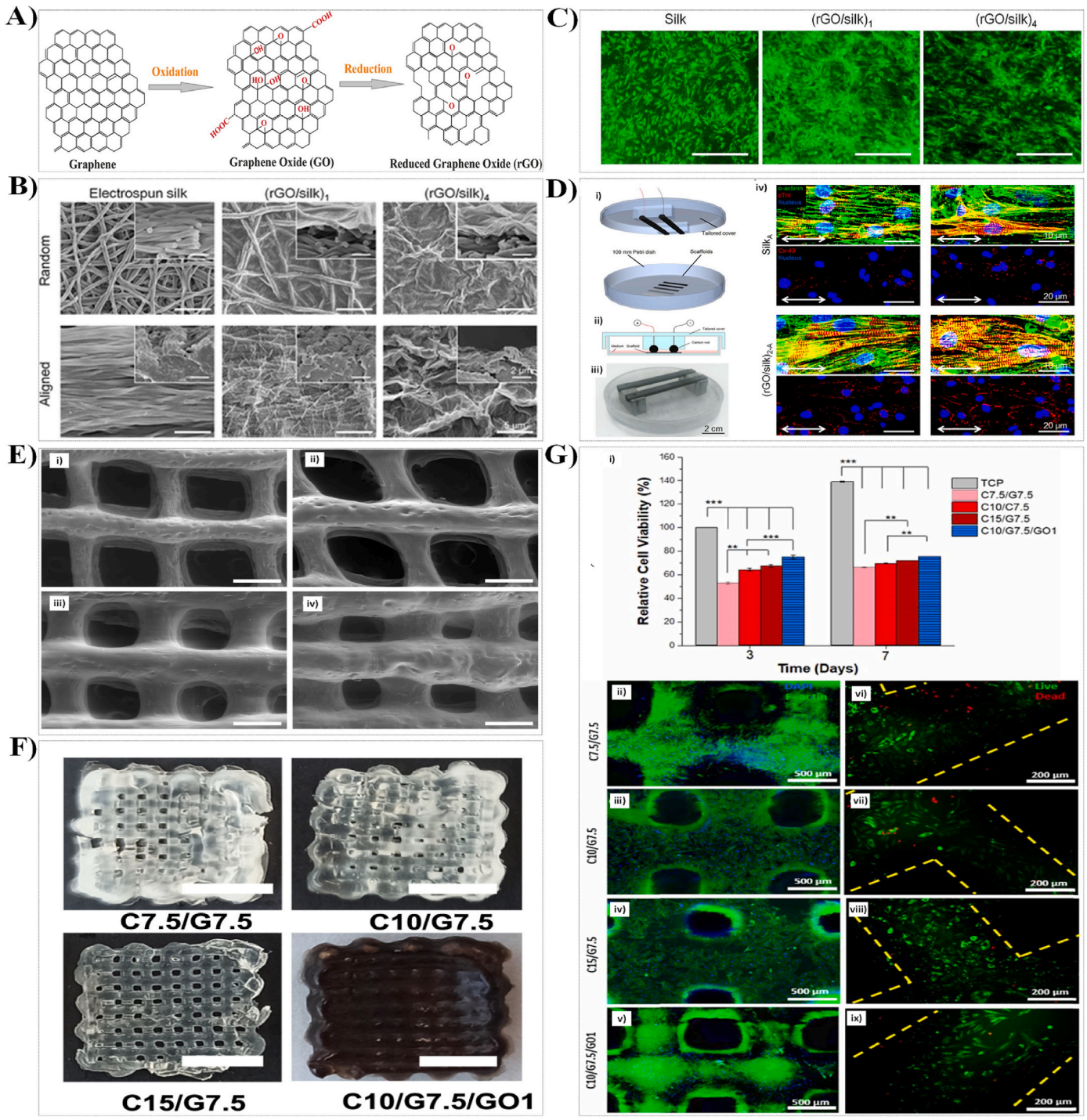

Fig. 19. (A) Schematic representation of the structures of graphene, GO, and rGO. Reproduced with permission from Ref. [423] Copyright © 2018 Springer Nature. (B) SEM images depicting the surface and cross-section of silk and rGO/silk scaffolds, showcasing an integrated rGO layer and a tunable nanofibrous morphology dependent on the coating thickness. (C) Live-dead staining of cardiomyocytes cultured on silk and rGO/silk scaffolds on day 7. (D) (i) 3D, (ii) 2D schematics, and (iii) photograph of a specially designed Petri dish cover that establishes parallel electric fields for cells when connected to an electrostimulator; iv) Immunofluorescence images illustrating the expression of α-actinin, cTnI, and Cx-43 in cardiomyocytes cultured on electrospun aligned silk ($silk_A$) and electrospun aligned silk enriched with reduced graphene oxide at a specific concentration $(rGO/silk)_{2\text{-}A}$ without and with electrical stimulation. The double arrows indicate the orientation of the nanofibers in the aligned groups. Reproduced with permission from Ref. [421] Copyright © 2018 Springer Nature. (E) SEM images of cardiac patches: (i) C7.5/G7.5, (ii) C10/G7.5, (iii) C15/G7.5, and (iv) C10/G7.5/GO1 (F) Images of samples after 28 days of incubation. (G) i). Relative cell viability of H9c2 cardiomyoblasts cultured on CMC/Gel cardiac patches at days 3 and 7. (ii–v) Fluorescence images and (vi–ix) live/dead staining of H9c2 cells on 3D-printed cardiac patches at day 3. The dotted yellow lines indicate the locations of the filaments. Results are presented as mean ± SD. Reproduced with permission from Ref. [422] Copyright © 2025 IOPscience.

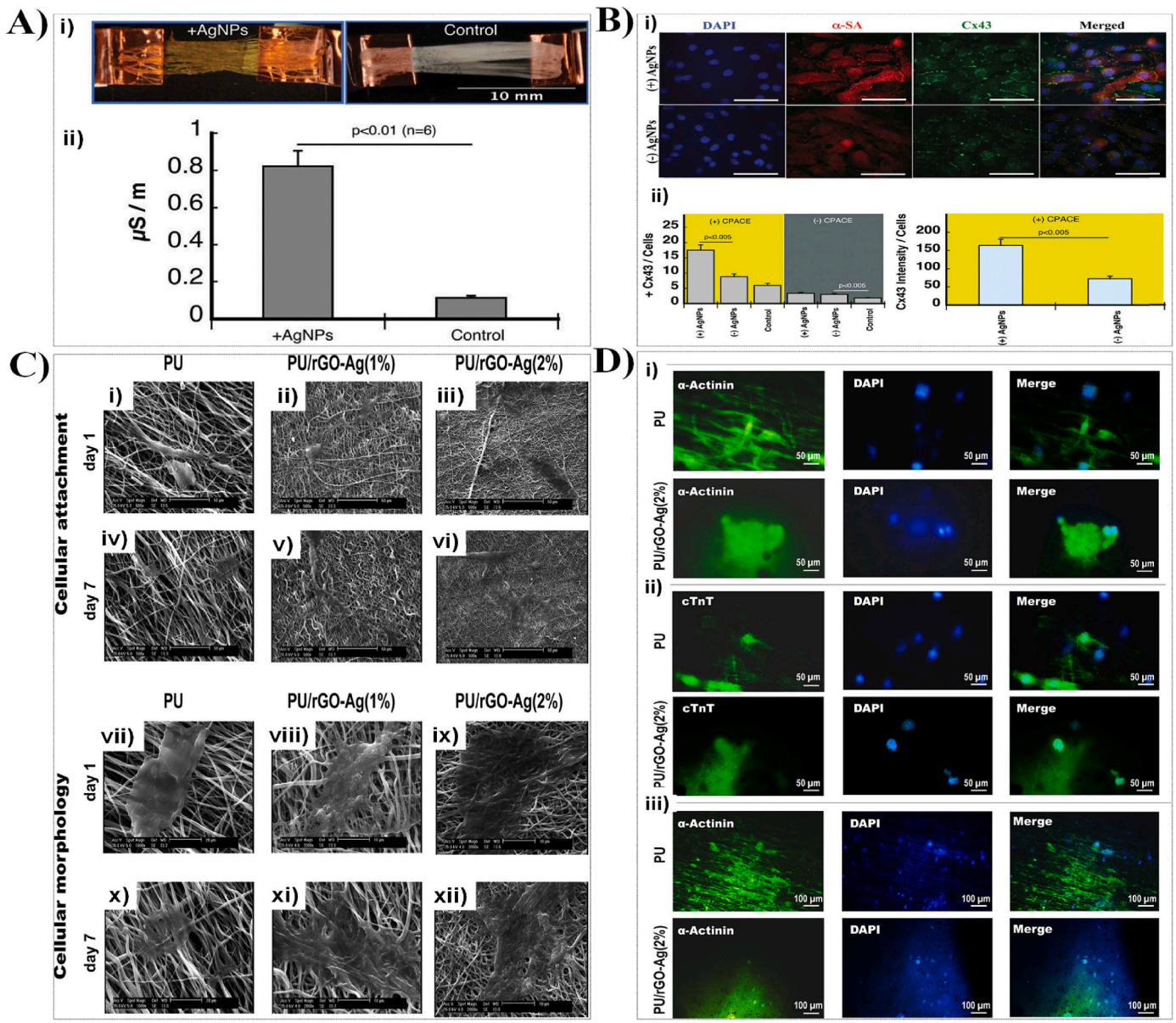

Fig. 20. (A) (i) Images of collagen fibers with and without silver nanoparticles (AgNPs) used for electrical conductivity measurement, (ii) Electrical conductivity results for collagen fibers with and without AgNPs. (B) (i) Confocal fluorescence microscopy images of neonatal cardiomyocytes on collagen fibers with and without AgNPs after 24 h electrical stimulation. Cells were stained for nuclei (DAPI), alpha-sarcomeric actinin (a-SA), and Cx43. Scale bar = 50 μm. (ii) Left: Cx43+ foci per cell for CPACE and non-stimulated cells. Control groups were cells on glass slides. Right: Average Cx43 intensity/cell by flow cytometry. Reproduced with permission from Ref. [433] Copyright © 2017 Royal Society of Chemistry. (C) Scanning electron microscopic images of PU, PU/rGO-Ag (1 %), and PU/rGO-Ag (2 %) scaffolds. Cell attachment of human cardiac progenitor cells seeded on (i) PU, (ii) PU/rGO-Ag (1 %), and (iii) PU/rGO-Ag (2 %) on day 1 and after 7 days of culturing on (iv) PU, (v) PU/rGO-Ag (1 %), and (vi) PU/rGO-Ag (2 %). Cellular morphology of human cardiac progenitor cells seeded on (vii) PU, (viii) PU/rGO-Ag (1 %), and (ix) PU/rGO-Ag (2 %) on day 1 and after 7 days of culturing on (x) PU, (xi) PU/rGO-Ag (1 %), and (xii) PU/rGO-Ag (2 %). (D) (i,ii,iii) Immunofluorescent staining of human cardiac progenitor cells seeded on PU, PU/rGO-Ag (1 %), and PU/rGO-Ag (2 %) scaffolds. Reproduced with permission from Ref. [377] Copyright © 2019 WILEY-VCH Verlag GmbH & Co. KGaA, Weinheim.

electroconductive hydrogels, when combined with hiPSC-derived cardiomyocytes, exhibited enhanced beating, improved sarcomere alignment, and advanced electrical coupling, with synchronous calcium flux (Fig. 21B). RNA-seq confirmed these findings, demonstrating the potential of bPEI-AuNP-collagen hydrogels for improving cardiac TE and possibly treating other electrically sensitive tissues [54]. Moreover, AuNPs-based hydrogels exhibit interesting biocompatibility, making them suitable candidates for cardiac TE [425,426]. The physicochemical properties of AuNPs, such as their stability and the ability to be functionalized with biocompatible polymers contribute to favorable interactions with biological tissues [438].

Zhu et al. [439] developed a novel bioink incorporating gold nanorods (GNRs) into gelatin methacryloyl (GelMA). The gold nanocomposite bioink, which included GelMA and alginate with commercial cetyltrimethylammonium bromide (CTAB)-coated gold nanorods (G-GNRs), showed broad compatibility with 3D bioprinting systems, including those using coaxial extrusion needles (Fig. 21C) [439]. Coextrusion of bioink and calcium chloride resulted in ionically crosslinked hydrogel microfibers. This GNR-infused bioink optimally balanced viscosity and GNR concentration to create a conducive microenvironment for cardiac cell spreading and organization (Fig. 21C). The resulting nanocomposite bioink allowed for easy

integration of cells at high densities, facilitating rapid, high-resolution deposition of cell-laden fibers while minimizing shear stress [439]. In this study, cardiac TE involved co-printing neonatal rat cardiac cells in G-GNR nanocomposite bioink. Homogeneous encapsulation was confirmed (Fig. 21D), with subsequent culture resulting in well-spread and highly confluent cells within the construct by day 12 (Fig. 21D). G-GNR constructs demonstrated higher Cx-43 expression and synchronized contractile frequency, indicating improved electrical coupling and contractile properties (Fig. 21D) [439]. Electrospinning was also used to fabricate gold-based biomaterial hydrogels for cardiac TE. To tackle the challenge of integrating cardiac patches without causing additional damage to the infarcted heart, Malki et al. [440] developed a suture-free methodology using nanocomposite scaffolds. The scaffolds, consisting of albumin protein electrospun fibers and gold nanorods (AuNRs), hosted cardiac cells to form a functional patch. Placed on the myocardium, the engineered tissue underwent near infrared laser irradiation at 808 nm [440]. The AuNRs absorbed the light, converting it into thermal energy. This localized energy altered the molecular structure of the fibrous scaffold, securely attaching it to the heart wall without causing harm. These hybrid biomaterials offer a promising solution for integrating

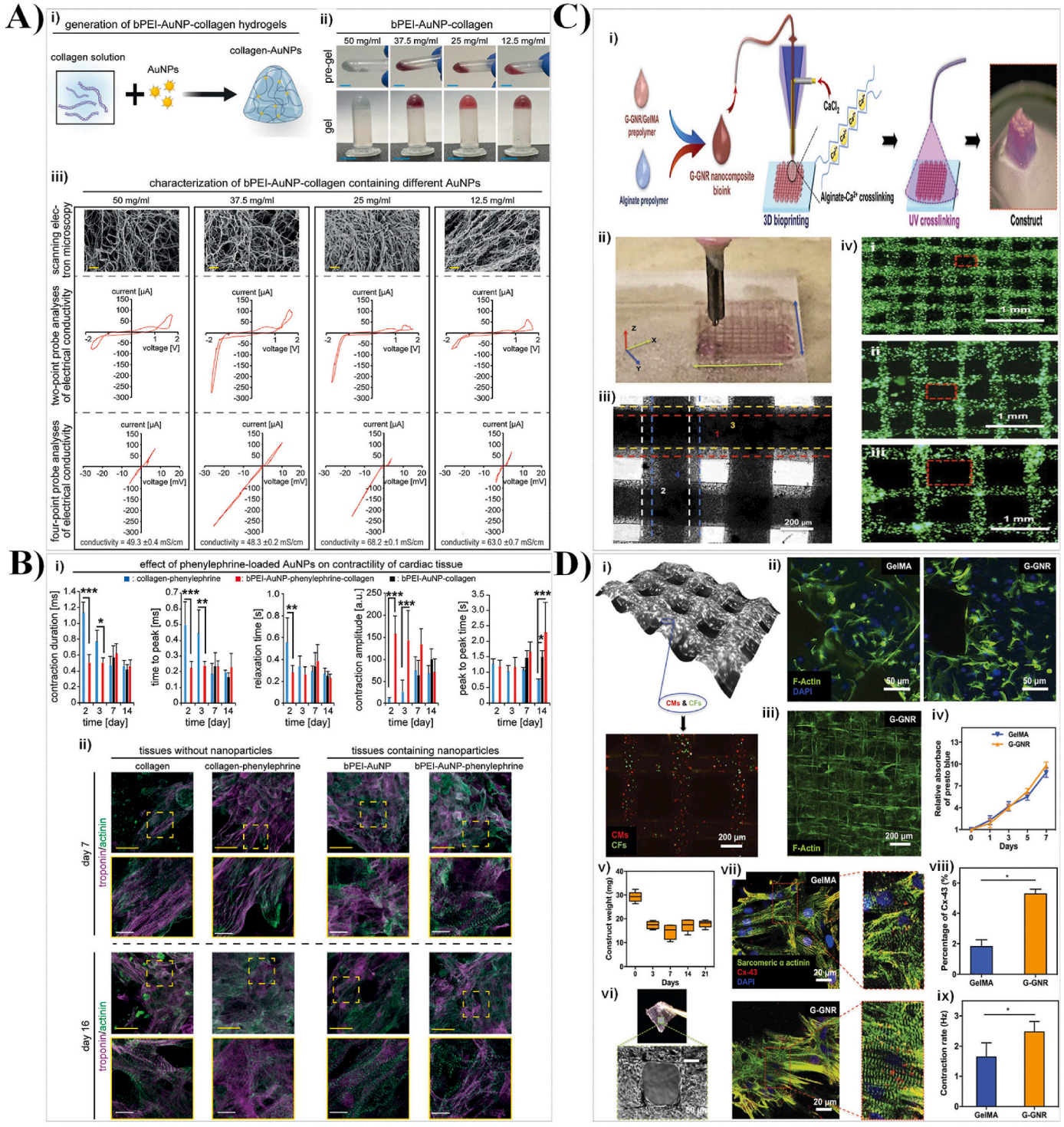

(caption on next page)

Fig. 21. (A) Microstructure and electrical conductivity of bPEI-AuNP-collagen hydrogels. (i) Schematic representation of hydrogel formation. (ii) Photographs of various hydrogels before and after gelation. (iii) SEM images of critically point-dried hydrogels with different gold nanoparticle types, alongside quantitative graphs of electrical conductivity measurements using two-point and four-point analysis. Scale bars: 2 μm. (B) Drug delivery and contractility enhancement in cardiomyocytes by bPEI-AuNPs. (i) Muscle motion-based analysis of engineered cardiac tissue contractility over time. (ii) Confocal projections of hiPSC-derived cardiomyocyte-laden tissue constructs stained for sarcomeric-α-actinin and troponin I at 7 and 16 days post-fabrication. Data are presented as mean ± SD. Scale bars: yellow: 25 μm; white: 4 μm. Reproduced with permission from Ref. [54] Copyright © 2023 WILEY-VCH Verlag GmbH & Co. KGaA, Weinheim. (C) G-GNR nanocomposite bioink 3D bioprinting. a) Schematic representation of the bioprinting process using G-GNR nanocomposite bioink, with an inset displaying the bioprinted 30-layered construct. b) Visualization of the printing procedure along x, y, and z axes. (iii) Microscopic observation of stacked layers using G-GNR nanocomposite bioink. (iv) Bioprinting of constructs with varying inner grids, where green beads were embedded in G-GNR nanocomposite bioink to highlight the printed fibers. (D) Bioprinted cardiac tissue Construct. (i) Pseudo-3D bright field image showing homogeneous cell distribution in the bioprinted construct using G-GNR nanocomposite bioink. Fluorescently labeled cardiomyocytes in red and cardiac fibroblasts in green observed after printing. (ii-iii) Fluorescence images of bioprinted cardiac cells within G-GNR nanocomposite bioink-printed constructs on days 5 and 12, respectively. (iv) Presto Blue assay indicating no significant differences in cell proliferation between GelMA/alginate bioink and G-GNR nanocomposite bioink-printed constructs. (v) Dry weight change of cell-laden G-GNR nanocomposite bioink-printed constructs during culture. (vi) Maintenance of morphology and inner grids during culture. (vii) Immunostaining revealing phenotypic differences in cardiac tissues within GelMA/alginate bioink and G-GNR nanocomposite bioink-printed constructs. (viii) Quantification of Cx-43 expression. (ix) Spontaneous beating rates of GelMA/alginate bioink and G-GNR nanocomposite bioink-printed constructs. Reproduced with permission from Ref. [439] Copyright © 2017 WILEY-VCH Verlag GmbH & Co. KGaA, Weinheim.

engineered tissues into damaged organs, thereby reducing the risks associated with traditional stitching methods and additional patient injury [440]. In another work, electrospun nanofibrous scaffolds were fabricated from polyurethane, chitosan, collagen, and saffron extract-synthesized AuNPs. Successful synthesis of AuNPs was confirmed by UV–Vis spectroscopy, with nanoparticles exhibiting a hydrodynamic size of approximately 13 nm and a zeta potential of −37 mV [441]. The biocompatibility of the prepared scaffolds was evaluated by seeding HUVEC cells on the nanofibers, followed by an alamar blue assay at 1, 3, and 5 days post-seeding. The results showed that all scaffolds exhibited good cytocompatibility with good cell survival. Additionally, the presence of saffron extract-synthesized AuNPs at the surface of nanofibers reduced contact angles and enhanced surface hydrophilicity, facilitating cell attachment and proliferation due to their topological features. AuNPs also contributed to minimal inflammatory responses and improved biocompatibility of AuNPs-based nanofibers [441].

6. Bioactive functionalities in electroconductive hydrogels for cardiac tissue engineering

To enhance the efficacy of hydrogels for cardiac TE, it is necessary to add bioactive functionalities by incorporating bioactive molecules and materials into the hydrogels. Foremost, hydrogels must exhibit high biocompatibility and support cell survival and function. Biocompatible hydrogels minimize adverse reactions and inflammation, fostering a conducive environment for cardiac cell integration. Materials such as natural polymers (e.g., collagen, chitosan, cellulose, gelatin and hyaluronic acid) and synthetic polymers (e.g., polyethylene glycol) have been widely explored for their biocompatibility [40,41,63,442]. Furthermore, incorporation of biochemical factors could be necessary to mimic the native cardiac microenvironment. Hydrogels can be functionalized with bioactive molecules such as growth factors (e.g., VEGF, TGF-β) and peptides (e.g., RGD peptides) to regulate cellular behavior. These molecules play a pivotal role in promoting angiogenesis, cell migration, and tissue regeneration within the engineered cardiac construct [96]. Moreover, cardiac tissue requires an electrically conductive microenvironment to support synchronized contraction. Hydrogels with inherent or engineered electrical conductivity facilitate the transmission of electrical signals, promoting the maturation and functionality of cardiac cells [53]. Incorporating conductive polymers, carbon-based materials, and metal nanoparticles into hydrogels enhances their electrical properties, creating a more biomimetic environment for cardiac tissue development [96,380,443]. In addition, the mechanical properties of hydrogels need to be close to those of native cardiac tissue to provide adequate structural support. Tunable stiffness is crucial for guiding cell differentiation and tissue maturation [444]. By adjusting the composition and crosslinking density, hydrogels can be engineered to achieve mechanical properties that closely resemble the native myocardium, ensuring optimal support for cardiac cells [63,445]. Additionally, hydrogels should have controllable degradation kinetics to align with the tissue regeneration process. Degradation that occurs too quickly or too slowly may hinder proper tissue development [446]. Enzymatically or hydrolytically degradable hydrogels can be tailored to match the desired degradation rate, enabling the gradual replacement of the scaffolds by newly formed tissues [446]. Moreover, effective transport of oxygen and nutrients is vital for the survival and functionality of cardiac cells in the hydrogel scaffold. Pore size and interconnectivity in the hydrogel structure must be carefully designed to facilitate efficient diffusion [447,448]. Incorporating bioactive components that promote angiogenesis further ensures an adequate supply of oxygen and nutrients throughout the engineered cardiac tissue [320,449,450].

6.1. Cardiac cell functionality in engineered electroconductive hydrogels for enhanced TE

In cardiac TE, cell delivery and integration into hydrogels could contribute to the regeneration of functionalities of cardiac tissues [445]. Hydrogels designed for cardiac applications can be carefully engineered to incorporate and facilitate the precise delivery of various cell types, such as cardiomyocytes, endothelial cells, cardiac fibroblasts and stem cells, each playing a specific role in restoring cardiac tissues [451]. Anisotropy in hydrogels is also important for cardiac TE because such hydrogels have the ability to mimic the directional properties found in native cardiac tissues. This feature promotes alignment and orientation of cardiomyocytes along specific axes, which is essential for proper electrical conduction and mechanical function of the heart [452,453]. Wu et al. [43] fabricated a 3D hybrid scaffold with aligned conductive nanofiber yarns network (NFYs-NET, composed of polycaprolactone, silk fibroin, and carbon nanotubes) in a hydrogel shell, demonstrating potential for 3D cardiac anisotropy engineering. Using dry-wet electrospinning, they developed an interwoven structure reminiscent of native cardiac tissue. The scaffold, depicted in Fig. 22A, featured a network design advantageous for cardiac tissue regeneration. Fluorescence images of NFYs-NET scaffolds, prepared using nanofiber yarns with varying diameters, are shown in Fig. 22B. These scaffolds facilitated aligned and elongated cardiomyocyte maturation on each layer, with the ability to individually control cellular orientation in a 3D environment (Fig. 22C) [43]. Additionally, co-culturing cardiomyocytes on electroconductive layered hydrogels and endothelial cells within the hydrogel shell induced cellular orientation, maturation, and anisotropy, providing a suitable 3D environment for endothelialization and significant potential in engineering 3D cardiac anisotropy (Fig. 22D) [43]. Furthermore, endothelial cells play a significant role in vascularization by aiding in the formation of blood vessels within hydrogels. This vascular network is crucial for ensuring adequate oxygen and nutrient

supply to engineered tissue, thereby promoting its overall health and functionality [454,455]. Stem cells, known for their regenerative abilities, can further enhance the hydrogel capacity to support tissue repair and regeneration. Under controlled conditions, stem cells can undergo specific differentiation protocols, facilitating the development of specialized cell lineages relevant to tissues affected by specific conditions [456].

The conductivity of myocardium is important for cardiac function,

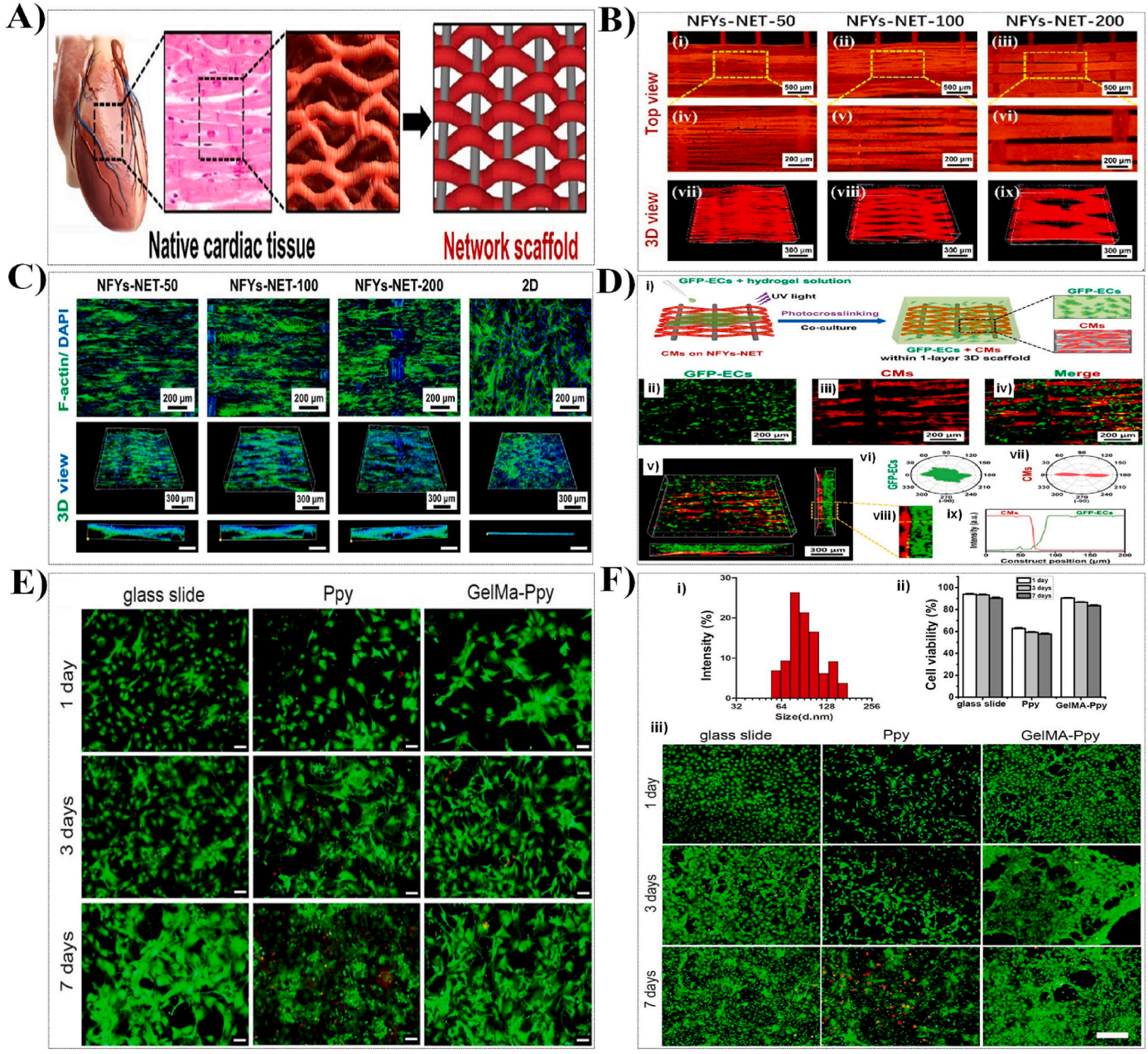

Fig. 22. (A) The interwoven structure observed in native cardiac tissue highlights the potential benefits of a scaffold with a network structure for cardiac tissue regeneration. (B) Fluorescent images of NFYs-NET scaffolds, prepared using NFYs with different diameters (50, 100, and 200 μm), featuring top views (i−vi) and 3D views (vii−ix) stained with Nile red dye. (C) Top views and 3D views of fluorescent images of cardiomyocytes on NFYs-NET scaffolds, stained with F-actin (green) and DAPI (blue) after 5 days of cultivation (scale bar: 300 μm). (D) Construction of endothelialized myocardium through the coculture of cardiomyocytes and green fluorescent protein-positive endothelial cells (GFP-ECs) within a 1-layer 3D scaffold. (i) Schematics illustrate the co-culture procedure, where cardiomyocytes (CMs) were cultured on the NFYs-NET layer, while GFP-ECs were encapsulated within the hydrogel shell. Fluorescent images of GFP-ECs (green) (ii), CMs (red) (iii), and their merged image (iv) are presented. The 3D view of confocal images of GFP-ECs and CMs within the scaffolds is shown (v). Quantitative analysis of cellular orientation distribution for GFP-ECs (vi) and CMs (vii) is provided. Fluorescence intensity analysis for the cross-section of this cell-laden scaffold illustrates the distribution of ECs in the hydrogel and CMs on NFYs-NET (viii, ix). Reproduced with permission from Ref. [43] Copyright © 2017, American Chemical Society. (E) Live/dead staining of untreated CMs, CMs treated with 25 mg/mL PPy, and CMs treated with 50 mg/mL GelMA-Ppy nanoparticles at 1, 3, and 7 days. Live cells are shown in green, and dead cells are shown in red. Scale bar: 50 μm. (F) Biocompatibility of GelMA-Ppy nanoparticles. (i) Size distribution of GelMA-Ppy nanoparticles analyzed by DLS. (ii) Quantitative cell viability of untreated CMs, CMs treated with 25 mg/mL Ppy, and CMs treated with 50 mg/mL GelMA-Ppy nanoparticles at 1, 3, and 7 days. (iii) Live/dead staining of untreated cardiac fibroblasts, fibroblasts treated with 25 mg/mL PPy, and fibroblasts treated with 50 mg/mL GelMA-Ppy nanoparticles at 1, 3, and 7 days. Live cells are shown in green, and dead cells are shown in red. Scale bar: 100 μm. Reproduced with permission from Ref. [458] Copyright © 2018, Ivyspring International Publisher.

facilitating the transmission of electrical signals for synchronized heart contractions [96,115]. Conductive polymers like PPy are widely used in scaffolds for their high conductivity and electrical stability [221,241,387]. However, achieving highly conductive and biocompatible fibers with high concentrations of conductive polymers remains challenging, as they can become cytotoxic to cardiac cells, leading to cell death and tissue malfunction. This effect can be attenuated by blending conductive polymers with functional biocompatible biomaterials [96,457,458]. To address this issue, the researchers recently combined conductive polymers with biocompatible biomaterials such as GelMA, to develop GelMA-PPy nanoparticles [458]. GelMA served as both a shape inducer and a toxicity-neutralizer during the formation of the nanoparticles through oxidative polymerization. The study demonstrated that GelMA-PPy nanoparticles highlighted suitable biocompatibility even at high concentrations (50 mg/mL) [458]. Live/dead staining of cardiomyocytes and myocardial fibroblasts showed that cell viability remained stable from day 1 to day 7 for cardiomyocytes treated with GelMA-PPy nanoparticles (Fig. 22E–F). In contrast, significant cell death was observed in the control group treated with pure PPy. Quantitative analysis revealed that over 80 % of cardiomyocytes survived with GelMA-PPy nanoparticles, similar to the CMs on glass slides, while only 60 % survived with pure PPy (Fig. 22E–F). This approach shows a interesting solution to balancing conductivity and cell viability making them suitable for cardiac TE [458].

6.2. Enhancing vascularization in cardiac tissues through endothelial cell culture in engineered electroconductive hydrogels

Another important aspect to integrate when designing hydrogels for cardiovascular tissue regeneration is vascularization [455]. Establishing effective vascularization is crucial for ensuring the survival and optimal functionality of engineered tissue. This aspect is addressed in recent research studies through the incorporation of specific features in hydrogels designed to promote the formation of blood vessels [163,228,459]. To enhance vascularization in engineered cardiac tissue constructs, numerous studies have shown successful outcomes by incorporating angiogenic factors [317], or integrating endothelial cells [173,320,454] into functional hydrogels. These strategies are pivotal in promoting the development and maturation of a functional vascular network within the hydrogel matrix. The incorporation of growth factors within hydrogels represents a cornerstone in promoting cardiovascular tissue regeneration. Growth factors such as VEGF and basic fibroblast growth factor (bFGF) have demonstrated the ability to stimulate angiogenesis, a fundamental process for establishing a functional vascular network in regenerating tissues [460,461]. Controlled incorporation of these growth factors into hydrogel matrices containing specific cells capable of promoting vascularization ensures a temporally and spatially coordinated response, facilitating the formation of new blood vessels and enhancing nutrient delivery to the regenerating tissue. These bioactive molecules can stimulate the migration and proliferation of endothelial cells, thereby fostering the creation of a well-organized and interconnected vascular network [462]. Furthermore, directly incorporating endothelial cells into the hydrogel also provides a biological component essential for vascular development, as these cells play a central role in forming the inner lining of blood vessels, contributing to their structural integrity and functionality [463]. Mehrabi et al. [464] recently used electrospinning technology to fabricate electroactive cardiac patches composed of carbon nanofibers (CNF) and gelatin (Gel) nanofibers. SEM assessment of developed fibrous scaffolds revealed randomly oriented nanofibers and electrical conductivity was in the semiconducting range ($\sim 10^{-5}$ S/m) as determined by a four-probe device. MTT assays highlighted suitable biocompatibility and human umbilical vein endothelial cells (HUVECs) cytotoxicity studies demonstrated robust cell attachment on scaffolds (Fig. 23A) [464]. Notably, electroactive scaffolds (CNF/Gel) exhibited complete cell coverage, creating a favorable functional HUVECs-based platform. CNF-containing scaffolds facilitated cardiomyocyte adhesion and elevated cardiac gene expression compared to non-conductive counterparts. Angiogenic assessment after subcutaneous implantation in mices for 2 and 4 weeks indicated enhanced vascularization in CNF/Gel scaffolds, which almost fully integrated with host tissue (Fig. 23B). CNF/Gel scaffolds further demonstrated significant cell migration, reaching about 85 % after 4 weeks (Fig. 23C). Immunofluorescence staining revealed increased capillary formation in CNF-containing scaffolds, confirming their angiogenic potential for cardiac TE [464]. He et al. [458] developed a mussel-inspired conductive electrospun (ES)-based engineered cardiac patch (ECP) to address challenges in the biocompatibility and aggregation of polypyrrole (PPy) in cardiac TE (Fig. 23D). Spherical methyl acrylic anhydride-gelatin (GelMA)-PPy nanoparticles were synthesized via oxidative polymerization and crosslinked onto an ES-GelMA/polycaprolactone (PCL) nanofibrous membrane using a dopamine-N'N'-methylene-bis-acrylamide (dopa-MBA) crosslinker. This strategy yielded a conductive and biocompatible scaffold [458]. GelMA-PPy nanoparticles exhibited suitable biocompatibility and improved cardiomyocyte (CM) synchronization and function in vitro. The modified topography of the membrane enhanced vascularization, with Ki67-positive HUVEC proliferation increasing fourfold and tube formation density tripling compared to pristine membranes. Angiogenic gene expression (eNOS, VEGF, KDR) was significantly elevated on the conductive membrane (Fig. 23E). In vivo, transplantation of the ECP decreased infarct size by 50 %, improved left ventricular shortening fraction by 20 %, and increased neovascular density in infarcted regions by ninefold compared to myocardial infarction controls (Fig. 23F). The study highlights a promising ECP design that leverages mussel-inspired conductive membranes to enhance cardiac function and revascularization, addressing myocardial infarction repair challenges [458]. Meng et al. [465] designed a composite scaffold by combining carbon fibers with coaxial fibrous mesh of poly(lactide)/gelatin (PLA@Gel), leveraging the high modulus and electrical conductivity of carbon fibers alongside the fibrous and porous properties of electrospun fibers. The scaffold was constructed through a straightforward process of integrating coaxial electrospun PLA@Gel fibers and carbon fibers via freeze-drying process [465]. In this study, the fibrous composite prepared from poly(lactide)/gelatin and carbon fibers (CF) were named PLA@Gel/CF. SEM analysis revealed homogeneous fibers with an average diameter of 760 nm and CFs were evenly distributed in the porous scaffolds (Fig. 23G). Immunohistological staining of Cx43 and α-SMA was performed on heart tissue (Fig. 23H(i)). In the myocardial infarcted group, no Cx43-positive cells were found in the infarcted area, indicating complete replacement of muscle tissue by scar tissue [465]. The PLA@Gel group showed a slight increase in Cx43 expression, while the PLA@Gel/CF3 group exhibited a significant rise in Cx43, suggesting effective tissue regeneration. α-SMA staining revealed more blood vessels in the PLA@Gel/CF3 group, with larger-diameter vessels compared to the PLA@Gel group, indicating enhanced angiogenesis. Vessel density, assessed by counting α-SMA-positive structures, was significantly higher in the PLA@Gel/CF3 group, approximately three times that of the myocardial infarcted group and significantly higher than in the PLA@Gel group (Fig. 23H(ii)), highlighting the positive impact of PLA@Gel/CF3 on myocardial regeneration [465].

6.3. Engineering electroconductive hydrogels with tuned mechanical properties for enhanced cardiac tissue regeneration

Hydrogels engineered for cardiac tissue regeneration are essential for providing suitable mechanical support to damaged or weakened heart tissue, thereby preventing further deterioration and actively supporting natural healing processes within the cardiac environment [466]. This mechanical support is commonly tailored to meet the specific needs of the myocardium, ensuring optimal functionality and integration. The mechanical properties of cardiac patches, such as elasticity and stiffness, are precisely engineered to closely mimic those of native myocardium

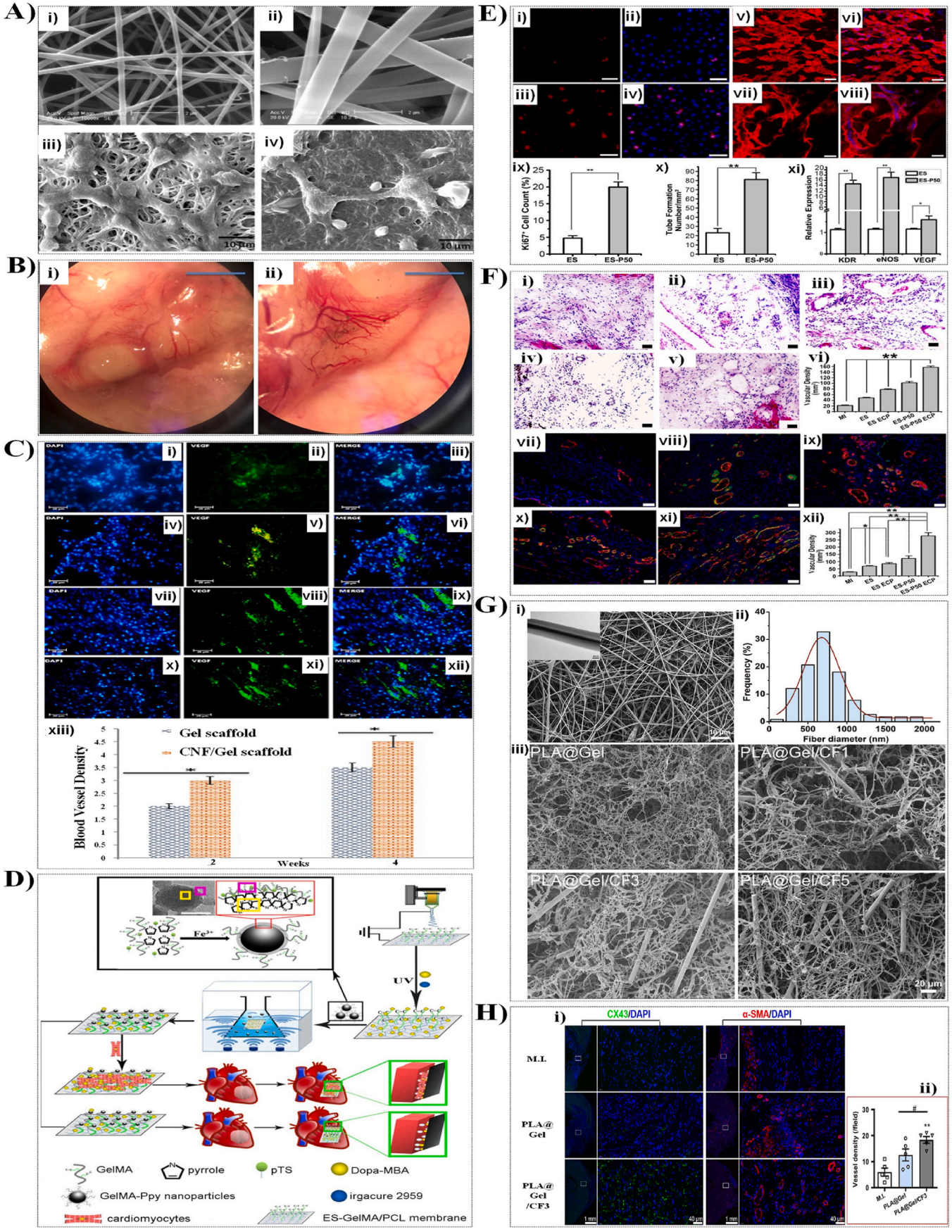

(caption on next page)

Fig. 23. (A) SEM analysis of nanofiber morphology for i) Gel and ii) CNF/Gel. HUVECs morphology on iii) CNF/Gel and iv) Gel nanofibers after 48 h. (B) Macroscopic view of scaffolds after 4 weeks subcutaneous implantation for Gel (i) and CNF/Gel (ii) scaffolds, Scale bar, 10 mm. (C) Immunohistological assessment of microvasculature stained with anti-VEGF after 2 (i–vi) and 4 (vii–xii) weeks subcutaneous implantation. Gel (i–iii, vii–ix) and CNF/Gel (iv–vi, x–xii). Corresponding quantitative analysis of blood vessel density after 2 and 4 weeks of subcutaneous implantation (xiii). Reproduced with permission from Ref. [464] Copyright © 2019, Springer Nature. (D) Schematic representation of the fabrication of the mussel-inspired conductive membrane and its application as an ECP in a rat myocardial infarction (MI) model. Scale bar: 50 nm. (E) The ES-P50 membrane promoted HUVEC proliferation and vascularization in vitro. Ki67-positive cells (red) on ES (i,ii) and ES-P50 (iii,iv). Scale bar: 50 μm; vWF-positive HUVECs (red) on ES (v,vi) and ES-P50 (vii,viii). Scale bar: 20 μm; (ix) Percentage of Ki67-positive cells; (x) Number of tubes formed per mm^2; (xi) Expression of KDR, eNOS, and VEGF genes. ES: pristine ES-GelMA/PCL; ES-P50: dopa-based ES-P50. Data are shown as mean ± SD. Nuclei were stained with DAPI. (F) Mussel-inspired conductive ECP enhanced vascularization in the infarct myocardium. H&E staining in MI (i), ES (ii), ES ECP (iii), ES-P50 (iv), and ES-P50 ECP (v) groups. Scale bar: 50 μm. (vi) Microvessel density based on H&E staining. Data are mean ± SD. vWF (red) and α-SMA (green) immunostaining in MI (vii), ES (viii), ES ECP (ix), ES-P50 (x), and ES-P50 ECP (xi). Scale bar: 50 μm. (xii) Microvessel density from vWF immunostaining. ES: pristine ES-GelMA/PCL; ES ECP: pristine ES-GelMA/PCL ECP; ES-P50: dopa-based ES-P50; ES-P50 ECP: dopa-based ES-P50 ECP. Data are mean ± SD. Reproduced with permission from Ref. [458] Copyright © 2018, Ivyspring International Publisher. (G) Morphology of the fibrous film and composite scaffolds. (i) SEM and TEM images (inset) of coaxial electrospun fibers. (ii) Diameter distribution of electrospun fibers. (iii) SEM images of PLA@Gel, PLA@Gel/CF1, PLA@Gel/CF3, and PLA@Gel/CF5 composite scaffolds. (H) Immunofluorescence analysis of muscle and vessel maturation in infarcted hearts post-MI treatment. (i) Representative images of Cx43 (green), α-SMA (red), and nuclei (DAPI, blue). (ii) Vessel density calculation in infarcted hearts across groups. Reproduced with permission from Ref. [465] Copyright © 2022, Elsevier.

[467]. This precise tuning is crucial for several reasons. Firstly, it prevents mechanical mismatch, enabling seamless integration of the hydrogel with surrounding tissue and without causing undue stress or strain. The objective is to establish a harmonious interface that facilitates proper functioning of the engineered tissue [395]. Secondly, aligning the mechanical properties with those of native myocardium enables the cardiac hydrogel to promote physiological responses in the regenerated tissue. This includes synchronized contractions and relaxations, facilitating more natural and coordinated heart function [73,184]. The tuned mechanical characteristics could also contribute to the overall structural integrity of the hydrogel construct, enhancing its ability to withstand the dynamic mechanical forces exerted during the cardiac cycle [184]. Integrating electroconductive components into hydrogels for cardiac TE can further enhance their mechanical properties through synergistic mechanisms [457]. These electroconductive components significantly reinforce the hydrogel matrix, improving mechanical strength, electrical conductivity, and structural integrity. Acting as reinforcing agents, they form a robust network within the hydrogel structure [395]. This reinforcement enhances tensile strength, elastic modulus, and toughness, rendering the hydrogel more resilient to mechanical stresses and better mimicking the mechanical properties of native cardiac tissue [56,96]. In a recent study, various electrospun fiber mats were evaluated for their mechanical properties. The study included combinations of electrically conductive PANi, collagen, and hyaluronic acid (HA) to fabricate electrospun and electroconductive scaffolds [60]. Neat collagen fiber mats exhibited an ultimate tensile strength (UTS) of 10 ± 2 MPa, a failure strain (FS) of 3.2 ± 0.4 %, and Young's modulus of 4 ± 1 MPa. Introduction of HA in collagen matrix increased UTS to 14 ± 4 MPa, while fiber mats with lower PANi content showed similar results. PANi concentrations up to PANi3 initially increased FS and UTS, but further increases (PANi4) led to a decline [60]. The lower collagen concentration in PANi4 contributed to reduced mechanical properties. Despite having a higher Young's modulus than native myocardium, the fiber mats demonstrated favorable environment for cardiomyocyte growth and function. In comparison to other materials used in cardiac TE, these fiber mats exhibited elastic modulus and tensile strength closer to native myocardium (Fig. 24A) [60].

6.4. *Electroconductive hydrogels for remolding and maturation of engineered cardiac tissues*

Remodeling and maturation are also main aspects to consider when designing functional hydrogels for cardiac TE. Beyond their anti-inflammatory properties, these hydrogels should be engineered to facilitate the gradual transformation of the artificial construct into functional native tissue over time [468]. This dynamic process involves the stepwise replacement of hydrogel materials with host-derived tissue components as the engineered construct integrates and matures within the surrounding biological environment [27]. The process of remodeling and maturation begins with the introduction of the hydrogel into the damaged or weakened cardiac tissue. As the hydrogel integrates, it serves as a temporary scaffold, providing mechanical support to the damaged tissue and creating a conducive environment for cellular activities [73]. Importantly, the hydrogel is designed to mimic the ECM of the native myocardium, offering cues for proper cell adhesion, migration, and tissue organization [469]. Over time, as the host cells infiltrate the hydrogel scaffold, they actively participate in tissue remodeling. This involves the synthesis and deposition of endogenous ECM components, such as collagen and elastin. Simultaneously, the hydrogel should begin to undergo controlled degradation, allowing for the gradual replacement of synthetic materials by the host tissue [335]. The process of maturation is characterized by the development of functional tissue properties resembling those of the native myocardium. Cardiomyocytes cultured in the hydrogel should align themselves in a more organized manner, and the mechanical properties of the developing tissue should approach those of the natural cardiac muscle [470]. This transition from hydrogel to native tissue is crucial for the fabrication of a seamlessly integrated and fully functional hydrogel for cardiac tissue repair. The engineered hydrogel is evidenced by its capacity to direct and facilitate the remodeling and maturation processes [470]. The incorporation of electroconductive polymers into hydrogels could play a crucial role in influencing the maturation of cardiomyocytes for cardiac TE. The interaction between the electroconductive polymers and cardiomyocytes could promote alignment and elongation of the cells, resembling the natural organization of cardiac tissues. Additionally, the conductive properties of these polymers contribute to improved contractile function, alignment of sarcomeres, and expression of cardiac-specific genes, leading to the maturation of cardiomyocytes. The conductive cues provided by electroconductive polymers in hydrogels create a supportive niche for cardiomyocyte development, ultimately enhancing the functionality and maturity of engineered cardiac tissues in vitro and in vivo. Sun et al. [471] demonstrated enhanced adhesion, intercalated disc-related protein expression, assembly, and functionality in neonatal cardiomyocytes (CMs) in single-walled-incorporated collagen hydrogels (Fig. 24B(i−iii)). Examining the organization, proliferation and phenotypes of cardiac cells on various hybrid scaffolds, the study focused on immunostaining of focal adhesion marker vinculin on day 3 and cardiac markers sarcomeric α-actin, CX43, and troponin I on day 5 (Fig. 24B(iv)) [471]. The results revealed that engineered cardiac tissues matured on CNT- and reduced graphene oxide (rGO)--GelMA had higher expression levels of these markers compared to graphene oxide (GO)-GelMA [471]. In particular, immunofluorescence staining revealed that engineered cardiac tissues cultured on CNT-GelMA and rGO-GelMA showed enhanced maturation compared to those on GO-GelMA. Vinculin expression was ~1.5-fold higher on CNT-GelMA and ~1.6-fold higher on rGO-GelMA. Sarcomeric α-actin

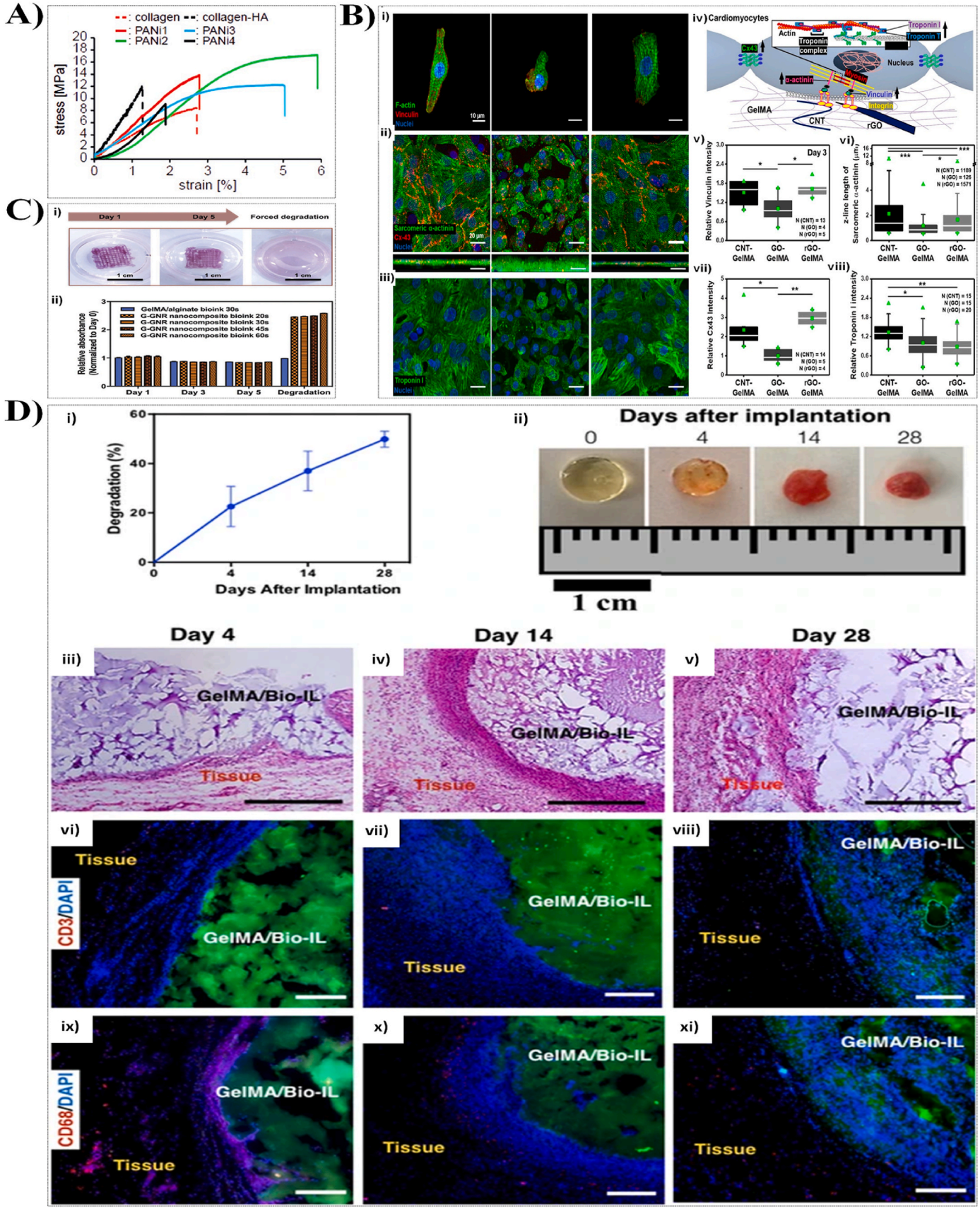

(caption on next page)

Fig. 24. (A) Mechanical properties of collagen, collagen/HA, and collagen/HA/PANi blends illustrated through representative stress–strain graphs. Reproduced with permission from Ref. [60] Copyright © 2020 WILEY-VCH Verlag GmbH & Co. KGaA, Weinheim. (B) Phenotypes of cardiac cells cultured on different scaffolds, evaluated through expression of cardiac-specific markers. (i) Immunofluorescence images of cardiomyocytes on CNT-, GO-, and rGO-GelMA stained for F-actin (green), vinculin (red), and nuclei (blue). (ii) Immunostaining of sarcomeric α-actinin (green), Cx-43 (red), and nuclei (blue) shows phenotypic differences in cardiac tissues cultured for 5 days on CNT-, GO-, and rGO-GelMA. Cross-section images of cardiac tissues are displayed at the bottom. (iii) Immunofluorescence images of cardiomyocytes on CNT-, GO-, and rGO-GelMA stained for troponin I (green) and nuclei (blue). (iv) Schematic representation of essential proteins for cardiomyocytes maturation, including integrin (yellow), vinculin (royal), α-actinin (pink), myosin (red), troponin I (purple), T (blue), and Cx43 (green). (v) Relative intensity of vinculin, (vi) Z-line length of sarcomeric α-actinin, and relative intensity of (vii) Cx43 and (viii) troponin I for cells cultured for 5 days on CNT-, GO-, and rGO-GelMA. Reproduced with permission from Ref. [471] Copyright © 2019 American Chemical Society. (C) i) Bioprinted constructs, stable in culture medium up to day 5, undergo forced degradation using a collagenase solution at 37 °C. ii) Absorbance spectrum analysis of culture medium confirms G-GNR retention within bioprinted constructs, released upon forced degradation. Reproduced with permission from Ref. [439] Copyright © 2017 WILEY-VCH Verlag GmbH & Co. KGaA, Weinheim. (D) In vivo biodegradation and biocompatibility of GelMA/Bio-IL composite hydrogels using a rat subcutaneous model. (i, ii) Assessment of in vivo degradation of GelMA/Bio-IL hydrogels at days 0, 4, 14, and 28 post-implantation. (i) In vivo degradation profile based on the weight loss of the implants, showing a nearly linear degradation behavior over 28 days. ii) Photographs of GelMA/Bio-IL composite hydrogels at 0, 4, 14, and 28 days after implantation. (iii–v) Hematoxylin and eosin (H&E) staining of GelMA/Bio-IL sections after iii) 4, (iv) 14, and (v) 28 days of implantation (scale bars = 500 μm), indicating minimal inflammatory cell presence. (vi–viii) Fluorescent immunohistochemical analysis of implanted GelMA/Bio-IL hydrogels showing no significant local lymphocyte infiltration (CD3) at days (vi) 4, (vii) 14, and (viii) 28 (scale bars = 200 μm), and prominent macrophage presence (CD68) at day 4 (ix), which diminished by day 14 (x) and day 28 (xi) (scale bars = 200 μm). Green, red, and blue colors represent the GelMA/Bio-IL hydrogels, immune cells, and cell nuclei (DAPI), respectively. The hydrogels were synthesized with a 15 % final polymer concentration and 50/50 GelMA/Bio-IL ratio. Reproduced with permission from Ref. [482] Copyright © 2017 Springer Nature.

lengths were ~1.8-fold and ~1.4-fold longer for CNT-GelMA and rGO-GelMA, respectively. Additionally, Cx43 expression was ~2.3-fold higher on CNT-GelMA and ~3.0-fold higher on rGO-GelMA (Fig. 24B (v-viii)). Electroconductive hybrid scaffolds acting as electrical connections between cardiomyocytes were found to promote increased expression of cardiac markers. Specifically, CNT-GelMA was observed to enhance troponin I expression, indicating a targeted improvement in the development and maturation of engineered cardiac tissues (Fig. 24B) [471].

6.5. *Biodegradable and functional electroconductive hydrogels for cardiac TE*

Moreover, biodegradability is a fundamental attribute to be considered in the design of functional hydrogels for cardiac TE [446]. In essence, these hydrogels should be engineered to undergo a controlled and gradual degradation process over time, aligning with the pace of native tissue regeneration. This degradation serves a dual purpose: providing essential structural support during the early phases of tissue healing and subsequently allowing the hydrogel to dissipate as the native tissue undergoes regeneration [472]. The gradual degradation of the hydrogel should be carefully timed to coincide with the natural tissue repair process, ensuring that the engineered support is available when required. Upon the degradation, the hydrogel breaks down into biocompatible byproducts, which are either absorbed into surrounding tissue or safely removed from the body [473]. This process mitigates the risk of long-term foreign body reactions and promotes the integration of the newly regenerated tissue in the host environment [474]. In vitro biodegradation of these hydrogels is investigated under simulated physiological conditions to comprehensively assess their stability and breakdown mechanisms. Factors including pH levels, temperature variations, and enzymatic activity are crucial determinants influencing the degradation kinetics of these materials [474]. Enzymes that are either present in the culture medium or specifically designed to simulate biological conditions can catalyze the degradation of hydrogel components. [159,439]. For example, a 3D functional cardiac tissue construct was printed using a gold nanorod (GNR)-incorporated gelatin methacryloyl (GelMA)-based bioink. GelMA-coated GNRs (G-GNRs) diffusion was monitored in phenol red-free medium, with spectrophotometric measurements of the medium collected from day 1 to day 5 [439]. On day 5, constructs were dissolved in collagenase type II at 37 °C to quantify G-GNR release via spectrophotometer. The persistent red color of G-GNRs was visually observed in 3D printed constructs throughout a 5-day culture, with a noticeable red hue emerging upon collagenase-induced degradation. (Fig. 24C(i)). Absorbance spectrum analysis verified G-GNR retention and release solely upon forced degradation (Fig. 24C(ii)) [439]. In vivo biodegradation of electroconductive hydrogels involves their interaction within the intricate physiological environment of living tissues. Upon transplantation, biopolymer-based hydrogels respond naturally to enzymatic reactions, cellular interactions, and immune responses, leading to gradual material breakdown. These biological processes play a crucial role in determining the longevity and compatibility of hydrogels in vivo, influencing their functional integration and potential applications in TE and biomedical research [475,476]. Macrophages, for instance, may play a crucial role in the recognition and engulfment of the hydrogels, initiating a cascade of events leading to their degradation [477]. Additionally, the incorporation of biodegradable components in hydrogel formulations facilitates their gradual breakdown into biocompatible byproducts, reducing the risk of adverse reactions [474].

The use of electrically conductive materials in combination with biopolymer-based polymers, to develop electroconductive hydrogel scaffolds for cardiac TE presents significant challenges regarding their biodegradation and potential toxicity in living organisms. Traditional conductive materials, such as PPy, graphene, CNTs and PANi, often exhibit non-biodegradable or very slow biodegradation rates in vivo, which can lead to the accumulation of material residues within tissues, triggering chronic inflammatory responses, fibrosis, and potential toxic effects [478–480]. This slow degradation also hinders the efficient integration of the scaffold with native tissue, disrupting the natural regenerative process. Moreover, some conductive materials may leach toxic by-products during degradation, further exacerbating cellular damage and impairing tissue functionality [479,480]. To overcome these challenges, bio-ionic liquids (Bio-ILs) have emerged as a promising alternative. Particularly those derived from choline, Bio-ILs provide an interesting combination of biocompatibility, biodegradability, intrinsic electroconductivity, and non-cytotoxicity [481]. When incorporated into biopolymer-based polymers like GelMA, Bio-ILs can provide electroconductive properties while ensuring that the hydrogels degrade at a controlled, physiologically relevant rate. This strategy enables not only the safe and efficient degradation of the scaffolds but also minimizes the risk of toxicity, supporting the regeneration of cardiac tissue without compromising scaffold performance over time [482]. In addition, GelMA-based hydrogels are known to contain peptide sequences that facilitate cell-mediated degradation in vivo [483–485]. Noshadi et al. [482] synthesized the Bio-IL-functionalized GelMA hydrogels, and their conductivity was measured using a two-probe electrical station. The results showed that varying the GelMA concentrations and the Bio-IL ratios influenced the electrical properties of the resulting GelMA/Bio-IL hydrogels. For instance, the conductivity of 50/50 GelMA/Bio-IL hydrogels increased from 3.03×10^{-5} S/m to 5.03×10^{-5} S/m when the polymer concentration was raised from 10 % to 20 %. Moreover, when the GelMA/Bio-IL ratio was adjusted from 50/50 to 20/80, the conductivity of 15 % GelMA/Bio-IL hydrogels increased by

more than 63 times, from 4.27 × 10^{-5} S/m to 272 × 10^{-5} S/m, demonstrating the effective tuning of electroconductive properties [482]. Furthermore, the engineered hydrogels facilitated the growth and function of primary cardiomyocytes in both 2D and 3D in vitro cultures. The study also investigated the in vivo biodegradation and biocompatibility of GelMA/Bio-IL hydrogels, addressing a major limitation of conventional conductive polymers, which are often not biodegradable and can induce chronic inflammation due to their long half-lives in the body. When implanted subcutaneously in an animal model, GelMA/Bio-IL hydrogels were observed to undergo sustained biodegradation over a 28-day period, as shown by the recovery of explanted samples at different periods till 28 days (Fig. 24D(i)). The degradation of the hydrogel matrix occurred through enzymatic hydrolysis, with notable tissue infiltration observed within the hydrogels, as evidenced by the visual inspection of explanted samples shown in Fig. 24D(ii) [482]. Histological analysis of the explanted hydrogels showed that cellular ingrowth occurred with minimal inflammation, accompanied by low deposition of fibrous collagenous tissue (Fig. 24D (iii-v)). Immunohistofluorescent staining for CD3 confirmed the absence of sustained infiltration of pro-inflammatory leukocytes (Fig. 24D(vi-viii)). Additionally, a macrophage response, marked by CD68 expression, was observed at day 4 but decreased significantly by day 28 (Fig. 24D (ix-xi)), indicating minimal inflammatory reactions. These findings suggested that GelMA/Bio-IL hydrogels induced minimal inflammatory responses in vivo, and their biocompatibility and biodegradability could be further tailored depending on the specific biopolymers used [482]. Ideally, biodegradable cardiac TE biomaterials fully consisting of polymer and cells could be proposed. In those polymer-based biomaterials, produced for example by combining cardiac cell-laden 3D bioprinting and electrospinning, the achieved microstructure should match the needed for cell-cell interaction and electrical coupling of cardiac cells, to have gaing of the intrinsic electrical properties of cells in the 3D mimicking environment allowing for synchronous beating, possibly without the need of addition of non biodegradable conductive materials.

6.6. Immunomodulatory properties of electroconductive hydrogels

Electroconductive hydrogels hold great promise in advancing cardiac TE due to the combination of electrical conductivity and anti-inflammatory properties, both of which are crucial for enhancing tissue regeneration and minimizing immune responses [96]. These hydrogels are designed by integrating electrically conductive materials into a hydrophilic polymer matrix, enabling them to conduct electrical signals that support cellular communication, particularly in cardiac tissues that depend on synchronized electrical signaling for normal function [96,379,457]. Beyond their conductive capabilities, these hydrogels also modulate macrophage polarization, a crucial factor in managing inflammation. In cardiac TE, inflammation is a complex biological response triggered by injury or the implantation of foreign materials, leading to the recruitment of immune cells such as macrophages and neutrophils, which release pro-inflammatory cytokines and growth factors that alter the tissue microenvironment. This inflammatory process can result in fibrosis, impaired tissue regeneration, and poor graft integration, ultimately compromising the functionality of engineered constructs [477,486,487]. Electroconductive hydrogels mitigate these issues by promoting the polarization of macrophages toward the M2 phenotype, reducing chronic inflammation and accelerating healing, mainly through electrical stimulation or their inherent electrochemical properties [488,489]. This polarization activates key intracellular pathways, such as nuclear factor kappa-light-chain-enhancer of activated B cells (NF-κB) and mitogen-activated protein kinase (MAPK), which regulate inflammatory responses by controlling the transcription of pro-inflammatory genes. In M1 macrophages, NF-κB activation promotes the expression of pro-inflammatory genes, whereas its inhibition in M2 macrophages aids in resolving inflammation and enhancing tissue repair [477,486,489]. Moreover, these conductive hydrogels can also regulate ion flux, modulating immune cell behavior by influencing membrane potential and ion channel activation, which helps control cytokine production and reduce inflammation in damaged tissues [191,490].

Immunomodulation is an important aspect of cardiovascular engineering, where efforts are made to finely tune the immune response for optimal tissue integration. In this context, the hydrogels are designed to act as immunomodulatory agents, aiming to mitigate the risk of rejection while fostering a conducive environment for seamless tissue integration [490,491]. Through strategic engineering, these hydrogels should be tailored to interact with the immune system in a way that minimizes adverse reactions. The goal is to create a microenvironment that promotes immunological tolerance, preventing an excessive inflammatory response that could compromise the viability and functionality of the implanted hydrogel [492,493]. Hydrogels with immunomodulatory properties frequently integrate biomaterials such as hyaluronic acid, collagen, silk fibroin, chitosan, among others. These biomaterials either possess intrinsic immunomodulatory capabilities or can be modified to actively modulate immune cell behavior [490,491,494]. Furthermore, the hydrogels may be designed to promote the recruitment of regulatory immune cells, such as T regulatory cells, which play an important role in suppressing immune reactions and facilitating a more tolerogenic environment. This strategic modulation of immune cell dynamics is aimed at minimizing the risk of rejection and creating a permissive setting for the hydrogel to integrate seamlessly with the host tissue [495]. Furthermore, in cardiac TE, incorporating specific molecules and drugs into hydrogels shows significant promise for augmenting their immunomodulatory capabilities. Alongside biomaterials known for their enhanced immunomodulatory properties in hydrogel design for cardiac tissue regeneration, research has also investigated the inclusion of anti-inflammatory agents like cytokines or growth factors [494,496]. For instance, interleukin-10 (IL-10), an anti-inflammatory cytokine, has been explored for its potential to suppress immune responses [497,498]. Moreover, the controlled release of immunomodulatory drugs, including tacrolimus and cyclosporine, traditionally used as immunosuppressants can be tailored to regulate the immune microenvironment surrounding cardiac tissues [499,500].

Electroconductive hydrogels have demonstrated significant potential in modulating immune responses in cardiac TE, a specific aspect for fostering tissue repair and mitigating inflammatory complications [224,379,488]. This immunomodulation is intricately influenced by specific cardiac cell types, including cardiomyocytes, cardiac fibroblasts, endothelial cells, and macrophages, each contributing uniquely to inflammation regulation and healing [224,488]. Cardiomyocytes benefit from the conductive environment of electroconductive hydrogels, which supports their survival, reduces oxidative stress, and limits pro-inflammatory cytokine secretion [224,379,488]. Cardiac fibroblasts, essential for ECM remodeling, adopt a reparative phenotype in electroconductive hydrogels, minimizing pathological fibrosis and maintaining tissue integrity [91,460]. Endothelial cells are stimulated by electroconductive hydrogels to enhance angiogenesis, improving oxygenation and nutrient delivery while indirectly controlling immune cell behavior [31,379]. Macrophages play a central role in the immune response of the heart, acting as key regulators of inflammation and tissue repair. These cells exhibit significant plasticity, meaning they can shift between two primary functional states: the pro-inflammatory M1 phenotype and the anti-inflammatory M2 phenotype [86,477]. The M1 phenotype is typically associated with the release of cytokines and other mediators that exacerbate inflammation and contribute to tissue damage [489,501]. In contrast, the M2 phenotype is linked to tissue repair and resolution of inflammation, characterized by the secretion of anti-inflammatory cytokines and growth factors that promote cell proliferation and wound healing [489,501]. Recent studies have highlighted the potential of electrospun electroconductive hydrogels in influencing macrophage polarization, due to their interesting material properties including surface chemistry, electrical conductivity and

mechanical properties. These hydrogels can mimic the natural ECM, providing a microenvironment that encourages macrophages to adopt an M2 phenotype, thereby mitigating the harmful effects of excessive inflammation [224,488]. This polarization shift is particularly beneficial in the context of cardiac tissue repair, as M2 macrophages can release key growth factors such as VEGF and TGF-β, which facilitate angiogenesis and collagen remodeling, suitable processes in healing after myocardial injury. By modifying macrophage behavior through these material interactions, electroconductive hydrogels not only reduce local inflammation but also promote regenerative healing, thereby directly influencing the inflammatory microenvironment within the heart [224,488]. Wei et al. [224] developed a novel cardiac patch for cardiac remodeling post-myocardial infarction (MI) by combining brown adipose-derived stem cell (BADSC) sheets with electrospun polycaprolactone/silk fibroin nanofibers containing carbon nanotubes (CNTs). The electrically conductive electrospun hydrogels achieved were named CPSN. The study demonstrated that BADSCs on CPSN formed myocardium-like structures, promoting gap junction remodeling and restoring cardiac function. In a rat MI model, the CNBS patch significantly modulated the immune environment, decreasing the infiltration of CD45-positive leukocytes at the infarction site compared to the no-treatment control group (Fig. 25A(i,ii)) [224]. Additionally, CD68 protein expression, a marker of macrophages, was significantly reduced in the CNBS group (Fig. 25A(iii,iv)), suggesting decreased macrophage presence. Immunohistochemistry staining revealed that the CNBS patch decreased pro-inflammatory M1 macrophage marker IL-1β while increasing the anti-inflammatory M2 macrophage marker CD163 (Fig. 25A(v,vi)). The CNBS group also exhibited a higher CD163/IL-1β ratio compared to the CPSN-sus and no-treatment groups. Moreover, CNBS treatment led to decreased IL-1β and TNF-α mRNA expressions and increased IL-10 mRNA expression (Fig. 25A(vii)). ELISA assays confirmed that CNBS treatment significantly reduced inflammatory factors (IL-8, TNF-α, and IL-10) in rat serum (Fig. 25A(viii)), promoting an immunoreparative environment for tissue regeneration [224]. Gil-Castell et al. [488] designed electrospun nanofiber scaffolds based on polycaprolactone (PCL), gelatin (Ge), and PANi particles for cardiac TE applications. The researchers fabricated scaffolds with varying PCL/Ge ratios (60/40, 50/50, and 40/60) and PANi contents (0.25 wt%, 0.50 wt%, and 1.00 wt%). Fig. 25B shows SEM images of the electrospun composite scaffolds obtained. The study demonstrated that increasing gelatin content and dissolution time (DT) enhanced scaffold biocompatibility and degradation. The incorporation of PANi in electrospun fibrous scaffolds promoted a controlled increase in electrical conductivity of resulting composites, which stimulated cardiomyocyte proliferation without impairing cellular growth [488]. To confirm cell attachment to the scaffolds, cells were seeded, fixed after 48 and 96 h, and stained with DAPI. The images, shown in Fig. 25C, revealed cell presence on all scaffolds. Cell proliferation in the scaffolds increased with higher Ge content due to its higher biocompatibility. In the 60/40 PCL/Ge composition, few cells were observed, while in the 40/60 nanofibers, cell numbers increased and occupied more surface after 96 h. Scaffolds electrospun after 24 and 48 h showed similar results [488]. Moreover, the effect of combined PCL, Ge, and PANi on the macrophage profile was evaluated using PCL/Ge/PANi scaffolds with different compositions. The expression profiles of TNFα (M1 marker) and CD206 (M2 marker) were analyzed through qPCR, and the results are shown in Fig. 25D [488]. None of the scaffolds impaired macrophage polarization. Significant differences were observed between the control and cells seeded onto the scaffolds when assessing the change in TNFα marker. Macrophages seeded on scaffolds containing PANi (1.00 %wt) exhibited less expression of the proinflammatory cytokine TNFα than control cells. Moreover, all the compositions analyzed exhibited similar behavior, indicating that variations in the percentages of PCL and Ge had a negligible impact on the overall response. A similar trend was observed when assessing CD206, a specific marker of the M2 profile, where no relevant differences were found between control cells and cells seeded onto the scaffolds [488]. This study demonstrated that the incorporation of PANi at 1 %wt in PCL/Ge scaffolds modulated the inflammatory response of macrophages by downregulating the expression of the proinflammatory cytokine TNFα, typically associated with the M1 phenotype. However, this reduction does not conclusively indicate a shift in macrophage polarization, as polarization involves a complex interaction of multiple markers. Specifically, no significant differences in CD206 expression, a marker of the M2 phenotype, were observed between control cells and those seeded onto PANi-containing scaffolds. These findings suggest that while PANi may reduce M1-associated proinflammatory activity, it does not induce a complete shift toward the M2 phenotype. Therefore, PANi-containing scaffolds likely promote a moderated inflammatory response by attenuating M1 activity without significantly altering overall macrophage polarization [488].

7. Cellular interactions in electrically conductive hydrogels

7.1. Cell adhesion and spreading

Cells seeded in electrically conductive hydrogels undergo adhesion and spreading, where the interactions between the cells and the material significantly influence the early stages of tissue development. Electroconductive hydrogels offer specific biochemical and biophysical cues that enable cells to interact with the material chemical functions to support tissue development [472,502]. Initially, electroconductive hydrogels should present a biocompatible environment that could mimic properties and features of the native ECM. This similarity allows integrin receptors on the cell membrane to recognize and bind to specific ligands or functional groups on the hydrogel surface. This initial adhesion triggers signaling pathways within the cell, leading to the formation of focal adhesions and cytoskeletal rearrangements. These processes stabilize the cell on the hydrogel surface and facilitate spreading [384,503].

Once cells have successfully adhered, the next step in this coordinated process involves cell spreading. Cell spreading involves the extension of adhered cells across the surface of the hydrogel, a process that is significantly influenced by the functional and conductive properties of the hydrogel [504]. The electrical and biochemical cues provided by the electroconductive hydrogel can actively guide cytoskeletal organization, shaping cellular morphology and influencing the spatial arrangement of cells [505]. This dynamic interaction is particularly significant in cardiac TE, where the orchestrated spreading of cardiac cells holds paramount importance for the synchronized contraction necessary for optimal heart function [53,96]. Furthermore, the promotion of cell spreading within electroconductive hydrogels is crucial for tissue development. Cell spreading is a dynamic process where cells extend filopodia and lamellipodia, which are thin, finger-like projections and broad, sheet-like extensions, respectively [506,507]. These structures allow cells to explore and adhere to the surface of the hydrogel substrate, thereby increasing the contact area between the cell membrane and the material. This spreading process is influenced by various factors, including the topography, surface chemistry and electrical conductivity of the hydrogel. Enhanced cell spreading facilitates stronger interactions between cells and the hydrogel, promoting cellular adhesion, proliferation, and ultimately the formation of functional tissues constructs [507,508].

7.2. Cell proliferation and viability

Ensuring effective cell proliferation and viability in electroconductive biopolymer-based hydrogels is crucial for advancing cardiac TE. These hydrogels act as dynamic matrices that regulate cellular processes by providing tailored electrical, chemical, and mechanical cues, enabling seeded cells within the hydrogels to interact and perform their normal functions, facilitating the formation of functional tissue structures [159,160,248,326]. Electrical conductivity in the hydrogel

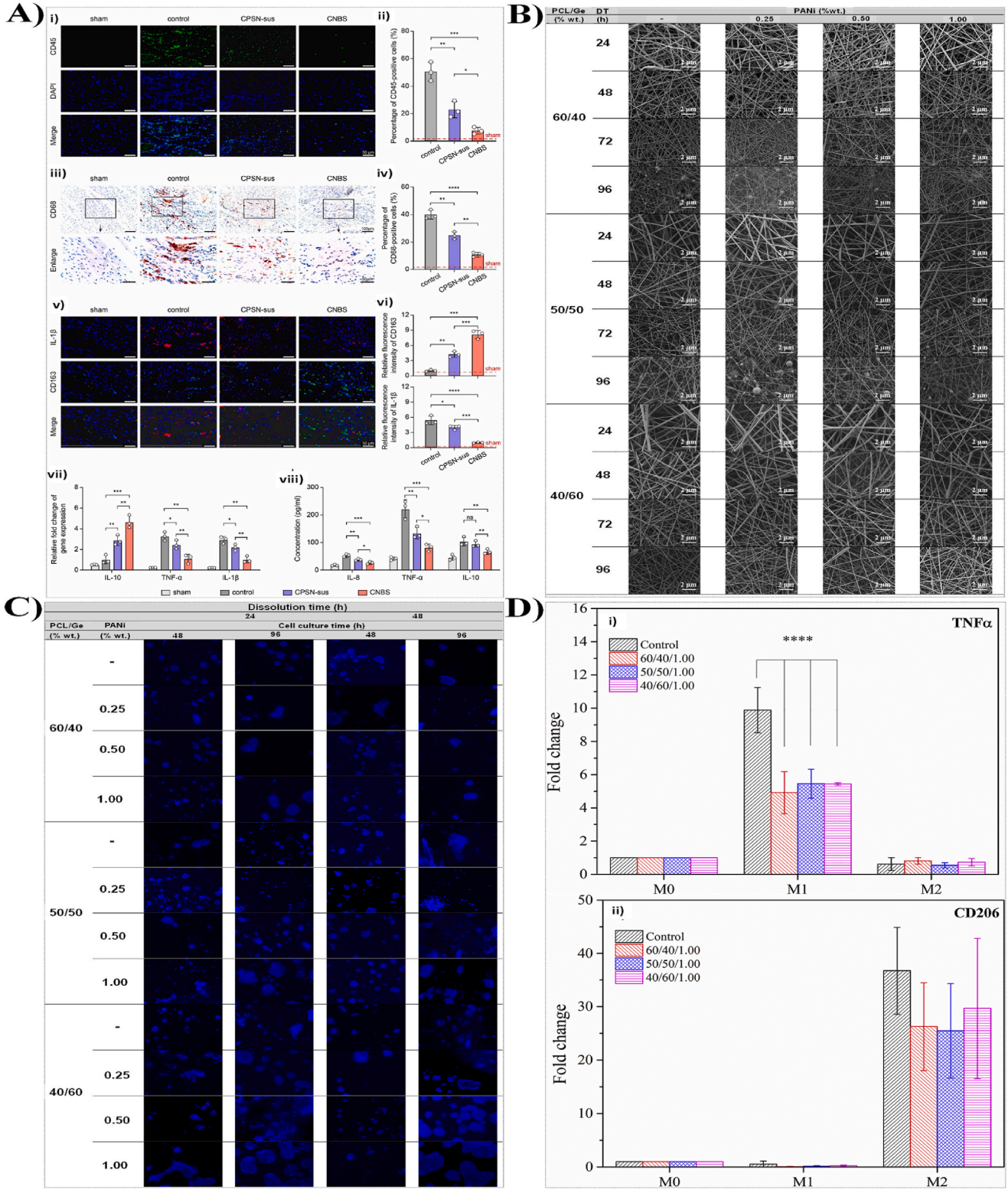

Fig. 25. (A) Immune modulation by CNBS patches in vivo post-MI. (i and ii) Immunofluorescent images of CD45 (green) showing leukocyte infiltration four weeks after transplantation, along with the quantification of CD45-positive cells. (iii and iv) Immunohistochemical images of CD68, depicting macrophage infiltration, with corresponding quantification. (v and vi) Immunohistochemistry staining showing a reduction in pro-inflammatory IL-1β (red) and an increase in anti-inflammatory CD163 (green). (vii) Relative mRNA expression of inflammation-related genes measured by RT-qPCR across the three groups. (viii) Serum levels of inflammatory cytokines IL-8, TNF-α, and IL-10 detected by ELISA. For panels (i) and (v), nuclei were counterstained with DAPI (blue). Data are presented as mean ± SD. Reproduced with permission from Ref. [224] Copyright © 2023, Elsevier. (B) Surface morphology of scaffolds based on PCL/Ge composition, PANi content, and DT (10000 × magnification). (C) Nuclear staining with DAPI after culturing cells on 60/40, 50/50, and 40/60 PCL/Ge scaffolds with varying PANi content over 48 and 96 h, based on DT. Reproduced with permission from Ref. [488] Copyright © 2022, Elsevier. (D) Gene expression associated with M1 (TNFα) (i) and M2 (CD206) markers (ii). Reproduced with permission from Ref. [488] Copyright © 2022, Elsevier.

enables the transmission of signals crucial for maintaining cell function and communication [433,509]. The incorporation of conductive polymers or nanoparticles endows these hydrogels with electrical conductivity. These electrical cues are not merely passive characteristics but actively guide cellular processes, fostering synchronized contractions in cardiomyocytes [510]. Furthermore, chemical cues provided by specific chemical functionalities present in hydrogels can facilitate essential processes such as cell adhesion, spreading, and differentiation, crucial for tissue development. The chemical composition of biomaterials and electroconductive polymers in the hydrogel offers a repertoire of cues influencing cellular responses. Meanwhile, the mechanical properties of the hydrogel, including its stiffness and elasticity, should provide structural support and mechanical cues that guide cellular activities [40,41,160]. In cardiac TE, the mechanical properties of electroconductive biopolymer-based hydrogels are commonly tailored to exert precise influences on cellular behavior through mechanotransduction processes [444]. The mechanical cues in the hydrogel matrix can profoundly affect cell morphology. Cells exhibit distinct morphological features in response to the mechanical properties of their surrounding environment [511]. Hydrogels engineered to mimic the stiffness and elasticity of native cardiac tissues guide cells to adopt shapes and structures conducive to their physiological functions, such as elongation and alignment of cardiomyocytes. Furthermore, the mechanical cues exert a regulatory influence on the proliferation rates of cells in the hydrogel. The stiffness and elasticity of the hydrogel matrix can either promote or inhibit cell division [445,512]. Mimicking the mechanical characteristics of the native cardiac tissue should provide cues that synchronize with the cell cycle, thereby modulating the rate at which cells proliferate in the engineered constructs. The mechanical cues extend their influence to the broader aspect of tissue development in the hydrogel. They guide processes such as tissue maturation, alignment of cells, and the formation of functional tissue structures [191,513].

7.3. Cell differentiation and maturation - phenotypic expression

The ability of electroconductive hydrogels to actively guide cellular differentiation is an important aspect, particularly in the context of stem cells [510]. Stem cell differentiation refers to the process by which undifferentiated or unspecialized cells undergo changes in gene expression and cellular characteristics to transform into specialized cells with specific functions [514]. Stem cells possess the unique capability to differentiate into diverse cell types, with differentiation serving as the primary mechanism that directs them toward a specific lineage or fate [515]. Electroconductive hydrogels, enriched with materials promoting the transmission of electrical signals within hydrogels introduce an advanced dimension to this differentiation phenomenon. The integration of electrical cues within the hydrogel matrix could exert a profound influence on the lineage commitment of stem cells [290,516]. Electrically conductive hydrogels transmit signals that act as instructive stimuli, influencing the fate of stem cells by modulating intracellular signaling pathways [290,425]. In addition, the unique electroconductive environment within the hydrogel actively facilitates the development of specific cell types relevant to the desired tissue regeneration [114]. Specific biochemical and physical signals incorporated into the hydrogel, such as growth factors, cytokines and mechanical stimuli, generally guide cell differentiation towards the cardiac lineage. The controlled release of these factors from the hydrogel matrix could influence gene expression and cellular behaviors, facilitating the maturation of cardiomyocytes with properties resembling those of native heart tissue [450,517,518].

Moreover, the hydrogel biomaterial composition and electrical conductivity acts as a regulatory factor guiding cells toward desired phenotypic expressions. Electroconductive hydrogel not only acts as a physical scaffold for cellular adherence but also actively communicates with cells, influencing their gene expression patterns [510]. The interaction between electrical components and the intrinsic biochemical environment in the hydrogel creates a microenvironment that supports the expression of specific proteins, transcription factors and signaling molecules conducive to the desired cellular phenotypes [519]. Cardiac cell phenotypic expression refers to the observable characteristics and functional traits that these cells exhibit in response to various stimuli within their microenvironment [520]. In electroconductive hydrogels, the phenotypic expression of cardiac cells involves intricate molecular and cellular responses. The properties of the hydrogels create an environment that influences the cells to adopt specific traits. This includes changes in gene expression, protein synthesis, and cellular morphology, all of which contribute to the overall function of the cardiac cells [25,291]. Electroconductive hydrogels interact with cells through multiple signaling pathways, including ion channels, membrane receptors, and intracellular cascades. This interaction facilitates a controlled differentiation process, enabling the generation of various cell types within these hydrogels [111,521]. Cardiac cells cultured in electrically conductive hydrogels, frequently showcased heightened contractile capabilities, improved alignment, and an upswing in the expression of cardiac-specific markers, including troponins and connexins. Navaei et al. [522] used micro- and nano-technologies to fabricate gelatin methacrylate (GelMA) hydrogels incorporating electrically conductive gold nanorods (GNRs) and microgrooves. In comparison to pure GelMA, GelMA–GNR hydrogels exhibited uniform, dense, and aligned cardiac tissues with enhanced connectivity and electrical properties, indicating potential functionality as cardiac patches in myocardial infarction scenarios (Fig. 26A) [522]. F-Actin stained images and fluorescent area coverage data depicted the formation of organized cardiac tissues on GelMA–GNR hydrogels, contrasting with disconnected cellular arrangements in pure GelMA constructs (Fig. 26B) [522]. Immunostaining images of cardiac markers, particularly sarcomeric α-actinin and connexin 43, revealed heightened cytoskeletal alignment and improved cellular connectivity on GelMA–GNR hydrogels (Fig. 26B). While tissues on both GelMA and GelMA–GNR constructs displayed spontaneous contractility from day 4–7 of culture, only electrically conductive GelMA–GNR cardiac tissues consistently responded to changes in beat rate upon external stimulation [522]. Roshanbinfar et al. [60] investigated the effects of incorporating PANi into electrospun collagen, and/or hyaluronic acid-based fiber mats on neonatal rat and hiPSC-derived cardiomyocytes. At day 5, cardiomyocytes attached and spread on all fiber mats, displaying striated sarcomeres, with no significant differences in surface coverage (Fig. 26C). However, connexin 43 expression increased with higher PANi concentrations, particularly in PANi3 and PANi4 (Fig. 26C), indicating improved intercellular coupling. PANi4, which exhibited thinner, more aligned fibers, also showed higher conductivity, enhancing cellular beating properties [60]. Despite this, no significant increase in cellular alignment was observed, likely due to fiber mat swelling and the scale of alignment cues. In testing with hiPSC-derived cardiomyocytes, PANi4 scaffolds exhibited the highest contraction amplitude and connexin 43 expression, with rhythmic beating. Confocal analysis revealed differences in microstructure among collagen, collagen-HA, and PANi4 mats, and no significant differences in cell viability (Fig. 26D). The hiPSC-derived cardiomyocytes developed organized striated structures on all scaffolds (Fig. 26D), supporting the potential of PANi-based scaffolds for cardiac TE [60]. A recent study examined the impact of electrical conductivity on the phenotypic expression of cardiac cells cultured on engineered electrospun hydrogels containing PPy nanoparticles compared to non-conductive substrates [458]. Alpha-actinin, a cytoskeletal protein vital for maintaining sarcomere integrity in cardiomyocytes, and connexin-43, a key component of gap junctions essential for intercellular electrical communication in the heart, were used as markers to assess cellular health and function. After 3 days of culture, cardiomyocytes on non-conductive electrospun GelMA/PCL membranes displayed a round morphology and lacked intact sarcomeres (Fig. 26E). In contrast, CMs on conductive membranes containing Ppy nanoparticles formed typical sarcomeres [458]. By day 7, CMs on the conductive membranes

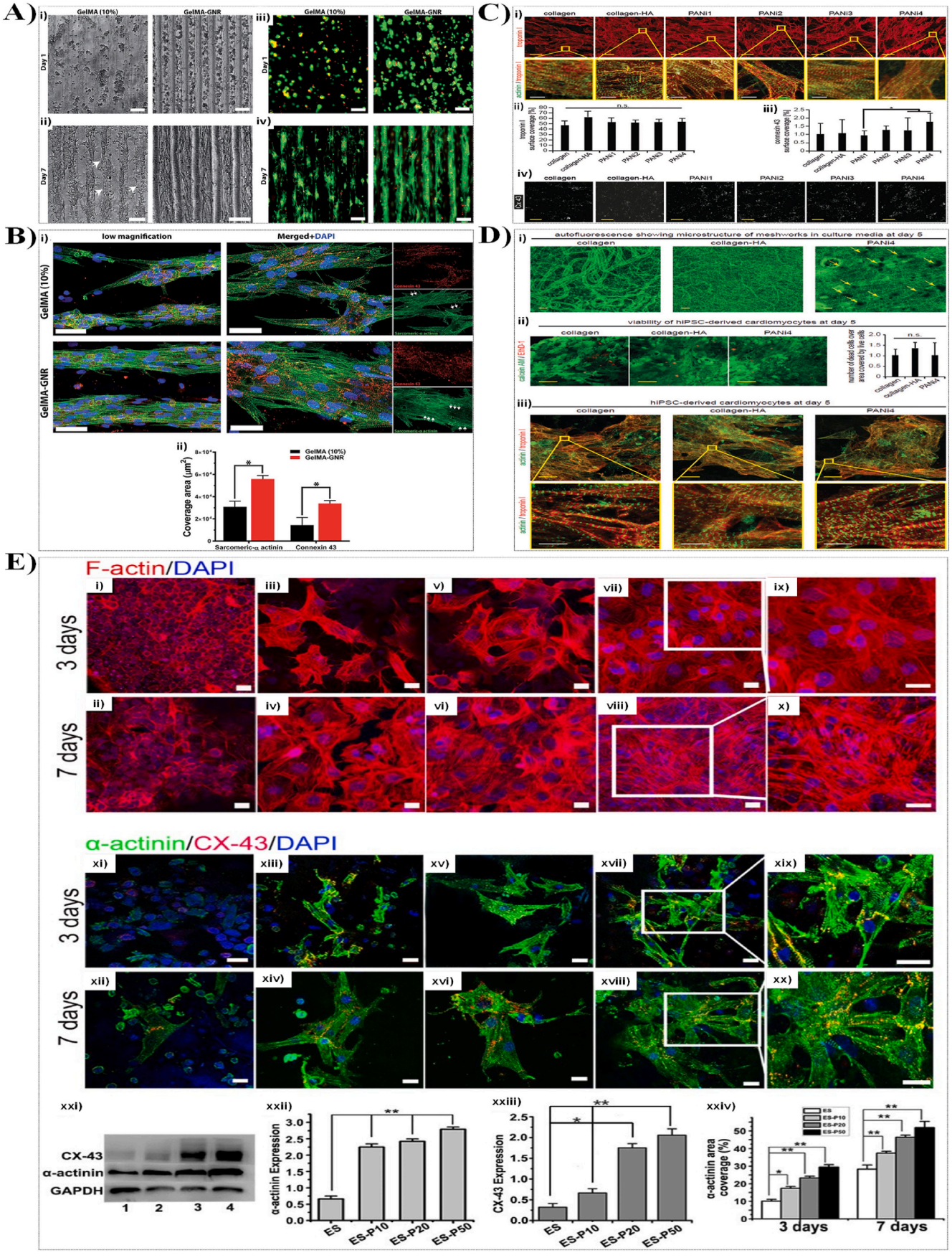

(caption on next page)

Fig. 26. (A) Phase-contrast micrographs depicting cardiac cell cultures on GelMA and GelMA–GNR micro-grooved hydrogels at (i) day 1 and (ii) day 7. White arrows indicate cellular cluster discontinuity. Fluorescent viability images of GelMA and GelMA–GNR micro-grooved cardiac tissues on (iii) day 1 and iv) day 7, with live cells stained in green and dead cells in red. Scale bars denote 100 μm. (B) i) Immunostained images illustrating SATN (green) and Cx43 gap junctions (red) in GelMA and GelMA–GNR micro-grooved cardiac tissues on day 7. White arrows highlight uniaxially aligned sarcomeric structures. Scale bars: 50 μm for low magnification, 20 μm for merged images. ii) Quantified area coverage of cardiac-specific markers on day 7. Reproduced with permission from Ref. [522] Copyright © 2017 Royal Society of Chemistry. (C) Cardiomyocyte Interaction with Electrospun Fiber Mats. (i) Confocal projections showing neonatal cardiomyocytes cultured on electrospun fiber mats at day 5, stained for cardiomyocyte markers troponin I, sarcomeric-α-actinin, and connexin 43. (ii) Quantitative analysis of surface coverage by troponin I-positive cells. (iii) Quantitative analysis of connexin 43 surface coverage. iv) Confocal projections highlighting connexin 43 distribution in cardiomyocytes. Data are mean ± SD, scale bars: yellow: 25 μm, white: 4 μm. (D) Fibrous Structure and hiPSC-Derived Cardiomyocyte Response. (i) Autofluorescent images of fiber mats, with yellow arrows indicating PANi presence. (ii) Live/dead staining of neonatal rat cardiomyocytes at day 5 using calcein-AM (green) and EthD-1 (red) with quantitative analysis. (iii) Confocal projections showing hiPSC-derived cardiomyocytes on fiber mats stained for troponin I and/or sarcomeric-α-actinin. Data are mean ± SD, n.s. indicates nonsignificant differences. Scale bars: yellow: 10 μm, white: 4 μm. Reproduced with permission from Ref. [60] Copyright © 2020 WILEY-VCH Verlag GmbH & Co. KGaA, Weinheim. (E) Mussel-inspired conductive membranes enhanced cardiomyocyte (CM) function. Filamentous actin (F-actin) staining of CMs cultured on various membranes for 3 and 7 days. (i,ii) Pristine ES-GelMA/PCL (ES); (iii,iv) dopa-based ES-P10; (v,vi) dopa-based ES-P20; (vii,viii,ix,x) dopa-based ES-P50. Scale bars, 20 μm. Staining for α-actinin (green) and Cx-43 (red) expression in CMs on membranes at day 3 and day 7. (xi,xii) ES; (xiii,xiv) ES-P10; (xv,xvi) ES-P20; (xvii, xviii,xix,xx) ES-P50. Scale bars, 20 μm. (xxi) Western blot analysis of α-actinin and CX-43 protein expression in CMs on membranes at day 7 of culture. Line 1: ES; Line 2: ES-P10; Line 3: ES-P20; Line 4: ES-P50. (xxii, xxiii) Quantitative analysis of α-actinin (xxii) and CX-43 protein expression (xxiii) in CMs based on Western blotting. (xxiv) α-actinin area coverage in CMs on membranes at days 3 and 7 based on immunofluorescence. ES: pristine ES-GelMA/PCL membrane; ES-P10: dopa-based ES-P10 membrane; ES-P20: dopa-based ES-P20 membrane; ES-P50: dopa-based ES-P50 membrane. All data are presented as mean ± SD. Reproduced with permission from Ref. [458] Copyright © 2018, Ivyspring International Publisher.

exhibited more elongated, highly packed sarcomeres, with a significantly higher expression of α-sarcomeric protein. Additionally, Cx43 expression was significantly higher in CMs cultured on conductive membranes, particularly at the inter-sarcomere and inter-cellular membranes (Fig. 26E). The conductive membranes, with a highest concentration of GelMA-Ppy nanoparticles, resulted in a significant increase in the sarcomeric α-actinin-positive area, which reached 30 % and 55 % on days 3 and 7, respectively, compared to only 10 % and 30 % on non-conductive membranes (Fig. 26E). These findings highlighted the importance of electrical conductivity, facilitated by PPy nanoparticles, in enhancing the structural and functional integration of cardiac cells, suggesting its potential for improving cardiac TE applications [458].

Stem cell-based therapy holds significant potential for cardiac repair and regeneration, yet its clinical application is often hindered by challenges related to the limited efficiency of cardiac differentiation [523, 524]. To address this, researchers have explored the incorporation of electrically conductive components like CNTs into hydrogel matrices as a means to design a more instructive extracellular microenvironment for stem cell cardiogenesis [523]. They aimed to investigate whether CNTs enhance the differentiation of stem cells into cardiomyocytes and to elucidate the molecular signaling pathways that mediate this process. The electroconductive properties of CNTs, when embedded within hydrogel scaffolds, have been shown to influence stem cell behavior by promoting cell adhesion, growth, and alignment, thereby facilitating the differentiation of stem cells into functional cardiac cells [523]. They demonstrated that incorporating CNTs into collagen substrates (CNT-Col) provided an electroconductive ECM that significantly enhanced cardiogenesis in brown adipose-derived stem cells (BASCs) via the β1-integrin-dependent transforming growth factor-beta 1 (TGF-β1) signaling pathway. BASCs cultured on CNT-Col substrates exhibited enhanced cell adhesion, spreading, and growth. Notably, fluorescence staining and quantitative real-time reverse transcription-polymerase chain reaction revealed that CNT-Col substrates markedly improved cardiac differentiation efficiency compared to collagen alone, with a higher percentage of α-sarcomeric actinin-positive ($\alpha\text{-SA}^{+}$) cells observed on CNT-Col substrates by day 3, 7, and 10 (Fig. 27A). BASCs on CNT-Col substrates adopted an elongated rod shape, displayed spontaneous contractile activity, and formed myofilaments indicative of mature cardiomyocytes. By day 10, these cells assembled into organized bundles with uniform contraction, aligning into sarcomere registers with superior structural maturity compared to those on collagen substrates (Fig. 27A) [523]. A detailed schematic model was proposed to elucidate the mechanism by which CNTs promote cardiac differentiation of brown adipose-derived stem cells (BASCs) via TGF-β1 signaling pathway (Fig. 27B). In this model, CNTs embedded in the ECM interact with β1-integrin, a transmembrane receptor, triggering its activation. This activation facilitates the release of active TGF-β1, a key growth factor involved in cellular differentiation and development. The released TGF-β1 binds to its receptor complexes on the BASC membrane, initiating downstream intracellular signaling (Fig. 27B) [523]. This cascade includes the phosphorylation and activation of Smad2 (p-Smad2), a central mediator in the TGF-β1 pathway. Activated p-Smad2 translocates to the nucleus, where it modulates the expression of cardiac-specific transcription factors. These transcription factors drive the differentiation of BASCs into cardiomyocytes by regulating genes responsible for sarcomeric organization, contractile protein expression, and functional maturation (Fig. 27B) [523].

Moreover, electroconductive CNT-based hydrogels were shown to enhance the assembly of intercalated discs (IDs) in cardiac myocytes through the β1-integrin-mediated signaling pathway, with results providing a mechanistic understanding of this enhancement [525]. Neonatal rat ventricular myocytes (NRVMs) cultured on CNT-Col substrates exhibited significant improvements in ID-related protein expression, including connexin43 (Cx43) for gap junctions, N-cadherin (NC) for adherens junctions, and plakophilin2 (PKP2) and plakoglobin (PG) for desmosomes. Immunofluorescence revealed that, by day 3, these proteins were more abundant and localized in intercellular regions in the CNT-Col group compared to controls (Fig. 27C) [525]. Western blotting confirmed significantly higher levels of these proteins in NRVMs on CNT-Col substrates relative to collagen-only (Col) substrates (Fig. 27C). By day 7, IDs in CNT-Col cultures showed progressive protein organization, with Cx43 forming linear plaques and NC, PKP2, and PG aligning in intercellular regions. This trend continued through day 14, with CNT-Col cultures displaying well-developed IDs, including larger and more numerous gap and mechanical junctions, compared to the control group (Fig. 27C). Functional assessment revealed that NRVMs on CNT-Col substrates formed a functional syncytium with stable rhythmic calcium transients by day 7, whereas controls displayed arrhythmic fluctuations (Fig. 27D) [525]. A schematic model was proposed to explain the mechanism by which CNTs accelerate the assembly of IDs in cardiac myocytes. The model highlights that CNTs interact with β1-integrin receptors at the cell membrane, initiating a cascade of intracellular signaling events important for ID formation (Fig. 27E). Upon activation, β1-integrin triggers the focal adhesion kinase (FAK) signaling pathway, which in turn activates downstream signaling molecules, including extracellular signal-regulated kinase (ERK). The ERK pathway plays a pivotal role in modulating transcriptional activity by stimulating cardiac-specific transcription factors such as GATA-binding protein 4 (GATA4) and myocyte enhancer factor-2c (MEF-2c) [525]. These transcription factors regulate the expression of genes coding for gap junction proteins, notably connexin43 (Cx43), a key component of

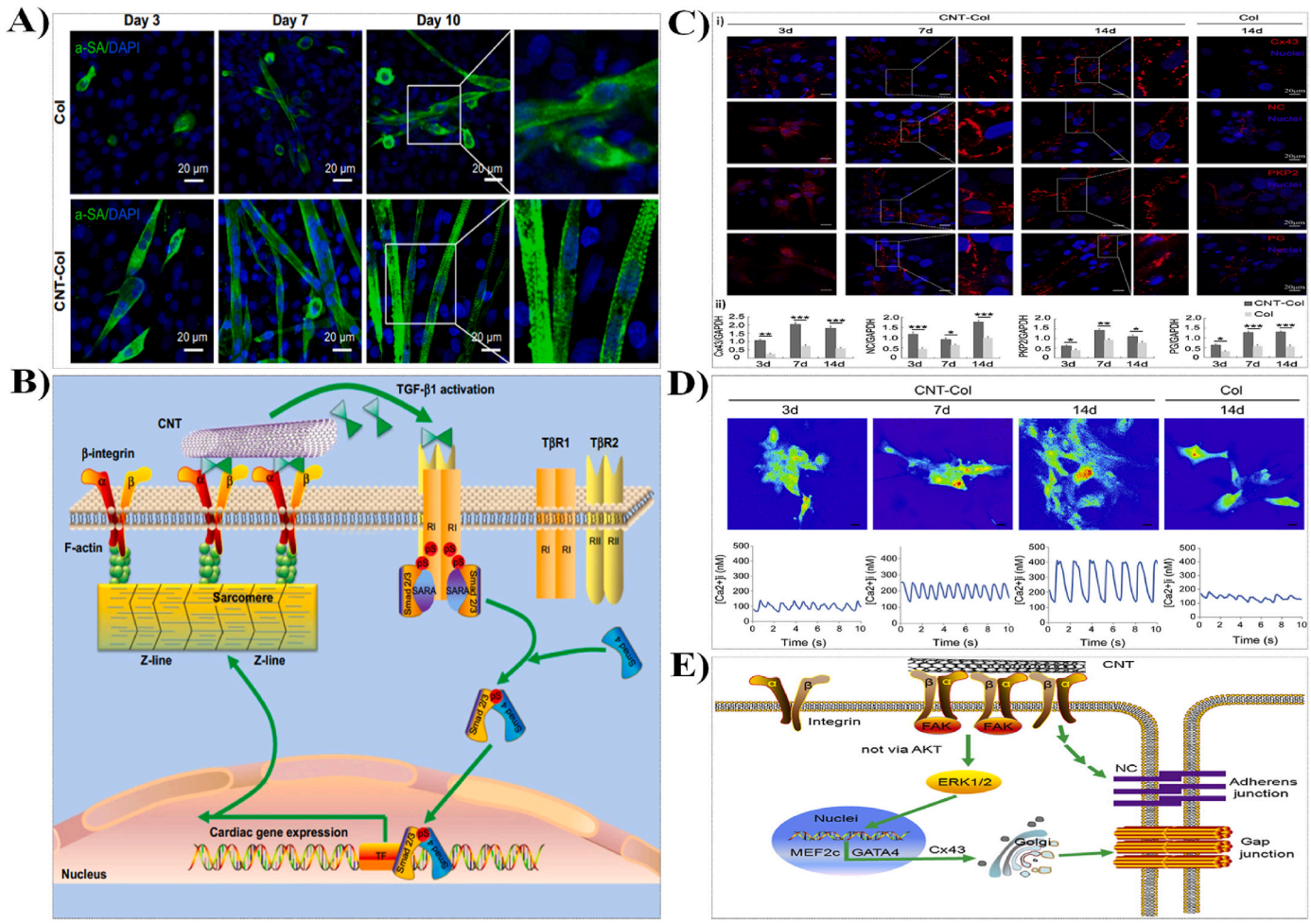

Fig. 27. (A) CNTs accelerated cardiogenesis in brown adipose-derived stem cells (BASCs) and enhanced the maturation of BASC-derived cardiomyocytes (BASC-CMs). Immunofluorescent staining of α-sarcomeric actin (α-SA) demonstrated BASCs cultured on CNT-collagen (CNT-Col) and collagen (Col) substrates at days 3, 7, and 10. (B) A schematic representation illustrating the promotion of BASC cardiac differentiation by CNTs via the β1 integrin-dependent TGF-β1 signaling pathway. Reproduced with permission from Ref. [523] Copyright © 2016, Dove Medical Press. (C) Immunofluorescent staining and quantification of intercalated disc (ID)-related proteins in neonatal rat ventricular myocytes (NRVMs) cultured on CNT-Col and Col substrates over 3, 7, and 14 days. (i) At day 3, connexin43 (Cx43) was scattered along the cell membrane, while N-cadherin (NC), plakophilin2 (PKP2), and plakoglobin (PG) accumulated in faint striped patterns near the perinuclear region and plasma membrane. By day 7, Cx43 formed numerous polymorphic gap junction plaques on CNT-Col substrates, while NC, PKP2, and PG gathered in large linear intercellular regions. By day 14, NRVMs on CNT-Col substrates exhibited localized ID structures, including punctate Cx43 plaques, strand-like fascia adherens, and whisker-like PKP2 distributions. In contrast, NRVMs on Col substrates showed smaller ID regions. Scale bars = 20 μm. (ii) Western blot analysis revealed significantly higher expression of Cx43, NC, PKP2, and PG in cardiac patches grown on CNT-Col substrates compared to Col substrates across all time points. Data are represented as mean ± standard error of the mean. (D) Spontaneous calcium transients in NRVMs cultured on CNT-Col substrates displayed more rhythmic patterns and higher amplitudes compared to Col substrates. Confocal laser microscopy images and corresponding intracellular calcium transient time-course plots are shown. Scale bars = 20 μm. (E) A schematic model illustrating CNT-induced β1-integrin activation, subsequent signaling through FAK and ERK pathways, and regulation of ID assembly via transcription factors GATA4 and MEF-2c. Reproduced with permission from Ref. [525] Copyright © 2015, Elsevier.

electrical coupling in cardiac myocytes. Consequently, this signaling cascade facilitates the organization and assembly of mechanical junctions, such as adherens junctions and desmosomes, as well as gap junctions, which are essential for the structural and functional integrity of IDs [525]. The enhanced localization and maturation of ID-related proteins, including Cx43, N-cadherin, plakophilin2 (PKP2), and plakoglobin (PG), on CNT-collagen substrates corroborate this mechanism. These findings elucidate the role of β1-integrin-mediated signaling in orchestrating the molecular and structural processes underlying the accelerated assembly of IDs facilitated by CNTs, offering valuable insights into the nanomaterial-induced modulation of cardiac cell behavior [525].

In the context of stem cell-derived cardiomyocytes cultured in electroconductive hydrogels, RNA-sequencing (RNA-seq) has been employed to analyze cardiomyocyte differentiation and maturation over time [90,526]. This has allowed for a comprehensive understanding of how electroconductive hydrogels influence the development and functionality of stem cell-derived cardiomyocytes, and has provided a platform for optimizing cardiac TE strategies. RNA-seq also enables the detection of genes involved in cellular processes like contractility, electrical signaling, and metabolic activity, which are essential for the functional maturation of cardiomyocytes [90,526,527]. The presence of electrically conductive materials in hydrogels promotes the maturation of hiPSC-cardiomyocytes. Several studies have demonstrated that incorporating PEDOT:PSS into hydrogels enhanced the expression of cardiac-related genes associated with cell maturation [90,526]. Gonzalez et al. [526] fabricated fibrillar electroconductive scaffolds by blending and electrospinning polyvinyl alcohol (PVA) and PEDOT:PSS, followed by crosslinking for 15 or 30 min to prevent PVA dissolution. The SEM images of electrospun fibrous scaffolds are shown in Fig. 28A (i,ii). The addition of PEDOT:PSS in PVA matrix increased the initial fiber diameter compared to the diameter of PVA-scaffolds (Fig. 28A(iii,

iv)). Scaffold stiffness, which influences stem cell behavior, scaled with PEDOT:PSS concentration (Fig. 28A(v)) and was consistent with normal cardiac muscle stiffness. The conductivity of the PEDOT:PSS/PVA scaffolds was measured using a transmission line model, revealing that the incorporation of PEDOT:PSS into PVA substantially increased the electrical conductivity of the resulting electroconductive fibrous scaffolds, reaching 7×10^{-3} S/cm^2 for 8 % PVA electrospun scaffolds containing 9.75 % PEDOT:PSS (Fig. 28A(vi)) [526]. In that study, the fabricated electroconductive PEDOT:PSS/PVA scaffolds were found to upregulate cardiac-related genes, improve cytoskeletal structures, and aid calcium handling and membrane depolarization in human pluripotent stem cell-derived cardiomyocytes (hPSC-CMs). Transcriptomic differences were examined through principal component analysis, which showed clustering based on substrate type, with increased dissimilarity between conductive and non-conductive scaffolds (Fig. 28B(i)). A total of 287 differentially expressed genes (DEGs) were identified between hPSC-CMs seeded on PVA-only and PEDOT:PSS/PVA-scaffolds (Fig. 28B (ii)) [526]. Gene ontology (GO) terms associated with PVA-only scaffolds highlighted stress responses, including immune and viral responses, while PEDOT:PSS/PVA scaffolds were linked to heart and muscle-related functions, including muscle contraction and decreased stress response (Fig. 28B(iii)). Further analysis revealed that gene expression related to hPSC-CM contractility (MYH6, MYH7, MYL7), sarcomere organization (TCAP), and electrophysiology (KCNIP2, ATP1A2, RNF207) was elevated on conductive scaffolds (Fig. 28B(iv)). Notably, MYH7, a marker of hPSC-CM maturity was upregulated, suggesting that the electroconductive environment promoted not only increased cardiomyocyte contractility but also enhanced cellular maturation. Additionally, while MYL2 expression was higher in hPSC-CMs on electroconductive scaffolds compared to neat PVA scaffolds [526].

Roshanbinfar et al. [90] demonstrated that incorporating PEDOT:PSS into collagen-based hydrogels promoted the maturation of hiPSC-cardiomyocytes cultured in these hydrogels. The expression of genes related to electric conduction (i.e., SCN5A, ITPR3, HCN4, KCNJ8, and KCNH2), structure (i.e., MYH7, ACTN2, AKAP6, JPH2, and TTN), energetics (i.e., PRKAA1, PPARGC1A, and SLC2A4), and calcium handling (i.e., CACNA1C, RYR2, CASQ2, PLN, AMPH, TRDN, ATP2A2, CAMK2D) were significantly upregulated in cardiomyocytes in collagen-PEDOT:PSS hydrogels compared to those in collagen hydrogels (Fig. 28C(i,ii)) [90]. Genes involved in oxidative phosphorylation and fatty acid oxidation (i.e., HK2, PFKM, and PGM2) as well as redox handling (i.e., NNT) were also upregulated. These findings suggested that PEDOT:PSS promoted the maturation of hiPSC-cardiomyocytes. Additionally, genes related to cell-ECM interactions, such as integrins (i.e., ITGB3, ITGAV, ITGA1, ITGB1, ITGA4, and ITGA7), were upregulated, supporting cell adhesion, migration, and signaling in the heart [90]. CDH2, crucial for structural integrity and electrical coupling between cardiomyocytes, was also upregulated, reinforcing the role of PEDOT:PSS in enhancing electrical coupling. Pathway analysis indicated positive enrichment in pathways associated with cardiac muscle development and morphogenesis, as well as membrane action potential and calcium ion regulation, while lipid metabolism and transcriptional factors were negatively enriched (Fig. 28C(iii)) [90]. The maturation of cardiomyocytes in collagen-PEDOT:PSS hydrogels was assessed through RNA-seq of 21-day-old tissues, revealing 7561 DEGs, with 3950 upregulated and 3611 downregulated (Fig. 28C). A comparison of gene expression between collagen-PEDOT:PSS and collagen hydrogels revealed that 69 % of selected maturation genes displayed concordant expression changes between the young versus fetal comparison and 74 % between the adult versus fetal comparison (Fig. 28C(iv)). In addition, Fig. 28C(v) presents a Venn diagram illustrating the number of overlapping DEGs among the three comparisons: collagen-PEDOT:PSS vs. collagen hydrogels, young vs. fetal, and adult vs.fetal [90].

8. Challenges and future directions

3D printing and electrospinning are remarkable technologies widely used for fabricating complex materials in biomedical applications [198,528,529]. In cardiac TE, integrating electrically conductive materials with biopolymer-based polymers presents a promising approach to construct advanced electroconductive composite hydrogel scaffolds. These scaffolds closely mimic the complex nature, architecture, properties, and functions of native cardiac tissues [49,96]. Significant challenges persist in developing multifunctional scaffolds that closely replicate the diverse features, properties and functions of native cardiac tissues.

A large number of studies have been published regarding cardiac TE [60,161,368,409]. One major issue in the field remains the use of cell lines that are not informative. H9c2 cells, often termed cardiomyoblasts, proliferate and, when differentiated, form myotubes with no contractile function. In addition, these cells express several skeletal muscle genes [229,371,422,426]. HL-1 cells are atrial cardiomyocytes. Notably, atrial and left ventricular cardiomyocytes exhibit significant differences, for example, in terms of morphology and contractility. Left ventricular cardiomyocytes are generally larger, possess more organized sarcomeric structures, and demonstrate stronger contractile capabilities than atrial cardiomyocytes, which are smaller and less contractile. These differences are important when selecting appropriate cell models for cardiac TE, as they can affect the functionality and behavior of the engineered tissues [221,530]. There are also other cell lines used that are not very representative in the field, as they do not exhibit the proper characteristics of cardiomyocytes. Even hiPSC-derived cardiomyocytes are suboptimal for several reasons, as they, for example, exhibit a fetal to neonatal cardiomyocyte developmental stage [54,291].

The application of electroconductive materials in cardiac TE has garnered significant attention due to their potential to support and enhance cardiomyocyte function, especially in relation to electrical signaling and conduction. While the effects of electroconductive materials, such as PEDOT [90,394], PPy [375], PANi [60], AuNPs [54,439], graphene [420,531] and CNTs [368], on cardiomyocytes have been well documented, less is known about how these materials influence other cardiac cell types, such as cardiac fibroblasts, endothelial cells, and smooth muscle cells. These non-myocyte cells are an integral part of the cardiac tissue microenvironment, contributing to the structural integrity, ECM remodeling, and vascularization processes essential for functional TE. The interactions between electroconductive materials and these non-myocyte populations are still underexplored, with limited studies examining how electroconductivity might modulate their behavior, phenotype, or functionality. Understanding these interactions is interesting for creating more comprehensive models of the heart that replicate not only the electrical properties of cardiac tissue but also the cellular diversity necessary for tissue regeneration.

Despite the promising potential of electroconductive materials, a significant gap in the field lies in demonstrating enhanced force generation due to the incorporation of these materials into cardiac tissue constructs. While there is substantial evidence supporting the idea that electrical conductivity can promote more synchronized cardiomyocyte beating and improve their electrophysiological properties, few studies have definitively shown that these enhancements translate into measurable improvements in force generation or mechanical contractility. Cardiac function, particularly in the context of force generation and contraction, is paramount for the long-term success of engineered tissues, especially when considering the goal of using these constructs in regenerative medicine or in vivo applications. Further research is needed to assess whether electroconductive scaffolds not only support electrical signaling but also promote the mechanical strength and force production necessary for heart tissue functionality.

Another key challenge in the development of electrically conductive hydrogels for cardiac TE is the successful 3D bioprinting of cell-laden conductive bioink materials to create functional cardiac tissues with

high cell density. While 3D bioprinting technologies have made significant strides in fabricating complex tissue architectures, including vascularized constructs and heart tissue models, no study has yet demonstrated the successful 3D bioprinting of high-density cell-laden electroconductive materials to get functional cardiac tissues. Maintaining high cardiac cell viability in cell-laden electroconductive bioinks during 3D bioprinting presents a significant challenge in cardiac TE. 3D bioprinting process which involves layer-by-layer deposition of cell-laden bioinks to create tissue constructs, exposes cells to various stresses, including mechanical forces, thermal changes, and potentially cytotoxic materials. Shear stress from the extrusion-based printing process is particularly detrimental, as it can damage cell membranes, leading to cell death or impaired functionality. Additionally, while electroconductive materials enhance electrical signaling, they may introduce cytotoxicity if not properly optimized, making it essential to balance conductivity and biocompatibility. Maintaining an appropriate microenvironment is also important, as factors like pH, temperature, and nutrient supply must be carefully controlled to support cell survival and proliferation. Any imbalance in these factors can lead to cell death and undermine tissue integrity. The spatial arrangement of cells within

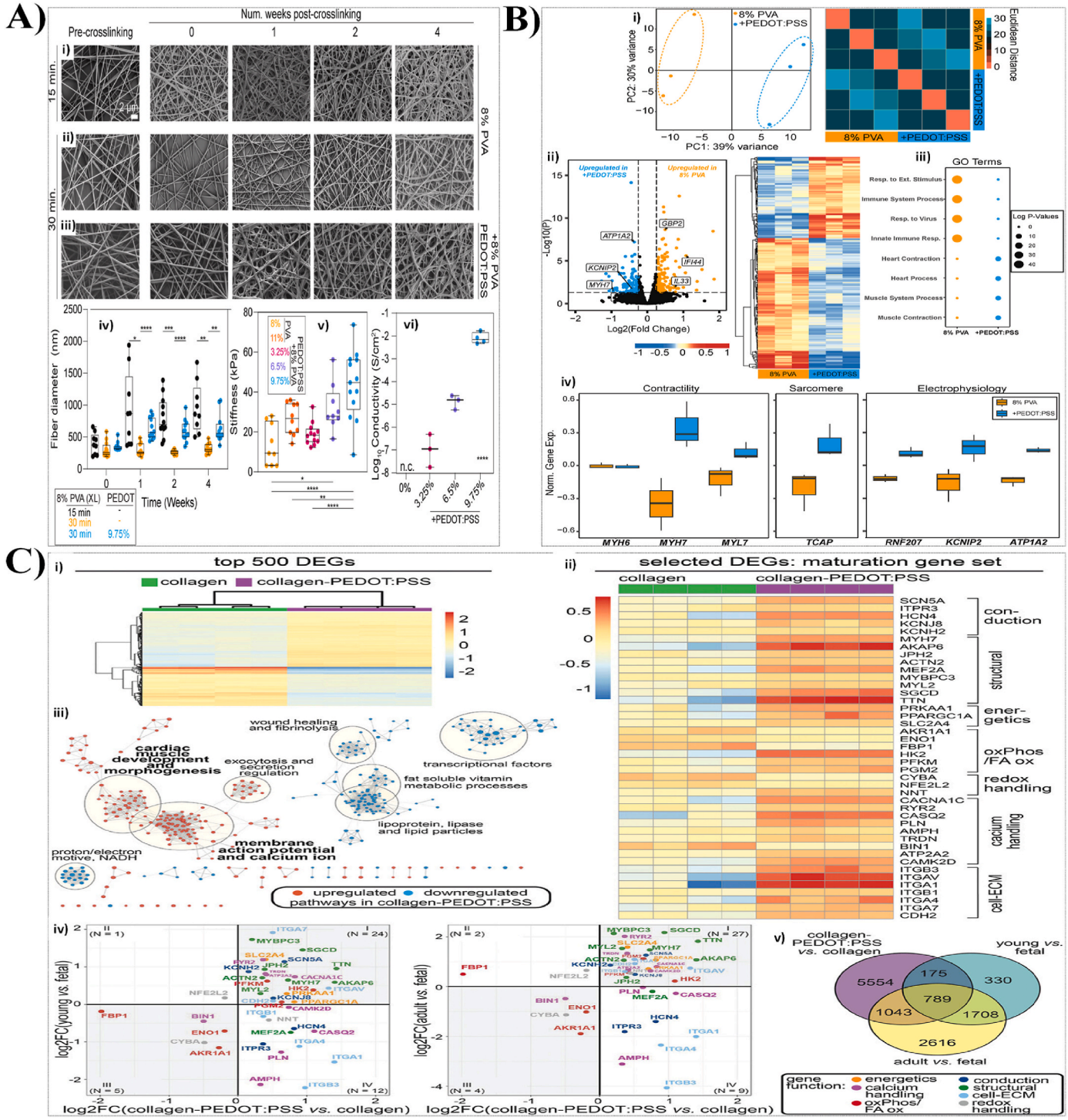

(caption on next page)

Fig. 28. (A) Physical characterization of electrospun scaffolds. (i) SEM images of 8 % PVA electrospun scaffolds incubated in DPBS for 4 weeks post-crosslinking with glutaraldehyde vapor for 15 min (ii), 30 min (iii), and 30 min with 9.75 % PEDOT:PSS/PVA. Scale bar = 2 μm. (iv) The median fiber diameter of 8 % PVA crosslinked for 15 min was 828.04 nm (n = 3 scaffolds for weeks 0, 1, and 4; n = 4 scaffolds for week 2; 3 average measurements per scaffold), while 8 % PVA crosslinked for 30 min had a median fiber diameter of 302.7 nm, and 560.1 nm with PEDOT:PSS (n = 4 scaffolds per timepoint, 3 average measurements per scaffold). (v) Bulk stiffness (kPa) of PVA-only (8 % and 11 %) and 8 % PVA with PEDOT:PSS (3.25 %, 6.5 %, and 9.75 % mass ratio) electrospun scaffolds crosslinked for 30 min measured by AFM. Median stiffness values for 8 % PVA, 11 % PVA, 3.25 %, 6.5 %, and 9.75 % were 9.30, 26.68, 18.36, 27.91, and 44.76 kPa, respectively (n = 4 scaffolds per condition; 1 point represents 1 force map). (vi) Conductivity measurements of 8 % PVA electrospun scaffolds containing 0–9.75 % PEDOT:PSS, measured by TLM. Median conductivity values for 3.25 %, 6.5 %, and 9.75 % were 1.09×10^{-7}, 1.57×10^{-5}, and 7.00×10^{-3} S/cm^2, respectively. Each point represents one scaffold (n.c. indicates not conductive, n = 2). Statistical significance was determined via a mixed-effects analysis (iv), a one-way ANOVA with Tukey's multiple comparison test (v), or a one-way ANOVA (vi). (B) RNA sequencing identifies upregulation of cardiac-related genes on conductive substrates. (i) PCA (post-batch correction) for hPSC-CMs seeded on 8 % PVA or 8 % PVA+9.75 % PEDOT:PSS scaffolds, with total contribution from each axis noted (left) and Euclidean distance matrix (right) indicating the similarity between groups, where 30 indicates the largest dissimilarity between samples. (ii) Volcano plot (left) indicating differences in DEGs between 8 % PVA and conductive scaffolds, and heatmap (right) illustrating transcriptomic clustering of the top 287 significant genes. (iii) Top four GO terms for each experimental condition and their statistical significance. (iv) Normalized expression of genes related to hPSC-CM contractility, sarcomere organization, and electrophysiology (p-adj. < 0.05). A FC cut-off >0.25 and p-adj. cut-off <0.05 for (ii) and (iii) were used. Reproduced with permission from Ref. [526], Copyright © 2023 Elsevier. (C) RNA-seq analysis of human induced pluripotent stem cell (hiPSC) cardiomyocyte maturation. (i,ii) Expression heatmap of the top 500 differentially expressed genes (DEGs) between collagen-PEDOT:PSS and collagen hydrogels, and (ii) selected DEGs belonging to the maturation gene set. Red = upregulated; blue = downregulated compared to the average expression in all samples. Ox Phos: oxidative phosphorylation; FA ox: fatty acid oxidation. (iii) Gene set enrichment analysis network. Nodes represent significantly dysregulated pathways (FDR <0.005). Edges (lines connecting nodes) indicate similarity between two connected pathways based on the proportion of shared genes (measured via the overlap coefficient, OC). Node size is proportional to the number of leading-edge genes associated with a given pathway, and edge thickness represents the OC (minimum OC = 0.5). Highly interconnected pathways form clusters. Circles with descriptive labels indicate clusters made up of at least 10 pathways. (iv) Scatterplots of the log base 2 fold changes (log2FCs) of the maturation gene set in collagen-PEDOT:PSS versus collagen hydrogels, compared to log2FCs in (left) young (n = 4) versus fetal (n = 6) or (right) adult (n = 11) versus fetal (n = 6). Gray highlights the quadrants where the maturation genes exhibit concordant expression changes in the two comparisons. OxPhos: oxidative phosphorylation; FA ox: fatty acid oxidation. (v) Venn diagram showing the number of overlapping DEGs among the three comparisons: collagen-PEDOT:PSS versus collagen hydrogels, young versus fetal, and adult versus fetal. Reproduced with permission from Ref. [90], Copyright © 2024 WILEY-VCH Verlag GmbH & Co. KGaA, Weinheim.

the bioink is another challenge, as the non-uniform distribution or cell clumping can hinder tissue functionality by creating areas of low cell density. To overcome these challenges, researchers are exploring strategies such as optimizing bioink formulations, developing gentler printing techniques, and incorporating protective agents into the bioink to minimize cell stresses and support their growth and function. Moreover, embedded 3D bioprinting, which utilizes low-viscosity bioinks and a gel-in-a-gel approach, offers a promising method for fabricating complex tissue models by embedding cell-laden bioinks in a supportive hydrogel. This technique minimizes gravitational effects and enables the precise deposition of bioinks, which are stabilized after printing [532,533]. However, challenges arise when attempting to print high-density cell-laden hydrogels, as the increased viscosity from higher cell concentrations conflicts with the low viscosity typically required for successful embedded bioprinting. The incorporation of cells into bioinks for bioprinting cell-laden constructs can significantly alter the rheological properties of the resulting formulation, particularly its viscosity. The magnitude of this effect is influenced by several parameters, including the cell type, cell concentration, and the physicochemical characteristics of the base bioink. For instance, when highly viscous bioinks are combined with dense cell suspensions, the resulting mixture often exhibits complex rheological behavior, which can adversely impact both printability and the uniformity of cell distribution within the construct [534,535]. To date, no studies have successfully demonstrated the bioprinting of high-cell-density electroconductive hydrogels using embedded technologies like SWIFT (sacrificial writing in functional tissue) and SPIRIT (sequential printing in a reversible ink template), indicating a significant gap in the current literature. Additionally, while embedded bioprinting holds potential for overcoming size limitations in organ fabrication, difficulties persist in achieving functional integration of vascular networks and maintaining cell viability during prolonged printing durations. Furthermore, the clinical translation of bioprinted tissues is hindered by challenges such as material compatibility, support material removal, and the need for rigorous in vitro and in vivo evaluations.

Furthermore, the current body of literature on the in vivo applications of electroconductive biopolymer-based hydrogels fabricated using 3D printing, electrospinning technologies, or a combination of both for cardiac tissue engineering remains extremely limited. While these hydrogels show promise due to their conductive properties, as well as their potential for in vitro mimicking the electromechanical and functional characteristics of native cardiac tissues, the lack of comprehensive results on their in vivo applications underscores the need for future research focused on evaluating their biocompatibility, cytotoxicity, and functional efficacy in cardiac live models. Further investigation is particularly necessary to assess the long-term integration, biodegradability, and impact of these 3D printed and/or electrospun electrically conductive hydrogels on cardiac regeneration, as well as their potential to overcome the challenges posed by the complex environment of heart tissue. Such studies are crucial for advancing the clinical translation of electroconductive biopolymer-based hydrogels for cardiac repair and regeneration.

Moreover, the long-term effects of implanted electroconductive patches in cardiac tissues remain largely unexplored, particularly regarding the degradation of electroconductive materials over time. These electroconductive materials, often employed to enhance electrical conductivity and support tissue regeneration, face significant challenges related to their breakdown and the subsequent effects within the living organisms. As the electroconductive patch degrades, it may release various degradation products that can provoke inflammatory responses in the surrounding tissue. Depending on their chemical nature, these products could alter the local microenvironment, leading to chronic inflammation, immune reactions, and fibrosis, ultimately impairing tissue healing and integration. The degradation of the material may also result in a loss of mechanical and electrical properties of the cardiac, which are crucial for the regeneration process. For instance, the breakdown of the electroconductive material may reduce its ability to facilitate proper electrical signaling across the myocardium, hindering the restoration of normal heart rhythm and function. In addition, the degradation products of electroconductive materials could potentially be toxic to surrounding cells, either directly through chemical interactions or indirectly by disrupting cellular functions and signaling pathways. This toxicity may lead to cell death or inhibition of tissue regeneration, extending healing times and decreasing the long-term success of the TE strategy. Furthermore, the impact of degradation on the ECM is another concern, as the materials used in these patches could interfere with the ECM structural and biochemical properties, potentially compromising cell adhesion, migration, and differentiation. Importantly, the interactions between the degradation products and the surrounding tissue have not been fully characterized, leaving a gap in our understanding of how these degradation products influence tissue

integration and long-term functional outcomes. Therefore, comprehensive studies on the degradation mechanisms of electroconductive materials, as well as their impact on both the electrical and mechanical properties of the patches in which they are incorporated, are essential to ensure the development of safe, functional, and high-performance implantable patches for cardiac repair and regeneration.

Finally, one of the most challenging goals in cardiac TE is the reconstruction of Purkinje fibers, which are responsible for the coordinated contraction of the ventricles. These fibers are specialized for fast electrical conduction and are crucial for maintaining the synchronized heartbeat. The incorporation of electroconductive materials into scaffolds designed to recreate these fibers could play a significant role in advancing TE strategies aimed at controlling ventricular contraction. However, there is still much to learn about how electroconductive materials can be specifically tailored to mimic the function and structure of Purkinje fibers. The ability to control the formation of Purkinje-like fibers within engineered cardiac tissues would be a major breakthrough in creating tissues that more closely resemble native heart function. This would require not only advancements in electroconductive materials but also a deeper understanding of the signaling pathways, cellular organization, and mechanical properties that govern Purkinje fiber development and function. Further studies should explore how electroconductive scaffolds can be used to direct the formation of these specialized structures, and how they can be incorporated into larger-scale engineered tissues for functional cardiac regeneration.

Looking ahead, significant advancements in electrically functional biopolymer-based hydrogels for cardiac TE and heart-on-a-chip platforms are essential for the development of more effective cardiac treatments. A shift is occurring from traditional in vitro studies to more rigorous in vivo research, where the safety, biocompatibility, and functional efficacy of these hydrogels are thoroughly evaluated within the complex environment of a living organism. In vivo studies are necessary to understand the interactions between the hydrogel materials and the native cardiac tissue, and to assess long-term effects such as degradation, immune responses, and tissue integration. Positive results from these studies could provide a strong foundation for future clinical applications, potentially revolutionizing treatments for cardiovascular diseases by improving tissue repair, heart regeneration, and the management of heart failure. Simultaneously, personalized medicine is becoming an integral part of this progress, utilizing patient-specific genetic and cardiac data to create tailored 3D-printed and electrospun hydrogel constructs that optimize treatment outcomes. By customizing these bioinks to meet individual patient profiles, a more precise and effective approach to cardiac repair could be realized, enhancing the overall success of implantable tissue constructs. Moreover, in heart-on-a-chip platforms, microfabrication technologies could play a pivotal role in seamlessly integrating biopolymer-based hydrogels into microscale systems that closely mimic the heart physiology, allowing for more accurate drug screening, disease modeling, and personalized therapy. These advanced systems could replicate the mechanical and electrical properties of human cardiac tissues more accurately, enabling better assessment of pharmacological responses and providing valuable insights into disease progression. Moreover, the integration of real-time monitoring with embedded sensors can enhance the understanding of cellular responses enabling dynamic and continuous observation of the effects of various drugs or treatments. This capability is particularly important for modeling disease states, as it provides more reliable, real-time data on the physiological behavior of cardiac tissues under different conditions.

9. Conclusion

Given the limited regenerative capacity of the heart and the formation of scar tissue after injury, electroconductive biopolymer-based hydrogel scaffolds hold significant potential for cardiac tissue repair and regeneration. These electroconductive hydrogels are high-performance materials designed to replicate or promote the functionality of native heart tissue in cardiac TE applications. Depending on their composition, these hydrogels can function as a 3D matrix and deliver essential biochemical, mechanical, and electrical signals that support the growth, proliferation, and differentiation of cardiac cells. By incorporating conductive materials into biopolymer matrices, the resulting electroconductive hydrogels exhibit enhanced electrical conductivity, mechanical strength, and biological properties, making them ideal for repairing heart tissue following infarction. Recent advancements in 3D printing and electrospinning technologies, alongside evaluations of material biocompatibility in vitro and in animal models, have demonstrated promising results in clinical settings. 3D printing and electrospinning enable the precise deposition of fiber/hydrogel constructs, often incorporating cells and bioactive molecules to closely replicate the architecture, properties, and functions of native cardiac tissue. Numerous studies have highlighted the successful application of biofabricated electroconductive hydrogels in cardiac TE offering a promising approach to overcoming challenges in cardiovascular regenerative medicine.

For myocardial regeneration, a combination of new therapies and existing treatments to induce both endogenous and exogenous effects is required for maximum efficacy. Strategies combining nanofiber-based networks, such as those produced by electrospinning, with hydrogels in 3D printing technologies to produce fibrous/hydrogel scaffolds may serve as an innovative repair tool for effective cardiac TE. In native cardiac tissue, the myocardium exhibits uniformly aligned cardiac cells in each layer, with a gradual transition of alignment between the cell layers. To be clinically relevant, engineered cardiac tissue scaffolds must not only induce regeneration of a single oriented cardiac layer but also enhance the organization of multiple anisotropic cardiac layers. Thus, designing a 3D tissue model that can individually control cellular orientation and organization in different cell layers would be effective. Furthermore, the specifically aligned fibrous network in the scaffolds can be easily disrupted when used in complex (pre)clinical environments. The preparation of multilayer scaffolds with controlled assembly between layers and nanofiber arrangement is both complex and challenging. More intricate architectured fibrous/hydrogel scaffolds, such as those with more than two or three layers and gradient fiber orientation between interpenetrated layers should not only induce cardiomyocyte alignment and elongation in each layer but also control the relative cellular orientation within the layers in a more sophisticated 3D mimicking environment. These insights highlight the great potential of nanofibrous 3D hydrogel scaffolds produced by combining electrospinning and 3D bioprinting, to engineer 3D multilayer cardiac anisotropy. Future research should focus on optimizing the microstructure and properties of these fibrous hydrogels and integrating cutting-edge technologies to enhance tissue functionality, ultimately improving patient outcomes and quality of life. Major challenges remain to be explored in vivo, including optimizing the technical parameters for fabricating small-diameter nanofibers and considering patient sensitivity to these biomaterial/technology treatments for personalized diagnoses and therapies, due to individual physiological and physical differences.

CRediT authorship contribution statement

Arnaud Kamdem Tamo: Writing – review & editing, Writing – original draft, Software, Project administration, Funding acquisition, Formal analysis, Data curation, Conceptualization. **Ingo Doench:** Writing – review & editing, Resources, Investigation, Formal analysis, Data curation. **Kaveh Roshanbinfar:** Writing – review & editing, Software, Resources, Formal analysis, Data curation. **Alexandra Montembault:** Writing – review & editing, Software, Resources, Investigation, Data curation. **Anatoli Serghei:** Writing – review & editing, Supervision, Software, Resources. **Felix B. Engel:** Writing – review & editing, Supervision, Resources, Project administration,

Funding acquisition. **Anayancy Osorio-Madrazo:** Writing – review & editing, Supervision, Software, Resources, Project administration, Funding acquisition.

Ethics approval and consent to participate

Not Applicable.

Funding

This work received financial support from the Emmy Noether Programme of the German Research Foundation DFG (Grant number: OS 497/6-1, AOBJ: 660891), the Walter Benjamin Programme of the German Research Foundation DFG (Grant number: KA 6604/2-1, AOBJ: 708768), and the German Heart Foundation e.V. (to F.B.E.). The article processing charge (APC) was funded by the Open Access Publishing Fund of the University of Bayreuth.

Declaration of competing interest

The authors declare that they have no known competing financial interests or personal relationships that could have influenced the work reported in this review.

Acknowledgments

We thank the Emmy Noether Programme of the German Research Foundation DFG (Grant number: OS 497/6-1, AOBJ: 660891), the Walter Benjamin Programme of the German Research Foundation DFG (Grant number: KA 6604/2-1, AOBJ: 708768), and the German Heart Foundation e.V. (to F.B.E.) for funding. We also acknowledge funding by the Open Access Publishing Fund of the University of Bayreuth.

References

[1] W.-H. Zimmermann, I. Melnychenko, T. Eschenhagen, Engineered heart tissue for regeneration of diseased hearts, Biomaterials 25 (2004) 1639–1647, https://doi.org/10.1016/S0142-9612(03)00521-0.

[2] J.J. Zhang, S.M. Pogwizd, K. Fukuda, W.-H. Zimmermann, C. Fan, J.M. Hare, R. Bolli, P. Menasché, Trials and tribulations of cell therapy for heart failure: an update on ongoing trials, Nat. Rev. Cardiol. (2024), https://doi.org/10.1038/s41569-024-01098-8.

[3] M. Längin, M. Bender, M. Schmoeckel, B. Reichart, Progress in orthotopic pig heart transplantation in nonhuman primates, Transpl. Int. 37 (2024) 13607, https://doi.org/10.3389/ti.2024.13607.

[4] S. Jou, S.R. Mendez, J. Feinman, L.R. Mitrani, V. Fuster, M. Mangiola, N. Moazami, C. Gidea, Heart transplantation: advances in expanding the donor pool and xenotransplantation, Nat. Rev. Cardiol. 21 (2024) 25–36, https://doi.org/10.1038/s41569-023-00902-1.

[5] T. Eschenhagen, R. Bolli, T. Braun, L.J. Field, B.K. Fleischmann, J. Frisén, M. Giacca, J.M. Hare, S. Houser, R.T. Lee, E. Marbán, J.F. Martin, J.D. Molkentin, C.E. Murry, P.R. Riley, P. Ruiz-Lozano, H.A. Sadek, M.A. Sussman, J.A. Hill, Cardiomyocyte regeneration: a consensus statement, Circulation (New York, N. Y.) 136 (2017) 680–686, https://doi.org/10.1161/CIRCULATIONAHA.117.029343.

[6] M. Leone, F.B. Engel, Advances in heart regeneration based on cardiomyocyte proliferation and regenerative potential of binucleated cardiomyocytes and polyploidization, Clin. Sci. 133 (2019) 1229–1253, https://doi.org/10.1042/CS20180560.

[7] J. Riegler, M. Tiburcy, A. Ebert, E. Tzatzalos, U. Raaz, O.J. Abilez, Q. Shen, N. G. Kooreman, E. Neofytou, V.C. Chen, M. Wang, T. Meyer, P.S. Tsao, A. J. Connolly, L.A. Couture, J.D. Gold, W.H. Zimmermann, J.C. Wu, Human engineered heart muscles engraft and survive long term in a rodent myocardial infarction model, Circ. Res. 117 (2015) 720–730, https://doi.org/10.1161/CIRCRESAHA.115.306985.

[8] T. Stüdemann, J. Rössinger, C. Manthey, B. Geertz, R. Srikantharajah, C. Von Bibra, A. Shibamiya, M. Köhne, A. Wiehler, J.S. Wiegert, T. Eschenhagen, F. Weinberger, Contractile force of transplanted cardiomyocytes actively supports heart function after injury, Circulation (New York, N. Y.) 146 (2022) 1159–1169, https://doi.org/10.1161/CIRCULATIONAHA.122.060124.

[9] S. Ensminger, B. Fujita, A. Aboud, C. Paitazoglou, I. Eitel, D. Jurczyk, M. Mezger, F. Yebran, I. Kutschka, M. Tiburcy, T. Legler, J. Riggert, M. Placzek, T. Friede, A. F. Jebran, T. Seidler, W.H. Zimmermann, Safety and efficacy of induced pluripotent stem cell-derived engineered human myocardium as biological ventricular assist tissue in terminal heart failure (BioVAT-DZHK20): trial design and experience at UKSH lübeck, in: Congress Center Hamburg, 2024, https://doi.org/10.1055/s-0044-1780639 p. s-0044-1780639.

[10] W.-H. Zimmermann, I. Melnychenko, G. Wasmeier, M. Didié, H. Naito, U. Nixdorff, A. Hess, L. Budinsky, K. Brune, B. Michaelis, S. Dhein, A. Schwoerer, H. Ehmke, T. Eschenhagen, Engineered heart tissue grafts improve systolic and diastolic function in infarcted rat hearts, Nat. Med. 12 (2006) 452–458, https://doi.org/10.1038/nm1394.

[11] A.-F. Jebran, T. Seidler, M. Tiburcy, M. Daskalaki, I. Kutschka, B. Fujita, S. Ensminger, F. Bremmer, A. Moussavi, H. Yang, X. Qin, S. Mißbach, C. Drummer, H. Baraki, S. Boretius, C. Hasenauer, T. Nette, J. Kowallick, C. O. Ritter, J. Lotz, M. Didié, M. Mietsch, T. Meyer, G. Kensah, D. Krüger, M. S. Sakib, L. Kaurani, A. Fischer, R. Dressel, I. Rodriguez-Polo, M. Stauske, S. Diecke, K. Maetz-Rensing, E. Gruber-Dujardin, M. Bleyer, B. Petersen, C. Roos, L. Zhang, L. Walter, S. Kaulfuß, G. Yigit, B. Wollnik, E. Levent, B. Roshani, C. Stahl-Henning, P. Ströbel, T. Legler, J. Riggert, K. Hellenkamp, J.-U. Voigt, G. Hasenfuß, R. Hinkel, J.C. Wu, R. Behr, W.-H. Zimmermann, Engineered heart muscle allografts for heart repair in primates and humans, Nature 639 (2025) 503–511, https://doi.org/10.1038/s41586-024-08463-0.

[12] C.V.C. Bouten, C. Cheng, I.M. Vermue, D. Gawlitta, R. Passier, Cardiovascular tissue engineering and regeneration: a plead for further knowledge convergence, Tissue Eng. 28 (2022) 525–541, https://doi.org/10.1089/ten.tea.2021.0231.

[13] Z.-S. Razavi, M. Soltani, G. Mahmoudvand, S. Farokhi, A. Karimi-Rouzbahani, B. Farasati-Far, S. Tahmasebi-Ghorabi, H. Pazoki-Toroudi, H. Afkhami, Advancements in tissue engineering for cardiovascular health: a biomedical engineering perspective, Front. Bioeng. Biotechnol. 12 (2024) 1385124, https://doi.org/10.3389/fbioe.2024.1385124.

[14] L.R. Simon, K.S. Masters, Disease-inspired tissue engineering: investigation of cardiovascular pathologies, ACS Biomater. Sci. Eng. 6 (2020) 2518–2532, https://doi.org/10.1021/acsbiomaterials.9b01067.

[15] G. Del Monte-Nieto, J.W. Fischer, D.J. Gorski, R.P. Harvey, J.C. Kovacic, Basic biology of extracellular matrix in the cardiovascular system, Part 1/4, J. Am. Coll. Cardiol. 75 (2020) 2169–2188, https://doi.org/10.1016/j.jacc.2020.03.024.

[16] A. Khanna, M. Zamani, N.F. Huang, Extracellular matrix-based biomaterials for cardiovascular tissue engineering, JCDD 8 (2021) 137, https://doi.org/10.3390/jcdd8110137.

[17] G.M. Abouna, Organ shortage crisis: problems and possible solutions, Transplant. Proc. 40 (2008) 34–38, https://doi.org/10.1016/j.transproceed.2007.11.067.

[18] G. Vunjak-Novakovic, N. Tandon, A. Godier, R. Maidhof, A. Marsano, T. P. Martens, M. Radisic, Challenges in cardiac tissue engineering, Tissue Eng. B Rev. 16 (2010) 169–187, https://doi.org/10.1089/ten.teb.2009.0352.

[19] A. Mancuso, A. Barone, M.C. Cristiano, E. Cianflone, M. Fresta, D. Paolino, Cardiac stem cell-loaded delivery systems: a new challenge for myocardial tissue regeneration, IJMS 21 (2020) 7701, https://doi.org/10.3390/ijms21207701.

[20] M. Wysoczynki, A. Khan, R. Bolli, New paradigms in cell therapy: repeated dosing, intravenous delivery, immunomodulatory actions, and new cell types, Circ. Res. 123 (2018) 138–158, https://doi.org/10.1161/CIRCRESAHA.118.313251.

[21] S. Baldari, G. Di Rocco, M. Piccoli, M. Pozzobon, M. Muraca, G. Toietta, Challenges and strategies for improving the regenerative effects of mesenchymal stromal cell-based therapies, IJMS 18 (2017) 2087, https://doi.org/10.3390/ijms18102087.

[22] X. Liu, W. Li, X. Fu, Y. Xu, The immunogenicity and immune tolerance of pluripotent stem cell derivatives, Front. Immunol. 8 (2017) 645, https://doi.org/10.3389/fimmu.2017.00645.

[23] T. Rademakers, J.M. Horvath, C.A. Blitterswijk, V.L.S. LaPointe, Oxygen and nutrient delivery in tissue engineering: approaches to graft vascularization, J. Tissue Eng. Regen. Med. 13 (2019) 1815–1829, https://doi.org/10.1002/term.2932.

[24] D.S. Masson-Meyers, L. Tayebi, Vascularization strategies in tissue engineering approaches for soft tissue repair, J. Tissue Eng. Regen. Med. 15 (2021) 747–762, https://doi.org/10.1002/term.3225.

[25] W.L. Stoppel, D.L. Kaplan, L.D. Black, Electrical and mechanical stimulation of cardiac cells and tissue constructs, Adv. Drug Deliv. Rev. 96 (2016) 135–155, https://doi.org/10.1016/j.addr.2015.07.009.

[26] L.M. Monteiro, F. Vasques-Nóvoa, L. Ferreira, P. Pinto-do-Ó, D.S. Nascimento, Restoring heart function and electrical integrity: closing the circuit, NPJ Regen. Med. 2 (2017) 9, https://doi.org/10.1038/s41536-017-0015-2.

[27] M.F. Tenreiro, A.F. Louro, P.M. Alves, M. Serra, Next generation of heart regenerative therapies: progress and promise of cardiac tissue engineering, NPJ Regen. Med. 6 (2021) 30, https://doi.org/10.1038/s41536-021-00140-4.

[28] M.A. Garza, Cardiac remodeling and physical training post myocardial infarction, WJC 7 (2015) 52, https://doi.org/10.4330/wjc.v7.i2.52.

[29] M. Domenech, L. Polo-Corrales, J.E. Ramirez-Vick, D.O. Freytes, Tissue engineering strategies for myocardial regeneration: acellular versus cellular scaffolds? Tissue Eng. B Rev. 22 (2016) 438–458, https://doi.org/10.1089/ten.teb.2015.0523.

[30] A. Khan, P. Kumari, N. Kumari, U. Shaikh, C. Ekhator, R. Halappa Nagaraj, V. Yadav, A.W. Khan, S. Lazarevic, B. Bharati, G. Lakshmipriya Vetrivendan, A. Mulmi, H. Mohamed, A. Ullah, B. Kadel, S.B. Bellegarde, A. Rehman, Biomimetic approaches in cardiac tissue engineering: replicating the native heart microenvironment, Cureus (2023), https://doi.org/10.7759/cureus.43431.

[31] V. Talman, R. Kivelä, Cardiomyocyte—endothelial cell interactions in cardiac remodeling and regeneration, Front. Cardiovasc. Med. 5 (2018) 101, https://doi.org/10.3389/fcvm.2018.00101.

[32] T. Agarwal, S.N.G.H. Narayana, K. Pal, K. Pramanik, S. Giri, I. Banerjee, Calcium alginate-carboxymethyl cellulose beads for colon-targeted drug delivery, Int. J.

Biol. Macromol. 75 (2015) 409–417, https://doi.org/10.1016/j.ijbiomac.2014.12.052.
[33] F. Xing, J. Xu, P. Yu, Y. Zhou, M. Zhe, R. Luo, M. Liu, Z. Xiang, X. Duan, U. Ritz, Recent advances in biofabrication strategies based on bioprinting for vascularized tissue repair and regeneration, Mater. Des. 229 (2023) 111885, https://doi.org/10.1016/j.matdes.2023.111885.
[34] P. Hanna, P.S. Rajendran, O.A. Ajijola, M. Vaseghi, J. Andrew Armour, J. L. Ardell, K. Shivkumar, Cardiac neuroanatomy - imaging nerves to define functional control, Auton. Neurosci. 207 (2017) 48–58, https://doi.org/10.1016/j.autneu.2017.07.008.
[35] J.A. Borovac, D. D'Amario, J. Bozic, D. Glavas, Sympathetic nervous system activation and heart failure: current state of evidence and the pathophysiology in the light of novel biomarkers, WJC 12 (2020) 373–408, https://doi.org/10.4330/wjc.v12.i8.373.
[36] G. Bernava, L. Iop, Advances in the design, generation, and application of tissue-engineered myocardial equivalents, Front. Bioeng. Biotechnol. 11 (2023) 1247572, https://doi.org/10.3389/fbioe.2023.1247572.
[37] A.H. Nguyen, P. Marsh, L. Schmiess-Heine, P.J. Burke, A. Lee, J. Lee, H. Cao, Cardiac tissue engineering: state-of-the-art methods and outlook, J. Biol. Eng. 13 (2019) 57, https://doi.org/10.1186/s13036-019-0185-0.
[38] T.B. Wissing, V. Bonito, C.V.C. Bouten, A.I.P.M. Smits, Biomaterial-driven in situ cardiovascular tissue engineering—a multi-disciplinary perspective, NPJ Regen. Med. 2 (2017) 18, https://doi.org/10.1038/s41536-017-0023-2.
[39] A.-F. Jebran, I. Kutschka, W.-H. Zimmermann, Tissue engineered heart repair, in: Emerging Technologies for Heart Diseases, Elsevier, 2020, pp. 285–290, https://doi.org/10.1016/B978-0-12-813706-2.00014-2.
[40] A.K. Tamo, Nanocellulose-based hydrogels as versatile materials with interesting functional properties for tissue engineering applications, J. Mater. Chem. B (2024), https://doi.org/10.1039/D4TB00397G, 10.1039.D4TB00397G.
[41] A.K. Tamo, L.D.W. Djouonkep, N.B.S. Selabi, 3D printing of polysaccharide-based hydrogel scaffolds for tissue engineering applications: a review, Int. J. Biol. Macromol. 270 (2024) 132123, https://doi.org/10.1016/j.ijbiomac.2024.132123.
[42] M.M. Sayed, H.M. Mousa, M.R. El-Aassar, N.M. El-Deeb, N.M. Ghazaly, M. M. Dewidar, A. Abdal-hay, Enhancing mechanical and biodegradation properties of polyvinyl alcohol/silk fibroin nanofibers composite patches for Cardiac Tissue Engineering, Mater. Lett. 255 (2019) 126510, https://doi.org/10.1016/j.matlet.2019.126510.
[43] Y. Wu, L. Wang, B. Guo, P.X. Ma, Interwoven aligned conductive nanofiber yarn/hydrogel composite scaffolds for engineered 3D cardiac anisotropy, ACS Nano 11 (2017) 5646–5659, https://doi.org/10.1021/acsnano.7b01062.
[44] K.D. Dwyer, K.L.K. Coulombe, Cardiac mechanostructure: using mechanics and anisotropy as inspiration for developing epicardial therapies in treating myocardial infarction, Bioact. Mater. 6 (2021) 2198–2220, https://doi.org/10.1016/j.bioactmat.2020.12.015.
[45] A. Haleem, M. Javaid, A. Saxena, Additive manufacturing applications in cardiology: a review, Egyptian Heart J. 70 (2018) 433–441, https://doi.org/10.1016/j.ehj.2018.09.008.
[46] M.H. Mobarak, MdA. Islam, N. Hossain, MdZ. Al Mahmud, MdT. Rayhan, N. J. Nishi, M.A. Chowdhury, Recent advances of additive manufacturing in implant fabrication – a review, Appl. Surf. Sci. Adv. 18 (2023) 100462, https://doi.org/10.1016/j.apsadv.2023.100462.
[47] G. Prashar, H. Vasudev, D. Bhuddhi, Additive manufacturing: expanding 3D printing horizon in industry 4.0, Int. J. Interact. Des. Manuf. 17 (2023) 2221–2235, https://doi.org/10.1007/s12008-022-00956-4.
[48] T.D. Ngo, A. Kashani, G. Imbalzano, K.T.Q. Nguyen, D. Hui, Additive manufacturing (3D printing): a review of materials, methods, applications and challenges, Compos. B Eng. 143 (2018) 172–196, https://doi.org/10.1016/j.compositesb.2018.02.012.
[49] A. Ghofrani, L. Taghavi, B. Khalilivavdareh, A. Rohani Shirvan, A. Nouri, Additive manufacturing and advanced functionalities of cardiac patches: a review, Eur. Polym. J. 174 (2022) 111332, https://doi.org/10.1016/j.eurpolymj.2022.111332.
[50] A. Harding, A. Pramanik, A.K. Basak, C. Prakash, S. Shankar, Application of additive manufacturing in the biomedical field- A review, Annals of 3D Printed Medicine 10 (2023) 100110, https://doi.org/10.1016/j.stlm.2023.100110.
[51] J.A. Roacho-Pérez, E.N. Garza-Treviño, N.K. Moncada-Saucedo, P.A. Carriquiry-Chequer, L.E. Valencia-Gómez, E.R. Matthews, V. Gómez-Flores, M. Simental-Mendía, P. Delgado-Gonzalez, J.L. Delgado-Gallegos, G.R. Padilla-Rivas, J. F. Islas, Artificial scaffolds in cardiac tissue engineering, Life 12 (2022) 1117, https://doi.org/10.3390/life12081117.
[52] A. Gleadall, D. Visscher, J. Yang, D. Thomas, J. Segal, Review of additive manufactured tissue engineering scaffolds: relationship between geometry and performance, Burns & Trauma 6 (2018), https://doi.org/10.1186/s41038-018-0121-4.
[53] M. Lee, M.C. Kim, J.Y. Lee, Nanomaterial-based electrically conductive hydrogels for cardiac tissue repair, IJN 17 (2022) 6181–6200, https://doi.org/10.2147/IJN.S386763.
[54] K. Roshanbinfar, M. Kolesnik-Gray, M. Angeloni, S. Schruefer, M. Fiedler, D. W. Schubert, F. Ferrazzi, V. Krstic, F.B. Engel, Collagen hydrogel containing polyethylenimine-gold nanoparticles for drug release and enhanced beating properties of engineered cardiac tissues, Adv. Healthcare Mater. 12 (2023) 2202408, https://doi.org/10.1002/adhm.202202408.
[55] K. Roshanbinfar, Z. Mohammadi, A. Sheikh-Mahdi Mesgar, M.M. Dehghan, O. P. Oommen, J. Hilborn, F.B. Engel, Carbon nanotube doped pericardial matrix derived electroconductive biohybrid hydrogel for cardiac tissue engineering, Biomater. Sci. 7 (2019) 3906–3917, https://doi.org/10.1039/C9BM00434C.
[56] M. Ghovvati, M. Kharaziha, R. Ardehali, N. Annabi, Recent advances in designing electroconductive biomaterials for cardiac tissue engineering, Adv. Healthcare Mater. 11 (2022) 2200055, https://doi.org/10.1002/adhm.202200055.
[57] J. Xing, M. Zhang, X. Liu, C. Wang, N. Xu, D. Xing, Multi-material electrospinning: from methods to biomedical applications, Mater. Today Bio 21 (2023) 100710, https://doi.org/10.1016/j.mtbio.2023.100710.
[58] M. Tallawi, D. Dippold, R. Rai, D. D'Atri, J.A. Roether, D.W. Schubert, E. Rosellini, F.B. Engel, A.R. Boccaccini, Novel PGS/PCL electrospun fiber mats with patterned topographical features for cardiac patch applications, Mater. Sci. Eng. C 69 (2016) 569–576, https://doi.org/10.1016/j.msec.2016.06.083.
[59] M. Tallawi, D.C. Zebrowski, R. Rai, J.A. Roether, D.W. Schubert, M. El Fray, F. B. Engel, K.E. Aifantis, A.R. Boccaccini, Poly(Glycerol sebacate)/poly(butylene succinate-butylene dilinoleate) fibrous scaffolds for cardiac tissue engineering, Tissue Eng. C Methods 21 (2015) 585–596, https://doi.org/10.1089/ten.tec.2014.0445.
[60] K. Roshanbinfar, L. Vogt, F. Ruther, J.A. Roether, A.R. Boccaccini, F.B. Engel, Nanofibrous composite with tailorable electrical and mechanical properties for cardiac tissue engineering, Adv. Funct. Mater. 30 (2020) 1908612, https://doi.org/10.1002/adfm.201908612.
[61] M. Kitsara, O. Agbulut, D. Kontziampasis, Y. Chen, P. Menasché, Fibers for hearts: a critical review on electrospinning for cardiac tissue engineering, Acta Biomater. 48 (2017) 20–40, https://doi.org/10.1016/j.actbio.2016.11.014.
[62] P.-H. Kim, J.-Y. Cho, Myocardial tissue engineering using electrospun nanofiber composites, BMB Rep. 49 (2016) 26–36, https://doi.org/10.5483/BMBRep.2016.49.1.165.
[63] Z. Li, J. Guan, Hydrogels for cardiac tissue engineering, Polymers 3 (2011) 740–761, https://doi.org/10.3390/polym3020740.
[64] A. Fatimi, O.V. Okoro, D. Podstawczyk, J. Siminska-Stanny, A. Shavandi, Natural hydrogel-based bio-inks for 3D bioprinting in tissue engineering: a review, Gels 8 (2022) 179, https://doi.org/10.3390/gels8030179.
[65] W. Li, J. Hu, C. Chen, X. Li, H. Zhang, Y. Xin, Q. Tian, S. Wang, Emerging advances in hydrogel-based therapeutic strategies for tissue regeneration, Regenerative Therapy 24 (2023) 459–471, https://doi.org/10.1016/j.reth.2023.09.007.
[66] J. Nicolas, S. Magli, L. Rabbachin, S. Sampaolesi, F. Nicotra, L. Russo, 3D extracellular matrix mimics: fundamental concepts and role of materials chemistry to influence stem cell fate, Biomacromolecules 21 (2020) 1968–1994, https://doi.org/10.1021/acs.biomac.0c00045.
[67] A. Nicosia, M. Salamone, S. Costa, M.A. Ragusa, G. Ghersi, Mimicking molecular pathways in the design of smart hydrogels for the design of vascularized engineered tissues, IJMS 24 (2023) 12314, https://doi.org/10.3390/ijms241512314.
[68] C. Zhao, Q. Lv, W. Wu, Application and prospects of hydrogel additive manufacturing, Gels 8 (2022) 297, https://doi.org/10.3390/gels8050297.
[69] L. Alzoubi, A.A.A. Aljabali, M.M. Tambuwala, Empowering precision medicine: the impact of 3D printing on personalized therapeutic, AAPS PharmSciTech 24 (2023) 228, https://doi.org/10.1208/s12249-023-02682-w.
[70] A. Redaelli, J. Cooper-White, Bioengineering of the heart, APL Bioeng. 4 (2020) 010402, https://doi.org/10.1063/1.5144525.
[71] C.M. Kofron, U. Mende, *In vitro* models of the cardiac microenvironment to study myocyte and non-myocyte crosstalk: bioinspired approaches beyond the polystyrene dish, J. Physiol. 595 (2017) 3891–3905, https://doi.org/10.1113/JP273100.
[72] T. Takada, D. Sasaki, K. Matsuura, K. Miura, S. Sakamoto, H. Goto, T. Ohya, T. Iida, J. Homma, T. Shimizu, N. Hagiwara, Aligned human induced pluripotent stem cell-derived cardiac tissue improves contractile properties through promoting unidirectional and synchronous cardiomyocyte contraction, Biomaterials 281 (2022) 121351, https://doi.org/10.1016/j.biomaterials.2021.121351.
[73] D.A. Dickerson, Advancing engineered heart muscle tissue complexity with hydrogel composites, Adv. Biol. 7 (2023) 2200067, https://doi.org/10.1002/adbi.202200067.
[74] L. Andrés-Delgado, N. Mercader, Interplay between cardiac function and heart development, Biochim. Biophys. Acta Mol. Cell Res. 1863 (2016) 1707–1716, https://doi.org/10.1016/j.bbamcr.2016.03.004.
[75] R. Avazmohammadi, J.S. Soares, D.S. Li, S.S. Raut, R.C. Gorman, M.S. Sacks, A contemporary look at biomechanical models of myocardium, Annu. Rev. Biomed. Eng. 21 (2019) 417–442, https://doi.org/10.1146/annurev-bioeng-062117-121129.
[76] P. Montero, M. Flandes-Iparraguirre, S. Musquiz, M. Pérez Araluce, D. Plano, C. Sanmartín, G. Orive, J.J. Gavira, F. Prosper, M.M. Mazo, Cells, materials, and fabrication processes for cardiac tissue engineering, Front. Bioeng. Biotechnol. 8 (2020) 955, https://doi.org/10.3389/fbioe.2020.00955.
[77] A. Månsson, Hypothesis: single actomyosin properties account for ensemble behavior in active muscle shortening and isometric contraction, IJMS 21 (2020) 8399, https://doi.org/10.3390/ijms21218399.
[78] G.L. Crawford, R. Horowits, Scaffolds and chaperones in myofibril assembly: putting the striations in striated muscle, Biophys Rev 3 (2011) 25–32, https://doi.org/10.1007/s12551-011-0043-x.
[79] D.A. Eisner, J.L. Caldwell, K. Kistamás, A.W. Trafford, Calcium and excitation-contraction coupling in the heart, Circ. Res. 121 (2017) 181–195, https://doi.org/10.1161/CIRCRESAHA.117.310230.

[80] Y. Sun, S.-M. Lee, B.-J. Ku, M.-J. Moon, Fine structure of the intercalated disc and cardiac junctions in the black widow spider Latrodectus mactans, Appl. Microsc. 50 (2020) 20, https://doi.org/10.1186/s42649-020-00040-9.

[81] M. Golob, R.L. Moss, N.C. Chesler, Cardiac tissue structure, properties, and performance: a materials science perspective, Ann. Biomed. Eng. 42 (2014) 2003–2013, https://doi.org/10.1007/s10439-014-1071-z.

[82] C.A. Opitz, M. Kulke, M.C. Leake, C. Neagoe, H. Hinssen, R.J. Hajjar, W.A. Linke, Damped elastic recoil of the titin spring in myofibrils of human myocardium, Proc. Natl. Acad. Sci. USA 100 (2003) 12688–12693, https://doi.org/10.1073/pnas.2133733100.

[83] E.C. James, E. Tomaskovic-Crook, J.M. Crook, Bioengineering clinically relevant cardiomyocytes and cardiac tissues from pluripotent stem cells, IJMS 22 (2021) 3005, https://doi.org/10.3390/ijms22063005.

[84] R. Micheletti, M. Alexanian, Transcriptional plasticity of fibroblasts in heart disease, Biochem. Soc. Trans. 50 (2022) 1247–1255, https://doi.org/10.1042/BST20210864.

[85] E. Grandi, M.F. Navedo, J.J. Saucerman, D.M. Bers, N. Chiamvimonvat, R. E. Dixon, D. Dobrev, A.M. Gomez, O.F. Harraz, B. Hegyi, D.K. Jones, T. Krogh-Madsen, W.L. Murfee, M.A. Nystoriak, N.G. Posnack, C.M. Ripplinger, R. Veeraraghavan, S. Weinberg, Diversity of cells and signals in the cardiovascular system, J. Physiol. 601 (2023) 2547–2592, https://doi.org/10.1113/JP284011.

[86] M. Hulsmans, S. Clauss, L. Xiao, A.D. Aguirre, K.R. King, A. Hanley, W.J. Hucker, E.M. Wülfers, G. Seemann, G. Courties, Y. Iwamoto, Y. Sun, A.J. Savol, H. B. Sager, K.J. Lavine, G.A. Fishbein, D.E. Capen, N. Da Silva, L. Miquerol, H. Wakimoto, C.E. Seidman, J.G. Seidman, R.I. Sadreyev, K. Naxerova, R. N. Mitchell, D. Brown, P. Libby, R. Weissleder, F.K. Swirski, P. Kohl, C. Vinegoni, D.J. Milan, P.T. Ellinor, M. Nahrendorf, Macrophages facilitate electrical conduction in the heart, Cell 169 (2017) 510–522.e20, https://doi.org/10.1016/j.cell.2017.03.050.

[87] S. Ghonim, I. Voges, P.D. Gatehouse, J. Keegan, M.A. Gatzoulis, P.J. Kilner, S. V. Babu-Narayan, Myocardial architecture, mechanics, and fibrosis in congenital heart disease, Front. Cardiovasc. Med. 4 (2017) 30, https://doi.org/10.3389/fcvm.2017.00030.

[88] C. Mekkaoui, S. Huang, H.H. Chen, G. Dai, T.G. Reese, W.J. Kostis, A. Thiagalingam, P. Maurovich-Horvat, J.N. Ruskin, U. Hoffmann, M. P. Jackowski, D.E. Sosnovik, Fiber architecture in remodeled myocardium revealed with a quantitative diffusion CMR tractography framework and histological validation, J. Cardiovasc. Magn. Reson. 14 (2012) 70, https://doi.org/10.1186/1532-429X-14-70.

[89] I. Valiente-Alandi, A.E. Schafer, B.C. Blaxall, Extracellular matrix-mediated cellular communication in the heart, J. Mol. Cell. Cardiol. 91 (2016) 228–237, https://doi.org/10.1016/j.yjmcc.2016.01.011.

[90] K. Roshanbinfar, M. Schiffer, E. Carls, M. Angeloni, M. Koleśnik-Gray, S. Schruefer, D.W. Schubert, F. Ferrazzi, V. Krstić, B.K. Fleischmann, W. Roell, F. B. Engel, Electrically conductive collagen-PEDOT:PSS hydrogel prevents post-infarct cardiac arrhythmia and supports hiPSC-cardiomyocyte function, Adv. Mater. 36 (2024) 2403642, https://doi.org/10.1002/adma.202403642.

[91] D. Fan, A. Takawale, J. Lee, Z. Kassiri, Cardiac fibroblasts, fibrosis and extracellular matrix remodeling in heart disease, Fibrogenesis Tissue Repair 5 (2012) 15, https://doi.org/10.1186/1755-1536-5-15.

[92] A.J. Cocciolone, J.Z. Hawes, M.C. Staiculescu, E.O. Johnson, M. Murshed, J. E. Wagenseil, Elastin, arterial mechanics, and cardiovascular disease, Am. J. Physiol. Heart Circ. Physiol. 315 (2018) H189–H205, https://doi.org/10.1152/ajpheart.00087.2018.

[93] M. Lockhart, E. Wirrig, A. Phelps, A. Wessels, Extracellular matrix and heart development, Birth Defects Research 91 (2011) 535–550, https://doi.org/10.1002/bdra.20810.

[94] J.K. Mouw, G. Ou, V.M. Weaver, Extracellular matrix assembly: a multiscale deconstruction, Nat. Rev. Mol. Cell Biol. 15 (2014) 771–785, https://doi.org/10.1038/nrm3902.

[95] N.G. Frangogiannis, The extracellular matrix in myocardial injury, repair, and remodeling, J. Clin. Investig. 127 (2017) 1600–1612, https://doi.org/10.1172/JCI87491.

[96] H. Esmaeili, A. Patino-Guerrero, M. Hasany, M.O. Ansari, A. Memic, A. Dolatshahi-Pirouz, M. Nikkhah, Electroconductive biomaterials for cardiac tissue engineering, Acta Biomater. 139 (2022) 118–140, https://doi.org/10.1016/j.actbio.2021.08.031.

[97] X.F. Figueroa, B.R. Duling, Gap junctions in the control of vascular function, Antioxidants Redox Signal. 11 (2009) 251–266, https://doi.org/10.1089/ars.2008.2117.

[98] R. Johnson, P. Camelliti, Role of non-myocyte gap junctions and connexin hemichannels in cardiovascular health and disease: novel therapeutic targets? IJMS 19 (2018) 866, https://doi.org/10.3390/ijms19030866.

[99] H. Abriel, J.-S. Rougier, J. Jalife, Ion Channel macromolecular complexes in cardiomyocytes: roles in sudden cardiac death, Circ. Res. 116 (2015) 1971–1988, https://doi.org/10.1161/CIRCRESAHA.116.305017.

[100] H. Dimke, J.G.J. Hoenderop, R.J.M. Bindels, Molecular basis of epithelial Ca^{2+} and Mg^{2+} transport: insights from the TRP channel family, J. Physiol. 589 (2011) 1535–1542, https://doi.org/10.1113/jphysiol.2010.199869.

[101] B.S. Romero-Martínez, B. Sommer, H. Solís-Chagoyán, E. Calixto, A. Aquino-Gálvez, R. Jaimez, J.C. Gomez-Verjan, G. González-Avila, E. Flores-Soto, L. M. Montaño, Estrogenic modulation of ionic channels, pumps and exchangers in airway smooth muscle, IJMS 24 (2023) 7879, https://doi.org/10.3390/ijms24097879.

[102] K.R. DeMarco, C.E. Clancy, Cardiac Na channels, in: Current Topics in Membranes, Elsevier, 2016, pp. 287–311, https://doi.org/10.1016/bs.ctm.2016.05.001.

[103] M.J. Cutler, D. Jeyaraj, D.S. Rosenbaum, Cardiac electrical remodeling in health and disease, Trends Pharmacol. Sci. 32 (2011) 174–180, https://doi.org/10.1016/j.tips.2010.12.001.

[104] R. Veeraraghavan, R.G. Gourdie, S. Poelzing, Mechanisms of cardiac conduction: a history of revisions, Am. J. Physiol. Heart Circ. Physiol. 306 (2014) H619–H627, https://doi.org/10.1152/ajpheart.00760.2013.

[105] G. Ronan, G. Bahcecioglu, N. Aliyev, P. Zorlutuna, Engineering the cardiac tissue microenvironment, Prog. Biomed, Eng. 6 (2024) 012002, https://doi.org/10.1088/2516-1091/ad0ea7.

[106] A.G. Kléber, Y. Rudy, Basic mechanisms of cardiac impulse propagation and associated arrhythmias, Physiol. Rev. 84 (2004) 431–488, https://doi.org/10.1152/physrev.00025.2003.

[107] H.C. Coghlan, A.R. Coghlan, G.D. Buckberg, J.L. Cox, 'The electrical spiral of the heart': its role in the helical continuum.The hypothesis of the anisotropic conducting matrix, Eur. J. Cardio. Thorac. Surg. 29 (2006) S178–S187, https://doi.org/10.1016/j.ejcts.2006.02.046.

[108] P. Ambesh, A. Kapoor, Biological pacemakers: concepts and techniques, Natl. Med. J. India 30 (2017) 324, https://doi.org/10.4103/0970-258X.239072.

[109] E.A. MacDonald, R.A. Rose, T.A. Quinn, Neurohumoral control of sinoatrial node activity and heart rate: insight from experimental models and findings from humans, Front. Physiol. 11 (2020) 170, https://doi.org/10.3389/fphys.2020.00170.

[110] F.I.M. Bonke, C.J.H.J. Kirchhof, M.A. Allessie, A.L. Wit, Impulse propagation from the SA-node to the ventricles, Experientia 43 (1987) 1044–1049, https://doi.org/10.1007/BF01956037.

[111] D.C. Bartos, E. Grandi, C.M. Ripplinger, Ion channels in the heart, in: R. Terjung (Ed.), Comprehensive Physiology, first ed., Wiley, 2015, pp. 1423–1464, https://doi.org/10.1002/cphy.c140069.

[112] M. Watanabe, A. Rollins, L. Polo-Parada, P. Ma, S. Gu, M. Jenkins, Probing the electrophysiology of the developing heart, JCDD 3 (2016) 10, https://doi.org/10.3390/jcdd3010010.

[113] E.R. Pfeiffer, J.R. Tangney, J.H. Omens, A.D. McCulloch, Biomechanics of cardiac electromechanical coupling and mechanoelectric feedback, J. Biomech. Eng. 136 (2014) 021007, https://doi.org/10.1115/1.4026221.

[114] K. Roshanbinfar, L. Vogt, B. Greber, S. Diecke, A.R. Boccaccini, T. Scheibel, F. B. Engel, Electroconductive biohybrid hydrogel for enhanced maturation and beating properties of engineered cardiac tissues, Adv. Funct. Mater. 28 (2018) 1803951, https://doi.org/10.1002/adfm.201803951.

[115] F. Edrisi, N. Baheiraei, M. Razavi, K. Roshanbinfar, R. Imani, N. Jalilinejad, Potential of graphene-based nanomaterials for cardiac tissue engineering, J. Mater. Chem. B 11 (2023) 7280–7299, https://doi.org/10.1039/D3TB00654A.

[116] J. Liu, K. Miller, X. Ma, S. Dewan, N. Lawrence, G. Whang, P. Chung, A. D. McCulloch, S. Chen, Direct 3D bioprinting of cardiac micro-tissues mimicking native myocardium, Biomaterials 256 (2020) 120204, https://doi.org/10.1016/j.biomaterials.2020.120204.

[117] E. Rosellini, M.G. Cascone, L. Guidi, D.W. Schubert, J.A. Roether, A.R. Boccaccini, Mending a broken heart by biomimetic 3D printed natural biomaterial-based cardiac patches: a review, Front. Bioeng. Biotechnol. 11 (2023) 1254739, https://doi.org/10.3389/fbioe.2023.1254739.

[118] M.R. Gomes, F. Castelo Ferreira, P. Sanjuan-Alberte, Electrospun piezoelectric scaffolds for cardiac tissue engineering, Biomater. Adv. 137 (2022) 212808, https://doi.org/10.1016/j.bioadv.2022.212808.

[119] A.S. Theus, M.L. Tomov, A. Cetnar, B. Lima, J. Nish, K. McCoy, M. Mahmoudi, V. Serpooshan, Biomaterial approaches for cardiovascular tissue engineering, Emergent Mater 2 (2019) 193–207, https://doi.org/10.1007/s42247-019-00039-3.

[120] J.A. Smith, E. Mele, Electrospinning and additive manufacturing: adding three-dimensionality to electrospun scaffolds for tissue engineering, Front. Bioeng. Biotechnol. 9 (2021) 674738, https://doi.org/10.3389/fbioe.2021.674738.

[121] D.G. Tamay, T. Dursun Usal, A.S. Alagoz, D. Yucel, N. Hasirci, V. Hasirci, 3D and 4D printing of polymers for tissue engineering applications, Front. Bioeng. Biotechnol. 7 (2019) 164, https://doi.org/10.3389/fbioe.2019.00164.

[122] R. Gonzales, M. Park, L. Tijing, D. Han, S. Phuntsho, H. Shon, Modification of nanofiber support layer for thin film composite forward osmosis membranes via layer-by-layer polyelectrolyte deposition, Membranes 8 (2018) 70, https://doi.org/10.3390/membranes8030070.

[123] H. Kumar, K. Kim, Stereolithography 3D bioprinting, in: J.M. Crook (Ed.), 3D Bioprinting, Springer US, New York, NY, 2020, pp. 93–108, https://doi.org/10.1007/978-1-0716-0520-2_6.

[124] S. Miao, H. Cui, M. Nowicki, S. Lee, J. Almeida, X. Zhou, W. Zhu, X. Yao, F. Masood, M.W. Plesniak, M. Mohiuddin, L.G. Zhang, Photolithographic-stereolithographic-tandem fabrication of 4D smart scaffolds for improved stem cell cardiomyogenic differentiation, Biofabrication 10 (2018) 035007, https://doi.org/10.1088/1758-5090/aabe0b.

[125] A. Hoffmann, H. Leonards, N. Tobies, L. Pongratz, K. Kreuels, F. Kreimendahl, C. Apel, M. Wehner, N. Nottrodt, New stereolithographic resin providing functional surfaces for biocompatible three-dimensional printing, J. Tissue Eng. 8 (2017) 204173141774448, https://doi.org/10.1177/2041731417744485.

[126] J. Choi, E.J. Lee, W.B. Jang, S.-M. Kwon, Development of biocompatible 3D-printed artificial blood vessels through multidimensional approaches, J. Forensic Biomech. 14 (2023) 497, https://doi.org/10.3390/jfb14100497.

[127] B. Huber, S. Engelhardt, W. Meyer, H. Krüger, A. Wenz, V. Schönhaar, G. Tovar, P. Kluger, K. Borchers, Blood-vessel mimicking structures by stereolithographic

fabrication of small porous tubes using cytocompatible polyacrylate elastomers, Biofunctionalization and Endothelialization, JFB 7 (2016) 11, https://doi.org/10.3390/jfb7020011.
[128] S. Kumar, M. Hofmann, B. Steinmann, E.J. Foster, C. Weder, Reinforcement of stereolithographic resins for rapid prototyping with cellulose nanocrystals, ACS Appl. Mater. Interfaces 4 (2012) 5399–5407, https://doi.org/10.1021/am301321v.
[129] W.Y. Yeong, N. Sudarmadji, H.Y. Yu, C.K. Chua, K.F. Leong, S.S. Venkatraman, Y. C.F. Boey, L.P. Tan, Porous polycaprolactone scaffold for cardiac tissue engineering fabricated by selective laser sintering, Acta Biomater. 6 (2010) 2028–2034, https://doi.org/10.1016/j.actbio.2009.12.033.
[130] T. Gharate, T. Karanwad, S. Lekurwale, S. Banerjee, Effect of laser power ratios on sinterability and physical properties of 3D prototypes sintered using selective laser sintering, J. 3D Print. Med 7 (2023) 3DP011, https://doi.org/10.2217/3dp-2023-0007.
[131] Y.A. Gueche, N.M. Sanchez-Ballester, S. Cailleaux, B. Bataille, I. Soulairol, Selective laser sintering (SLS), a new chapter in the production of solid oral forms (SOFs) by 3D printing, Pharmaceutics 13 (2021) 1212, https://doi.org/10.3390/pharmaceutics13081212.
[132] G.V. Salmoria, P. Klauss, R.A. Paggi, L.A. Kanis, A. Lago, Structure and mechanical properties of cellulose based scaffolds fabricated by selective laser sintering, Polym. Test. 28 (2009) 648–652, https://doi.org/10.1016/j.polymertesting.2009.05.008.
[133] F. Lupone, E. Padovano, F. Casamento, C. Badini, Process phenomena and material properties in selective laser sintering of polymers, A Review, Materials 15 (2021) 183, https://doi.org/10.3390/ma15010183.
[134] D.I. Stoia, E. Linul, L. Marsavina, Influence of manufacturing parameters on mechanical properties of porous materials by selective laser sintering, Materials 12 (2019) 871, https://doi.org/10.3390/ma12060871.
[135] B. Duan, M. Wang, W.Y. Zhou, W.L. Cheung, Z.Y. Li, W.W. Lu, Three-dimensional nanocomposite scaffolds fabricated via selective laser sintering for bone tissue engineering, Acta Biomater. 6 (2010) 4495–4505, https://doi.org/10.1016/j.actbio.2010.06.024.
[136] S.F.S. Shirazi, S. Gharehkhani, M. Mehrali, H. Yarmand, H.S.C. Metselaar, N. Adib Kadri, N.A.A. Osman, A review on powder-based additive manufacturing for tissue engineering: selective laser sintering and inkjet 3D printing, Sci. Technol. Adv. Mater. 16 (2015) 033502, https://doi.org/10.1088/1468-6996/16/3/033502.
[137] E.N. Antonov, V.N. Bagratashvili, M.J. Whitaker, J.J.A. Barry, K.M. Shakesheff, A. N. Konovalov, V.K. Popov, S.M. Howdle, Three-dimensional bioactive and biodegradable scaffolds fabricated by surface-selective laser sintering, Adv. Mater. 17 (2005) 327–330, https://doi.org/10.1002/adma.200400838.
[138] R.K. Kankala, K. Zhu, J. Li, C.-S. Wang, S.-B. Wang, A.-Z. Chen, Fabrication of arbitrary 3D components in cardiac surgery: from macro-, micro- to nanoscale, Biofabrication 9 (2017) 032002, https://doi.org/10.1088/1758-5090/aa8113.
[139] J.N. DiNoro, N.C. Paxton, J. Skewes, Z. Yue, P.M. Lewis, R.G. Thompson, S. Beirne, M.A. Woodruff, G.G. Wallace, Laser sintering approaches for bone tissue engineering, Polymers 14 (2022) 2336, https://doi.org/10.3390/polym14122336.
[140] A.G. Tabriz, H. Kuofie, J. Scoble, S. Boulton, D. Douroumis, Selective Laser Sintering for printing pharmaceutical dosage forms, J. Drug Deliv. Sci. Technol. 86 (2023) 104699, https://doi.org/10.1016/j.jddst.2023.104699.
[141] D.L. Bourell, T.J. Watt, D.K. Leigh, B. Fulcher, Performance limitations in polymer laser sintering, Phys. Procedia 56 (2014) 147–156, https://doi.org/10.1016/j.phpro.2014.08.157.
[142] J. Korpela, A. Kokkari, H. Korhonen, M. Malin, T. Närhi, J. Seppälä, Biodegradable and bioactive porous scaffold structures prepared using fused deposition modeling, J. Biomed. Mater. Res. 101B (2013) 610–619, https://doi.org/10.1002/jbm.b.32863.
[143] I. Zein, D.W. Hutmacher, K.C. Tan, S.H. Teoh, Fused deposition modeling of novel scaffold architectures for tissue engineering applications, Biomaterials 23 (2002) 1169–1185, https://doi.org/10.1016/S0142-9612(01)00232-0.
[144] J. Domínguez-Robles, E. Utomo, V.A. Cornelius, Q.K. Anjani, A. Korelidou, Z. Gonzalez, R.F. Donnelly, A. Margariti, M. Delgado-Aguilar, Q. Tarrés, E. Larrañeta, TPU-based antiplatelet cardiovascular prostheses prepared using fused deposition modelling, Mater. Des. 220 (2022) 110837, https://doi.org/10.1016/j.matdes.2022.110837.
[145] S. Ghaziof, S. Shojaei, M. Mehdikhani, M. Khodaei, M. Jafari Nodoushan, Electro-conductive 3D printed polycaprolactone/gold nanoparticles nanocomposite scaffolds for myocardial tissue engineering, J. Mech. Behav. Biomed. Mater. 132 (2022) 105271, https://doi.org/10.1016/j.jmbbm.2022.105271.
[146] C. Parulski, O. Jennotte, A. Lechanteur, B. Evrard, Challenges of fused deposition modeling 3D printing in pharmaceutical applications: where are we now? Adv. Drug Deliv. Rev. 175 (2021) 113810 https://doi.org/10.1016/j.addr.2021.05.020.
[147] M. Zeraatkar, M.D. De Tullio, A. Pricci, F. Pignatelli, G. Percoco, Exploiting limitations of fused deposition modeling to enhance mixing in 3D printed microfluidic devices, RPJ 27 (2021) 1850–1859, https://doi.org/10.1108/RPJ-03-2021-0051.
[148] A. Boschetto, L. Bottini, Accuracy prediction in fused deposition modeling, Int. J. Adv. Manuf. Technol. 73 (2014) 913–928, https://doi.org/10.1007/s00170-014-5886-4.
[149] T. Xu, C. Baicu, M. Aho, M. Zile, T. Boland, Fabrication and characterization of bio-engineered cardiac pseudo tissues, Biofabrication 1 (2009) 035001, https://doi.org/10.1088/1758-5082/1/3/035001.
[150] L.D. Garma, L.M. Ferrari, P. Scognamiglio, F. Greco, F. Santoro, Inkjet-printed PEDOT:PSS multi-electrode arrays for low-cost *in vitro* electrophysiology, Lab Chip 19 (2019) 3776–3786, https://doi.org/10.1039/C9LC00636B.
[151] X. Li, B. Liu, B. Pei, J. Chen, D. Zhou, J. Peng, X. Zhang, W. Jia, T. Xu, Inkjet bioprinting of biomaterials, Chem. Rev. 120 (2020) 10793–10833, https://doi.org/10.1021/acs.chemrev.0c00008.
[152] X. Cui, T. Boland, Human microvasculature fabrication using thermal inkjet printing technology, Biomaterials 30 (2009) 6221–6227, https://doi.org/10.1016/j.biomaterials.2009.07.056.
[153] R. Zimmermann, C. Hentschel, F. Schrön, D. Moedder, T. Büttner, P. Atallah, T. Wegener, T. Gehring, S. Howitz, U. Freudenberg, C. Werner, High resolution bioprinting of multi-component hydrogels, Biofabrication 11 (2019) 045008, https://doi.org/10.1088/1758-5090/ab2aa1.
[154] W.L. Ng, X. Huang, V. Shkolnikov, R. Suntornnond, W.Y. Yeong, Polyvinylpyrrolidone-based bioink: influence of bioink properties on printing performance and cell proliferation during inkjet-based bioprinting, Bio-Des. Manuf 6 (2023) 676–690, https://doi.org/10.1007/s42242-023-00245-3.
[155] H. Gudapati, M. Dey, I. Ozbolat, A comprehensive review on droplet-based bioprinting: past, present and future, Biomaterials 102 (2016) 20–42, https://doi.org/10.1016/j.biomaterials.2016.06.012.
[156] W.L. Ng, J.M. Lee, W.Y. Yeong, M. Win Naing, Microvalve-based bioprinting – process, bio-inks and applications, Biomater. Sci. 5 (2017) 632–647, https://doi.org/10.1039/C6BM00861E.
[157] D. Venkata Krishna, M. Ravi Sankar, Persuasive factors on the bioink printability and cell viability in the extrusion-based 3D bioprinting for tissue regeneration applications, Eng. Regen. 4 (2023) 396–410, https://doi.org/10.1016/j.engreg.2023.07.002.
[158] X.B. Chen, A. Fazel Anvari-Yazdi, X. Duan, A. Zimmerling, R. Gharraei, N. K. Sharma, S. Sweilem, L. Ning, Biomaterials/bioinks and extrusion bioprinting, Bioact. Mater. 28 (2023) 511–536, https://doi.org/10.1016/j.bioactmat.2023.06.006.
[159] A.K. Tamo, T.A. Tran, I. Doench, S. Jahangir, A. Lall, L. David, C. Peniche-Covas, A. Walther, A. Osorio-Madrazo, 3D printing of cellulase-laden cellulose nanofiber/chitosan hydrogel composites: towards tissue engineering functional biomaterials with enzyme-mediated biodegradation, Materials 15 (2022) 6039, https://doi.org/10.3390/ma15176039.
[160] A.K. Tamo, I. Doench, L. Walter, A. Montembault, G. Sudre, L. David, A. Morales-Helguera, M. Selig, B. Rolauffs, A. Bernstein, D. Hoenders, A. Walther, A. Osorio-Madrazo, Development of bioinspired functional chitosan/cellulose nanofiber 3D hydrogel constructs by 3D printing for application in the engineering of mechanically demanding tissues, Polymers 13 (2021) 1663, https://doi.org/10.3390/polym13101663.
[161] M. Izadifar, D. Chapman, P. Babyn, X. Chen, M.E. Kelly, UV-assisted 3D bioprinting of nanoreinforced hybrid cardiac patch for myocardial tissue engineering, Tissue Eng. C Methods 24 (2018) 74–88, https://doi.org/10.1089/ten.tec.2017.0346.
[162] T.U. Esser, A. Anspach, K.A. Muenzebrock, D. Kah, S. Schrüfer, J. Schenk, K. G. Heinze, D.W. Schubert, B. Fabry, F.B. Engel, Direct 3D-bioprinting of hiPSC-derived cardiomyocytes to generate functional cardiac tissues, Adv. Mater. (2023) 2305911, https://doi.org/10.1002/adma.202305911.
[163] F. Maiullari, M. Costantini, M. Milan, V. Pace, M. Chirivì, S. Maiullari, A. Rainer, D. Baci, H.E.-S. Marei, D. Seliktar, C. Gargioli, C. Bearzi, R. Rizzi, A multi-cellular 3D bioprinting approach for vascularized heart tissue engineering based on HUVECs and iPSC-derived cardiomyocytes, Sci. Rep. 8 (2018) 13532, https://doi.org/10.1038/s41598-018-31848-x.
[164] S.H. Hwang, J. Kim, C. Heo, J. Yoon, H. Kim, S.-H. Lee, H.W. Park, M.S. Heo, H. E. Moon, C. Kim, S.H. Paek, J. Jang, 3D printed multi-growth factor delivery patches fabricated using dual-crosslinked decellularized extracellular matrix-based hybrid inks to promote cerebral angiogenesis, Acta Biomater. 157 (2023) 137–148, https://doi.org/10.1016/j.actbio.2022.11.050.
[165] G. Gillispie, P. Prim, J. Copus, J. Fisher, A.G. Mikos, J.J. Yoo, A. Atala, S.J. Lee, Assessment methodologies for extrusion-based bioink printability, Biofabrication 12 (2020) 022003, https://doi.org/10.1088/1758-5090/ab6f0d.
[166] I. Donderwinkel, J.C.M. Van Hest, N.R. Cameron, Bio-inks for 3D bioprinting: recent advances and future prospects, Polym. Chem. 8 (2017) 4451–4471, https://doi.org/10.1039/C7PY00826K.
[167] Z. Yue, X. Liu, P.T. Coates, G.G. Wallace, Advances in printing biomaterials and living cells: implications for islet cell transplantation, Curr. Opin. Organ Transplant. 21 (2016) 467–475, https://doi.org/10.1097/MOT.0000000000000346.
[168] S. Liu, H. Zhang, T. Ahlfeld, D. Kilian, Y. Liu, M. Gelinsky, Q. Hu, Evaluation of different crosslinking methods in altering the properties of extrusion-printed chitosan-based multi-material hydrogel composites, Bio-Des, Manuf 6 (2023) 150–173, https://doi.org/10.1007/s42242-022-00194-3.
[169] Q. Zhang, H.-P. Bei, M. Zhao, Z. Dong, X. Zhao, Shedding light on 3D printing: printing photo-crosslinkable constructs for tissue engineering, Biomaterials 286 (2022) 121566, https://doi.org/10.1016/j.biomaterials.2022.121566.
[170] A. Jafari, S. Vahid Niknezhad, M. Kaviani, W. Saleh, N. Wong, P.P. Van Vliet, C. Moraes, A. Ajji, L. Kadem, N. Azarpira, G. Andelfinger, H. Savoji, Formulation and evaluation of PVA/Gelatin/Carrageenan inks for 3D printing and development of tissue-engineered heart valves, Adv. Funct. Mater. (2023) 2305188, https://doi.org/10.1002/adfm.202305188.
[171] F. Wang, Y. Xue, X. Chen, P. Zhang, L. Shan, Q. Duan, J. Xing, Y. Lan, B. Lu, J. Liu, 3D printed implantable hydrogel bioelectronics for electrophysiological monitoring and electrical modulation, Adv. Funct. Mater. 34 (2024) 2314471, https://doi.org/10.1002/adfm.202314471.

[172] A. Lee, A.R. Hudson, D.J. Shiwarski, J.W. Tashman, T.J. Hinton, S. Yerneni, J. M. Bliley, P.G. Campbell, A.W. Feinberg, 3D bioprinting of collagen to rebuild components of the human heart, Science 365 (2019) 482–487, https://doi.org/10.1126/science.aav9051.
[173] R. Gaebel, N. Ma, J. Liu, J. Guan, L. Koch, C. Klopsch, M. Gruene, A. Toelk, W. Wang, P. Mark, F. Wang, B. Chichkov, W. Li, G. Steinhoff, Patterning human stem cells and endothelial cells with laser printing for cardiac regeneration, Biomaterials 32 (2011) 9218–9230, https://doi.org/10.1016/j.biomaterials.2011.08.071.
[174] R. Brighenti, M.P. Cosma, L. Marsavina, A. Spagnoli, M. Terzano, Laser-based additively manufactured polymers: a review on processes and mechanical models, J. Mater. Sci. 56 (2021) 961–998, https://doi.org/10.1007/s10853-020-05254-6.
[175] C. Dou, V. Perez, J. Qu, A. Tsin, B. Xu, J. Li, A state-of-the-art review of laser-assisted bioprinting and its future research trends, ChemBioEng Rev. 8 (2021) 517–534, https://doi.org/10.1002/cben.202000037.
[176] L. Koch, M. Gruene, C. Unger, B. Chichkov, Laser assisted cell printing, Curr. Pharm. Biotechnol. 14 (2013) 91–97, https://doi.org/10.2174/1389201013804805368.
[177] C. Klopsch, R. Gäbel, A. Kaminski, P. Mark, W. Wang, A. Toelk, E. Delyagina, G. Kleiner, L. Koch, B. Chichkov, P. Mela, S. Jockenhoevel, N. Ma, G. Steinhoff, Spray- and laser-assisted biomaterial processing for fast and efficient autologous cell-plus-matrix tissue engineering: spray- and lased-based advances in tissue engineering, J. Tissue Eng. Regen. Med. 9 (2015) E177–E190, https://doi.org/10.1002/term.1657.
[178] T.C. Suh, A.Y. Amanah, J.M. Gluck, Electrospun scaffolds and induced pluripotent stem cell-derived cardiomyocytes for cardiac tissue engineering applications, Bioengineering 7 (2020) 105, https://doi.org/10.3390/bioengineering7030105.
[179] M. Rahmati, D.K. Mills, A.M. Urbanska, M.R. Saeb, J.R. Venugopal, S. Ramakrishna, M. Mozafari, Electrospinning for tissue engineering applications, Prog. Mater. Sci. 117 (2021) 100721, https://doi.org/10.1016/j.pmatsci.2020.100721.
[180] E.G.R. Fernandes, V. Zucolotto, A.A.A. De Queiroz, Electrospinning of hyperbranched poly-L-lysine/polyaniline nanofibers for application in cardiac tissue engineering, J. Macromol. Sci., Part A 47 (2010) 1203–1207, https://doi.org/10.1080/10601325.2010.518847.
[181] F. Flaig, H. Ragot, A. Simon, G. Revet, M. Kitsara, L. Kitasato, A. Hébraud, O. Agbulut, G. Schlatter, Design of functional electrospun scaffolds based on poly (glycerol sebacate) elastomer and poly(lactic acid) for cardiac tissue engineering, ACS Biomater. Sci. Eng. 6 (2020) 2388–2400, https://doi.org/10.1021/acsbiomaterials.0c00243.
[182] P. Ahmadi, N. Nazeri, M.A. Derakhshan, H. Ghanbari, Preparation and characterization of polyurethane/chitosan/CNT nanofibrous scaffold for cardiac tissue engineering, Int. J. Biol. Macromol. 180 (2021) 590–598, https://doi.org/10.1016/j.ijbiomac.2021.03.001.
[183] X. Wang, B. Ding, B. Li, Biomimetic electrospun nanofibrous structures for tissue engineering, Mater. Today 16 (2013) 229–241, https://doi.org/10.1016/j.mattod.2013.06.005.
[184] S. Baghersad, A. Sathish Kumar, M.J. Kipper, K. Popat, Z. Wang, Recent advances in tissue-engineered cardiac scaffolds—the progress and gap in mimicking native myocardium mechanical behaviors, J. Forensic Biomech. 14 (2023) 269, https://doi.org/10.3390/jfb14050269.
[185] P.T. Bertuoli, J. Ordoño, E. Armelin, S. Pérez-Amodio, A.F. Baldissera, CarlosA. Ferreira, J. Puiggalí, E. Engel, L.J. Del Valle, C. Alemán, Electrospun conducting and biocompatible uniaxial and core–shell fibers having poly(lactic acid), poly(ethylene glycol), and polyaniline for cardiac tissue engineering, ACS Omega 4 (2019) 3660–3672, https://doi.org/10.1021/acsomega.8b03411.
[186] D. Kai, M.P. Prabhakaran, G. Jin, S. Ramakrishna, Guided orientation of cardiomyocytes on electrospun aligned nanofibers for cardiac tissue engineering, J. Biomed. Mater. Res. 98B (2011) 379–386, https://doi.org/10.1002/jbm.b.31862.
[187] E. Ehler, S.N. Jayasinghe, Cell electrospinning cardiac patches for tissue engineering the heart, Analyst 139 (2014) 4449–4452, https://doi.org/10.1039/C4AN00766B.
[188] A. Townsend-Nicholson, S.N. Jayasinghe, Cell electrospinning: a unique biotechnique for encapsulating living organisms for generating active biological microthreads/scaffolds, Biomacromolecules 7 (2006) 3364–3369, https://doi.org/10.1021/bm060649h.
[189] L.A. Bosworth, L.-A. Turner, S.H. Cartmell, State of the art composites comprising electrospun fibres coupled with hydrogels: a review, Nanomed. Nanotechnol. Biol. Med. 9 (2013) 322–335, https://doi.org/10.1016/j.nano.2012.10.008.
[190] B. Freystetter, M. Grab, L. Grefen, L. Bischof, L. Isert, P. Mela, D. Bezuidenhout, C. Hagl, N. Thierfelder, Combining 3D-printing and electrospinning to manufacture biomimetic heart valve leaflets, JoVE J. (2022) 63604, https://doi.org/10.3791/63604.
[191] M. Qasim, F. Haq, M.H. Kang, J.H. Kim, 3D printing approaches for cardiac tissue engineering and role of immune modulation in tissue regeneration, IJN 14 (2019) 1311–1333, https://doi.org/10.2147/IJN.S189587.
[192] A. Ghosh, J.T. Orasugh, S.S. Ray, D. Chattopadhyay, Integration of 3D printing–coelectrospinning: concept shifting in biomedical applications, ACS Omega 8 (2023) 28002–28025, https://doi.org/10.1021/acsomega.3c03920.
[193] M.Z.A. Zulkifli, D. Nordin, N. Shaari, S.K. Kamarudin, Overview of electrospinning for tissue engineering applications, Polymers 15 (2023) 2418, https://doi.org/10.3390/polym15112418.
[194] D. Yang, F. Faraz, J. Wang, N. Radacsi, Combination of 3D printing and electrospinning techniques for biofabrication, Adv Materials Technologies 7 (2022) 2101309, https://doi.org/10.1002/admt.202101309.
[195] P. Romero-Araya, V. Pino, A. Nenen, V. Cárdenas, F. Pavicic, P. Ehrenfeld, G. Serandour, J.G. Lisoni, I. Moreno-Villoslada, M.E. Flores, Combining materials obtained by 3D-printing and electrospinning from commercial polylactide filament to produce biocompatible composites, Polymers 13 (2021) 3806, https://doi.org/10.3390/polym13213806.
[196] H. Wu, F. Xu, H. Jin, M. Xue, W. Zhang, J. Yang, J. Huang, Y. Jiang, B. Qiu, B. Lin, Q. Gao, S. Chen, D. Sun, 3D nanofiber-assisted embedded extrusion bioprinting for oriented cardiac tissue fabrication, ACS Biomater. Sci. Eng. 10 (2024) 7256–7265, https://doi.org/10.1021/acsbiomaterials.4c01611.
[197] S. Liu, Z. Wang, X. Chen, M. Han, J. Xu, T. Li, L. Yu, M. Qin, M. Long, M. Li, H. Zhang, Y. Li, L. Wang, W. Huang, Y. Wu, Multiscale anisotropic scaffold integrating 3D printing and electrospinning techniques as a heart-on-a-chip platform for evaluating drug-induced cardiotoxicity, Adv. Healthcare Mater. 12 (2023) 2300719, https://doi.org/10.1002/adhm.202300719.
[198] C. Vyas, G. Ates, E. Aslan, J. Hart, B. Huang, P. Bartolo, Three-dimensional printing and electrospinning dual-scale polycaprolactone scaffolds with low-density and oriented fibers to promote cell alignment, 3D Print. Addit. Manuf. 7 (2020) 105–113, https://doi.org/10.1089/3dp.2019.0091.
[199] R. Li, A. McCarthy, Y.S. Zhang, J. Xie, Decorating 3D printed scaffolds with electrospun nanofiber segments for tissue engineering, Adv. Biosyst. 3 (2019) 1900137, https://doi.org/10.1002/adbi.201900137.
[200] M. Kharaziha, M. Nikkhah, S.-R. Shin, N. Annabi, N. Masoumi, A.K. Gaharwar, G. Camci-Unal, A. Khademhosseini, PGS:Gelatin nanofibrous scaffolds with tunable mechanical and structural properties for engineering cardiac tissues, Biomaterials 34 (2013) 6355–6366, https://doi.org/10.1016/j.biomaterials.2013.04.045.
[201] L. Ikonen, E. Kerkelä, G. Metselaar, M.C.A. Stuart, M.R. De Jong, K. Aalto-Setälä, 2D and 3D self-assembling nanofiber hydrogels for cardiomyocyte culture, BioMed Res. Int. 2013 (2013) 1–12, https://doi.org/10.1155/2013/285678.
[202] K.T. Shalumon, P.R. Sreerekha, D. Sathish, H. Tamura, S.V. Nair, K.P. Chennazhi, R. Jayakumar, Hierarchically designed electrospun tubular scaffolds for cardiovascular applications, J. Biomed. Nanotechnol. 7 (2011) 609–620, https://doi.org/10.1166/jbn.2011.1337.
[203] K.T. Shalumon, K.P. Chennazhi, S.V. Nair, R. Jayakumar, Development of small diameter fibrous vascular grafts with outer wall multiscale architecture to improve cell penetration, J. Biomed. Nanotechnol. 9 (2013) 1299–1305, https://doi.org/10.1166/jbn.2013.1630.
[204] M.N. Hirt, A. Hansen, T. Eschenhagen, Cardiac tissue engineering: state of the art, Circ. Res. 114 (2014) 354–367, https://doi.org/10.1161/CIRCRESAHA.114.300522.
[205] H. Jawad, N.N. Ali, A.R. Lyon, Q.Z. Chen, S.E. Harding, A.R. Boccaccini, Myocardial tissue engineering: a review, J. Tissue Eng. Regen. Med. 1 (2007) 327–342, https://doi.org/10.1002/term.46.
[206] L. Tian, M.P. Prabhakaran, X. Ding, D. Kai, S. Ramakrishna, Emulsion electrospun nanofibers as substrates for cardiomyogenic differentiation of mesenchymal stem cells, J. Mater. Sci. Mater. Med. 24 (2013) 2577–2587, https://doi.org/10.1007/s10856-013-5003-5.
[207] H.-J. Wei, C.-H. Chen, W.-Y. Lee, I. Chiu, S.-M. Hwang, W.-W. Lin, C.-C. Huang, Y.-C. Yeh, Y. Chang, H.-W. Sung, Bioengineered cardiac patch constructed from multilayered mesenchymal stem cells for myocardial repair, Biomaterials 29 (2008) 3547–3556, https://doi.org/10.1016/j.biomaterials.2008.05.009.
[208] G. Zhao, X. Zhang, T.J. Lu, F. Xu, Recent advances in electrospun nanofibrous scaffolds for cardiac tissue engineering, Adv. Funct. Mater. 25 (2015) 5726–5738, https://doi.org/10.1002/adfm.201502142.
[209] Y. Orlova, N. Magome, L. Liu, Y. Chen, K. Agladze, Electrospun nanofibers as a tool for architecture control in engineered cardiac tissue, Biomaterials 32 (2011) 5615–5624, https://doi.org/10.1016/j.biomaterials.2011.04.042.
[210] B. Qiu, D. Wu, M. Xue, L. Ou, Y. Zheng, F. Xu, H. Jin, Q. Gao, J. Zhuang, J. Cen, B. Lin, Y.-C. Su, S. Chen, D. Sun, 3D aligned nanofiber scaffold fabrication with trench-guided electrospinning for cardiac tissue engineering, Langmuir 40 (2024) 4709–4718, https://doi.org/10.1021/acs.langmuir.3c03358.
[211] Z. Wang, S. Liu, M. Han, J. Xu, M. Qin, Q. Yang, G. Zeng, M. Long, T. Li, J. Yin, L. Yu, W. Huang, L. Wang, Y. Wu, 3D printing-electrospinning hybrid nanofibrous scaffold as LEGO-like bricks for modular assembling skeletal muscle-on-a-chip functional platform, Adv. Fiber Mater. (2024), https://doi.org/10.1007/s42765-024-00433-5.
[212] I. Mayoral, E. Bevilacqua, G. Gómez, A. Hmadcha, I. González-Loscertales, E. Reina, J. Sotelo, A. Domínguez, P. Pérez-Alcántara, Y. Smani, P. González-Puertas, A. Mendez, S. Uribe, T. Smani, A. Ordoñez, I. Valverde, Tissue engineered in-vitro vascular patch fabrication using hybrid 3D printing and electrospinning, Mater. Today Bio 14 (2022) 100252, https://doi.org/10.1016/j.mtbio.2022.100252.
[213] S.J. Lee, D.N. Heo, J.S. Park, S.K. Kwon, J.H. Lee, J.H. Lee, W.D. Kim, I.K. Kwon, S.A. Park, Characterization and preparation of bio-tubular scaffolds for fabricating artificial vascular grafts by combining electrospinning and a 3D printing system, Phys. Chem. Chem. Phys. 17 (2015) 2996–2999, https://doi.org/10.1039/C4CP04801F.
[214] M. Yeo, G. Kim, Nano/microscale topographically designed alginate/PCL scaffolds for inducing myoblast alignment and myogenic differentiation, Carbohydr. Polym. 223 (2019) 115041, https://doi.org/10.1016/j.carbpol.2019.115041.
[215] M. Yeo, G. Kim, Micro/nano-hierarchical scaffold fabricated using a cell electrospinning/3D printing process for co-culturing myoblasts and HUVECs to induce myoblast alignment and differentiation, Acta Biomater. 107 (2020) 102–114, https://doi.org/10.1016/j.actbio.2020.02.042.

[216] L. Lou, A.S. Rubfiaro, V. Deng, J. He, T. Thomas, M. Roy, D. Dickerson, A. Agarwal, Harnessing 3D printing and electrospinning for multiscale hybrid patches mimicking the native myocardium, ACS Appl. Mater. Interfaces 16 (2024) 37596–37612, https://doi.org/10.1021/acsami.4c06505.
[217] T. Xu, K.W. Binder, M.Z. Albanna, D. Dice, W. Zhao, J.J. Yoo, A. Atala, Hybrid printing of mechanically and biologically improved constructs for cartilage tissue engineering applications, Biofabrication 5 (2012) 015001, https://doi.org/10.1088/1758-5082/5/1/015001.
[218] M.J. Mirzaali, V. Moosabeiki, S.M. Rajaai, J. Zhou, A.A. Zadpoor, Additive manufacturing of biomaterials—design principles and their implementation, Materials 15 (2022) 5457, https://doi.org/10.3390/ma15155457.
[219] M. Krishani, W.Y. Shin, H. Suhaimi, N.S. Sambudi, Development of scaffolds from bio-based natural materials for tissue regeneration applications: a review, Gels 9 (2023) 100, https://doi.org/10.3390/gels9020100.
[220] Y. Wang, S. Yang, H. Cai, H. Hu, K. Hu, Z. Sun, R. Liu, Y. Wei, L. Han, A dual-crosslinking electroactive hydrogel based on gelatin methacrylate and dibenzaldehyde-terminated telechelic polyethylene glycol for 3D bio-printing, Sci. Rep. 14 (2024) 4118, https://doi.org/10.1038/s41598-024-54853-9.
[221] Y. Liang, A. Mitriashkin, T.T. Lim, J.C.-H. Goh, Conductive polypyrrole-encapsulated silk fibroin fibers for cardiac tissue engineering, Biomaterials 276 (2021) 121008, https://doi.org/10.1016/j.biomaterials.2021.121008.
[222] T. Mei, H. Cao, L. Zhang, Y. Cao, T. Ma, Z. Sun, Z. Liu, Y. Hu, W. Le, 3D printed conductive hydrogel patch incorporated with MSC@GO for efficient myocardial infarction repair, ACS Biomater. Sci. Eng. 10 (2024) 2451–2462, https://doi.org/10.1021/acsbiomaterials.3c01837.
[223] S. Saghebasl, A. Nobakht, H. Saghebasl, S. Hayati, O. Naturi, R. Rahbarghazi, Sandwich-like electro-conductive polyurethane-based gelatin/soybean oil nanofibrous scaffolds with a targeted release of simvastatin for cardiac tissue engineering, J. Biol. Eng. 17 (2023) 42, https://doi.org/10.1186/s13036-023-00364-6.
[224] X. Wei, L. Wang, C. Duan, K. Chen, X. Li, X. Guo, P. Chen, H. Liu, Y. Fan, Cardiac patches made of brown adipose-derived stem cell sheets and conductive electrospun nanofibers restore infarcted heart for ischemic myocardial infarction, Bioact. Mater. 27 (2023) 271–287, https://doi.org/10.1016/j.bioactmat.2023.03.023.
[225] S. Ghaziof, S. Shojaei, M. Mehdikhani, M. Khodaei, M. Jafari Nodoushan, The effect of spironolactone loading on the properties of 3D-printed polycaprolactone/gold nanoparticles composite scaffolds for myocardial tissue engineering, J Bionic Eng 21 (2024) 924–937, https://doi.org/10.1007/s42235-023-00458-3.
[226] A. Abedi, M. Hasanzadeh, L. Tayebi, Conductive nanofibrous Chitosan/PEDOT: PSS tissue engineering scaffolds, Mater. Chem. Phys. 237 (2019) 121882, https://doi.org/10.1016/j.matchemphys.2019.121882.
[227] T.C. Suh, J. Twiddy, N. Mahmood, K.M. Ali, M.M. Lubna, P.D. Bradford, M. A. Daniele, J.M. Gluck, Electrospun carbon nanotube-based scaffolds exhibit high conductivity and cytocompatibility for tissue engineering applications, ACS Omega 7 (2022) 20006–20019, https://doi.org/10.1021/acsomega.2c01807.
[228] B. Lu, M. Ye, J. Xia, Z. Zhang, Z. Xiong, T. Zhang, Electrical stimulation promotes the vascularization and functionalization of an engineered biomimetic human cardiac tissue, Adv. Healthcare Mater. 12 (2023) 2300607, https://doi.org/10.1002/adhm.202300607.
[229] A.F. Branco, S.P. Pereira, S. Gonzalez, O. Gusev, A.A. Rizvanov, P.J. Oliveira, Gene expression profiling of H9c2 myoblast differentiation towards a cardiac-like phenotype, PLoS One 10 (2015) e0129303, https://doi.org/10.1371/journal.pone.0129303.
[230] M. Suhaeri, R. Subbiah, S.Y. Van, P. Du, I.G. Kim, K. Lee, K. Park, Cardiomyoblast (H9c2) differentiation on tunable extracellular matrix microenvironment, Tissue Eng. 21 (2015) 1940–1951, https://doi.org/10.1089/ten.tea.2014.0591.
[231] W. Wang, M. Watanabe, T. Nakamura, Y. Kudo, R. Ochi, Properties and expression of Ca^{2+} -activated K^{+} channels in H9c2 cells derived from rat ventricle, Am. J. Physiol. Heart Circ. Physiol. 276 (1999) H1559–H1566, https://doi.org/10.1152/ajpheart.1999.276.5.H1559.
[232] L. Del Valle, A. Díaz, J. Puiggalí, Hydrogels for biomedical applications: cellulose, chitosan, and protein/peptide derivatives, Gels 3 (2017) 27, https://doi.org/10.3390/gels3030027.
[233] Q. Wei, J. Zhou, Y. An, M. Li, J. Zhang, S. Yang, Modification, 3D printing process and application of sodium alginate based hydrogels in soft tissue engineering: a review, Int. J. Biol. Macromol. 232 (2023) 123450, https://doi.org/10.1016/j.ijbiomac.2023.123450.
[234] Y. Rioux, J. Fradette, Y. Maciel, A. Bégin-Drolet, J. Ruel, Biofabrication of sodium alginate hydrogel scaffolds for heart valve tissue engineering, IJMS 23 (2022) 8567, https://doi.org/10.3390/ijms23158567.
[235] J.A. Burdick, G.D. Prestwich, Hyaluronic acid hydrogels for biomedical applications, Adv. Mater. 23 (2011), https://doi.org/10.1002/adma.201003963.
[236] A. Yasin, Y. Ren, J. Li, Y. Sheng, C. Cao, K. Zhang, Advances in hyaluronic acid for biomedical applications, Front. Bioeng. Biotechnol. 10 (2022) 910290, https://doi.org/10.3389/fbioe.2022.910290.
[237] F. Munarin, P. Petrini, M.C. Tanzi, M.A. Barbosa, P.L. Granja, Biofunctional chemically modified pectin for cell delivery, Soft Matter 8 (2012) 4731, https://doi.org/10.1039/c2sm07260b.
[238] R. Joy, P.N. Vigneshkumar, F. John, J. George, Hydrogels based on carrageenan, in: Plant and Algal Hydrogels for Drug Delivery and Regenerative Medicine, Elsevier, 2021, pp. 293–325, https://doi.org/10.1016/B978-0-12-821649-1.00003-9.
[239] N.S. Said, I.F. Olawuyi, W.Y. Lee, Pectin hydrogels: gel-forming behaviors, mechanisms, and food applications, Gels 9 (2023) 732, https://doi.org/10.3390/gels9090732.
[240] C. Dong, Y. Lv, Application of collagen scaffold in tissue engineering: recent advances and new perspectives, Polymers 8 (2016) 42, https://doi.org/10.3390/polym8020042.
[241] A. Serafin, M. Culebras, J.M. Oliveira, J. Koffler, M.N. Collins, 3D printable electroconductive gelatin-hyaluronic acid materials containing polypyrrole nanoparticles for electroactive tissue engineering, Adv. Compos. Hybrid Mater. 6 (2023) 109, https://doi.org/10.1007/s42114-023-00665-w.
[242] M.C. Barsotti, F. Felice, A. Balbarini, R. Di Stefano, Fibrin as a scaffold for cardiac tissue engineering, Biotechnol. Appl. Biochem. 58 (2011) 301–310, https://doi.org/10.1002/bab.49.
[243] H. Trębacz, A. Barzycka, Mechanical properties and functions of elastin: an overview, Biomolecules 13 (2023) 574, https://doi.org/10.3390/biom13030574.
[244] S. Lee, E.S. Sani, A.R. Spencer, Y. Guan, A.S. Weiss, N. Annabi, Human-recombinant-elastin-based bioinks for 3D bioprinting of vascularized soft tissues, Adv. Mater. 32 (2020) 2003915, https://doi.org/10.1002/adma.202003915.
[245] X. Yao, S. Zou, S. Fan, Q. Niu, Y. Zhang, Bioinspired silk fibroin materials: from silk building blocks extraction and reconstruction to advanced biomedical applications, Mater. Today Bio 16 (2022) 100381, https://doi.org/10.1016/j.mtbio.2022.100381.
[246] D.M. Pedrotty, V. Kuzmenko, E. Karabulut, A.M. Sugrue, C. Livia, V.R. Vaidya, C. J. McLeod, S.J. Asirvatham, P. Gatenholm, S. Kapa, Three-dimensional printed biopatches with conductive ink facilitate cardiac conduction when applied to disrupted myocardium, Circ: Arrhythmia and Electrophysiology 12 (2019) e006920, https://doi.org/10.1161/CIRCEP.118.006920.
[247] S.N.H. Karimi, R.M. Aghdam, S.A.S. Ebrahimi, Y. Chehrehsaz, Tri-layered alginate/poly(ε -caprolactone) electrospun scaffold for cardiac tissue engineering, Polym. Int. 71 (2022) 1099–1108, https://doi.org/10.1002/pi.6371.
[248] I. Doench, M. Torres-Ramos, A. Montembault, P. Nunes De Oliveira, C. Halimi, E. Viguier, L. Heux, R. Siadous, R. Thiré, A. Osorio-Madrazo, Injectable and gellable chitosan formulations filled with cellulose nanofibers for intervertebral disc tissue engineering, Polymers 10 (2018) 1202, https://doi.org/10.3390/polym10111202.
[249] A. Lall, A. Kamdem Tamo, I. Doench, L. David, P. Nunes De Oliveira, C. Gorzelanny, A. Osorio-Madrazo, Nanoparticles and colloidal hydrogels of chitosan–caseinate polyelectrolyte complexes for drug-controlled release applications, IJMS 21 (2020) 5602, https://doi.org/10.3390/ijms21165602.
[250] O. Domengé, H. Ragot, R. Deloux, A. Crépet, G. Revet, S.E. Boitard, A. Simon, N. Mougenot, L. David, T. Delair, A. Montembault, O. Agbulut, Efficacy of epicardial implantation of acellular chitosan hydrogels in ischemic and nonischemic heart failure: impact of the acetylation degree of chitosan, Acta Biomater. 119 (2021) 125–139, https://doi.org/10.1016/j.actbio.2020.10.045.
[251] O. Domengé, R. Deloux, G. Revet, L. Mazière, E. Pillet-Michelland, L. Commin, C. Bonnefont-Rebeix, A. Simon, N. Mougenot, A. Cavagnino, M. Baraibar, N. Saulnier, A. Crépet, T. Delair, O. Agbulut, A. Montembault, Bio-functionalized hydrogel patches of chitosan for the functional recovery of infarcted myocardial tissue, Int. J. Biol. Macromol. 281 (2024) 136400, https://doi.org/10.1016/j.ijbiomac.2024.136400.
[252] F.E. Bentley, R. Passieux, L. David, A. Osorio-Madrazo, Pure chitosan biomedical textile fibers from mixtures of low- and high-molecular weight bidisperse polymer solutions: processing and understanding of microstructure–mechanical properties' relationship, IJMS 23 (2022) 4767, https://doi.org/10.3390/ijms23094767.
[253] J. Toeri, A. Osorio-Madrazo, M.-P. Laborie, Preparation and chemical/microstructural characterization of azacrown ether-crosslinked chitosan films, Materials 10 (2017) 400, https://doi.org/10.3390/ma10040400.
[254] A.K. Tamo, I. Doench, A. Morales Helguera, D. Hoenders, A. Walther, A. Osorio-Madrazo, Biodegradation of crystalline cellulose nanofibers by means of enzyme immobilized-alginate beads and microparticles, Polymers 12 (2020) 1522, https://doi.org/10.3390/polym12071522.
[255] K. Gwon, E. Kim, G. Tae, Heparin-hyaluronic acid hydrogel in support of cellular activities of 3D encapsulated adipose derived stem cells, Acta Biomater. 49 (2017) 284–295, https://doi.org/10.1016/j.actbio.2016.12.001.
[256] S. Marquez-Bravo, I. Doench, P. Molina, F.E. Bentley, A.K. Tamo, R. Passieux, F. Lossada, L. David, A. Osorio-Madrazo, Functional bionanocomposite fibers of chitosan filled with cellulose nanofibers obtained by gel spinning, Polymers 13 (2021) 1563, https://doi.org/10.3390/polym13101563.
[257] C. Sun, Y. Xie, H. Zhu, X. Zheng, R. Hou, Z. Shi, J. Li, Q. Yang, Highly electroactive tissue engineering scaffolds based on nanocellulose/sulfonated carbon nanotube composite hydrogels for myocardial tissue repair, Biomacromolecules 24 (2023) 5989–5997, https://doi.org/10.1021/acs.biomac.3c01034.
[258] H. Abushammala, J.F. Pontes, G.H. Gomes, A. Osorio-Madrazo, R.M.S.M. Thiré, F. V. Pereira, M.-P.G. Laborie, Swelling, viscoelastic, and anatomical studies on ionic liquid-swollen Norway spruce as a screening tool toward ionosolv pulping, Holzforschung (Berl.) 69 (2015) 1059–1067, https://doi.org/10.1515/hf-2014-0292.
[259] A. Osorio-Madrazo, M. Laborie, Morphological and thermal investigations of cellulosic bionanocomposites, in: A. Dufresne, S. Thomas, L.A. Pothen (Eds.), Biopolymer Nanocomposites, first ed., Wiley, 2013, pp. 411–436, https://doi.org/10.1002/9781118609958.ch18.
[260] L.D.W. Djouonkep, A.K. Tamo, I. Doench, N.B.S. Selabi, E.M. Ilunga, A.R. K. Lenwoue, M. Gauthier, Z. Cheng, A. Osorio-Madrazo, Synthesis of high performance thiophene–aromatic polyesters from bio-sourced organic acids and

polysaccharide-derived diol: characterization and degradability studies, Molecules 27 (2022) 325, https://doi.org/10.3390/molecules27010325.
[261] A. Papagiannopoulos, S.-P. Nikolakis, A. Pamvouxoglou, E. Koutsopoulou, Physicochemical properties of electrostatically crosslinked carrageenan/chitosan hydrogels and carrageenan/chitosan/Laponite nanocomposite hydrogels, Int. J. Biol. Macromol. 225 (2023) 565–573, https://doi.org/10.1016/j.ijbiomac.2022.11.113.
[262] H. Mokhtari, S. Tavakoli, F. Safarpour, M. Kharaziha, H.R. Bakhsheshi-Rad, S. Ramakrishna, F. Berto, Recent advances in chemically-modified and hybrid carrageenan-based platforms for drug delivery, wound healing, and tissue engineering, Polymers 13 (2021) 1744, https://doi.org/10.3390/polym13111744.
[263] N. Li, F. Xue, H. Zhang, H.J. Sanyour, A.P. Rickel, A. Uttecht, B. Fanta, J. Hu, Z. Hong, Fabrication and characterization of pectin hydrogel nanofiber scaffolds for differentiation of mesenchymal stem cells into vascular cells, ACS Biomater. Sci. Eng. 5 (2019) 6511–6519, https://doi.org/10.1021/acsbiomaterials.9b01178.
[264] M.D. Shoulders, R.T. Raines, Collagen structure and stability, Annu. Rev. Biochem. 78 (2009) 929–958, https://doi.org/10.1146/annurev.biochem.77.032207.120833.
[265] S.D. Melton, E.A.E. Brackhahn, S.J. Orlin, P. Jin, D.M. Chenoweth, Rules for the design of aza-glycine stabilized triple-helical collagen peptides, Chem. Sci. 11 (2020) 10638–10646, https://doi.org/10.1039/D0SC03003A.
[266] C.W. Kim, C.J. Kim, E.-H. Park, S. Ryu, Y. Lee, E. Kim, K. Kang, K.Y. Lee, E.-H. Choo, B.-H. Hwang, H.-J. Youn, K.D. Park, K. Chang, MSC-encapsulating in situ cross-linkable gelatin hydrogels to promote myocardial repair, ACS Appl. Bio Mater. 3 (2020) 1646–1655, https://doi.org/10.1021/acsabm.9b01215.
[267] S. Mohanto, S. Narayana, K.P. Merai, J.A. Kumar, A. Bhunia, U. Hani, A. Al Fatease, B.H.J. Gowda, S. Nag, M.G. Ahmed, K. Paul, L.K. Vora, Advancements in gelatin-based hydrogel systems for biomedical applications: a state-of-the-art review, Int. J. Biol. Macromol. 253 (2023) 127143, https://doi.org/10.1016/j.ijbiomac.2023.127143.
[268] J.W. Weisel, R.I. Litvinov, Fibrin Formation, structure and properties, in: D.A. D. Parry, J.M. Squire (Eds.), Fibrous Proteins: Structures and Mechanisms, Springer International Publishing, Cham, 2017, pp. 405–456, https://doi.org/10.1007/978-3-319-49674-0_13.
[269] I. Gonzalez De Torre, M. Alonso, J.-C. Rodriguez-Cabello, Elastin-based materials: promising candidates for cardiac tissue regeneration, Front. Bioeng. Biotechnol. 8 (2020) 657, https://doi.org/10.3389/fbioe.2020.00657.
[270] T. Fukayama, K. Takagi, R. Tanaka, Y. Hatakeyama, D. Aytemiz, Y. Suzuki, T. Asakura, Biological reaction to small-diameter vascular grafts made of silk fibroin implanted in the abdominal aortae of rats, Ann. Vasc. Surg. 29 (2015) 341–352, https://doi.org/10.1016/j.avsg.2014.10.008.
[271] J. Loureiro, S.P. Miguel, V. Galván-Chacón, D. Patrocinio, J.B. Pagador, F. M. Sánchez-Margallo, M.P. Ribeiro, P. Coutinho, Three-dimensionally printed hydrogel cardiac patch for infarct regeneration based on natural polysaccharides, Polymers 15 (2023) 2824, https://doi.org/10.3390/polym15132824.
[272] A.K.A. Silva, M. Juenet, A. Meddahi-Pellé, D. Letourneur, Polysaccharide-based strategies for heart tissue engineering, Carbohydr. Polym. 116 (2015) 267–277, https://doi.org/10.1016/j.carbpol.2014.06.010.
[273] A. Sood, A. Gupta, G. Agrawal, Recent advances in polysaccharides based biomaterials for drug delivery and tissue engineering applications, Carbohydrate Polymer Technologies and Applications 2 (2021) 100067, https://doi.org/10.1016/j.carpta.2021.100067.
[274] A. Kavand, F. Noverraz, S. Gerber-Lemaire, Recent advances in alginate-based hydrogels for cell transplantation applications, Pharmaceutics 16 (2024) 469, https://doi.org/10.3390/pharmaceutics16040469.
[275] S.S. Ho, K.C. Murphy, B.Y.K. Binder, C.B. Vissers, J.K. Leach, Increased survival and function of mesenchymal stem cell spheroids entrapped in instructive alginate hydrogels, Stem Cells Transl. Med. 5 (2016) 773–781, https://doi.org/10.5966/sctm.2015-0211.
[276] E. Karakaya, L. Gleichauf, L. Schöbel, A. Hassan, A.A. Soufivand, J. Tessmar, S. Budday, A.R. Boccaccini, R. Detsch, Engineering peptide-modified alginate-based bioinks with cell-adhesive properties for biofabrication, RSC Adv. 14 (2024) 13769–13786, https://doi.org/10.1039/D3RA08394B.
[277] M.D. Sarker, S. Naghieh, A.D. McInnes, L. Ning, D.J. Schreyer, X. Chen, Bio-fabrication of peptide-modified alginate scaffolds: printability, mechanical stability and neurite outgrowth assessments, Bioprinting 14 (2019) e00045, https://doi.org/10.1016/j.bprint.2019.e00045.
[278] S. Naveenkumar, N. Venkateshan, K. Kaviyarasu, J.R.S.S. Christyraj, A. Muthukumaran, Optimum performance of a novel biocompatible scaffold comprising alginate-pectin-selenium nanoparticles for cardiac tissue engineering using C2C12 cells, J. Mol. Struct. 1294 (2023) 136457, https://doi.org/10.1016/j.molstruc.2023.136457.
[279] F. Ketabat, T. Maris, X. Duan, Z. Yazdanpanah, M.E. Kelly, I. Badea, X. Chen, Optimization of 3D printing and in vitro characterization of alginate/gelatin lattice and angular scaffolds for potential cardiac tissue engineering, Front. Bioeng. Biotechnol. 11 (2023) 1161804, https://doi.org/10.3389/fbioe.2023.1161804.
[280] A.M. Martins, G. Eng, S.G. Caridade, J.F. Mano, R.L. Reis, G. Vunjak-Novakovic, Electrically conductive chitosan/carbon scaffolds for cardiac tissue engineering, Biomacromolecules 15 (2014) 635–643, https://doi.org/10.1021/bm401679q.
[281] A. Osorio-Madrazo, L. David, S. Trombotto, J.-M. Lucas, C. Peniche-Covas, A. Domard, Kinetics study of the solid-state acid hydrolysis of chitosan: evolution of the crystallinity and macromolecular structure, Biomacromolecules 11 (2010) 1376–1386, https://doi.org/10.1021/bm1001685.
[282] A. Osorio-Madrazo, L. David, C. Peniche-Covas, C. Rochas, J.-L. Putaux, S. Trombotto, P. Alcouffe, A. Domard, Fine microstructure of processed chitosan nanofibril networks preserving directional packing and high molecular weight, Carbohydr. Polym. 131 (2015) 1–8, https://doi.org/10.1016/j.carbpol.2015.05.011.
[283] Y. Liu, S. Wang, R. Zhang, Composite poly(lactic acid)/chitosan nanofibrous scaffolds for cardiac tissue engineering, Int. J. Biol. Macromol. 103 (2017) 1130–1137, https://doi.org/10.1016/j.ijbiomac.2017.05.101.
[284] M.Z. Albanna, T.H. Bou-Akl, H.L. Walters, H.W.T. Matthew, Improving the mechanical properties of chitosan-based heart valve scaffolds using chitosan fibers, J. Mech. Behav. Biomed. Mater. 5 (2012) 171–180, https://doi.org/10.1016/j.jmbbm.2011.08.021.
[285] M.I. Wahba, Enhancement of the mechanical properties of chitosan, J. Biomater. Sci. Polym. Ed. 31 (2020) 350–375, https://doi.org/10.1080/09205063.2019.1692641.
[286] B. Patel, R. Manne, D.B. Patel, S. Gorityala, A. Palaniappan, M. Kurakula, Chitosan as functional biomaterial for designing delivery systems in cardiac therapies, Gels 7 (2021) 253, https://doi.org/10.3390/gels7040253.
[287] M. Zarei, A. Samimi, M. Khorram, M.M. Abdi, S.I. Golestaneh, Fabrication and characterization of conductive polypyrrole/chitosan/collagen electrospun nanofiber scaffold for tissue engineering application, Int. J. Biol. Macromol. 168 (2021) 175–186, https://doi.org/10.1016/j.ijbiomac.2020.12.031.
[288] A. Poerio, B. Guibert, M.M. Leroux, J.F. Mano, F. Cleymand, J.-P. Jehl, Mechanical characterization of 3D-printed patterned membranes for cardiac tissue engineering: an experimental and numerical study, Biomedicines 11 (2023) 963, https://doi.org/10.3390/biomedicines11030963.
[289] A. Abedi, B. Bakhshandeh, A. Babaie, J. Mohammadnejad, S. Vahdat, R. Mombeiny, S.R. Moosavi, J. Amini, L. Tayebi, Concurrent application of conductive biopolymeric chitosan/polyvinyl alcohol/MWCNTs nanofibers, intracellular signaling manipulating molecules and electrical stimulation for more effective cardiac tissue engineering, Mater. Chem. Phys. 258 (2021) 123842, https://doi.org/10.1016/j.matchemphys.2020.123842.
[290] X. Xu, L. Wang, J. Jing, J. Zhan, C. Xu, W. Xie, S. Ye, Y. Zhao, C. Zhang, F. Huang, Conductive collagen-based hydrogel combined with electrical stimulation to promote neural stem cell proliferation and differentiation, Front. Bioeng. Biotechnol. 10 (2022) 912497, https://doi.org/10.3389/fbioe.2022.912497.
[291] F. Zhang, K. Qu, X. Li, C. Liu, L.S. Ortiz, K. Wu, X. Wang, N. Huang, Gelatin-based hydrogels combined with electrical stimulation to modulate neonatal rat cardiomyocyte beating and promote maturation, Bio-Des, Manuf 4 (2021) 100–110, https://doi.org/10.1007/s42242-020-00100-9.
[292] Q. Wei, J. Ma, L. Jia, H. Zhao, Y. Dong, Y. Jiang, W. Zhang, Z. Hu, Enzymatic one-pot preparation of carboxylmethyl chitosan-based hydrogel with inherent antioxidant and antibacterial properties for accelerating wound healing, Int. J. Biol. Macromol. 226 (2023) 823–832, https://doi.org/10.1016/j.ijbiomac.2022.12.035.
[293] K. Wu, Z. Yan, Z. Wu, J. Li, W. Zhong, L. Ding, T. Zhong, T. Jiang, Recent advances in the preparation, antibacterial mechanisms, and applications of chitosan, J. Forensic Biomech. 15 (2024) 318, https://doi.org/10.3390/jfb15110318.
[294] P.K. Dutta, K. Rinki, J. Dutta, Chitosan: a promising biomaterial for tissue engineering scaffolds, in: R. Jayakumar, M. Prabaharan, R.A.A. Muzzarelli (Eds.), Chitosan for Biomaterials II, Springer Berlin Heidelberg, Berlin, Heidelberg, 2011, pp. 45–79, https://doi.org/10.1007/12_2011_112.
[295] K.B. Rufato, J.P. Galdino, K.S. Ody, A.G.B. Pereira, E. Corradini, A.F. Martins, A. T. Paulino, A.R. Fajardo, F.A. Aouada, F.A. La Porta, A.F. Rubira, E.C. Muniz, Hydrogels based on chitosan and chitosan derivatives for biomedical applications, in: L. Popa, M. Violeta Ghica, C.-E. Dinu-Pîrvu (Eds.), Hydrogels - Smart Materials for Biomedical Applications, IntechOpen, 2019, https://doi.org/10.5772/intechopen.81811.
[296] F. Croisier, C. Jérôme, Chitosan-based biomaterials for tissue engineering, Eur. Polym. J. 49 (2013) 780–792, https://doi.org/10.1016/j.eurpolymj.2012.12.009.
[297] A. Almasi-Jaf, A. Shamloo, H. Shaygani, S. Seifi, Fabrication of heparinized bi-layered vascular graft with PCL/PU/gelatin co-electrospun and chitosan/silk fibroin/gelatin freeze-dried hydrogel for improved endothelialization and enhanced mechanical properties, Int. J. Biol. Macromol. 253 (2023) 126807, https://doi.org/10.1016/j.ijbiomac.2023.126807.
[298] A. Liberski, N. Latif, C. Raynaud, C. Bollensdorff, M. Yacoub, Alginate for cardiac regeneration: from seaweed to clinical trials, Gcsp 2016 (2016), https://doi.org/10.21542/gcsp.2016.4.
[299] K.Y. Lee, D.J. Mooney, Alginate: properties and biomedical applications, Prog. Polym. Sci. 37 (2012) 106–126, https://doi.org/10.1016/j.progpolymsci.2011.06.003.
[300] H. Zhang, J. Cheng, Q. Ao, Preparation of alginate-based biomaterials and their applications in biomedicine, Mar. Drugs 19 (2021) 264, https://doi.org/10.3390/md19050264.
[301] J. Jang, J. Lee, Y.-J. Seol, Y.H. Jeong, D.-W. Cho, Improving mechanical properties of alginate hydrogel by reinforcement with ethanol treated polycaprolactone nanofibers, Compos. B Eng. 45 (2013) 1216–1221, https://doi.org/10.1016/j.compositesb.2012.09.059.
[302] G. Ochbaum, M. Davidovich-Pinhas, R. Bitton, Tuning the mechanical properties of alginate–peptide hydrogels, Soft Matter 14 (2018) 4364–4373, https://doi.org/10.1039/C8SM00059J.
[303] A. Hurtado, A.A.A. Aljabali, V. Mishra, M.M. Tambuwala, Á. Serrano-Aroca, Alginate: enhancement strategies for advanced applications, IJMS 23 (2022) 4486, https://doi.org/10.3390/ijms23094486.

[304] P. Rosiak, I. Latanska, P. Paul, W. Sujka, B. Kolesinska, Modification of alginates to modulate their physic-chemical properties and obtain biomaterials with different functional properties, Molecules 26 (2021) 7264, https://doi.org/10.3390/molecules26237264.
[305] J. Dahlmann, A. Krause, L. Möller, G. Kensah, M. Möwes, A. Diekmann, U. Martin, A. Kirschning, I. Gruh, G. Dräger, Fully defined in situ cross-linkable alginate and hyaluronic acid hydrogels for myocardial tissue engineering, Biomaterials 34 (2013) 940–951, https://doi.org/10.1016/j.biomaterials.2012.10.008.
[306] R. Ucm, M. Aem, Z. Lhb, V. Kumar, M.J. Taherzadeh, V.K. Garlapati, A. K. Chandel, Comprehensive review on biotechnological production of hyaluronic acid: status, innovation, market and applications, Bioengineered 13 (2022) 9645–9661, https://doi.org/10.1080/21655979.2022.2057760.
[307] M.Y. Kwon, C. Wang, J.H. Galarraga, E. Puré, L. Han, J.A. Burdick, Influence of hyaluronic acid modification on CD44 binding towards the design of hydrogel biomaterials, Biomaterials 222 (2019) 119451, https://doi.org/10.1016/j.biomaterials.2019.119451.
[308] F. Bonafè, M. Govoni, E. Giordano, C.M. Caldarera, C. Guarnieri, C. Muscari, Hyaluronan and cardiac regeneration, J. Biomed. Sci. 21 (2014) 100, https://doi.org/10.1186/s12929-014-0100-4.
[309] S. Amorim, D.S. Da Costa, D. Freitas, C.A. Reis, R.L. Reis, I. Pashkuleva, R. A. Pires, Molecular weight of surface immobilized hyaluronic acid influences CD44-mediated binding of gastric cancer cells, Sci. Rep. 8 (2018) 16058, https://doi.org/10.1038/s41598-018-34445-0.
[310] S. Misra, V.C. Hascall, R.R. Markwald, S. Ghatak, Interactions between hyaluronan and its receptors (CD44, RHAMM) regulate the activities of inflammation and cancer, Front. Immunol. 6 (2015), https://doi.org/10.3389/fimmu.2015.00201.
[311] R. Gaetani, D.A.M. Feyen, V. Verhage, R. Slaats, E. Messina, K.L. Christman, A. Giacomello, P.A.F.M. Doevendans, J.P.G. Sluijter, Epicardial application of cardiac progenitor cells in a 3D-printed gelatin/hyaluronic acid patch preserves cardiac function after myocardial infarction, Biomaterials 61 (2015) 339–348, https://doi.org/10.1016/j.biomaterials.2015.05.005.
[312] G. Basara, S.G. Ozcebe, B.W. Ellis, P. Zorlutuna, Tunable human myocardium derived decellularized extracellular matrix for 3D bioprinting and cardiac tissue engineering, Gels 7 (2021) 70, https://doi.org/10.3390/gels7020070.
[313] G. Sun, J.J. Mao, Engineering dextran-based scaffolds for drug delivery and tissue repair, Nanomedicine 7 (2012) 1771–1784, https://doi.org/10.2217/nnm.12.149.
[314] S. Banerjee, M. Szepes, N. Dibbert, J.-C. Rios-Camacho, A. Kirschning, I. Gruh, G. Dräger, Dextran-based scaffolds for in-situ hydrogelation: use for next generation of bioartificial cardiac tissues, Carbohydr. Polym. 262 (2021) 117924, https://doi.org/10.1016/j.carbpol.2021.117924.
[315] W.N.E. Van Dijk-Wolthuis, J.A.M. Hoogeboom, M.J. Van Steenbergen, S.K. Y. Tsang, W.E. Hennink, Degradation and release behavior of dextran-based hydrogels, Macromolecules 30 (1997) 4639–4645, https://doi.org/10.1021/ma9704018.
[316] X. Ke, M. Li, X. Wang, J. Liang, X. Wang, S. Wu, M. Long, C. Hu, An injectable chitosan/dextran/β -glycerophosphate hydrogel as cell delivery carrier for therapy of myocardial infarction, Carbohydr. Polym. 229 (2020) 115516, https://doi.org/10.1016/j.carbpol.2019.115516.
[317] J. O'Dwyer, R. Murphy, E.B. Dolan, L. Kovarova, M. Pravda, V. Velebny, A. Heise, G.P. Duffy, S.A. Cryan, Development of a nanomedicine-loaded hydrogel for sustained delivery of an angiogenic growth factor to the ischaemic myocardium, Drug Deliv. and Transl. Res. 10 (2020) 440–454, https://doi.org/10.1007/s13346-019-00684-5.
[318] J. Qu, Y. Liang, M. Shi, B. Guo, Y. Gao, Z. Yin, Biocompatible conductive hydrogels based on dextran and aniline trimer as electro-responsive drug delivery system for localized drug release, Int. J. Biol. Macromol. 140 (2019) 255–264, https://doi.org/10.1016/j.ijbiomac.2019.08.120.
[319] T. Simon-Yarza, M.-N. Labour, R. Aid, D. Letourneur, Channeled polysaccharide-based hydrogel reveals influence of curvature to guide endothelial cell arrangement in vessel-like structures, Mater. Sci. Eng. C 118 (2021) 111369, https://doi.org/10.1016/j.msec.2020.111369.
[320] L. Tian, M.P. Prabhakaran, X. Ding, D. Kai, S. Ramakrishna, Emulsion electrospun vascular endothelial growth factor encapsulated poly(l-lactic acid-co-ε-caprolactone) nanofibers for sustained release in cardiac tissue engineering, J. Mater. Sci. 47 (2012) 3272–3281, https://doi.org/10.1007/s10853-011-6166-4.
[321] S. Amine, A. Montembault, M. Fumagalli, A. Osorio-Madrazo, L. David, Controlled polyelectrolyte association of chitosan and carboxylated nano-fibrillated cellulose by desalting, Polymers 13 (2021) 2023, https://doi.org/10.3390/polym13122023.
[322] P. Samyn, A. Osorio-Madrazo, Native crystalline polysaccharide nanofibers: processing and properties, in: A. Barhoum, M. Bechelany, A.S.H. Makhlouf (Eds.), Handbook of Nanofibers, Springer International Publishing, Cham, 2019, pp. 287–321, https://doi.org/10.1007/978-3-319-53655-2_17.
[323] M. Beaumont, E. Jahn, A. Mautner, S. Veigel, S. Böhmdorfer, A. Potthast, W. Gindl-Altmutter, T. Rosenau, Facile preparation of mechanically robust and functional silica/cellulose nanofiber gels reinforced with soluble polysaccharides, Nanomaterials 12 (2022) 895, https://doi.org/10.3390/nano12060895.
[324] P.-H. Chen, H.-C. Liao, S.-H. Hsu, R.-S. Chen, M.-C. Wu, Y.-F. Yang, C.-C. Wu, M.-H. Chen, W.-F. Su, A novel polyurethane/cellulose fibrous scaffold for cardiac tissue engineering, RSC Adv. 5 (2015) 6932–6939, https://doi.org/10.1039/C4RA12486C.
[325] H. Tohidi, N. Maleki-Jirsaraei, A. Simchi, F. Mohandes, Z. Emami, L. Fassina, F. Naro, B. Conti, F. Barbagallo, An electroconductive, thermosensitive, and injectable chitosan/pluronic/gold-decorated cellulose nanofiber hydrogel as an efficient carrier for regeneration of cardiac tissue, Materials 15 (2022) 5122, https://doi.org/10.3390/ma15155122.
[326] I. Doench, T. Tran, L. David, A. Montembault, E. Viguier, C. Gorzelanny, G. Sudre, T. Cachon, M. Louback-Mohamed, N. Horbelt, C. Peniche-Covas, A. Osorio-Madrazo, Cellulose nanofiber-reinforced chitosan hydrogel composites for intervertebral disc tissue repair, Biomimetics (New York, N. Y.) 4 (2019) 19, https://doi.org/10.3390/biomimetics4010019.
[327] C. Xu, B. Zhang Molino, X. Wang, F. Cheng, W. Xu, P. Molino, M. Bacher, D. Su, T. Rosenau, S. Willför, G. Wallace, 3D printing of nanocellulose hydrogel scaffolds with tunable mechanical strength towards wound healing application, J. Mater. Chem. B 6 (2018) 7066–7075, https://doi.org/10.1039/C8TB01757C.
[328] A. Rees, L.C. Powell, G. Chinga-Carrasco, D.T. Gethin, K. Syverud, K.E. Hill, D. W. Thomas, 3D bioprinting of carboxymethylated-periodate oxidized nanocellulose constructs for wound dressing applications, BioMed Res. Int. 2015 (2015) 1–7, https://doi.org/10.1155/2015/925757.
[329] G.M. Rodriguez, D. Trueb, J. Köser, J. Schoelkopf, M. Gullo, An origami like 3D patterned cellulose-based scaffold for bioengineering cardiovascular applications, Cellulose (Lond.) (2023), https://doi.org/10.1007/s10570-023-05492-2.
[330] R. Ajdary, N.Z. Ezazi, A. Correia, M. Kemell, S. Huan, H.J. Ruskoaho, J. Hirvonen, H.A. Santos, O.J. Rojas, Multifunctional 3D-printed patches for long-term drug release therapies after myocardial infarction, Adv. Funct. Mater. 30 (2020) 2003440, https://doi.org/10.1002/adfm.202003440.
[331] C. Chen, C. Zhan, X. Huang, S. Zhang, J. Chen, Three-dimensional printing of cell-laden bioink for blood vessel tissue engineering: influence of process parameters and components on cell viability, J. Biomater. Sci. Polym. Ed. 34 (2023) 2411–2437, https://doi.org/10.1080/09205063.2023.2251781.
[332] C.E. Campiglio, A. Carcano, L. Draghi, RGD -pectin microfiber patches for guiding muscle tissue regeneration, J. Biomed. Mater. Res. 110 (2022) 515–524, https://doi.org/10.1002/jbm.a.37301.
[333] F. Chen, Y. Ni, B. Liu, T. Zhou, C. Yu, Y. Su, X. Zhu, X. Yu, Y. Zhou, Self-crosslinking and injectable hyaluronic acid/RGD-functionalized pectin hydrogel for cartilage tissue engineering, Carbohydr. Polym. 166 (2017) 31–44, https://doi.org/10.1016/j.carbpol.2017.02.059.
[334] A. Aazmi, D. Zhang, C. Mazzaglia, M. Yu, Z. Wang, H. Yang, Y.Y.S. Huang, L. Ma, Biofabrication methods for reconstructing extracellular matrix mimetics, Bioact. Mater. 31 (2024) 475–496, https://doi.org/10.1016/j.bioactmat.2023.08.018.
[335] A.C. Silva, C. Pereira, A.C.R.G. Fonseca, P. Pinto-do-Ó, D.S. Nascimento, Bearing my heart: the role of extracellular matrix on cardiac development, homeostasis, and injury response, Front. Cell Dev. Biol. 8 (2021) 621644, https://doi.org/10.3389/fcell.2020.621644.
[336] C. Wittig, R. Szulcek, Extracellular matrix protein ratios in the human heart and vessels: how to distinguish pathological from physiological changes? Front. Physiol. 12 (2021) 708656 https://doi.org/10.3389/fphys.2021.708656.
[337] H.A. Awad, G.P. Boivin, M.R. Dressler, F.N.L. Smith, R.G. Young, D.L. Butler, Repair of patellar tendon injuries using a cell–collagen composite, J. Orthop. Res. 21 (2003) 420–431, https://doi.org/10.1016/S0736-0266(02)00163-8.
[338] Y. Kaizawa, J. Leyden, A.W. Behn, U.S. Tulu, A. Franklin, Z. Wang, G. Abrams, J. Chang, P.M. Fox, Human tendon–derived collagen hydrogel significantly improves biomechanical properties of the tendon-bone interface in a chronic rotator cuff injury model, J. Hand Surg. 44 (2019) 899.e1–899.e11, https://doi.org/10.1016/j.jhsa.2018.11.021.
[339] B. Sun, The mechanics of fibrillar collagen extracellular matrix, Cell Rep. Phys. Sci. 2 (2021) 100515, https://doi.org/10.1016/j.xcrp.2021.100515.
[340] S. Choy, D.V. Lam, S.-M. Lee, D.S. Hwang, Prolonged biodegradation and improved mechanical stability of collagen via vapor-phase Ti stitching for long-term tissue regeneration, ACS Appl. Mater. Interfaces 11 (2019) 38440–38447, https://doi.org/10.1021/acsami.9b12196.
[341] D. Zhang, X. Wu, J. Chen, K. Lin, The development of collagen based composite scaffolds for bone regeneration, Bioact. Mater. 3 (2018) 129–138, https://doi.org/10.1016/j.bioactmat.2017.08.004.
[342] S.S. Karapehlivan, M.N. Danisik, Z. Akdag, E.N. Yildiz, O.V. Okoro, L. Nie, A. Shavandi, S. Ulag, A. Sahin, F. Dumludag, O. Gunduz, Fabrication and in vitro characterization of polycaprolactone/graphene oxide/collagen nanofibers for myocardial repair, Macromol. Mater. Eng. 309 (2024) 2300189, https://doi.org/10.1002/mame.202300189.
[343] S. Cesur, S. Ulag, L. Ozak, A. Gumussoy, S. Arslan, B.K. Yilmaz, N. Ekren, M. Agirbasli, D.M. Kalaskar, O. Gunduz, Production and characterization of elastomeric cardiac tissue-like patches for Myocardial Tissue Engineering, Polym. Test. 90 (2020) 106613, https://doi.org/10.1016/j.polymertesting.2020.106613.
[344] A. Salleh, N. Mustafa, Y.H. Teow, M.N. Fatimah, F.A. Khairudin, I. Ahmad, M. B. Fauzi, Dual-layered approach of ovine collagen-gelatin/cellulose hybrid biomatrix containing graphene oxide-silver nanoparticles for cutaneous wound healing: fabrication, physicochemical, cytotoxicity and antibacterial characterisation, Biomedicines 10 (2022) 816, https://doi.org/10.3390/biomedicines10040816.
[345] Gaspar-Pintiliescu Stefan, Berger Anton, Negreanu-Pirjol Matei, Moldovan, physicochemical and biological properties of gelatin extracted from marine snail rapana venosa, Mar. Drugs 17 (2019) 589, https://doi.org/10.3390/md17100589.
[346] F. Mushtaq, Z.A. Raza, S.R. Batool, M. Zahid, O.C. Onder, A. Rafique, M. A. Nazeer, Preparation, properties, and applications of gelatin-based hydrogels (GHs) in the environmental, technological, and biomedical sectors, Int. J. Biol. Macromol. 218 (2022) 601–633, https://doi.org/10.1016/j.ijbiomac.2022.07.168.

[347] C.S. Julie Chandra, S. Sasi, T.K. Bindu Sharmila, Material applications of gelatin, in: S. Thomas, A. Ar, C. Jose Chirayil, B. Thomas (Eds.), Handbook of Biopolymers, Springer Nature Singapore, Singapore, 2023, pp. 749–782, https://doi.org/10.1007/978-981-19-0710-4_28.
[348] D.R. Bagal-Kestwal, M.H. Pan, B. Chiang, Properties and applications of gelatin, pectin, and carrageenan gels, in: P.M. Visakh, O. Bayraktar, G. Menon (Eds.), Bio Monomers for Green Polymeric Composite Materials, first ed., Wiley, 2019, pp. 117–140, https://doi.org/10.1002/9781119301714.ch6.
[349] F. Zhang, N. Zhang, H.-X. Meng, H.-X. Liu, Y.-Q. Lu, C.-M. Liu, Z.-M. Zhang, K.-Y. Qu, N.-P. Huang, Easy applied gelatin-based hydrogel system for long-term functional cardiomyocyte culture and myocardium formation, ACS Biomater. Sci. Eng. 5 (2019) 3022–3031, https://doi.org/10.1021/acsbiomaterials.9b00515.
[350] A. Tijore, S.A. Irvine, U. Sarig, P. Mhaisalkar, V. Baisane, S. Venkatraman, Contact guidance for cardiac tissue engineering using 3D bioprinted gelatin patterned hydrogel, Biofabrication 10 (2018) 025003, https://doi.org/10.1088/1758-5090/aaa15d.
[351] N. Nagiah, R. El Khoury, M.H. Othman, J. Akimoto, Y. Ito, D.A. Roberson, B. Joddar, Development and characterization of furfuryl-gelatin electrospun scaffolds for cardiac tissue engineering, ACS Omega 7 (2022) 13894–13905, https://doi.org/10.1021/acsomega.2c00271.
[352] C. Schneider-Barthold, S. Baganz, M. Wilhelmi, T. Scheper, I. Pepelanova, Hydrogels based on collagen and fibrin – frontiers and applications, BioNanoMaterials 17 (2016) 3–12, https://doi.org/10.1515/bnm-2015-0025.
[353] N.J. Kaiser, R.J. Kant, A.J. Minor, K.L.K. Coulombe, Optimizing blended collagen-fibrin hydrogels for cardiac tissue engineering with human iPSC-derived cardiomyocytes, ACS Biomater. Sci. Eng. 5 (2019) 887–899, https://doi.org/10.1021/acsbiomaterials.8b01112.
[354] S. Li, X. Dan, H. Chen, T. Li, B. Liu, Y. Ju, Y. Li, L. Lei, X. Fan, Developing fibrin-based biomaterials/scaffolds in tissue engineering, Bioact. Mater. 40 (2024) 597–623, https://doi.org/10.1016/j.bioactmat.2024.08.006.
[355] P. Yang, F. Xie, L. Zhu, J.N. Selvaraj, D. Zhang, J. Cai, Fabrication of chitin-fibrin hydrogels to construct the 3D artificial extracellular matrix scaffold for vascular regeneration and cardiac tissue engineering, J. Biomed. Mater. Res. (2024), https://doi.org/10.1002/jbm.a.37774 jbm.a.37774.
[356] P.R. Sreerekha, D. Menon, S.V. Nair, K.P. Chennazhi, Fabrication of electrospun poly (Lactide-co-Glycolide)–Fibrin multiscale scaffold for myocardial regeneration *in vitro*, Tissue Eng. 19 (2013) 849–859, https://doi.org/10.1089/ten.tea.2012.0374.
[357] S. Anil Kumar, M. Alonzo, S.C. Allen, L. Abelseth, V. Thakur, J. Akimoto, Y. Ito, S. M. Willerth, L. Suggs, M. Chattopadhyay, B. Joddar, A. Visible Light-Cross-Linkable, Fibrin–gelatin-based bioprinted construct with human cardiomyocytes and fibroblasts, ACS Biomater. Sci. Eng. 5 (2019) 4551–4563, https://doi.org/10.1021/acsbiomaterials.9b00505.
[358] K. Wang, X. Meng, Z. Guo, Elastin structure, synthesis, regulatory mechanism and relationship with cardiovascular diseases, Front. Cell Dev. Biol. 9 (2021) 596702, https://doi.org/10.3389/fcell.2021.596702.
[359] L.D. Muiznieks, J.T. Cirulis, A. Van Der Horst, D.P. Reinhardt, G.J.L. Wuite, R. Pomès, F.W. Keeley, Modulated growth, stability and interactions of liquid-like coacervate assemblies of elastin, Matrix Biol. 36 (2014) 39–50, https://doi.org/10.1016/j.matbio.2014.03.008.
[360] C.E.H. Schmelzer, L. Duca, Elastic fibers: formation, function, and fate during aging and disease, FEBS J. 289 (2022) 3704–3730, https://doi.org/10.1111/febs.15899.
[361] B. Sivaraman, C.A. Bashur, A. Ramamurthi, Advances in biomimetic regeneration of elastic matrix structures, Drug Deliv. and Transl. Res. 2 (2012) 323–350, https://doi.org/10.1007/s13346-012-0070-6.
[362] X. Wang, M. Ali, C. Lacerda, A three-dimensional collagen-elastin scaffold for heart valve tissue engineering, Bioengineering 5 (2018) 69, https://doi.org/10.3390/bioengineering5030069.
[363] C. Patra, S. Talukdar, T. Novoyatleva, S.R. Velagala, C. Mühlfeld, B. Kundu, S. C. Kundu, F.B. Engel, Silk protein fibroin from Antheraea mylitta for cardiac tissue engineering, Biomaterials 33 (2012) 2673–2680, https://doi.org/10.1016/j.biomaterials.2011.12.036.
[364] B. Kundu, N.E. Kurland, S. Bano, C. Patra, F.B. Engel, V.K. Yadavalli, S.C. Kundu, Silk proteins for biomedical applications: bioengineering perspectives, Prog. Polym. Sci. 39 (2014) 251–267, https://doi.org/10.1016/j.progpolymsci.2013.09.002.
[365] J. Petzold, T.B. Aigner, F. Touska, K. Zimmermann, T. Scheibel, F.B. Engel, Surface features of recombinant spider silk protein eADF4(κ16)-Made materials are well-suited for cardiac tissue engineering, Adv. Funct. Mater. 27 (2017) 1701427, https://doi.org/10.1002/adfm.201701427.
[366] P.J. Babu, L. Suamte, Applications of silk-based biomaterials in biomedicine and biotechnology, Eng. Regen. 5 (2024) 56–69, https://doi.org/10.1016/j.engreg.2023.11.002.
[367] G. Li, S. Sun, Silk fibroin-based biomaterials for tissue engineering applications, Molecules 27 (2022) 2757, https://doi.org/10.3390/molecules27092757.
[368] G. Zhao, X. Zhang, B. Li, G. Huang, F. Xu, X. Zhang, Solvent-free fabrication of carbon nanotube/silk fibroin electrospun matrices for enhancing cardiomyocyte functionalities, ACS Biomater. Sci. Eng. 6 (2020) 1630–1640, https://doi.org/10.1021/acsbiomaterials.9b01682.
[369] S. Mehrotra, B.A.G. De Melo, M. Hirano, W. Keung, R.A. Li, B.B. Mandal, S. R. Shin, Nonmulberry silk based ink for fabricating mechanically robust cardiac patches and endothelialized myocardium-on-a-chip application, Adv. Funct. Mater. 30 (2020) 1907436, https://doi.org/10.1002/adfm.201907436.
[370] H. Liu, C. Wang, X. Sun, C. Zhan, Z. Li, L. Qiu, R. Luo, H. Liu, X. Sun, R. Li, J. Zhang, Silk fibroin/collagen/hydroxyapatite scaffolds obtained by 3D printing technology and loaded with recombinant human erythropoietin in the reconstruction of alveolar bone defects, ACS Biomater. Sci. Eng. 8 (2022) 5245–5256, https://doi.org/10.1021/acsbiomaterials.2c00690.
[371] J. Liu, Y. Shen, K. Duan, X. He, R. Wang, Y. Chen, R. Li, J. Sun, X. Qiu, T. Chen, J. Wang, H. Wang, Novel biomimetic sandwich-structured electrospun cardiac patches with moderate adhesiveness and excellent electrical conductivity, J. Mech. Behav. Biomed. Mater. 163 (2025) 106828, https://doi.org/10.1016/j.jmbbm.2024.106828.
[372] J.P.M. Kramer, T.B. Aigner, J. Petzold, K. Roshanbinfar, T. Scheibel, F.B. Engel, Recombinant spider silk protein eADF4(C16)-RGD coatings are suitable for cardiac tissue engineering, Sci. Rep. 10 (2020) 8789, https://doi.org/10.1038/s41598-020-65786-4.
[373] T.U. Esser, V.T. Trossmann, S. Lentz, F.B. Engel, T. Scheibel, Designing of spider silk proteins for human induced pluripotent stem cell-based cardiac tissue engineering, Mater. Today Bio 11 (2021) 100114, https://doi.org/10.1016/j.mtbio.2021.100114.
[374] H. Sun, J. Zhou, Z. Huang, L. Qu, N. Lin, C. Liang, R. Dai, L. Tang, F. Tian, Carbon nanotube-incorporated collagen hydrogels improve cell alignment and the performance of cardiac constructs, IJN 12 (2017) 3109–3120, https://doi.org/10.2147/IJN.S128030.
[375] B.S. Spearman, A.J. Hodge, J.L. Porter, J.G. Hardy, Z.D. Davis, T. Xu, X. Zhang, C. E. Schmidt, M.C. Hamilton, E.A. Lipke, Conductive interpenetrating networks of polypyrrole and polycaprolactone encourage electrophysiological development of cardiac cells, Acta Biomater. 28 (2015) 109–120, https://doi.org/10.1016/j.actbio.2015.09.025.
[376] S. McMahan, A. Taylor, K.M. Copeland, Z. Pan, J. Liao, Y. Hong, Current advances in biodegradable synthetic polymer based cardiac patches, J. Biomed. Mater. Res. 108 (2020) 972–983, https://doi.org/10.1002/jbm.a.36874.
[377] H. Nazari, S. Azadi, S. Hatamie, M.S. Zomorrod, K. Ashtari, M. Soleimani, S. Hosseinzadeh, Fabrication of graphene-silver/polyurethane nanofibrous scaffolds for cardiac tissue engineering, Polym. Adv. Techs 30 (2019) 2086–2099, https://doi.org/10.1002/pat.4641.
[378] D. Testore, A. Zoso, G. Kortaberria, M. Sangermano, V. Chiono, Electroconductive photo-curable PEGDA-gelatin/PEDOT:PSS hydrogels for prospective cardiac tissue engineering application, Front. Bioeng. Biotechnol. 10 (2022) 897575, https://doi.org/10.3389/fbioe.2022.897575.
[379] M. Morsink, P. Severino, E. Luna-Ceron, M.A. Hussain, N. Sobahi, S.R. Shin, Effects of electrically conductive nano-biomaterials on regulating cardiomyocyte behavior for cardiac repair and regeneration, Acta Biomater. 139 (2022) 141–156, https://doi.org/10.1016/j.actbio.2021.11.022.
[380] H. Lu, N. Zhang, M. Ma, Electroconductive hydrogels for biomedical applications, WIREs Nanomed Nanobiotechnol 11 (2019) e1568, https://doi.org/10.1002/wnan.1568.
[381] M. Zamani, E. Karaca, N.F. Huang, Multicellular interactions in 3D engineered myocardial tissue, Front. Cardiovasc. Med. 5 (2018) 147, https://doi.org/10.3389/fcvm.2018.00147.
[382] B. Yi, Q. Xu, W. Liu, An overview of substrate stiffness guided cellular response and its applications in tissue regeneration, Bioact. Mater. 15 (2022) 82–102, https://doi.org/10.1016/j.bioactmat.2021.12.005.
[383] Z. Zhang, H. Zhu, G. Zhao, Y. Miao, L. Zhao, J. Feng, H. Zhang, R. Miao, L. Sun, B. Gao, W. Zhang, Z. Wang, J. Zhang, Y. Zhang, H. Guo, F. Xu, T.J. Lu, G. M. Genin, M. Lin, Programmable and reversible integrin-mediated cell adhesion reveals hysteresis in actin kinetics that alters subsequent mechanotransduction, Adv. Sci. 10 (2023) 2302421, https://doi.org/10.1002/advs.202302421.
[384] J. Labat-Robert, Cell–Matrix interactions, the role of fibronectin and integrins, A survey, Pathologie Biologie 60 (2012) 15–19, https://doi.org/10.1016/j.patbio.2011.10.003.
[385] D. Hao, R. Liu, K. Gao, C. He, S. He, C. Zhao, G. Sun, D.L. Farmer, A. Panitch, K. S. Lam, A. Wang, Developing an injectable nanofibrous extracellular matrix hydrogel with an integrin αvβ3 ligand to improve endothelial cell survival, engraftment and vascularization, Front. Bioeng. Biotechnol. 8 (2020) 890, https://doi.org/10.3389/fbioe.2020.00890.
[386] S. Maji, H. Lee, Engineering hydrogels for the development of three-dimensional in vitro models, IJMS 23 (2022) 2662, https://doi.org/10.3390/ijms23052662.
[387] D. Kai, M.P. Prabhakaran, G. Jin, S. Ramakrishna, Polypyrrole-contained electrospun conductive nanofibrous membranes for cardiac tissue engineering, J. Biomed. Mater. Res. 99A (2011) 376–385, https://doi.org/10.1002/jbm.a.33200.
[388] R. Rai, J.A. Roether, A.R. Boccaccini, Polyaniline based polymers in tissue engineering applications: a review, Prog. Biomed. Eng. 4 (2022) 042004, https://doi.org/10.1088/2516-1091/ac93d3.
[389] W. Łużny, E. Bańka, Relations between the structure and electric conductivity of polyaniline protonated with camphorsulfonic acid, Macromolecules 33 (2000) 425–429, https://doi.org/10.1021/ma9913663.
[390] A. Ul Haq, L. Montaina, F. Pescosolido, F. Carotenuto, F. Trovalusci, F. De Matteis, E. Tamburri, P. Di Nardo, Electrically conductive scaffolds mimicking the hierarchical structure of cardiac myofibers, Sci. Rep. 13 (2023) 2863, https://doi.org/10.1038/s41598-023-29780-w.
[391] Q. Lei, J. He, D. Li, Electrohydrodynamic 3D printing of layer-specifically oriented, multiscale conductive scaffolds for cardiac tissue engineering, Nanoscale 11 (2019) 15195–15205, https://doi.org/10.1039/C9NR04989D.
[392] F. Furlani, E. Campodoni, N. Sangiorgi, M. Montesi, A. Sanson, M. Sandri, S. Panseri, Electroconductive scaffolds based on gelatin and PEDOT:PSS for cardiac regeneration, Int. J. Biol. Macromol. 224 (2023) 266–280, https://doi.org/10.1016/j.ijbiomac.2022.10.122.

[393] D. Mawad, A. Artzy-Schnirman, J. Tonkin, J. Ramos, S. Inal, M.M. Mahat, N. Darwish, L. Zwi-Dantsis, G.G. Malliaras, J.J. Gooding, A. Lauto, M.M. Stevens, Electroconductive hydrogel based on functional poly(ethylenedioxy thiophene), Chem. Mater. 28 (2016) 6080–6088, https://doi.org/10.1021/acs.chemmater.6b01298.

[394] G.C. Luque, M.L. Picchio, B. Daou, H. Lasa-Fernandez, M. Criado-Gonzalez, R. Querejeta, D. Filgueiras-Ramas, M. Prato, D. Mecerreyes, J. Ruiz-Cabello, N. Alegret, Printable poly(3,4-ethylenedioxythiophene)-based conductive patches for cardiac tissue remodeling, ACS Appl. Mater. Interfaces 16 (2024) 34467–34479, https://doi.org/10.1021/acsami.4c03784.

[395] D.M. Alshangiti, T.K. El-damhougy, A. Zaher, M. Madani, M. Mohamady Ghobashy, Revolutionizing biomedicine: advancements, applications, and prospects of nanocomposite macromolecular carbohydrate-based hydrogel biomaterials: a review, RSC Adv. 13 (2023) 35251–35291, https://doi.org/10.1039/D3RA07391B.

[396] M.N. Norizan, M.H. Moklis, S.Z. Ngah Demon, N.A. Halim, A. Samsuri, I. S. Mohamad, V.F. Knight, N. Abdullah, Carbon nanotubes: functionalisation and their application in chemical sensors, RSC Adv. 10 (2020) 43704–43732, https://doi.org/10.1039/D0RA09438B.

[397] P.R. Bandaru, Electronic transport and electrical properties of carbon nanotubes, in: J. Abraham, S. Thomas, N. Kalarikkal (Eds.), Handbook of Carbon Nanotubes, Springer International Publishing, Cham, 2022, pp. 173–211, https://doi.org/10.1007/978-3-030-91346-5_59.

[398] M.A. Morsi, A. Rajeh, A.A. Al-Muntaser, Reinforcement of the optical, thermal and electrical properties of PEO based on MWCNTs/Au hybrid fillers: nanodielectric materials for organoelectronic devices, Compos. B Eng. 173 (2019) 106957, https://doi.org/10.1016/j.compositesb.2019.106957.

[399] S. Bose, R.A. Khare, P. Moldenaers, Assessing the strengths and weaknesses of various types of pre-treatments of carbon nanotubes on the properties of polymer/carbon nanotubes composites: a critical review, Polymer 51 (2010) 975–993, https://doi.org/10.1016/j.polymer.2010.01.044.

[400] P.N. Yaron, B.D. Holt, P.A. Short, M. Lösche, M.F. Islam, K.N. Dahl, Single wall carbon nanotubes enter cells by endocytosis and not membrane penetration, J. Nanobiotechnol. 9 (2011) 45, https://doi.org/10.1186/1477-3155-9-45.

[401] B. Huang, Carbon nanotubes and their polymeric composites: the applications in tissue engineering, Biomanuf. Rev. 5 (2020) 3, https://doi.org/10.1007/s40898-020-00009-x.

[402] X. Yuan, X. Zhang, L. Sun, Y. Wei, X. Wei, Cellular toxicity and immunological effects of carbon-based nanomaterials, Part. Fibre Toxicol. 16 (2019) 18, https://doi.org/10.1186/s12989-019-0299-z.

[403] D. Van Berlo, V. Wilhelmi, A.W. Boots, M. Hullmann, T.A.J. Kuhlbusch, A. Bast, R. P.F. Schins, C. Albrecht, Apoptotic, inflammatory, and fibrogenic effects of two different types of multi-walled carbon nanotubes in mouse lung, Arch. Toxicol. 88 (2014) 1725–1737, https://doi.org/10.1007/s00204-014-1220-z.

[404] M.R. Chetyrkina, F.S. Fedorov, A.G. Nasibulin, *In vitro* toxicity of carbon nanotubes: a systematic review, RSC Adv. 12 (2022) 16235–16256, https://doi.org/10.1039/D2RA02519A.

[405] G. Kougkolos, M. Golzio, L. Laudebat, Z. Valdez-Nava, E. Flahaut, Hydrogels with electrically conductive nanomaterials for biomedical applications, J. Mater. Chem. B 11 (2023) 2036–2062, https://doi.org/10.1039/D2TB02019J.

[406] S.R. Shin, S.M. Jung, M. Zalabany, K. Kim, P. Zorlutuna, S.B. Kim, M. Nikkhah, M. Khabiry, M. Azize, J. Kong, K. Wan, T. Palacios, M.R. Dokmeci, H. Bae, X. Shirley Tang, A. Khademhosseini, Carbon-nanotube-embedded hydrogel sheets for engineering cardiac constructs and bioactuators, ACS Nano 7 (2013) 2369–2380, https://doi.org/10.1021/nn305559j.

[407] S. Mombini, J. Mohammadnejad, B. Bakhshandeh, A. Narmani, J. Nourmohammadi, S. Vahdat, S. Zirak, Chitosan-PVA-CNT nanofibers as electrically conductive scaffolds for cardiovascular tissue engineering, Int. J. Biol. Macromol. 140 (2019) 278–287, https://doi.org/10.1016/j.ijbiomac.2019.08.046.

[408] A.Yu Gerasimenko, U.E. Kurilova, M.S. Savelyev, D.T. Murashko, O.E. Glukhova, Laser fabrication of composite layers from biopolymers with branched 3D networks of single-walled carbon nanotubes for cardiovascular implants, Compos. Struct. 260 (2021) 113517, https://doi.org/10.1016/j.compstruct.2020.113517.

[409] F. Tondnevis, H. Keshvari, J.A. Mohandesi, Fabrication, characterization, and in vitro evaluation of electrospun polyurethane-gelatin-carbon nanotube scaffolds for cardiovascular tissue engineering applications, J. Biomed. Mater. Res. 108 (2020) 2276–2293, https://doi.org/10.1002/jbm.b.34564.

[410] M. Kharaziha, S.R. Shin, M. Nikkhah, S.N. Topkaya, N. Masoumi, N. Annabi, M. R. Dokmeci, A. Khademhosseini, Tough and flexible CNT–polymeric hybrid scaffolds for engineering cardiac constructs, Biomaterials 35 (2014) 7346–7354, https://doi.org/10.1016/j.biomaterials.2014.05.014.

[411] V.B. Mbayachi, E. Ndayiragije, T. Sammani, S. Taj, E.R. Mbuta, A.U. Khan, Graphene synthesis, characterization and its applications: a review, Results Chem. 3 (2021) 100163, https://doi.org/10.1016/j.rechem.2021.100163.

[412] W. Xue, J. Du, Q. Li, Y. Wang, Y. Lu, J. Fan, S. Yu, Y. Yang, Preparation, properties, and application of graphene-based materials in tissue engineering scaffolds, Tissue Eng. B Rev. 28 (2022) 1121–1136, https://doi.org/10.1089/ten.teb.2021.0127.

[413] Z. Xu, C. Gao, Graphene fiber: a new trend in carbon fibers, Mater. Today 18 (2015) 480–492, https://doi.org/10.1016/j.mattod.2015.06.009.

[414] C. Shen, S.O. Oyadiji, The processing and analysis of graphene and the strength enhancement effect of graphene-based filler materials: a review, Materials Today Physics 15 (2020) 100257, https://doi.org/10.1016/j.mtphys.2020.100257.

[415] F. Olate-Moya, L. Arens, M. Wilhelm, M.A. Mateos-Timoneda, E. Engel, H. Palza, Chondroinductive alginate-based hydrogels having graphene oxide for 3D printed scaffold fabrication, ACS Appl. Mater. Interfaces 12 (2020) 4343–4357, https://doi.org/10.1021/acsami.9b22062.

[416] K. Ławkowska, M. Pokrywczyńska, K. Koper, L.A. Kluth, T. Drewa, J. Adamowicz, Application of graphene in tissue engineering of the nervous system, IJMS 23 (2021) 33, https://doi.org/10.3390/ijms23010033.

[417] A. Ambrosi, C.K. Chua, A. Bonanni, M. Pumera, Electrochemistry of graphene and related materials, Chem. Rev. 114 (2014) 7150–7188, https://doi.org/10.1021/cr500023c.

[418] C. Jiang, D. An, Z. Wang, S. Zhang, X. An, J. Bo, G. Yan, K.-S. Moon, C. Wong, A sustainable reduction route of graphene oxide by industrial waste lignin for versatile applications in energy and environment, J. Clean. Prod. 268 (2020) 122019, https://doi.org/10.1016/j.jclepro.2020.122019.

[419] A. Najafi Tireh Shabankareh, P. Samadi Pakchin, M. Hasany, H. Ghanbari, Development of a new electroconductive nanofibrous cardiac patch based on polyurethane-reduced graphene oxide nanocomposite scaffolds, Mater. Chem. Phys. 305 (2023) 127961, https://doi.org/10.1016/j.matchemphys.2023.127961.

[420] S.R. Shin, C. Zihlmann, M. Akbari, P. Assawes, L. Cheung, K. Zhang, V. Manoharan, Y.S. Zhang, M. Yüksekkaya, K. Wan, M. Nikkhah, M.R. Dokmeci, X. (Shirley, Tang, A. Khademhosseini, Reduced graphene oxide-GelMA hybrid hydrogels as scaffolds for cardiac tissue engineering, Small 12 (2016) 3677–3689, https://doi.org/10.1002/smll.201600178.

[421] G. Zhao, H. Qing, G. Huang, G.M. Genin, T.J. Lu, Z. Luo, F. Xu, X. Zhang, Reduced graphene oxide functionalized nanofibrous silk fibroin matrices for engineering excitable tissues, NPG Asia Mater. 10 (2018) 982–994, https://doi.org/10.1038/s41427-018-0092-8.

[422] Ş. Arıcı, A.R. Kamali, D. Ege, CMC/Gel/GO 3D-printed cardiac patches: GO and CMC improve flexibility and promote H9C2 cell proliferation, while EDC/NHS enhances stability, Biofabrication 17 (2025) 015025, https://doi.org/10.1088/1758-5090/ad8e87.

[423] S. Priyadarsini, S. Mohanty, S. Mukherjee, S. Basu, M. Mishra, Graphene and graphene oxide as nanomaterials for medicine and biology application, J. Nanostruct. Chem. 8 (2018) 123–137, https://doi.org/10.1007/s40097-018-0265-6.

[424] M. Fathi-Achachelouei, H. Knopf-Marques, C.E. Ribeiro Da Silva, J. Barthès, E. Bat, A. Tezcaner, N.E. Vrana, Use of nanoparticles in tissue engineering and regenerative medicine, Front. Bioeng. Biotechnol. 7 (2019) 113, https://doi.org/10.3389/fbioe.2019.00113.

[425] P. Baei, S. Jalili-Firoozinezhad, S. Rajabi-Zeleti, M. Tafazzoli-Shadpour, H. Baharvand, N. Aghdami, Electrically conductive gold nanoparticle-chitosan thermosensitive hydrogels for cardiac tissue engineering, Mater. Sci. Eng. C 63 (2016) 131–141, https://doi.org/10.1016/j.msec.2016.02.056.

[426] B. Maharjan, D. Kumar, G.P. Awasthi, D.P. Bhattarai, J.Y. Kim, C.H. Park, C. S. Kim, Synthesis and characterization of gold/silica hybrid nanoparticles incorporated gelatin methacrylate conductive hydrogels for H9C2 cardiac cell compatibility study, Compos. B Eng. 177 (2019) 107415, https://doi.org/10.1016/j.compositesb.2019.107415.

[427] A.-C. Burduşel, O. Gherasim, A.M. Grumezescu, L. Mogoantă, A. Ficai, E. Andronescu, Biomedical applications of silver nanoparticles: an up-to-date overview, Nanomaterials 8 (2018) 681, https://doi.org/10.3390/nano8090681.

[428] K.M.F. Hasan, L. Xiaoyi, Z. Shaoqin, P.G. Horváth, M. Bak, L. Bejó, G. Sipos, T. Alpár, Functional silver nanoparticles synthesis from sustainable point of view: 2000 to 2023 – A review on game changing materials, Heliyon 8 (2022) e12322, https://doi.org/10.1016/j.heliyon.2022.e12322.

[429] A.K. Mittal, Y. Chisti, U.C. Banerjee, Synthesis of metallic nanoparticles using plant extracts, Biotechnol. Adv. 31 (2013) 346–356, https://doi.org/10.1016/j.biotechadv.2013.01.003.

[430] Y. Liu, F. Li, Z. Guo, Y. Xiao, Y. Zhang, X. Sun, T. Zhe, Y. Cao, L. Wang, Q. Lu, J. Wang, Silver nanoparticle-embedded hydrogel as a photothermal platform for combating bacterial infections, Chemical Engineering Journal 382 (2020) 122990, https://doi.org/10.1016/j.cej.2019.122990.

[431] A.S. Dove, D.I. Dzurny, W.R. Dees, N. Qin, C.C. Nunez Rodriguez, L.A. Alt, G. L. Ellward, J.A. Best, N.G. Rudawski, K. Fujii, D.M. Czyż, Silver nanoparticles enhance the efficacy of aminoglycosides against antibiotic-resistant bacteria, Front. Microbiol. 13 (2023) 1064095, https://doi.org/10.3389/fmicb.2022.1064095.

[432] K. Kang, D.-H. Lim, I.-H. Choi, T. Kang, K. Lee, E.-Y. Moon, Y. Yang, M.-S. Lee, J.-S. Lim, Vascular tube formation and angiogenesis induced by polyvinylpyrrolidone-coated silver nanoparticles, Toxicol. Lett. 205 (2011) 227–234, https://doi.org/10.1016/j.toxlet.2011.05.1033.

[433] S. Allison, M. Ahumada, C. Andronic, B. McNeill, F. Variola, M. Griffith, M. Ruel, V. Hamel, W. Liang, E.J. Suuronen, E.I. Alarcon, Electroconductive nanoengineered biomimetic hybrid fibers for cardiac tissue engineering, J. Mater. Chem. B 5 (2017) 2402–2406, https://doi.org/10.1039/C7TB00405B.

[434] X. Huang, M.A. El-Sayed, Gold nanoparticles: optical properties and implementations in cancer diagnosis and photothermal therapy, J. Adv. Res. 1 (2010) 13–28, https://doi.org/10.1016/j.jare.2010.02.002.

[435] M.R. Ivanov, H.R. Bednar, A.J. Haes, Investigations of the mechanism of gold nanoparticle stability and surface functionalization in capillary electrophoresis, ACS Nano 3 (2009) 386–394, https://doi.org/10.1021/nn8005619.

[436] X. Zhao, X. Ding, Z. Deng, Z. Zheng, Y. Peng, C. Tian, X. Long, A kind of smart gold nanoparticle–hydrogel composite with tunable thermo-switchable electrical properties, New J. Chem. 30 (2006) 915–920, https://doi.org/10.1039/B601069E.

[437] Y. Zhang, W. Fan, K. Wang, H. Wei, R. Zhang, Y. Wu, Novel preparation of Au nanoparticles loaded Laponite nanoparticles/ECM injectable hydrogel on cardiac

differentiation of resident cardiac stem cells to cardiomyocytes, J. Photochem. Photobiol. B Biol. 192 (2019) 49–54, https://doi.org/10.1016/j.jphotobiol.2018.12.022.
[438] P. Tiwari, K. Vig, V. Dennis, S. Singh, Functionalized gold nanoparticles and their biomedical applications, Nanomaterials 1 (2011) 31–63, https://doi.org/10.3390/nano1010031.
[439] K. Zhu, S.R. Shin, T. Van Kempen, Y. Li, V. Ponraj, A. Nasajpour, S. Mandla, N. Hu, X. Liu, J. Leijten, Y. Lin, M.A. Hussain, Y.S. Zhang, A. Tamayol, A. Khademhosseini, Gold nanocomposite bioink for printing 3D cardiac constructs, Adv. Funct. Mater. 27 (2017) 1605352, https://doi.org/10.1002/adfm.201605352.
[440] M. Malki, S. Fleischer, A. Shapira, T. Dvir, Gold nanorod-based engineered cardiac patch for suture-free engraftment by near IR, Nano Lett. 18 (2018) 4069–4073, https://doi.org/10.1021/acs.nanolett.7b04924.
[441] A. Khanbaba, H. Mozaffari, R. Faridi-Majidi, M.A. Derakhshan, Electrospun polyurethane/collagen/chitosan nanofibers containing gold nanoparticles for cardiac tissue regeneration, BioNanoScience 15 (2025) 16, https://doi.org/10.1007/s12668-024-01652-1.
[442] R. Chaudhuri, M. Ramachandran, P. Moharil, M. Harumalani, A.K. Jaiswal, Biomaterials and cells for cardiac tissue engineering: current choices, Mater. Sci. Eng. C 79 (2017) 950–957, https://doi.org/10.1016/j.msec.2017.05.121.
[443] J. Min, M. Patel, W.-G. Koh, Incorporation of conductive materials into hydrogels for tissue engineering applications, Polymers 10 (2018) 1078, https://doi.org/10.3390/polym10101078.
[444] U. Blache, E.M. Ford, B. Ha, L. Rijns, O. Chaudhuri, P.Y.W. Dankers, A.M. Kloxin, J.G. Snedeker, E. Gentleman, Engineered hydrogels for mechanobiology, Nat Rev Methods Primers 2 (2022) 98, https://doi.org/10.1038/s43586-022-00179-7.
[445] G. Camci-Unal, N. Annabi, M.R. Dokmeci, R. Liao, A. Khademhosseini, Hydrogels for cardiac tissue engineering, NPG Asia Mater. 6 (2014), https://doi.org/10.1038/am.2014.19 e99–e99.
[446] S. Mohammadi Nasr, N. Rabiee, S. Hajebi, S. Ahmadi, Y. Fatahi, M. Hosseini, M. Bagherzadeh, A.M. Ghadiri, M. Rabiee, V. Jajarmi, T.J. Webster, Biodegradable nanopolymers in cardiac tissue engineering: from concept towards nanomedicine, IJN 15 (2020) 4205–4224, https://doi.org/10.2147/IJN.S245936.
[447] G. Guan, D. Huo, Y. Li, X. Zhao, Y. Li, Z. Qin, D. Sun, G. Yang, M. Yang, J. Tan, W. Zeng, C. Zhu, Engineering hiPSC-CM and hiPSC-EC laden 3D nanofibrous splenic hydrogel for improving cardiac function through revascularization and remuscularization in infarcted heart, Bioact. Mater. 6 (2021) 4415–4429, https://doi.org/10.1016/j.bioactmat.2021.04.010.
[448] I.M. El-Sherbiny, M.H. Yacoub, Hydrogel scaffolds for tissue engineering: progress and challenges, Global Cardiol. Sci. Pract. 2013 (2013) 38, https://doi.org/10.5339/gcsp.2013.38.
[449] R.J. Kant, K.L.K. Coulombe, Integrated approaches to spatiotemporally directing angiogenesis in host and engineered tissues, Acta Biomater. 69 (2018) 42–62, https://doi.org/10.1016/j.actbio.2018.01.017.
[450] S. Smagul, Y. Kim, A. Smagulova, K. Raziyeva, A. Nurkesh, A. Saparov, Biomaterials loaded with growth factors/cytokines and stem cells for cardiac tissue regeneration, IJMS 21 (2020) 5952, https://doi.org/10.3390/ijms21175952.
[451] N. Liu, X. Ye, B. Yao, M. Zhao, P. Wu, G. Liu, D. Zhuang, H. Jiang, X. Chen, Y. He, S. Huang, P. Zhu, Advances in 3D bioprinting technology for cardiac tissue engineering and regeneration, Bioact. Mater. 6 (2021) 1388–1401, https://doi.org/10.1016/j.bioactmat.2020.10.021.
[452] H. Cui, Z.-X. Yu, Y. Huang, S.Y. Hann, T. Esworthy, Y.-L. Shen, L.G. Zhang, 3D printing of thick myocardial tissue constructs with anisotropic myofibers and perfusable vascular channels, Biomater. Adv. 153 (2023) 213579, https://doi.org/10.1016/j.bioadv.2023.213579.
[453] X. Li, P. Lu, Z. Liu, Z. Wen, X. Li, C. Wang, W. Jin, B. Zhou, N. Huang, M. Song, X. Wang, An anisotropic electromagnetic hydrogel promotes cardiomyocyte maturation and post-infarction cardiac repair, Chemical Engineering Journal 476 (2023) 146745, https://doi.org/10.1016/j.cej.2023.146745.
[454] C.H. Chew, B.-L. Sheu, A. Chen, W.-T. Huang, T.-M. Cheng, C.-M. Shih, A. Chang, C.-C. Chen, Tissue-engineered vascular graft with Co-culture of smooth muscle cells and human endothelial vein cells on an electrospun poly(lactic-co-glycolic acid) microtube array membrane, Membranes 11 (2021) 732, https://doi.org/10.3390/membranes11100732.
[455] C. O'Connor, E. Brady, Y. Zheng, E. Moore, K.R. Stevens, Engineering the multiscale complexity of vascular networks, Nat. Rev. Mater. 7 (2022) 702–716, https://doi.org/10.1038/s41578-022-00447-8.
[456] R. Augustine, P. Dan, A. Hasan, I.M. Khalaf, P. Prasad, K. Ghosal, C. Gentile, L. McClements, P. Maureira, Stem cell-based approaches in cardiac tissue engineering: controlling the microenvironment for autologous cells, Biomed. Pharmacother. 138 (2021) 111425, https://doi.org/10.1016/j.biopha.2021.111425.
[457] N. Jalilinejad, M. Rabiee, N. Baheiraei, R. Ghahremanzadeh, R. Salarian, N. Rabiee, O. Akhavan, P. Zarrintaj, A. Hejna, M.R. Saeb, A. Zarrabi, E. Sharifi, S. Yousefiasl, E.N. Zare, Electrically conductive carbon-based (bio)-nanomaterials for cardiac tissue engineering, Bioeng.; Transla Med. 8 (2023) e10347, https://doi.org/10.1002/btm2.10347.
[458] Y. He, G. Ye, C. Song, C. Li, W. Xiong, L. Yu, X. Qiu, L. Wang, Mussel-inspired conductive nanofibrous membranes repair myocardial infarction by enhancing cardiac function and revascularization, Theranostics 8 (2018) 5159–5177, https://doi.org/10.7150/thno.27760.
[459] M. Yeo, A. Sarkar, Y.P. Singh, I.D. Derman, P. Datta, I.T. Ozbolat, Synergistic coupling between 3D bioprinting and vascularization strategies, Biofabrication 16 (2024) 012003, https://doi.org/10.1088/1758-5090/ad0b3f.
[460] Z. Fan, Z. Xu, H. Niu, Y. Sui, H. Li, J. Ma, J. Guan, Spatiotemporal delivery of basic fibroblast growth factor to directly and simultaneously attenuate cardiac fibrosis and promote cardiac tissue vascularization following myocardial infarction, J. Contr. Release 311–312 (2019) 233–244, https://doi.org/10.1016/j.jconrel.2019.09.005.
[461] R. Lakshmanan, P. Kumaraswamy, U.M. Krishnan, S. Sethuraman, Engineering a growth factor embedded nanofiber matrix niche to promote vascularization for functional cardiac regeneration, Biomaterials 97 (2016) 176–195, https://doi.org/10.1016/j.biomaterials.2016.02.033.
[462] R. Chapla, J.L. West, Hydrogel biomaterials to support and guide vascularization, Prog. Biomed. Eng. 3 (2021) 012002, https://doi.org/10.1088/2516-1091/abc947.
[463] U. Blache, M. Ehrbar, Inspired by nature: hydrogels as versatile tools for vascular engineering, Adv. Wound Care 7 (2018) 232–246, https://doi.org/10.1089/wound.2017.0760.
[464] A. Mehrabi, N. Baheiraei, M. Adabi, Z. Amirkhani, Development of a novel electroactive cardiac patch based on carbon nanofibers and gelatin encouraging vascularization, Appl. Biochem. Biotechnol. 190 (2020) 931–948, https://doi.org/10.1007/s12010-019-03135-6.
[465] J. Meng, B. Xiao, F. Wu, L. Sun, B. Li, W. Guo, X. Hu, X. Xu, T. Wen, J. Liu, H. Xu, Co-axial fibrous scaffolds integrating with carbon fiber promote cardiac tissue regeneration post myocardial infarction, Mater. Today Bio 16 (2022) 100415, https://doi.org/10.1016/j.mtbio.2022.100415.
[466] V.C. Vetter, C.V.C. Bouten, A. Van Der Pol, Hydrogels for cardiac restorative support: relevance of gelation mechanisms for prospective clinical use, Curr. Heart Fail. Rep. 20 (2023) 519–529, https://doi.org/10.1007/s11897-023-00630-0.
[467] P. Li, J. Hu, J. Wang, J. Zhang, L. Wang, C. Zhang, The role of hydrogel in cardiac repair and regeneration for myocardial infarction: recent advances and future perspectives, Bioengineering 10 (2023) 165, https://doi.org/10.3390/bioengineering10020165.
[468] A. Sesena-Rubfiaro, N.J. Prajapati, L. Paolino, L. Lou, D. Cotayo, P. Pandey, M. Shaver, J.D. Hutcheson, A. Agarwal, J. He, Membrane remodeling of human-engineered cardiac tissue by chronic electric stimulation, ACS Biomater. Sci. Eng. 9 (2023) 1644–1655, https://doi.org/10.1021/acsbiomaterials.2c01370.
[469] J. Song, S. Gerecht, Hydrogels to recapture extracellular matrix cues that regulate vascularization, ATVB 43 (2023), https://doi.org/10.1161/ATVBAHA.122.318235.
[470] K. Ronaldson-Bouchard, S.P. Ma, K. Yeager, T. Chen, L. Song, D. Sirabella, K. Morikawa, D. Teles, M. Yazawa, G. Vunjak-Novakovic, Advanced maturation of human cardiac tissue grown from pluripotent stem cells, Nature 556 (2018) 239–243, https://doi.org/10.1038/s41586-018-0016-3.
[471] J. Lee, V. Manoharan, L. Cheung, S. Lee, B.-H. Cha, P. Newman, R. Farzad, S. Mehrotra, K. Zhang, F. Khan, M. Ghaderi, Y.-D. Lin, S. Aftab, P. Mostafalu, M. Miscuglio, J. Li, B.B. Mandal, M.A. Hussain, K. Wan, X.S. Tang, A. Khademhosseini, S.R. Shin, Nanoparticle-based hybrid scaffolds for deciphering the role of multimodal cues in cardiac tissue engineering, ACS Nano 13 (2019) 12525–12539, https://doi.org/10.1021/acsnano.9b03050.
[472] A. Kantaros, T. Ganetsos, From static to dynamic: smart materials pioneering additive manufacturing in regenerative medicine, IJMS 24 (2023) 15748, https://doi.org/10.3390/ijms242115748.
[473] A. Samir, F.H. Ashour, A.A.A. Hakim, M. Bassyouni, Recent advances in biodegradable polymers for sustainable applications, npj Mater. Degrad. 6 (2022) 68, https://doi.org/10.1038/s41529-022-00277-7.
[474] A. Yaacob, N.S. Jamaludin, Biodegradable polymers for cardiac tissue engineering, in: G.A.M. Ali, A.S.H. Makhlouf (Eds.), Handbook of Biodegradable Materials, Springer International Publishing, Cham, 2023, pp. 979–1013, https://doi.org/10.1007/978-3-031-09710-2_44.
[475] M. Gomez-Florit, A. Pardo, R.M.A. Domingues, A.L. Graça, P.S. Babo, R.L. Reis, M. E. Gomes, Natural-based hydrogels for tissue engineering applications, Molecules 25 (2020) 5858, https://doi.org/10.3390/molecules25245858.
[476] D.A. Ahmad Ruzaidi, M.M. Mahat, S.A. Shafiee, Z. Mohamed Sofian, A. S. Mohmad Sabere, R. Ramli, H. Osman, H.H. Hamzah, Z. Zainal Ariffin, K. K. Sadasivuni, Advocating electrically conductive scaffolds with low immunogenicity for biomedical applications: a review, Polymers 13 (2021) 3395, https://doi.org/10.3390/polym13193395.
[477] M. Suku, L. Forrester, M. Biggs, M.G. Monaghan, Resident macrophages and their potential in cardiac tissue engineering, Tissue Eng. B Rev. 28 (2022) 579–591, https://doi.org/10.1089/ten.teb.2021.0036.
[478] G. Abd, R.S. Díaz, A. Gupta, T.H.R. Niepa, K. Mondal, S. Ramakrishna, A. Sharma, A.D. Lantada, M. Islam, Carbon nanomaterials-based electrically conductive scaffolds for tissue engineering applications, MedComm – Biomaterials and Applications 3 (2024) e76, https://doi.org/10.1002/mba2.76.
[479] E. Sancar, B. Oktay, E. Ahlatcıoğlu Özerol, Carbon based materials in conducting tissue engineering, Mater. Res. Express 11 (2024) 122001, https://doi.org/10.1088/2053-1591/ad9549.
[480] A. Saberi, F. Jabbari, P. Zarrintaj, M.R. Saeb, M. Mozafari, Electrically conductive materials: opportunities and challenges in tissue engineering, Biomolecules 9 (2019) 448, https://doi.org/10.3390/biom9090448.
[481] Y. Fukaya, Y. Iizuka, K. Sekikawa, H. Ohno, Bio ionic liquids: room temperature ionic liquids composed wholly of biomaterials, Green Chem. 9 (2007) 1155, https://doi.org/10.1039/b706571j.
[482] I. Noshadi, B.W. Walker, R. Portillo-Lara, E. Shirzaei Sani, N. Gomes, M. R. Aziziyan, N. Annabi, Engineering biodegradable and biocompatible bio-ionic liquid conjugated hydrogels with tunable conductivity and mechanical properties, Sci. Rep. 7 (2017) 4345, https://doi.org/10.1038/s41598-017-04280-w.

[483] J.W. Nichol, S.T. Koshy, H. Bae, C.M. Hwang, S. Yamanlar, A. Khademhosseini, Cell-laden microengineered gelatin methacrylate hydrogels, Biomaterials 31 (2010) 5536–5544, https://doi.org/10.1016/j.biomaterials.2010.03.064.
[484] S.T. Koshy, T.C. Ferrante, S.A. Lewin, D.J. Mooney, Injectable, porous, and cell-responsive gelatin cryogels, Biomaterials 35 (2014) 2477–2487, https://doi.org/10.1016/j.biomaterials.2013.11.044.
[485] Y. Chen, R. Lin, H. Qi, Y. Yang, H. Bae, J.M. Melero-Martin, A. Khademhosseini, Functional human vascular network generated in photocrosslinkable gelatin methacrylate hydrogels, Adv. Funct. Mater. 22 (2012) 2027–2039, https://doi.org/10.1002/adfm.201101662.
[486] J.G. Rurik, H. Aghajanian, J.A. Epstein, Immune cells and immunotherapy for cardiac injury and repair, Circ. Res. 128 (2021) 1766–1779, https://doi.org/10.1161/CIRCRESAHA.121.318005.
[487] W.P. Lafuse, D.J. Wozniak, M.V.S. Rajaram, Role of cardiac macrophages on cardiac inflammation, fibrosis and tissue repair, Cells 10 (2020) 51, https://doi.org/10.3390/cells10010051.
[488] O. Gil-Castell, I. Ontoria-Oviedo, J.D. Badia, E. Amaro-Prellezo, P. Sepúlveda, A. Ribes-Greus, Conductive polycaprolactone/gelatin/polyaniline nanofibres as functional scaffolds for cardiac tissue regeneration, React. Funct. Polym. 170 (2022) 105064, https://doi.org/10.1016/j.reactfunctpolym.2021.105064.
[489] K. Kohno, S. Koya-Miyata, A. Harashima, T. Tsukuda, M. Katakami, T. Ariyasu, S. Ushio, K. Iwaki, Inflammatory M1-like macrophages polarized by NK-4 undergo enhanced phenotypic switching to an anti-inflammatory M2-like phenotype upon co-culture with apoptotic cells, J. Inflamm. 18 (2021) 2, https://doi.org/10.1186/s12950-020-00267-z.
[490] W. Bu, Y. Wu, A.M. Ghaemmaghami, H. Sun, A. Mata, Rational design of hydrogels for immunomodulation, Regen. Biomater. 9 (2022), https://doi.org/10.1093/rb/rbac009 rbac009.
[491] M. Kharaziha, A. Baidya, N. Annabi, Rational design of immunomodulatory hydrogels for chronic wound healing, Adv. Mater. 33 (2021) 2100176, https://doi.org/10.1002/adma.202100176.
[492] D. Salthouse, K. Novakovic, C.M.U. Hilkens, A.M. Ferreira, Interplay between biomaterials and the immune system: challenges and opportunities in regenerative medicine, Acta Biomater. 155 (2023) 1–18, https://doi.org/10.1016/j.actbio.2022.11.003.
[493] Z. Rezaei, D. Yilmaz-Aykut, F.M. Tourk, N. Bassous, M. Barroso-Zuppa, A.I. Shawl, S.S. Ashraf, H. Avci, S. Hassan, Immunomodulating hydrogels as stealth platform for drug delivery applications, Pharmaceutics 14 (2022) 2244, https://doi.org/10.3390/pharmaceutics14102244.
[494] J.I. Andorko, C.M. Jewell, Designing biomaterials with immunomodulatory properties for tissue engineering and regenerative medicine, Bioeng.; Transla Med. 2 (2017) 139–155, https://doi.org/10.1002/btm2.10063.
[495] X. Wang, H. Zhou, Q. Liu, P. Cheng, T. Zhao, T. Yang, Y. Zhao, W. Sha, Y. Zhao, H. Qu, Targeting regulatory T cells for cardiovascular diseases, Front. Immunol. 14 (2023) 1126761, https://doi.org/10.3389/fimmu.2023.1126761.
[496] A. Vishwakarma, N.S. Bhise, M.B. Evangelista, J. Rouwkema, M.R. Dokmeci, A. M. Ghaemmaghami, N.E. Vrana, A. Khademhosseini, Engineering immunomodulatory biomaterials to tune the inflammatory response, Trends Biotechnol. 34 (2016) 470–482, https://doi.org/10.1016/j.tibtech.2016.03.009.
[497] M.C.P. Sok, N. Baker, C. McClain, H.S. Lim, T. Turner, L. Hymel, M. Ogle, C. Olingy, J.I. Palacios, J.R. Garcia, K. Srithar, A.J. García, P. Qiu, E.A. Botchwey, Dual delivery of IL-10 and AT-RvD1 from PEG hydrogels polarize immune cells towards pro-regenerative phenotypes, Biomaterials 268 (2021) 120475, https://doi.org/10.1016/j.biomaterials.2020.120475.
[498] S. Xu, J. Zhang, J. Liu, J. Ye, Y. Xu, Z. Wang, J. Yu, D. Ye, M. Zhao, Y. Feng, W. Pan, M. Wang, J. Wan, The role of interleukin-10 family members in cardiovascular diseases, Int. Immunopharmacol. 94 (2021) 107475, https://doi.org/10.1016/j.intimp.2021.107475.
[499] D.V. Dzhonova, R. Olariu, J. Leckenby, Y. Banz, J.-C. Prost, A. Dhayani, P. K. Vemula, E. Voegelin, A. Taddeo, R. Rieben, Local injections of tacrolimus-loaded hydrogel reduce systemic immunosuppression-related toxicity in vascularized composite allotransplantation, Transplantation 102 (2018) 1684–1694, https://doi.org/10.1097/TP.0000000000002283.
[500] W. Qian, D. Liu, Y. Han, M. Liu, B. Liu, Q. Ji, B. Zhang, Q. Mei, S. Zhou, Y. Cheng, Cyclosporine A-loaded apoferritin alleviates myocardial ischemia-reperfusion injury by simultaneously blocking ferroptosis and apoptosis of cardiomyocytes, Acta Biomater. 160 (2023) 265–280, https://doi.org/10.1016/j.actbio.2023.02.025.
[501] S. Kang, B. Wang, Y. Xie, X. Cao, M. Wang, The role of M1 and M2 myocardial macrophages in promoting proliferation and healing via activating epithelial-to-mesenchymal transition, Biomedicines 11 (2023) 2666, https://doi.org/10.3390/biomedicines11102666.
[502] W. Xie, X. Wei, H. Kang, H. Jiang, Z. Chu, Y. Lin, Y. Hou, Q. Wei, Static and dynamic: evolving biomaterial mechanical properties to control cellular mechanotransduction, Adv. Sci. 10 (2023) 2204594, https://doi.org/10.1002/advs.202204594.
[503] A. Mariano, C. Lubrano, U. Bruno, C. Ausilio, N.B. Dinger, F. Santoro, Advances in cell-conductive polymer biointerfaces and role of the plasma membrane, Chem. Rev. 122 (2022) 4552–4580, https://doi.org/10.1021/acs.chemrev.1c00363.
[504] Y.M. Chen, J.J. Yang, J.P. Gong, Adhesion, spreading, and proliferation of endothelial cells on charged hydrogels, J. Adhes. 85 (2009) 839–868, https://doi.org/10.1080/00218460903291486.
[505] C. Wu, A. Liu, S. Chen, X. Zhang, L. Chen, Y. Zhu, Z. Xiao, J. Sun, H. Luo, H. Fan, Cell-laden electroconductive hydrogel simulating nerve matrix to deliver electrical cues and promote neurogenesis, ACS Appl. Mater. Interfaces 11 (2019) 22152–22163, https://doi.org/10.1021/acsami.9b05520.
[506] F. Xue, D.M. Janzen, D.A. Knecht, Contribution of filopodia to cell migration: a mechanical link between protrusion and contraction, Int. J. Cell Biol. 2010 (2010) 1–13, https://doi.org/10.1155/2010/507821.
[507] K. Adebowale, Z. Gong, J.C. Hou, K.M. Wisdom, D. Garbett, H. Lee, S. Nam, T. Meyer, D.J. Odde, V.B. Shenoy, O. Chaudhuri, Enhanced substrate stress relaxation promotes filopodia-mediated cell migration, Nat. Mater. 20 (2021) 1290–1299, https://doi.org/10.1038/s41563-021-00981-w.
[508] M. Innocenti, New insights into the formation and the function of lamellipodia and ruffles in mesenchymal cell migration, Cell Adhes. Migrat. (2018) 1–16, https://doi.org/10.1080/19336918.2018.1448352.
[509] M. Solazzo, F.J. O'Brien, V. Nicolosi, M.G. Monaghan, The rationale and emergence of electroconductive biomaterial scaffolds in cardiac tissue engineering, APL Bioeng. 3 (2019) 041501, https://doi.org/10.1063/1.5116579.
[510] Z.J. Rogers, M.P. Zeevi, R. Koppes, S.A. Bencherif, Electroconductive hydrogels for tissue engineering: current status and future perspectives, Bioelectricity 2 (2020) 279–292, https://doi.org/10.1089/bioe.2020.0025.
[511] C.T. Mierke, Mechanical cues affect migration and invasion of cells from three different directions, Front. Cell Dev. Biol. 8 (2020) 583226, https://doi.org/10.3389/fcell.2020.583226.
[512] T. Hendrickson, C. Mancino, L. Whitney, C. Tsao, M. Rahimi, F. Taraballi, Mimicking cardiac tissue complexity through physical cues: a review on cardiac tissue engineering approaches, Nanomed. Nanotechnol. Biol. Med. 33 (2021) 102367, https://doi.org/10.1016/j.nano.2021.102367.
[513] S. Mehrotra, S. Dey, K. Sachdeva, S. Mohanty, B.B. Mandal, Recent advances in tailoring stimuli-responsive hybrid scaffolds for cardiac tissue engineering and allied applications, J. Mater. Chem. B 11 (2023) 10297–10331, https://doi.org/10.1039/D3TB00450C.
[514] W. Zakrzewski, M. Dobrzyński, M. Szymonowicz, Z. Rybak, Stem cells: past, present, and future, Stem Cell Res. Ther. 10 (2019) 68, https://doi.org/10.1186/s13287-019-1165-5.
[515] E. Apostolou, H. Blau, K. Chien, M.A. Lancaster, P.R. Tata, E. Trompouki, F. M. Watt, Y.A. Zeng, M. Zernicka-Goetz, Progress and challenges in stem cell biology, Nat. Cell Biol. 25 (2023) 203–206, https://doi.org/10.1038/s41556-023-01087-y.
[516] Y. Xu, M. Cui, P.A. Patsis, M. Günther, X. Yang, K. Eckert, Y. Zhang, Reversibly assembled electroconductive hydrogel via a host–guest interaction for 3D cell culture, ACS Appl. Mater. Interfaces 11 (2019) 7715–7724, https://doi.org/10.1021/acsami.8b19482.
[517] J.D.S. Rebouças, N.S. Santos-Magalhães, F.R. Formiga, Cardiac regeneration using growth factors: advances and challenges, Arq. Bras. Cardiol. (2016), https://doi.org/10.5935/abc.20160097.
[518] B. Bakhshandeh, N. Ranjbar, A. Abbasi, E. Amiri, A. Abedi, M. Mehrabi, Z. Dehghani, C.P. Pennisi, Recent progress in the manipulation of biochemical and biophysical cues for engineering functional tissues, Bioeng.; Transla Med. 8 (2023) e10383, https://doi.org/10.1002/btm2.10383.
[519] Y. Wu, L. Wang, B. Guo, Y. Shao, P.X. Ma, Electroactive biodegradable polyurethane significantly enhanced Schwann cells myelin gene expression and neurotrophin secretion for peripheral nerve tissue engineering, Biomaterials 87 (2016) 18–31, https://doi.org/10.1016/j.biomaterials.2016.02.010.
[520] Kshitiz, J. Park, P. Kim, W. Helen, A.J. Engler, A. Levchenko, D.-H. Kim, Control of stem cell fate and function by engineering physical microenvironments, Integr. Biol. 4 (2012) 1008–1018, https://doi.org/10.1039/c2ib20080e.
[521] M. Zhang, C. Che, J. Cheng, P. Li, Y. Yang, Ion channels in stem cells and their roles in stem cell biology and vascular diseases, J. Mol. Cell. Cardiol. 166 (2022) 63–73, https://doi.org/10.1016/j.yjmcc.2022.02.002.
[522] A. Navaei, N. Moore, R.T. Sullivan, D. Truong, R.Q. Migrino, M. Nikkhah, Electrically conductive hydrogel-based micro-topographies for the development of organized cardiac tissues, RSC Adv. 7 (2017) 3302–3312, https://doi.org/10.1039/C6RA26279A.
[523] F. Tian, H. Sun, Y. Mou, Y. Li, X. Li, Z. Chen, K. Duval, Z. Huang, R. Dai, L. Tang, Carbon nanotube-based substrates promote cardiogenesis in brown adipose-derived stem cells via β1-integrin-dependent TGF-β1 signaling pathway, IJN 11 (2016) 4381–4395, https://doi.org/10.2147/IJN.S114357.
[524] A. Mousavi, S. Vahdat, N. Baheiraei, M. Razavi, M.H. Norahan, H. Baharvand, Multifunctional conductive biomaterials as promising platforms for cardiac tissue engineering, ACS Biomater. Sci. Eng. 7 (2021) 55–82, https://doi.org/10.1021/acsbiomaterials.0c01422.
[525] H. Sun, S. Lü, X.-X. Jiang, X. Li, H. Li, Q. Lin, Y. Mou, Y. Zhao, Y. Han, J. Zhou, C. Wang, Carbon nanotubes enhance intercalated disc assembly in cardiac myocytes via the β1-integrin-mediated signaling pathway, Biomaterials 55 (2015) 84–95, https://doi.org/10.1016/j.biomaterials.2015.03.030.
[526] G. Gonzalez, A.C. Nelson, A.R. Holman, A.J. Whitehead, E. LaMontagne, R. Lian, R. Vatsyayan, S.A. Dayeh, A.J. Engler, Conductive electrospun polymer improves stem cell-derived cardiomyocyte function and maturation, Biomaterials 302 (2023) 122363, https://doi.org/10.1016/j.biomaterials.2023.122363.
[527] C.B. Sim, B. Phipson, M. Ziemann, H. Rafehi, R.J. Mills, K.I. Watt, K.D. Abu-Bonsrah, R.K.R. Kalathur, H.K. Voges, D.T. Dinh, M. Ter Huurne, C.J. Vivien, A. Kaspi, H. Kaipananickal, A. Hidalgo, L.M.D. Delbridge, R.L. Robker, P. Gregorevic, C.G. Dos Remedios, S. Lal, A.T. Piers, I.E. Konstantinov, D. A. Elliott, A. El-Osta, A. Oshlack, J.E. Hudson, E.R. Porrello, Sex-specific control of human heart maturation by the progesterone receptor, Circulation (New York, N. Y.) 143 (2021) 1614–1628, https://doi.org/10.1161/CIRCULATIONAHA.120.051921.
[528] S.C. Ligon, R. Liska, J. Stampfl, M. Gurr, R. Mülhaupt, Polymers for 3D printing and customized additive manufacturing, Chem. Rev. 117 (2017) 10212–10290, https://doi.org/10.1021/acs.chemrev.7b00074.

[529] Y. Li, Y. Shi, Y. Lu, X. Li, J. Zhou, A.A. Zadpoor, L. Wang, Additive manufacturing of vascular stents, Acta Biomater. 167 (2023) 16–37, https://doi.org/10.1016/j.actbio.2023.06.014.
[530] N. Dark, M.-V. Cosson, L.I. Tsansizi, T.J. Owen, E. Ferraro, A.J. Francis, S. Tsai, C. Bouissou, A. Weston, L. Collinson, N. Abi-Gerges, P.E. Miller, K.T. MacLeod, E. Ehler, R. Mitter, S.E. Harding, J.C. Smith, A.S. Bernardo, Generation of left ventricle-like cardiomyocytes with improved structural, functional, and metabolic maturity from human pluripotent stem cells, Cell Reports Methods 3 (2023) 100456, https://doi.org/10.1016/j.crmeth.2023.100456.
[531] J. Wang, C. Cui, H. Nan, Y. Yu, Y. Xiao, E. Poon, G. Yang, X. Wang, C. Wang, L. Li, K.R. Boheler, X. Ma, X. Cheng, Z. Ni, M. Chen, Graphene sheet-induced global maturation of cardiomyocytes derived from human induced pluripotent stem cells, ACS Appl. Mater. Interfaces 9 (2017) 25929–25940, https://doi.org/10.1021/acsami.7b08777.
[532] M.A. Skylar-Scott, S.G.M. Uzel, L.L. Nam, J.H. Ahrens, R.L. Truby, S. Damaraju, J. A. Lewis, Biomanufacturing of organ-specific tissues with high cellular density and embedded vascular channels, Sci. Adv. 5 (2019) eaaw2459, https://doi.org/10.1126/sciadv.aaw2459.
[533] Y. Fang, Y. Guo, B. Wu, Z. Liu, M. Ye, Y. Xu, M. Ji, L. Chen, B. Lu, K. Nie, Z. Wang, J. Luo, T. Zhang, W. Sun, Z. Xiong, Expanding embedded 3D bioprinting capability for engineering complex organs with freeform vascular networks, Adv. Mater. 35 (2023) 2205082, https://doi.org/10.1002/adma.202205082.
[534] J. Wu, C. Wu, S. Zou, X. Li, B. Ho, R. Sun, C. Liu, M. Chen, Investigation of biomaterial ink viscosity properties and optimization of the printing process based on pattern path planning, Bioengineering 10 (2023) 1358, https://doi.org/10.3390/bioengineering10121358.
[535] S. Dani, T. Ahlfeld, F. Albrecht, S. Duin, P. Kluger, A. Lode, M. Gelinsky, Homogeneous and reproducible mixing of highly viscous biomaterial inks and cell suspensions to create bioinks, Gels 7 (2021) 227, https://doi.org/10.3390/gels7040227.